

Tfap2a, Irf6 & Grhl3: A NOVEL NETWORK THAT REGULATES BOTH
NEURULATION AND CRANIOFACIAL DEVELOPMENT

By

Youssef Ayoub Adly Kousa

A DISSERTATION

Submitted to
Michigan State University
in partial fulfillment of the requirements
for the degree of

Biochemistry and Molecular Biology – Doctor of Philosophy

2014

ABSTRACT

Tfap2a, *Irf6* & *Grhl3*: A NOVEL NETWORK THAT REGULATES BOTH NEURULATION AND CRANIOFACIAL DEVELOPMENT

By

Youssef Ayoub Adly Kousa

Interferon Regulatory Factors transcriptionally regulate development and differentiation of the innate and adaptive immune systems. Within this family, *IRF6* is unique because it regulates cutaneous and orofacial development in humans and mice. Common variants in *IRF6* are associated with 12% of all orofacial clefting risk. Critically, a DNA variant in the *IRF6* enhancer *MCS9.7*, rs642961, is found in 30% of the world's population.

Biochemically, we know that rs642961 abrogates one of four *TFAP2a* binding sites, suggesting regulatory function. Mutations in *TFAP2a* can lead to Cranio-oculo-facial Syndrome, a dominantly inherited orofacial clefting syndrome that includes upper lip pits. However, functional studies have not shown if *Tfap2a* regulates *MCS9.7* activity or endogenous *Irf6* expression in the mouse. In addition, rare mutations in *IRF6*, located within 1q32-q41, lead to Van der Woude and Popliteal Pterygium Syndromes, dominantly inherited orofacial clefting disorders. Currently, 70% of VWS families have mutations in *IRF6*. While the remaining 30% have unknown etiology, prior linkage analysis suggest locus heterogeneity.

We use a mouse models to determine how common variants in *IRF6* may be associated with orofacial clefting and to investigate locus heterogeneity in VWS. We find that knocking out *Tfap2a* leads to loss of *MCS9.7* enhancer activity and *Irf6* expression *in vivo*. On the other hand, *Irf6* also appears to stabilize *Tfap2a* protein in epidermis. The

necessity of *Tfap2a* for *Irf6* expression contributes to our understanding of the association between rs642961 and isolated orofacial clefting. Significantly, we also find that *Irf6* transcriptionally activates *Grhl3* in epithelium. Consistent with prior work showing locus heterogeneity, we find that mutations in *GRHL3* can also lead to Van der Woude Syndrome. These results suggest that *TFAP2a*, *IRF6*, and *GRHL3* share a conserved genetic pathway that is required for proper development of the lip and palate in humans and mice.

In the mouse, loss of *Grhl3* and *Tfap2a* leads to skin, limb, craniofacial and neural tube defects. Because *Irf6* is an intermediate node between *Tfap2a* and *Grhl3* in oral epithelium, we predict and find that changes in *Irf6* expression can lead to neural tube defects. Over-expressing *Irf6* leads to rostral neural tube defects, including loss of the cranial vault, i.e. acrania, and a split face. In addition, both reducing and over-expressing *Irf6* leads to caudal neural tube defects, a curled and kinked tail, respectively. Consistent with orofacial genetic regulation, we find that *Irf6* represses *Tfap2a* in rostral neural tube development. In the caudal neural tube, we find that *Irf6* activates both *Tfap2a* and *Grhl3* expression and that *Tfap2a* and *Grhl3* interact in caudal neurulation. Consistently, human sequencing reveals a rare *IRF6* mutation in an individual with spina bifida. Finally, we show that *Irf6* expression in skin development rescues perinatal lethality but not limb, tail and palatal development. These results suggest that *Tfap2a-Irf6-Grhl3* regulate the development of multiple ectodermal lineages. We conclude that cross-fertilization in orofacial and neural tube development provides candidate genes and potential therapeutic strategies for two congenital diseases with significant morbidity and mortality.

Copyright by
YOUSSEF AYOUB ADLY KOUSA
2014

I dedicate this work to my parents, my family and my teachers, younger and older; my parents for having the courage to come into an unknown land and language with nothing in hopes of a better future for my brother and I. I dedicate this book to Evon, David and Elijah, for not only supporting my passion but for motivating me to achieve more and for making life outside the lab truly enjoyable. I would not be here without my teachers, professors, mentors, co-workers, and undergrads...for teaching me that I have lots to learn from everyone.

ACKNOWLEDGMENTS

First and foremost, I would like to thank my lab. It all starts with my mentor, Dr. Brian C. Schutte, for letting me join his lab, creating a outstanding research environment and for teaching me how to be a scientist who strives for both depth and breadth. I would also like to thank the people in the lab that made research fun and possible. Arianna Smith and Tamer Mansour not only made these years enjoyable but also constantly helped me to think through experiments, work through models and interpret results. They are not only my co-workers but are also my friends and I deeply appreciate them. I also want to thank Dr. Walid Fakhouri for teaching me techniques and how to remain skeptical, the essence of being a good scientist.

I am also deeply indebted to Raeuf Roushangar, Nicole Patel and Ari Walter for all of the time they put toward this work, including days, nights, weekends and holidays. Mouse work is difficult and together Raeuf and Nicole performed over 5000 genotyping reactions. Ari Walter single handedly sectioned more than 100 boxes worth of tissue, totaling nearly 5000 slides. This work would not be possible without their dedication. I also want to thank Dr. Dina Moussa for her efficiency and dedication despite numerous family and work obligations. This work would also not be possible without Eric Fuller, Keith McAuley, Matt Thomas, Kendra Siegersma, Krysta Wierzbicki, Silus DeBacker and Rachel Han who gave freely of their time and have taught me so much about the art of teaching and learning. I also want to thank our collaborators who are technically at the University of Iowa but who I consider to be part of our lab. These especially include Dr.

Martine Dunnwald, Dr. Rob Cornell, Dr. Jeff Murray, Dr. Elizabeth Leslie, Dr. Leah Biggs and Tiffany Smith. My time as a PhD student would have been dramatically different if not for their mentorship and friendship.

I want to thank Dr. John Wang, for giving me a chance at Michigan State University, seeing that I could be successful and for being a person I truly admire and cherish. I am also truly indebted to the DO-PhD program at Michigan State University. Dr. Justin McCormick and Mrs. Bethany Heinlen have dedicated many years to this program and at every turn in the road they provided guidance and support. I am also very thankful for having, Dr. David Arnosti and Dr. John LaPres, brilliant scientists, as mentors and teachers. Finally, I want to sincerely thank Dr. Andy Amalfitano, Dr. Terrie Taylor, Dr. Karl Seydel and Dr. Douglas Postels for being mentors, friends and role models. They embody the spirit, intellect and clinical acumen that defines a physician-scientist. I can only hope to be as insightful, knowledgeable and creative as my mentors.

I want to also thank Dr. Jon Kaguni, Mrs. Jessica Lawrence and Kaillathe ‘Pappan’ Padmanabhan for not only helping and guiding but for also going above and beyond the call of duty on multiple occasions. I would also like to thank Rick Lillich and Rob Patten at Mager Scientific for sharing their insights, expertise and equipment to make this work possible. I would also like to sincerely thank Amy Porter and Kathy Joseph at Investigative Histopathology Laboratory at Michigan State University. They literally handled every piece of tissue we sectioned and stained. Therefore, I am deeply indebted to them for their dedication and persistence in processing our precious tissues.

I want to thank the people of Michigan State University who made the journey so complete, including Dr. John Fyfe, Dr. Sherif Ibrahim, Dr. Nermin Kady, Satyaki Sengupta, Dr. Bill Henry, Dr. Pat Venta, Dr. Jerry Dodgson, Dr. Ellen Wilch, Dr. Karen Friderici, Dr. Vilma Yuzbasiyan-Gurkan, Maciej Parys, Dr. Sandhya Payankaulam, Cho Rattanasinchai, Dr. Kathy Gallo, Sarah Roosa, Dr. Yasser Aldhamen and the ULAR Staff facilitating the humane treatment of research animals, including Mr. Don Harrington, Mr. Patrick Lee, Mr. Randy Shoemaker and Ms. Danielle Ferguson.

I want to also thank my friends in the DO-PhD program, including Darin Quach, Paul Beach, Steve Proper, Tyrell Simkins, Joe Prinsen, Eric Schauburger, My-Trang Dang, Nadine El-Ayache and Yirong Zhu. At the College of Osteopathic Medicine, I also want to thank Dr. Margaret Kingry, Ms. Robin Hastings and Erin Doelling for providing the support and instruction necessary to navigate the DO-PhD program. It would have been nearly impossible to finish this program in eight years without Dr. Kingry's support. Ms. Robin Hastings was essential in this process as well and I am deeply indebted to her. I am also very thankful for Dean William Strample, Dr. Reza Nassiri, Dr. H. Steven Williams, Dr. William Falls, and Ms. Beth Courey.

I also want to thank Dr. Myriam Peyrard-Janvid and Dr. Juha Kere at the Karolinska Institutet, Dr. Richard Finnell and Dr. Huiping Zhu at UT Austin, Dr. Laura Mitchell and Dr. AJ Agopian at UT Houston, Dr. Gary Shaw at Stanford University, Dr. Bogi Anderson and William Gordon at UC Irvine, Dr. Allison Ashley-Koch and Dr. Simon

Gregory at Duke University, Dr. Akira Kinoshita at Nagasaki University, Dr. Yang Chai at UCLA and Dr. Trevor Williams at UC Denver.

Most importantly, I would like to thank the National Institute of Dental and Craniofacial Research for supporting this work. I am also indebted to Dr. Leslie Frieden for always providing the support and feedback necessary to understand the process of getting and keeping NIH funding.

PREFACE

In my time as a graduate student, I have often found myself responding in one of three ways to research papers.

The first response is “Man, I wish I could have written this.”

The second is “Glad someone wrote this.”

The third, more of a question, is “Why would anyone write this?”

I have written this thesis to avoid the question.

“The dogmas of the quiet past, are inadequate to the stormy present. The occasion is piled high with difficulty, and we must rise -- with the occasion. As our case is new, so we must think anew, and act anew.”

Abraham Lincoln

TABLE OF CONTENTS

LIST OF TABLES.....	xiv
LIST OF FIGURES.....	xv
KEY TO ABBREVIATIONS.....	xvii
CHAPTER 1 - <i>Irf6</i> regulates development and differentiation in multiple ectodermal lineages.....	1
Historical.....	2
Variable expressivity suggests that VWS is a clinical model for iCLP.....	2
Clinical context and impact of orofacial clefting.....	4
Mutations in IRF6 cause VWS.....	6
Variants within IRF6 are associated with iCLP.....	10
IRF6.....	11
IRF6 structure-function in development and disease.....	13
Regulating IRF6 expression.....	19
<i>Irf6</i> knockout mice.....	21
Genotype-phenotype correlation: From morphology to molecule.....	22
Rescuing the knockout phenotype.....	24
Neurulation: Neural tube development.....	27
Conclusion.....	29
APPENDIX.....	30
BIBLIOGRAPHY.....	34
CHAPTER 2 - Dominant mutations in <i>GRHL3</i> cause Van der Woude syndrome and disrupt oral periderm development.....	50
Abstract.....	53
Introduction.....	54
Results.....	55
<i>Grainy-head like 3</i> is the <i>VWS2</i> gene.....	55
Affect of <i>GRHL3</i> alleles on zebrafish development.....	57
<i>Grhl3</i> ^{-/-} murine embryos have cleft palate at low penetrance.....	58
The oral phenotypes of <i>Irf6</i> and <i>Grhl3</i> heterozygous murine mutants are independent.....	60
Discussion.....	61
Supplemental Data Description.....	64
Acknowledgments.....	64
Web Resources.....	64
Materials and Methods.....	65
Human DNA samples.....	65
Targeted exome sequencing.....	65
Genotyping.....	66

Mutation screening by Sanger sequencing.....	66
Phenotype Analysis.....	67
Transfection of human GRHL3 mutation variants into Zebrafish embryos.....	67
Murine crosses.....	68
Morphological, histological and molecular analyses of mice.....	69
Imaging.....	69
Statistical analysis.....	70
APPENDIX.....	71
BIBLIOGRAPHY.....	99
CHAPTER 3 - <i>Irf6</i> regulates <i>Tfap2α</i> and <i>Grhl3</i> in neurulation.....	104
Abstract.....	106
Introduction.....	106
Results.....	109
<i>Tfap2α</i> is necessary for <i>MCS9.7</i> activity and <i>Irf6</i> expression.....	109
<i>Irf6</i> regulates <i>Tfap2α</i>	112
<i>Irf6</i> homeostasis is required for neurulation and <i>Tfap2α</i> expression in epidermis.....	113
Endogenous and transgenic <i>Irf6</i> expression regulate <i>Tfap2α</i> in neurulation.....	117
<i>Tfap2α</i> and <i>Grhl3</i> interact in caudal neurulation.....	119
Shared <i>IRF6</i> mutation in Spina Bifida and VWS.....	121
Discussion.....	122
Supplemental Data Description.....	126
Author Contributions.....	126
Acknowledgments.....	126
Web Resources.....	126
Materials and Methods.....	127
Murine crosses.....	127
<i>Irf6</i> hypomorphic allele.....	128
Murine genotyping.....	129
Morphological, histological and molecular analyses of murine tissue...	129
Skeletal prep.....	131
Bioimaging upright/fluorescent microscope.....	131
Transcriptional profiling using quantitative-PCR.....	132
Western blotting.....	134
Human sequencing and genotyping.....	134
Statistical analysis.....	134
APPENDIX.....	135
BIBLIOGRAPHY.....	182
CHAPTER 4 - Epithelial <i>Irf6</i> rescues lethality but not craniofacial and limb development.....	187
Abstract.....	188
Introduction.....	189

Results.....	191
Titrating <i>Irf6</i> dose shows that mandible-maxilla oral adhesions are not sufficient for clefting	191
<i>Irf6</i> expression using the <i>KRT14</i> promoter completely rescues cutaneous defects.....	193
Epithelial <i>Irf6</i> rescues perinatal lethality.....	194
Completely penetrant clefting despite basal <i>Irf6</i> expression.....	196
Palate-tongue oral adhesions prevent palatal elevation.....	197
Discussion.....	198
Author Contributions.....	202
Acknowledgments.....	203
Web Resources.....	203
Materials and Methods.....	203
Murine crosses.....	204
Morphological and histological analysis.....	204
Molecular analyses of murine tissue.....	205
Skeletal prep.....	205
Bioimaging upright/fluorescent microscope and stereomicroscope.....	206
Transcriptional profiling using quantitative-PCR.....	206
Statistical analysis.....	207
APPENDIX.....	208
BIBLIOGRAPHY.....	229
CHAPTER 5 - Conclusion and Future Directions	232
Major Themes: Orofacial Clefting.....	233
Major Themes: Neural Tube Defects.....	234
Genetic risk for orofacial and neural tube defects.....	236
Expanding the gene regulatory network: <i>Tfap2</i> and <i>Grhl</i> paralogs.....	237
Novel implications for <i>Irf6</i> knockout phenotype.....	239
Proposed gene regulatory network.....	241
Therapeutic consideration in congenital disease.....	242
Preventative strategies in orofacial clefting and neural tube defects.....	243
APPENDIX.....	247
BIBLIOGRAPHY.....	250

LIST OF TABLES

Table 1: <i>GRHL3</i> mutations in eight Van der Woude syndrome families	83
Table 2: Comparison of VWS phenotypes caused by mutations in <i>IRF6</i> and <i>GRHL3</i>	85
Table 3: Human <i>GRHL3</i> primers used in Sanger sequencing mutation screening.....	95
Table 4: Genomic SNPs used for confirming <i>de novo</i> mutations.....	96
Table 5: Frequency of genotypes and resorbing embryos from <i>Irf6</i> ^{+/-} x <i>Grhl3</i> ^{+/-} cross....	97
Table 6: Association between <i>IRF6</i> (rs642961) and risk of NTDs.....	160
Table 7: Association between <i>IRF6</i> (rs75012801) and risk of NTDs.....	161
Table 8: Association between <i>IRF6</i> (rs17317411) and risk of NTDs.....	162
Table 9: <i>Tfap2a</i> ^{+/-} ; <i>Tg</i> ^{MCS9.7-LacZ}	171
Table 10: <i>Irf6</i> ^{ey/-} vs. <i>Irf6</i> ^{ey/+}	172
Table 11: <i>Irf6</i> ^{+/+} ; <i>Tg</i> ^{KRT14-Irf6}	173
Table 12: <i>Tg</i> ^{KRT14-Irf6} ; <i>Tg</i> ^{KRT14-Irf6}	174
Table 13: <i>Tfap2a</i> ^{+/-} ; <i>Irf6</i> ^{+/-}	175
Table 14: <i>Tfap2a</i> ^{-/-}	176
Table 15: <i>Tfap2a</i> ^{+/-} ; <i>Tg</i> ^{KRT14-Irf6}	177
Table 16: <i>Tfap2a</i> ^{+/-} ; <i>Irf6</i> ^{+/-} ; <i>Tg</i> ^{KRT14-Irf6}	178
Table 17: <i>Tfap2a</i> ^{+/-} ; <i>Grhl3</i> ^{+/-}	179
Table 18: Murine qPCR primer sequences.....	180
Table 19: <i>IRF6</i> sequencing primers.....	181
Table 20: <i>Irf6</i> ^{-/-} ; <i>Tg</i> ^{KRT14::Irf6}	228

LIST OF FIGURES

Figure 1: Analogous processes lead to palate and neural tube development.....	31
Figure 2: Structure of <i>IRF6</i>	32
Figure 3: Proposed genetic network for orofacial and rostral, caudal neural tube development.....	33
Figure 4: Mutations in <i>GRHL3</i> cause Van der Woude syndrome.....	72
Figure 5: VWS-associated alleles of <i>GRHL3</i> disrupt the development of the periderm when expressed in zebrafish embryos.....	75
Figure 6: <i>Grhl3</i> is required for murine periderm and palatal development.....	77
Figure 7: No evidence for genetic interaction between <i>Irf6</i> and <i>Grhl3</i> in murine palatal development.....	80
Figure 8: Pedigrees of the eight VWS families with <i>GRHL3</i> mutation.....	86
Figure 9: Multiple alignment and protein domains of <i>GRHL3</i> gene products from human, mouse and zebrafish.....	91
Figure 10: Molecular changes in the oral epithelium of <i>Irf6</i> ^{-/-} and <i>Grhl3</i> ^{-/-} embryos.....	93
Figure 11: <i>Tfap2a</i> is necessary for <i>MCS9.7</i> activity and <i>Irf6</i> expression.....	136
Figure 12: <i>Irf6</i> regulates <i>Tfap2a</i>	141
Figure 13: <i>Irf6</i> homeostasis is required for neurulation and <i>Tfap2a</i> expression in epidermis.....	145
Figure 14: Endogenous and Transgenic <i>Irf6</i> expression regulate <i>Tfap2a</i> in neurulation.....	150
Figure 15: <i>Tfap2a</i> and <i>Grhl3</i> interact in caudal neurulation.....	155
Figure 16: Shared <i>IRF6</i> mutation in Spina Bifida and VWS.....	158
Figure 17: Generation of <i>Irf6</i> hypomorphic allele.....	163
Figure 18: <i>Irf6</i> transcriptionally regulates <i>Trp63</i> , <i>Tgm1</i> and <i>Krt1</i> but not <i>Krt14</i> and <i>Tfap2c</i> in skin.....	165

Figure 19: <i>Irf6</i> homeostasis is required for epidermal development.....	167
Figure 20: <i>Irf6</i> Transcriptionally regulates <i>Tfap2c</i> but not <i>Krt14</i> in tail development..	170
Figure 21: <i>Irf6</i> compound heterozygosity causes completely penetrant oral adhesions but not clefting.....	209
Figure 22: <i>Irf6</i> expression using the <i>KRT14</i> promoter rescues cutaneous defects in knockout embryos.....	213
Figure 23: Epidermal expression of <i>Irf6</i> rescues perinatal lethality without altering skeletal defects, limb clubbing or syndactyly.....	217
Figure 24: Rescued pups have completely penetrant palatal clefting and oral adhesions.....	220
Figure 25: Obliteration of the esophageal lumen contributes to postnatal lethality.....	222
Figure 26: Tongue-palate oral adhesions obstruct palatal development.....	224
Figure 27: Oral adhesions to the tongue prevent re-orientation and apposition of palatal shelves.....	226
Figure 28: Summary of genetic network in orofacial and neural tube development.....	248
Figure 29: Proposed IRF6 gene regulatory network	249

KEY TO ABBREVIATIONS

PPS.....	popliteal pterygium syndromes
BOFS.....	Branio-Oculo-Facial Syndrome
GRHL3.....	Grainy-Head Like 3
LOD	Logarithm (base 10) of the odds
REN.....	Renin gene
TDT.....	Transmission Disequilibrium Test
SNP.....	Single Nucleotide Polymorphisms
Trp63.....	Transformation Related Protein 63
TP63.....	Tumor Related Protein 63
EEC.....	Ectrodactyly, Ectodermal Dysplasia and Cleft lip and Palate
R84C.....	Arginine 84 Cytosine
Maspin.....	Mammary Serine Protease Inhibitor
SCC.....	Squamous Cell Carcinoma
HNSCC.....	Head and Neck Squamous Cell Carcinoma
TSS.....	Transcription Start Site
<i>Irf6</i> ^{gt/+}	<i>Irf6</i> ^{gt/+} Irf6 gene trap allele
<i>Irf6</i> ^{R84C/+}	Arginine 84 Cytosine mutation in a mouse allele
<i>Irf6</i> ^{C1f1/+}	ENU forward screen leading to mutation at Proline-39
<i>Ikkα</i>	Inhibitor of Nuclear Factor Kappa-B Kinase subunit alpha
TP53	Transformation Protein 53
G2/M.....	Growth 2/Mitosis DNA Damage Checkpoint

NF- κ BNucleor Factor Keppa-light-chain-enhancer of activated B cells
IKK.....IkB Kinase
Ripk4.....Receptor-Interacting Protein Kinase 4
Kdf1.....Keratinocytes Differentiation Factor 1
BPS.....Bartsocas-Papas Syndrome
Krt1.....Keratin 1
Krt6Keratin 6
Krt14.....Keratin 14
Celsr1.....Cadherin, EGF, LAG seven-pass G-type receptor 1
GRN.....Gene Regulator Network

Chapter 1 -

***Irf6* regulates development and differentiation in
multiple ectodermal lineages**

Historical

Clefts of the lip and palate have afflicted humanity since the dawn of civilization (1). According to Cervenka et al (1966) orofacial clefting with lip pits were first described in 1845 as a “very rare” congenital malformation by Demarquay (2). In 1947 Test and Falls described lip pits, cleft lip and palate syndrome in five generations of an affected family (3). Dr. Anne van der Woude, then at the University of Michigan, summarized the literature in 1954 and concluded an autosomal dominant inheritance pattern (4). From this point forth, lip pits along with orofacial clefting became known Van der Woude Syndrome (VWS). In 1962 Dr. Levy highlighted the presence of lip pits, symmetrically located on the medial edge of lower lips, pathognomonic feature of VWS (5). The earliest recorded survey of VWS prevalence among all forms of cleft lip and palate took place in 1971 when Dr. Dronamraju reported that eight of 260 clefting families (3%) had VWS (6). The incidence of VWS has been directly estimated at 3.6/100,000 live births (7).

Variable expressivity suggests that VWS is a clinical model for iCLP

Variable expressivity and incomplete penetrance continue to be important aspect of VWS. Dr. Baker studied one affected family and concluded variable expressivity as some presented with lip pits but not orofacial clefting (8). Cervenka et al reported 80% penetrance in 25 VWS cases, with lip pit present in 69.6% and clefting present in 36.0% of individuals (2). In 1980 Janku et al. (1980) (9) reported that penetrance was closer to 96.7%, with lip pit present in 88% and clefting present in 21% of individuals. Burdick et al (1985) examined 864 individuals from 164 families and found that VWS penetrance ranged from 89% to 99% using different methods, with cleft lip and palate occurring

more commonly than cleft palate (10). Hypodontia, bifid uvula, hypernasal voice, lip mounds that secrete mucus instead, Hirschsprung disease, congenital heart defects, popliteal webs, limb anomalies and accessory nipples have also been associated with VWS (4, 9, 11-13). By either estimate, a portion of VWS families has clefting but not lip pits. As such, patients with VWS may only present with orofacial clefting, mimicking patients with isolated cleft lip and palate (iCLP). iCLP is a common, complex disease with multiple genetic and environmental contributing factors (14). Considering the phenotypic overlap, Murray et al (1990) hypothesized that discovering the genetic etiology of VWS may also elucidate the genetic architecture of iCLP(15). However, unlike iCLP, VWS does not exhibit sex-specific differences (10, 16, 17).

Variable expressivity in Van der Woude Syndrome may result from locus heterogeneity, different types of mutations (mis-sense vs. truncation), location of mutation (DNA Binding Domain vs. Protein Interaction Domain vs. Activation Domain), affect on protein location (sequestration in sub-cellular organelle), affect on protein activity or stability (resistance to degradation/activation/turnover), regulation of expression (enhancer, promoter), or could be environmental modifiers. Consistent with this, prior work showed that 17p11.2-11.1 increased VWS clefting risk (18). However, a more recent hypothesis-driven search for common variants that modify VWS did not yield a formally significant association (19). Understanding the basis for this phenotypic variation may provide preventative strategies to reduce disease severity. For example, if VWS expressivity could be limited to lip pits, disease burden could be significantly reduced.

While the phenotypic evidence suggests that VWS can be a clinical model for iCLP, is there evidence that VWS could also be a genetic model for iCLP? As a Mendelian disorder, family studies are a critical component in VWS research (2, 20, 21). Houdayer et al (2001) used a family design to ask if VWS and iCLP were associated in a parametric linkage analysis and Transmission Disequilibrium Tests (TDT) (22). While parametric linkage was not supportive, TDT provided evidence for a genetic link between VWS and iCLP (22). TDT measures the over-transmitted allele from parents to affected offspring and as such is robust to population structure, e.g. population stratification.

Clinical context and impact of orofacial clefting

As a result of life-long utilization of medical resources and loss of productivity, each individual born with a CLP will require \$200,000 for medical treatment (23). Despite these enormous resources, surgical and clinical intervention are often inadequate and result in physical and psychological sequelae (24). In addition, individuals born with a CLP have an increased risk for cancer (25) and neurological (11, 17, 26-31), musculoskeletal and cardiovascular diseases (17). Importantly, individuals born with cleft lip and palate had an increased risk of mortality between birth and 55 years of age (32). In addition, recent studies have shown that patients with VWS have an increased risk of surgical complications after cleft repair (33). As a result, understanding the gene regulatory network leading to orofacial clefting and these associated phenotypes may lead to preventative strategies and therapies for other disease.

Orofacial clefting results from defective palate and lip closure between the 6th and 10th week of human gestation. First, and foremost, prevention is possible in at least a subset of cases because reduced maternal folate, alcohol consumption and maternal smoking can contribute risk toward iCLP (34, 35). Current standard of care for children born with a cleft lip and plate includes surgical closure of a cleft lip by 4 months and closure of the palate by 12 months. Closure of alveolar clefts with bone grafts should be complete by 11 years of age, correction of residual abnormalities by 12 years of age and final nasal contours and breathing problems by 17 years of age. In addition to these surgeries, children born with CLP need to undergo speech therapy until the age of 11. According to the American Society of Plastic Surgeons, children born with CLP require a multi-disciplinary team to receive appropriate care. This team includes a pediatrician, pediatric dentist, otolaryngologist, auditory specialist, speech pathologist, genetic counselor and a social worker. Costs include surgical procedure, hospital, anesthesia, medication, garments and devices and clinical tests. However, recent work also suggests brain anomalies in patients with orofacial clefting, suggesting that additional resources may still be required (11).

Despite team-based medical treatment and the enormous cost, several risks are associated with CLP repair. These commonly include bleeding, infection, irregular healing of scars and puckering of tissues (contractures), asymmetries and remaining deformities, anesthesia risks, allergies to suture material and glue, damage to deep structures, such as blood vessels, nerves and muscles, and possibility of surgery revision. In addition, changes in nose shape and teeth alignment may result from cleft repair. Finally, teeth

abnormalities associated with CLP may require additional repair (36). Finally, because the mouth and palate are integral tissues, CLP morbidity also includes poor feeding, growth retardation and repeated ear infections. Considering the complications and the number of healthcare providers need for treatment, there has been a shift of CLP repair to teaching hospitals and an associated increase in cost (37). While ongoing clinical investigation in CLP treatment has led to a dramatic decrease in the associated morbidity (38), the challenges are even greater for developing countries (39). The challenges highlighted above illustrate the need for prevention, rather than treatment of CLP. Folate and multi-vitamin use are playing a role in reducing disease risk and burden (35, 40).

Mutations in IRF6 cause VWS

The first study into the genetic etiology of VWS was by Schneider (1973)(41). Here, the author used the “Red Blood Cell antigen” for genetic linkage as well as several biochemical assays, including electrophoretic studies of glucose-6-phosphate-dehydrogenase, haptoglobin, phosphoglucomutase, and haemoglobin (41). A subsequent study examined additional genetic markers and several biochemical assays but also reported a LOD (logarithm of odds) as a measure of linkage (42). Spence et al. (1983) reported on VWS linkage using ten genetic markers, including three on chromosome one, but did not find a plausible genetic link (43). Wienker et al. (1987) studied 27 informative polymorphic markers and excluded several based on an analysis of a five-generation kindred. Interestingly, despite a paucity of markers examined, the authors reported positive linkage to the “VWS:Duffy” antigen, located on chromosome 1 (44).

A critical finding that further refined the VWS locus came with the discovery of a cytogenetic anomaly by Bocian and Walker (45). In their report, an interstitial deletion of chromosome 1 at q32-q41 was found in a 41-month-old girl of Polish-German descent who had lip pits. Murray et al. (1990) used a candidate-gene-and-region approach to study multiple generations in six families with VWS. The authors successfully identified linkage with the renin (REN) gene and the D1S65 locus in 1q using Restriction Fragment Length Polymorphisms, providing a LOD score of 10.83 (15). Additional studies confirmed linkage between REN and VWS (46). A report by Sander et al. (1994) showed a VWS family with deletion of D1S205, a highly polymorphic microsatellite within the 1q32-41 region (47). The observed microdeletion led to refinement of the VWS locus to an approximate 4.1 Mega base pair stretch within 1q32-41. Additional work by Houdayer et al (1999) supported the locus homogeneity of VWS and the chromosomal location reported previously (48). Another family allowed Schutte and colleagues to map the VWS locus to a 1.6 Mega base pair interval between D1S491 and D1S205. Cloning of the critical region allowed the production of a single YAC clone with an 850 Kb segment containing the microdeletion (49). Subsequent studies expanded the region (50) and work by Schutte et al. (2000) provided a 900 Kb gene map (51). The gene map included 11 novel and four previously described genes, along with nine putative genes (51). Additional mapping further confirmed these findings (52, 53).

Several important twin studies have contributed to our understanding of VWS (54). While zygoty was not determined, the VWS twins were discordant: one had lip pits and a cleft palate while the other had preauricular skin tags (54). Dizygotic twins discordant

for the VWS were described by Levy et al (1962), with one having lip pits and cleft palate while the other had a likely unrelated hemangioma (5). Cervenka et al (1963) characterized the first published description of concordant twins for VWS, who were then identified as “probably monozygotic” based on facial features and blood typing (2). While these twins had lip pits, only one had a unilateral cleft lip. Another monozygotic twin concordant for VWS came nearly 30 years later when Hersh and Verdi (1992) showed siblings with unilateral cleft lip and palate, and lip pits (55). At this point, four monozygotic twins concordant for VWS were reported (56, 57). Of these studies, Jobling et al (2011) was significant because it showed monozygotic twins who were concordant for VWS but had highly dissimilar features, with one twin showing lip pits only while the other sibling also showed a cleft lip and a cleft palate (56). Thus, multiple examples of monozygotic, diamniotic twins with variable expressivity are seen, suggesting that somatic mutations or stochastic interactions may be a common feature of VWS expressivity.

Nearly 150 years after Demarquay first described a clefting syndrome with lip pits, Kondo et al (2002) used discordant monozygotic twins to discover *Interferon Regulatory Factor 6 (IRF6)* as the VWS gene (21). Specifically, targeted sequencing in the twins found mutations in *IRF6* in the affected individual but not the unaffected sibling. Prevalence screening in 45 unrelated VWS families further showed both truncation and point mutations in *IRF6*. In addition, analysis of three families with popliteal pterygium syndromes (PPS) showed linkage to the Van der Woude Syndrome locus, at 1q32-q41 (58, 59). PPS, like VWS, can include orofacial clefting, lip pits, hypodontia and skin

anomalies. However, unlike VWS, PPS also includes webbing in the back of knee (popliteal fossa), genital anomalies (hypoplasia of the labia majora, cryptorchidism or bifid scrotum), webbing between toes or fingers (syndactyly), triangular folds of skin over nails and tissue connecting the upper and lower eyelids (ankyloblepharon) (60-62). Seeing linkage to the same locus and phenotypic similarity, *IRF6* was sequenced and mutations found in 13 families with PPS (21). Both protein truncations and substitutions were found throughout the *IRF6* open reading frame in patients with VWS. In contrast, the preponderance of mutations leading to PPS are single nucleotide substitution in exons three and four, the DNA binding domain (21, 63).

Since identification, numerous replication studies found *IRF6* mutations in Van der Woude Syndrome families displaying a broad phenotypic spectrum and geographical distribution (64-86). While most genetic studies identified point mutations in *IRF6*, deletions as large as 2.98 Mb, involving 25 genes, have also been reported in VWS (47, 50, 84). Considering genomic deletions, haploinsufficient etiology is strongly supported. Furthermore, phenotypic variation resulting from deletions relative to point mutations suggests that additional genes or regulatory sequences in 1q41-q32 may be interacting with *IRF6*. de Lima et al (2009) conducted a comprehensive study of *IRF6* mutations leading to VWS and found that 80% of newly discovered disease causing mutations were found in exons 3, 4, 7 and 9 (80). This information may guide targeted sequencing for *IRF6* mutations in patients with VWS and PPS. Importantly, de Lima et al (2009) did not find *IRF6* mutations in 30% of VWS families. However, prior work suggested locus heterogeneity, linking a large Finnish VWS family to 1p34, instead of 1q32-q41, where

IRF6 is located (87). The second VWS locus at 1p34 contains nearly 700 genes, necessitating a targeted approach for elucidation of a second VWS gene. Rorick and colleagues (2011) provided evidence suggesting that *WDR65* was a candidate gene and identified one disease-associated variant (88). At this point, it is not clear if this variant is etiologic.

Variants within *IRF6* are associated with iCLP

Considering that mutations in *IRF6* lead to VWS, and that VWS is a clinical model for iCLP, is it possible that *IRF6* may also be contributing risk to isolated orofacial clefting? Consistent with this rationale, three recent studies show a robust link between *IRF6* and isolated orofacial clefting (89-91). The first, by Zuccherro et al (2004), show that a non-synonymous substitution (V274I) within *IRF6* is associated with 12% of all orofacial clefting (89). Considering that V274I is the ancestral allele, the association with cleft lip and palate seems counter-intuitive because clefting is lethal in all non-human primates. Furthermore, V274I does not alter the protein-coding sequence of *IRF6*. Instead, the authors predicted that V274I is in Linkage Disequilibrium (LD) with the etiologic variant. Consistently, sequencing of highly conserved regions within this LD block (140 Kb in length) revealed an association to a non-coding variant 9.7 Kb upstream of the *IRF6* transcription start site (91). In contrast to V274I, the single nucleotide polymorphism (SNP), rs642961 is not ancestral. Furthermore, rs642961 lies within a 608 bp sequence that is highly conserved and has enhancer activity that highly recapitulates endogenous *IRF6* expression *in vivo* (92). The variant abrogates one of four binding sites for Transcription Factor Activating Protein 2 alpha (TFAP2a). However, functional

studies in cell culture on this associated variant did not reveal mechanistic insights. Plausibly, but untested, the variant reduces *IRF6* enhancer activity because the trans-activating factor (TFAP2a) binds less robustly, alters endogenous *IRF6* expression and therefore increases risk for a loss-of-function disease known to result from haploinsufficient *IRF6* mutations.

Interestingly, while the pathogenic affect of rs642961 is unaltered with prenatal vitamins, two variants within the *IRF6* locus do interact with prenatal multi-vitamin supplementation (93-95). These data suggest that both environmental and non-environmental pathways may be associated with *IRF6* function in orofacial development. If *IRF6* and environment interact in iCLP, they may also interact in VWS. Environmental interaction with *IRF6* in VWS and iCLP may be leveraged to alter disease penetrance and/or expressivity.

IRF6

Interferon Regulatory Factor 6 is a member of the IRF family of transcription factors, which are widely known to regulate innate and adaptive immune function (96). Unlike other members of IRF family, *IRF6* regulates orofacial, skin and limb development. *IRF6* is composed of nine exons, with the start codon in exon three and a stop codon in exon nine (97). Kondo et al. (2002) detected two *IRF6* transcripts (one at 4.4 Kb, the second larger) with Northern Blot analysis from whole mouse embryos from E4.5 to E18.5, with apparent differential regulation (21). Spatial dimension of *Irf6* expression is seen in the brain, eyes, heart, liver, lung, placenta, skin, testes and tongue but not the spleen (21).

During palatal development, *Irf6* expression is seen most robustly in the oral epithelium, which includes the periderm, a flat epithelial layer that envelops embryos, and the basal cell layer, a cuboidal epithelium that lies beneath periderm cells but is superficial to the dermis (98). IRF6 protein is 467 amino acids (97, 99) and western blot analysis shows two bands for IRF6; with one at 59 and the other at 63 kDa, a phosphorylated form of the protein is found in cell culture and murine mammary epithelium (97, 100).

Consistent with *IRF6* function in human orofacial development, *Irf6* expression is seen in murine palatal epithelium from E12.5 to E17.5 (Fig. 1). Two cell types that constitute the early oral epithelium and express *Irf6* are the periderm and the basal cell layer. The periderm is a flat, squamous monolayer that coats the palatal shelves and may be preventing pathological oral adhesion to surrounding oral structures, including tongue, maxilla and mandible. Basal epithelial cells are a cuboidal monolayer early in development (E12.5-E13.5) but proliferate to give rise to the periderm and other intermediate cell types (E12.5-E15.5) and undergo cell death to allow fusion. The palatal shelves start as mesenchymal buds covered by epithelium at E12.5. During the next 24 hours, the palatal shelves, mesenchyme and epithelium, proliferate to expand, to inhabit the space between the tongue and mandible bilaterally. Between E13.5 and E14.0, the palatal shelves elevate and pivot toward midline, ultimately apposing above the tongue. At E14.5, periderm cells along the medial contact points are lost, allowing the basal cells to form from the medial edge to adhere and then to interdigitate (adhere). Loss of the medial edge epithelium allows a mesenchymal bridge to form, generating the nasal and oral cavities (E15.5 - E17.5) (99).

Unlike the fused mouse palate, *Irf6* expression is not observed in the naturally cleft chick palate (99). To date, no study has directly tested if knocking down *Irf6* in the mouse or over-expressing it in the chick is necessary and sufficient for palatal development. *Irf6* expression is also seen at the fusion point of the lateral and medial nasal processes and the maxillary processes, which fuse at E11.5 in the mouse to form the upper lip (99).

IRF6 structure-function in development and disease

Based on the crystal structure of IRF1, IRF6 appears to contain a highly conserved pentatryptophan winged-helix-loop-helix DNA binding domain in exons three and four (Fig. 2) (21, 101). While *IRF6* is structurally characterized as transcription factor, it is mainly detected in the cytoplasm and rarely visualized in the nucleus with various antibodies. Therefore, does *IRF6* transcriptionally regulate downstream targets and is this activity important for development? If so, why don't we find *IRF6* in the nucleus? Several lines of evidence suggest that *IRF6* binds DNA and transcriptionally regulates gene expression in critical developmental pathways. First, injection of cDNA containing the *IRF6* DNA binding domain (dominant negative construct) leads to more severe developmental defects than knocking down the whole transcript (morpholino) in zebrafish and xenopus embryos (102, 103). These data suggest that while embryonic development is grossly resistant to some perturbations in *IRF6* dose, cDNA constructs that directly or indirectly affect *IRF6* DNA binding result in more severe developmental defects. Furthermore, in mice and humans, mutations in the DNA binding domain of *IRF6* lead to more severe developmental phenotypes. For example, in humans, a mutation in the DNA binding

domain, R84C, is associated with more severe developmental defects than deletion mutations (80). As a murine allele, R84C heterozygous embryos have more severe oral adhesions than embryos heterozygous for the gene trap (null) allele (104, 105). Unlike physiological adhesions or fusions between apposing surfaces of the palatal shelves, pathological adhesions or fusions occur between the palate and mandible or palate and tongue or mandible and maxilla. Biochemically, R84C appears to reduce *IRF6* DNA-binding affinity (101) and a concomitant reduction in transactivation of a luciferase reporter is observed (106).

In support of transcriptional regulation, we recently showed that *irf6* transcriptionally regulates *grhl3* in zebrafish embryos via a highly conserved binding element.

Consistently, *grhl3* mRNA partially rescues zebrafish embryos injected with a dominant negative *irf6* (103). In primary human keratinocytes, a genome wide screen showed that *IRF6* binds within this highly conserved element and that knocking down *IRF6* leads to a reduction of *GRHL3* expression (107). During palatal development, we found that *Irf6* is required for *Grhl3* expression in the epithelium and oral periderm (103). Considering that *IRF6* is required for palatal development and that *IRF6* regulates *GRHL3* in oral epithelium, we predicated that mutations in *GRHL3* could also contribute to orofacial clefting. Considering that *GRHL3* is at 1p36 and linkage to a second VWS locus at 1p34, we performed exome sequencing and examined this region for mutations. Consistently, we found *GRHL3* mutations only in the affected members of the pedigree. In addition, screen VWS families negative for *IRF6* mutations (30%, N=45) and discover seven families with *GRHL3* mutations. *In vivo* assays showed that VWS associated *GRHL3*

mutations disrupted endogenous gene function, suggesting dominant negative function. In the mouse, loss of *Grhl3* leads to neural tube defects (108). In the oral cavity, loss of *Grhl3* leads to bi-lateral oral adhesions and palatal clefting. However, compared to loss of *Irf6* in the mouse, the oral adhesions were less severe and the cleft was less penetrant. These results are consistent with *Grhl3* working downstream of *Irf6* in palatal development. Embryos heterozygous for *Irf6* had oral adhesions at the tooth germ and embryos heterozygous for *Grhl3* had oral adhesions and fusions posterior to the tooth germ. Embryos doubly heterozygous for *Irf6* and *Grhl3* had a combination of both phenotypes at and more posterior to the tooth germ but neither was more severe, suggesting function in the same cell types and time point if not the same location (Chapter 2). Together, these data suggest that *IRF6* transcriptionally regulates critical genes and tissues during development in multiple species.

While these results highlight *Irf6* transcriptional activity, recent work has also shown that *IRF6* directly binds fewer than 2,200 genes (107). In contrast, *TP63*, a transcription factor co-expressed with *IRF6* throughout epithelial development, binds over 7,500 targets (109). While differences in peak threshold may account for the number of binding sites reported, only 2.6% (56/2177) of putative downstream targets bound by *IRF6* were altered with knockdown (107). In contrast, 1,213 genes bound by *TP63* are differential expressed with knockdown studies (109). Therefore, as a transcription factor, *IRF6* does not seem to have robust transcriptional activity. Lack of nuclear staining, considering similar results with multiple antibodies, may therefore result from relatively minor transcriptional activity. However, more rapid *IRF6* turnover via the proteasome (110) or

cytoplasmic sequestration and exocytosis (100) may also be contributing to the nuclear/cytoplasmic localization ratio. Examining IRF6 expression in multiple tissues and time points along with inhibition of nuclear export with Leptomycin B may further elucidate the tendencies and targets of *IRF6*.

In fact, the majority of genes affected by *IRF6* perturbation are not bound *IRF6* (83%, 276/332). A useful example to contrast is TP63. In humans, mutations in *TP63* can lead to Ectrodactyly, Ectodermal Dysplasia (EEC), which includes CLP (OMIM #604292). While TP63 drives *IRF6* expression, IRF6 seems to be post-translationally targeting TP63 for degradation via the proteasome (111), in a negative feedback loop critical for palatal development (112). In the mouse, embryos doubly heterozygous for *Trp63* and *Irf6* can develop a cleft palate. Considering cytoplasmic localization and regulation of TP63 protein stability, post-translational regulation by *IRF6* seems increasingly important. Protein-protein interaction by IRF6 leading to *Trp63* degradation are likely to be mediated by a less well-conserved protein-binding domain in exons seven and eight (97). Protein-protein interaction by IRF6 have also been shown with the Mammary Serine Protease Inhibitor (Maspin) (97). However, in contrast to the inhibitory affect on TP63, IRF6 cooperatively binds to Maspin to regulate differentiation in mammary epithelium. In fact, transient re-expression of IRF6 reduced breast cancer invasiveness. In the skin, loss of *IRF6* is associated with squamous cell carcinoma (107, 113). Unlike breast cancer, this may result from an increase in TP63, which is a proliferative factor in the epidermis (107). *IRF6* also transcriptionally regulates OVOL1, a transcription factor regulating epithelial differentiation and a repressor of the oncogenic protein c-Myc (107,

114). Mutations in *IRF6* are also found in 5% of patients with head and neck squamous cell carcinoma (HNSCC)(115). While epithelial origin suggests oncogenic similarity to the epidermis, the regulatory partners and pathway of *IRF6* in HNSCC are undetermined. Aside from *TP63* and *Maspin*, little is known about protein-protein interactions mediated by *IRF6*. Important targets for future work include the E3 ubiquitin ligases that regulate and are regulated by *IRF6*.

Skin development, like palate development, includes both epithelium (known as epidermis in skin) and an underlying mesenchyme (known as dermis in skin). Like palatal development, the early epidermis (E9.5 – E12.5) includes squamous periderm cells, marked with Krt6, and cuboidal basal cells, marked with Krt14. While the periderm persists, basal cells of the epidermis proliferate between E13.0 and E16.5, leading to four cell types. Starting from the dermis and ending at the visible skin layers, basal cells are marked by Krt14 and Trp63, supraspinous cells are marked by Krt1, granular cells are marked by Loricrin, and cornified cells are marked by Krt6. As the epidermis develops, so does the dermis, leading to embryonically mature skin that acts as a permeability barrier by E17.5. Cells retaining periderm characteristics are found as late as E17.5, but are eventually sloughed off prior to birth. Early in cutaneous development (E9.5-E12.5), *Irf6* is expressed in both the periderm and basal cells. From E13.0 to E16.5, *Irf6* expression is also seen in the intermediate supra-spinous cells. In embryonically mature epithelium (E17.5), *Irf6* expression is primarily seen in the spinous cell layer and, to a lesser degree, the basal and granular cells. Pathological histological and molecular changes observed in *Irf6* knockout embryos include ectopic Krt14 and Trp63 expression,

proliferative supra-basal cells and loss of terminal differentiation (105). Consistently, loss of *IRF6* leads to reduced basal cell differentiation and results in a hyperproliferative epidermis that may give rise to squamous cell carcinoma (107). One model to explain these results would include either asymmetric *Irf6* deposition into a daughter basal cells to drive differentiation or de novo *Irf6* expression in an otherwise pre-programmed daughter cell. Together, these data suggest that *Irf6* expression drives differentiation and stratification of the epidermis from basal to spinous to granular cells.

In the c-terminus, exon nine is serine rich and appears to harbor the regulatory domain for *IRF6* in mammary epithelium (97). The generalization of an IRF6 c-terminal activation/repression domain seems plausible considering an analogous domain in *IRF3* and *IRF5* (116). In addition to biochemical and structural results consistent with a regulatory domain, this c-terminal domain in *IRF3* and *IRF5* is highly sensitive to mutagenesis (116). Like IRF3 and IRF5, activation of IRF6 most likely results from phosphorylation at amino acid 416 (97). In zebrafish (Rob Cornell, unpublished data) and human keratinocytes, creation of a phosphomimetic *IRF6* by converting serine and threonine to aspartic acid leads to constitutive activation and nuclear localization (106). The proteins regulating *IRF6* post-translational activation/repression are unknown.

Exons five and six appear to encode a less conserved proline-rich region. In direct contrast to the distribution of the DNA binding domain, of 19 etiologic mutations found in exons five and six, 16 are protein truncations. Underrepresentation of missense mutations along with less conservation, suggests that most coding changes in exons five

and six rarely led to orofacial clefting. We caution, however, against the assumption that paucity of mutations suggests a non-functional domain. Rather, this domain may be associated with other developmental processes and phenotypes.

Regulating IRF6 expression

Regulation of IRF6 expression is implicated in two disease processes. Rahimov and collaborators (2008) discovered an *IRF6* enhancer in a Multi-Species Conserved Sequence 9.7 Kb upstream of the *IRF6* Transcription Start Site (*MCS 9.7*) (91). *MCS9.7* highly recapitulates endogenous *Irf6* expression in skin and oral epithelium (92). A DNA variant, rs642961, in the *IRF6* enhancer is associated with isolated cleft lip and palate (CLP) but not cleft palate only (91). Biochemically, rs642961 abrogates one of four *TFAP2* binding sites within *MCS9.7*. The Transcription Factor Activating Protein 2 (*TFAP2*) family of transcription factors is composed of five members that homo or heterodimerize to repress or activate gene expression through a common, conserved binding element. A role in palatal development is most clearly demonstrated for *TFAP2a*. Mutations in *TFAP2a* can lead to Branio-Oculo-Facial Syndrome (BOFS OMIM # 113620), a dominantly inherited orofacial clefting disorder that can also include malformation of the eyes, ears and skin (117). Like VWS, BOFS can also include lip pits. Similar to *Irf6* knockout embryos (reviewed below), loss of *Tfap2α* leads to severe craniofacial, limb and skin defects (118, 119). However, *Tfap2α* knockout embryos are unique in the biomedical literature for absence of a thoracic and abdominal body wall as well as neural tube defects. Facial clefting, which results from failed neural tube closure, precludes analysis of palatal development in *Tfap2α*^{-/-} embryos. However, tissue-specific

deletion of *Tfap2α* suggests a requirement for palatal development that is independent of neural tube closure (120).

In vitro and in primary human keratinocytes, *TFAP2a* binds to *MCS9.7* (91, 109). *TFAP2a* and *TP63* also appear to cooperatively regulate *IRF6* expression in primary keratinocytes (109). In vivo, *Tfap2a* regulates *MCS9.7* and *Irf6* expression in murine epidermis (Chapter 3). As such, rs642961 may reduce *TFAP2a* trans-activation of *IRF6*, contributing to orofacial clefting risk. Furthermore, loss of *Irf6* expression in *Tfap2a* knockout embryos leads to pathological molecular changes associated with loss of *Irf6* (105, 107) but not *Tfap2a* (109). As such, *Irf6* may be more important for *Tfap2α* function than previously recognized. Considering numerous etiologic *TFAP2a* mutations in the DNA binding domain, altered trans-activation of *IRF6* may also be contributing to skin, lip pit and orofacial clefting in BOFS (Chapter 3). In addition to *TFAP2a*, *MCS9.7* also harbors binding sites for *TP63* and *MAFB*, the latter recently associated with CLP (111, 121). More recent work also suggests that *IRF6* is downstream of Notch signaling in keratinocytes. Notch appears to be acting through novel enhancers located 2.4 and 3.5 Kb upstream of the *IRF6* TSS (122).

Epigenetic regulation of *IRF6* expression has also been documented. Bisulfite sequencing showed that a ~300 bp CpG island in the *IRF6* promoter was methylated (107).

Methylation of the *IRF6* promoter represses expression and may increase risk for squamous cell carcinoma (107). *IRF6* expression is also found in post-utero mammary gland development and exhibited apical localization followed by luminal secretion into

milk (100). While regulation of this process is unknown, luminal secretion may be involved in delivering *IRF6* to the neonate, e.g. IgG, or in purging it from maternal mammary tissue.

***Irf6* knockout mice**

There are three mouse lines for *Irf6*. A gene trap allele (*Irf6^{gt/+}*), inserted 36 base pair into intron 1, has several splice donor/acceptor sites and stop codons, resulting in loss of *Irf6* translation (105). Targeted insertion of R84C, the human mutation disrupting the DNA binding domain and most frequently leading to PPS (*Irf6^{R84C/+}*), led to the second murine allele (104). A more recent third allele (*Irf6^{clfl1/+}*), resulted from a forward genetic screen using *N*-ethyl-*N*-Nitrosourea (ENU) mutagenesis (123). Interestingly, this approach led to a missense mutation at Proline-39, which was previously reported in a VWS pedigree (21). *IRF6* gene deletions and both mutations are found in human disease, providing robust tools to study human pathogenesis.

Murine embryos that lack *Irf6* has clubbed limbs, syndactyly, a bifid xiphoid, a shortened fused tail, palatal clefting and a grossly smaller head (104, 105). These embryos also have lingual (124) and mandibular defects (125). However, the most severely affected cell type is the epithelium. Epithelial abnormalities include a hyperproliferative epidermis that fails to differentiate, a permeable skin barrier, esophageal adhesions and pervasive oral adhesions. Intraoral adhesions seem to prevent palatal elevation leading to a cleft palate. While untested, the mechanical force generated by palate-tongue cohesion may be restraining the palatal shelves vertically and preventing elevation and midline

reorientation. That is, the force normally generated by the palatal shelves during elevation may not be sufficient with oral adhesions.

Genotype-phenotype correlation: From morphology to molecule

Loss of *Irf6* is phenocopied by four other genetic knockouts; *Stratifin (14-3-3sigma)*, *Ikka*, *Kdfl*, and, to a lesser extent, *Rpik4* (126-129). *14-3-3sigma* is a tumor suppressor protein that interacts with *TP53* via a positive feedback loop to regulate the G2/M cell cycle checkpoint (130, 131). *14-3-3sigma* also enhances Protein Kinase C activity and contains a Pleckstrin homology domain, critical in protein-protein interaction with serine/threonine phosphorylation (132-134). *Irf6* genetically interacts with *14-3-3sigma* in skin, limb, craniofacial and oral cavity development. If the genetic interaction is direct, *14-3-3sigma* may be involved in phosphorylation and post-translational activation of *Irf6*. Mutations in *14-3-3sigma* have not been associated with syndromic human disease. However, hypermethylation of a CpG regulatory island reduced *14-3-3sigma* expression in 91% of breast carcinoma cells (135), and likely constitutes an early oncogenic event (136).

In humans, homozygous recessive mutations in Nuclear Factor Kappa-B Kinase subunit alpha (*IKKA*) lead to Severe Fetal Encasement Malformation, also called Cocoon Syndrome (OMIM # 613630), which appears to include body wall, skin, limb and neural tube defects (137). *IKKA*, also known as CHUK, is a serine/threonine protein kinase that regulates the activation of NF-kB by marking its repressors (IkB Kinase) for ubiquitin-mediated degradation. However, in the skin, *Ikka* is a tumor suppressor protein and

functions independently of NF- κ B and I κ B Kinase (138). Instead, *Ikka* works downstream of Tgfb signaling in a complex with Smad2/3 that allows nuclear translocation independent of Smad4 (139). In skin, *Tgfb* signaling regulates *Irf6* (140), which in turn regulates OVOL1 (107), in a molecular cascade highly analogous to *Ikka* (139). In the palate, *Tgfb* signaling regulates *Irf6* through *Smad4* (141) but the molecular context of *Ikka* in this tissue are less clearly delineated. Despite the phenotypic similarity in skin and palate, and the common upstream and downstream molecular targets, preliminary work appears to show that *Ikka* does not interact with *Irf6* in the mouse (104). While analyzing *Irf6* expression in *Ikka* knockout murine skin would further elucidate this point, testing epistasis in the mouse is highly specific but not sensitive, i.e. absence of proof is not proof of absence. As such, *Ikka* may be upstream of *Irf6* in skin and palate development.

Like *14-3-3sigma*, the Receptor-Interacting serine/threonine Protein Kinase 4 (*Ripk4*) regulates keratinocytes differentiation and interacts with the Protein Kinase C (142). Like *Ikka*, *Ripk4* activates NF- κ B (143). However, *Ripk4* knockout embryos appear to be the least severely affected of the group (144). In contrast, human mutations in *RIPK4* can lead to a lethal type of Popliteal Pterygium Syndrome, called Bartsocas-Papas Syndrome (BPS) (OMIM # 263650). Like PPS, caused by mutation in *IRF6*, BPS is associated with popliteal webbing, ankyloblepharon, cleft lip and palate and syndactyly (145, 146). Like Cocoon Syndrome, caused by mutations in *Ikka*, BPS is associated with severe craniofacial defects, leading to superficial visualization of the nasal cavity, in what may be a form of facial clefting. As of this writing, a test for epistasis between *Ripk4* and each

of the other three murine models that it phenocopies, i.e. *Irf6*, *Ikka*, and *14-3-3sigma*, has not been reported.

A recently discovered gene, Keratinocytes Differentiation Factor 1 (*Kdfl*), like *Irf6*, appears to interact with *Trp63* and *14-3-3sigma* in skin, limb and craniofacial development (128). While the molecular nature of *Kdfl* is undetermined, cytoplasmic localization and association with the cellular membrane would suggest a signaling molecule.

Rescuing the knockout phenotype

Seeing multiple epithelial defects, several studies have tried to rescue the knockout phenotype with epithelial specific promoters, i.e. *KRT14* or *KRT5*, to drive expression in basal epithelial cells. Using the *KRT14* promoter to drive *Ikka* in *Ikka* knockout embryos led to rescue of skin, skeletal and limb defects (147). Skeletal and limb rescue is intriguing because it involves both cartilaginous and bony structures that lie beneath the epidermal cells driving *KRT14*, strongly suggesting *Ikka* non-cell autonomous function. However, unlike the skin and limbs, a curled tail persisted, suggesting additional cell autonomous function for *Ikka* in neural tube development. Furthermore, pups did not feed, as suggested by absence of a milk mark in the abdomen. Likely, esophageal adhesions occlude the gastrointestinal tract and result from minimal *KRT14* promoter activity in basal cells of the esophagus. In addition, using two different *KRT5* transgenic lines to drive *Ikka* in *Ikka* knockout embryos leads to rescue of skin, limb and skeletal development. However, rescue of tail morphology, classically a consequence of neural

tube closure, diverged more prominently between the two transgenic lines. While physiological expression of *Ikka* in the epidermis did not rescue tail development in one line, a super-physiological dose of *Ikka* completely rescues the tail in the other. First, as *KRT14* and *KRT5* are co-expressed intermediate filaments, these results suggest that at a certain dose, the *KRT14* promoter may also rescue the curled tail noted above. More importantly, how is *Ikka* expression in the epidermis rescuing a curled tail? Is it through rescue of the epidermis or is it through non-cell autonomous signaling of *Ikka* in neural tube? Considering highly similar epidermal rescues with both doses of *Ikka* yet divergent tail rescue, we favor a non-cell autonomous process.

An analogous experiment using the *KRT14* promoter to drive *Ripk4* in *Ripk4* knockout pups rescues skin defects. As seen with *Ikka*, *KRT14* spatio-temporal regulation of *Ripk4* was not sufficient to rescue esophageal adhesions (129). In a clever test for epistasis, epithelial expression of *Ripk4* using the *KRT14* promoter did not rescue *Ikka* and *14-3-3sigma* knockout embryos. Considering less severely affected knockout embryos and failure to rescue loss of *Ikka* and *14-3-3sigma*, *Ripk4* may be in a parallel, but converging pathway or require both *Ikka* and *14-3-3sigma* for function.

In direct contrast to non-cell autonomous *Ikka* function in limb and skeletal development, using the *KRT14* promoter to drive *Irf6* only rescues epidermal defects. Importantly, while the skin grossly appeared taut, both histological and molecular analysis revealed complete rescue. Despite epidermal rescue, limb, skeletal, tail and craniofacial defects persisted. The limb are free of adhesion to the body wall but clubbing and syndactyly

persisted. In the axial skeleton, a bifid xiphoid remained in rescue pups as seen in *Irf6* knockout pups. Despite epithelial re-expression of *Irf6*, palatal clefting is completely penetrant at P0. At E15.5, oral adhesions persisted between the tongue and palate and the mandible and maxilla but these are less severe. Dramatically, oral adhesions gripped the midline oriented palatal shelves to the tongue, physically restraining horizontal movement. Together, these data suggest that *Irf6* functions in limb and skeletal development through a cell autonomous mechanism (Chapter 4). In support of this model, we recently showed *Irf6* enhancer activity in limb bone and cartilage development.

In addition to genetic rescue, experimental embryonic gene therapy protocols to prevent disease in animal models have been developed for cystic fibrosis (148), Duchenne muscular dystrophy (149), Herlitz junctional epidermolysis bullosa (150, 151), Thrombotic thrombocytopenic purpura (152) and congenital blindness (153). Likewise, gene delivery to the oral epithelium and developing epidermis is highly feasible during development (154). In mature skin, epithelial stratification (cornified layer) and keratin secretion forms a physical barrier, leaving viral and bacterial pathogens refractory to host penetration. However, during early embryonic development, a cornified layer is not present, leaving the tissue highly susceptible to transduction. As such, intra-aminotic injection of a viral vector with tropism to epithelial tissue may provide robust targeting. Like the epithelium covering the skin, epithelium covering the oral cavity is also highly amenable to transduction. Considering that embryonic development of the lip and palate occurs between the 6th and 10th week of human gestation, such efforts could be highly

targeted using ultrasound to visualize the structures. Circulation of amniotic fluid in and through the embryos also ensures transduction of viral vectors into the oral cavity. Like numerous orofacial clefting genes, *Irf6* pathogenesis results from abnormal epithelial development. As such, gene delivery approaches may provide a feasible therapeutic modality for multiple, single gene clefting disorders. Furthermore, transduction of the periderm layer, a cell type lost before birth, limits side effects on post-embryonic development. Finally, immune-privileged status of amniotic fluid limits innate and adaptive blunting of the therapy.

Neurulation: Neural tube development

Like palate development, neural tube development is a highly orchestrated process that begins as flat epithelial layers followed by a period of proliferation to establish neural plates (E7.5 – E8.5) (Fig. 1). Unlike the palate, convergent extension and a median hinge point allows the bilateral neural plates to orient that growth toward a midline pivot (E8.5 – E9.5). Also like palatal development, additional growth allows midline oriented neural plates to appose (E10.0). Adhesion of the neural plates is mediated by bilateral lamelipodial cell protrusions. Midline cell death and epithelial remodeling ultimately leads to fusion of the neural plates and formation of the neural tube (reviewed fully in (155)). As such, palate and neural tube development occur in a highly analogous manner. However, unlike palate development, neural tube development is a highly complex process that involves multiple independent closure points. Defects in the rostral closure point can lead to anencephaly, as seen with *Tfap2a* knockout embryos. Defects in the caudal closure point can lead to an open lumbo-sacral defect or a curled tail, as seen with

Grhl3 knockout embryos (108). Defects in the intermediate closure points can lead to a craniorachischisis, as seen with the Cadherin, EGF, LAG seven-pass G-type receptor 1 (*Celsr1*) knockout embryos (155).

Unexpectedly, we found that over-expressing *Irf6* leads to rostral neural tube defect with variable penetrance and expressivity (Chapter 3). While 6% of embryos over-expressing *Irf6* had exencephaly, 5% of embryos had anencephaly, phenocopying *Tfap2a* knockout embryos. We further show that modulating *Irf6* expression in vivo completely and negatively correlates with *Tfap2a* mRNA. Despite an increase in *Tfap2a* transcript, we also found that reducing *Irf6* led to a reduction of *Tfap2a* protein. *Irf6* is expressed in both the rostral and caudal neural plates, the neural tube and the non-neural ectoderm. Consistent with *Tfap2a* dose regulating neural tube development, we also found that 10% of *Tfap2a* heterozygous embryos have exencephaly. Finally, we show that reducing endogenous *Irf6* in *Tfap2a*^{+/-};*Irf6*^{+/-} double heterozygous embryos completely rescues rostral neural tube defects seen with *Tfap2a* haploinsufficiency. In addition, we found that reducing *Irf6* expression led to a completely penetrant caudal neural tube defect, a curled tail. Like skin development, we show that *Tfap2a* regulates *Irf6* in the caudal neural tube. Transcriptional profiling shows that *Irf6* positively regulates both *Tfap2a* and *Grhl3* in the caudal neural tube. These data suggest that *Tfap2a* interacted with *Grhl3* via *Irf6*. Consistent with this model, we found that 13% of *Tfap2a*^{+/-};*Grhl3*^{+/-} double heterozygous embryos have a curled.

Conclusion

In summary, we show that *Tfap2a* regulates *Irf6*, which in turn regulates *Grhl3*. The link between *Tfap2a* and *Irf6* may explain the pathophysiological process involved in 12% of all oral facial clefting risk. Similarly, the link between *Irf6* and *Grhl3* in zebrafish and mouse led to the discovery of an additional orofacial clefting gene and to the etiology underpinning previously documented locus heterogeneity in VWS. Similar to the pathway in orofacial development, we further show that *Irf6* regulates neural tube development through genetic interactions with *Tfap2a* and *Grhl3*. In the caudal neural tube, we show that *Tfap2a* interacts with *Grhl3* (Fig. 3). Remarkably, we also show that *Irf6* expression in epithelium is not sufficient to rescue palatal development and that oral adhesions can physically restrain mid-line oriented palatal shelves from adhesion.

Finally, despite well-documented roles for *Irf6* in epithelium, we show that *Irf6* rescue of skin is not sufficient to rescue limb, skeletal and tail development. While the role of *Irf6* in tail development is orthogonally discovered in this work, these data strongly suggest multiple additional, as yet un-documented cell-autonomous roles for *Irf6* in embryonic development. Broadly, this work is significant because it shows that orofacial clefting genes also play a role neural tube development, underscoring the commonality of molecular pathways stemming from common ectodermal lineages. Considering these results, future work should seek to identify the role of this pathway in skin cancer. In addition, considering that multiple mouse models phenocopy the *Irf6* knockout, the role of *Ikka*, *14-3-3sigma*, *Ripk4* and *Kdfl* in neural tube development should be analyzed.

APPENDIX

APPENDIX

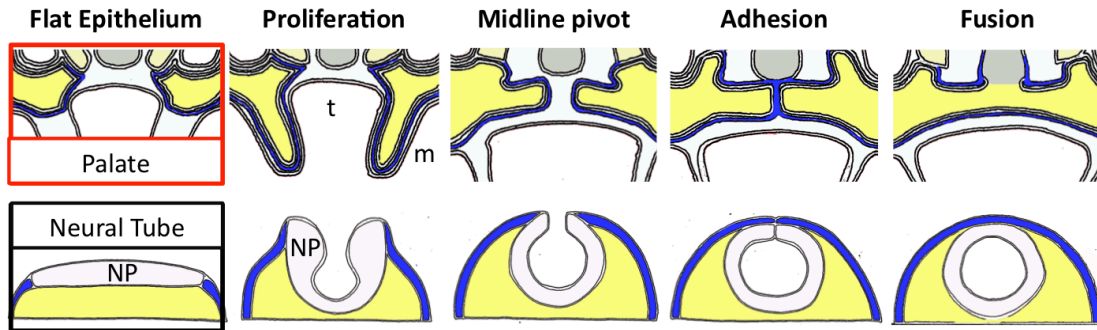


Figure 1: Analogous processes lead to palate and neural tube development. Top row: palate development begins at E12.5 as a flat epithelium, in blue, with an underlying mesenchyme, in yellow. A period of rapid proliferation leads to formation of palatal shelves alongside the tongue (t) and mandible (m). Reorientation of the palatal shelves leads to a midline pivot and a horizontal suspension above the tongue. Apposition of the palatal shelves leads to adhesion, or interdigitation of the epithelial cells. Breakdown of that epithelium leads to fusion of the shelves, forming a mesenchymal bridge that separates the nasal from the oral cavities. Bottom row: Like palate development, neural tube development happens through a highly choreographed progress. Flat epithelial layers, including the non-neural superficial ectoderm (blue) and neural plate (white, NP) undergo a period of rapid proliferation to expand. Neural tube specific processes (including a median hinge point and convergent extension, not shown) provide direction. Like palate development, a pivot toward midline is followed by adhesion. Breakdown of the epithelium leads to fusion.



Figure 2: Structure of *IRF6*. Exon one and two are not translated (orange). Exons three, beginning of translation, and four are the DNA binding domain of IRF6 (blue). Exons five and six are less highly conserved (yellow). The majority of exon seven and eight mark the Interferon Association Domain, or the protein binding domain of IRF6 (green). Exon nine is less highly conserved and includes a c-terminal helix thought to regulate IRF6 activation and repression (yellow). The 3'UTR of IRF6 is shown in orange.

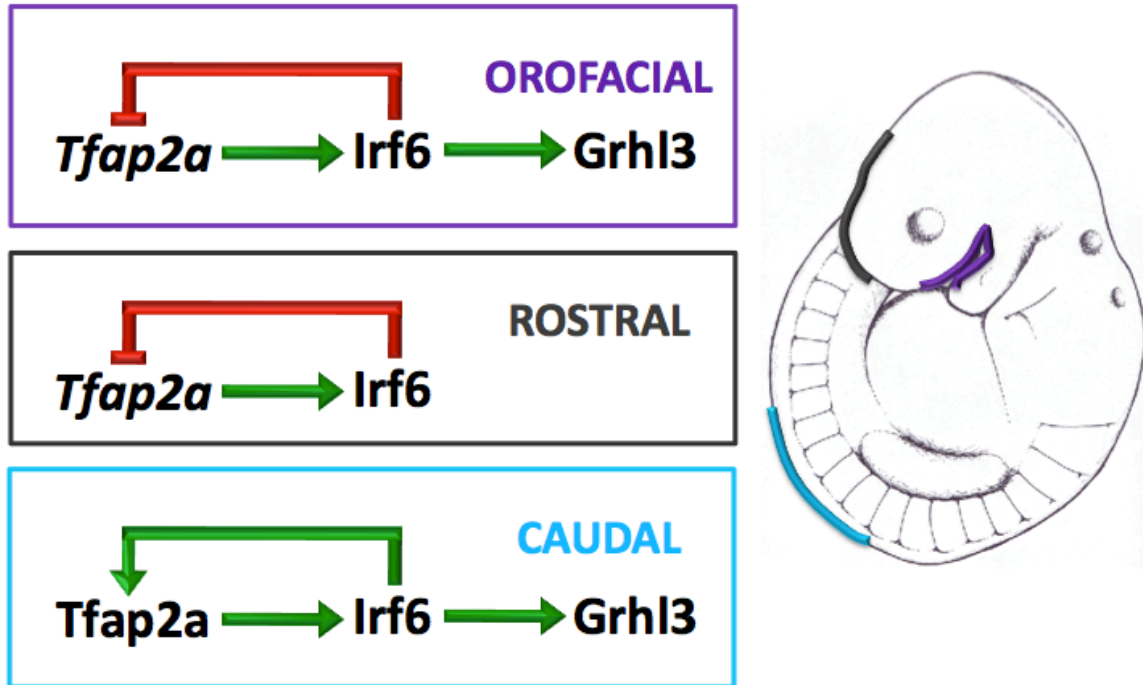


Figure 3: Proposed genetic network for orofacial and rostral, caudal neural tube development. Top: Orofacial development is likely to proceed through a negative feedback loop between *Irf6* and *Tfap2a* that lies upstream of *Grhl3*. Middle: Rostral neural tube development is likely mediated through a negative feedback loop between *Tfap2a* and *Irf6*. A role for *Grhl3* in this rostral neural tube pathway has not been investigated. Bottom: Caudal neural tube development is mediated through a positive

BIBLIOGRAPHY

BIBLIOGRAPHY

- 1 Hoffman, H. and Hudgins, P.A. (2002) Head and skull base features of nine Egyptian mummies: evaluation with high-resolution CT and reformation techniques. *AJR Am J Roentgenol*, **178**, 1367-1376.
- 2 Cervenka J, G.R., Anderson VE (1967) The syndrome of pits of the lower lip and cleft lip and/or palate. Genetic considerations. *Am J Hum Genet.* , **19**, 416-432.
- 3 Test, A.R. and Falls, H.F. (1947) Dominant inheritance of cleft lip and palate in five generations. *J Oral Surg (Chic)*, **5**, 292-297.
- 4 Van Der Woude, A. (1954) Fistula labii inferioris congenita and its association with cleft lip and palate. *Am J Hum Genet*, **6**, 244-256.
- 5 Levy, J. (1962) [Twins in a family with lower lip malformation]. *Acta Genet Stat Med*, **12**, 33-40.
- 6 Dronamraju, K.R. (1971) Genetic studies of a cleft palate clinic population. *Birth Defects Orig Artic Ser*, **7**, 54-57.
- 7 Burdick, A.B. (1986) Genetic epidemiology and control of genetic expression in van der Woude syndrome. *J Craniofac Genet Dev Biol Suppl*, **2**, 99-105.
- 8 Baker, B.R. (1964) A Family with Bilateral Congenital Pits of the Inferior Lip. *Oral Surg Oral Med Oral Pathol*, **18**, 494-497.
- 9 Janku, P., Robinow, M., Kelly, T., Bralley, R., Baynes, A. and Edgerton, M.T. (1980) The van der Woude syndrome in a large kindred: variability, penetrance, genetic risks. *Am J Med Genet*, **5**, 117-123.
- 10 Burdick, A.B., Bixler, D. and Puckett, C.L. (1985) Genetic analysis in families with van der Woude syndrome. *J Craniofac Genet Dev Biol*, **5**, 181-208.
- 11 Nopoulos, P., Richman, L., Andreasen, N.C., Murray, J.C. and Schutte, B. (2007) Abnormal brain structure in adults with Van der Woude syndrome. *Clin Genet*, **71**, 511-517.
- 12 Nopoulos, P., Richman, L., Andreasen, N., Murray, J.C. and Schutte, B. (2007) Cognitive dysfunction in adults with Van der Woude syndrome. *Genet Med*, **9**, 213-218.
- 13 Shprintzen, R.J., Goldberg, R.B. and Sidoti, E.J. (1980) The penetrance and variable expression of the Van der Woude syndrome: implications for genetic counseling. *Cleft Palate J*, **17**, 52-57.

- 14 Cobourne, M.T. (2004) The complex genetics of cleft lip and palate. *Eur J Orthod*, **26**, 7-16.
- 15 Murray, J.C., Nishimura, D.Y., Buetow, K.H., Ardinger, H.H., Spence, M.A., Sparkes, R.S., Falk, R.E., Falk, P.M., Gardner, R.J., Harkness, E.M. *et al.* (1990) Linkage of an autosomal dominant clefting syndrome (Van der Woude) to loci on chromosome 1q. *Am J Hum Genet*, **46**, 486-491.
- 16 Huang, J.J., Hou, J.W., Tan, Y.C., Chen, K.T., Lo, L.J. and Chen, Y.R. (2007) Van der Woude syndrome: clinical presentation in 64 patients. *Cleft Palate Craniofac J*, **44**, 649-652.
- 17 Calzolari, E., Pierini, A., Astolfi, G., Bianchi, F., Neville, A.J. and Rivieri, F. (2007) Associated anomalies in multi-malformed infants with cleft lip and palate: An epidemiologic study of nearly 6 million births in 23 EUROCAT registries. *Am J Med Genet A*, **143**, 528-537.
- 18 Sertie, A.L., Sousa, A.V., Steman, S., Pavanello, R.C. and Passos-Bueno, M.R. (1999) Linkage analysis in a large Brazilian family with van der Woude syndrome suggests the existence of a susceptibility locus for cleft palate at 17p11.2-11.1. *Am J Hum Genet*, **65**, 433-440.
- 19 Leslie, E.J., Mancuso, J.L., Schutte, B.C., Cooper, M.E., Durda, K.M., L'Heureux, J., Zuccherro, T.M., Marazita, M.L. and Murray, J.C. (2013) Search for genetic modifiers of IRF6 and genotype-phenotype correlations in Van der Woude and popliteal pterygium syndromes. *Am J Med Genet A*, **161**, 2535-2544.
- 20 Vignale, R., Araujo, J., Pascal, G., Reissenweber, N., Abulafia, J., Quadrelli, R., Vaglio, A., Larrandaburo, M. and Reyno, S. (1998) Van der Woude syndrome. A case report. *Pediatr Dermatol*, **15**, 459-463.
- 21 Kondo, S., Schutte, B.C., Richardson, R.J., Bjork, B.C., Knight, A.S., Watanabe, Y., Howard, E., de Lima, R.L., Daack-Hirsch, S., Sander, A. *et al.* (2002) Mutations in IRF6 cause Van der Woude and popliteal pterygium syndromes. *Nat Genet*, **32**, 285-289.
- 22 Houdayer, C., Bonaiti-Pellie, C., Erguy, C., Soupre, V., Dondon, M.G., Burglen, L., Cougoureux, E., Couderc, R., Vazquez, M.P. and Bahuau, M. (2001) Possible relationship between the van der Woude syndrome (vWS) locus and nonsyndromic cleft lip with or without cleft palate (NSCL/P). *Am J Med Genet*, **104**, 86-92.
- 23 Wehby, G.L. and Cassell, C.H. (2010) The impact of orofacial clefts on quality of life and healthcare use and costs. *Oral Dis*, **16**, 3-10.

- 24 Manna, F., Pensiero, S., Clarich, G., Guarneri, G.F. and Parodi, P.C. (2009) Cleft lip and palate: current status from the literature and our experience. *J Craniofac Surg*, **20**, 1383-1387.
- 25 Taioli, E., Ragin, C., Robertson, L., Linkov, F., Thurman, N.E. and Vieira, A.R. (2010) Cleft lip and palate in family members of cancer survivors. *Cancer Invest*, **28**, 958-962.
- 26 Conrad, A.L., Dailey, S., Richman, L., Canady, J., Karnell, M.P., Axelson, E. and Nopoulos, P. (2010) Cerebellum Structure Differences and Relationship to Speech in Boys and Girls With Nonsyndromic Cleft of the Lip and/or Palate. *Cleft Palate Craniofac J*, **47**, 469-475.
- 27 Boes, A.D., Murko, V., Wood, J.L., Langbehn, D.R., Canady, J., Richman, L. and Nopoulos, P. (2007) Social function in boys with cleft lip and palate: relationship to ventral frontal cortex morphology. *Behav Brain Res*, **181**, 224-231.
- 28 Rosen, H., Chiou, G.J., Stoler, J.M., Mulliken, J.B., Tarui, T., Meara, J.G. and Estroff, J.A. (2011) Magnetic Resonance Imaging for Detection of Brain Abnormalities in Fetuses With Cleft Lip and/or Cleft Palate. *Cleft Palate Craniofac J*, **48**, 619-622.
- 29 Shriver, A.S., Canady, J., Richman, L., Andreasen, N.C. and Nopoulos, P. (2006) Structure and function of the superior temporal plane in adult males with cleft lip and palate: pathologic enlargement with no relationship to childhood hearing deficits. *J Child Psychol Psychiatry*, **47**, 994-1002.
- 30 Conrad, A.L., Canady, J., Richman, L. and Nopoulos, P. (2008) Incidence of neurological soft signs in children with isolated cleft of the lip or palate. *Percept Mot Skills*, **106**, 197-206.
- 31 Conrad, A.L., Dailey, S., Richman, L., Canady, J., Karnell, M.P., Axelson, E. and Nopoulos, P. (2010) Cerebellum structure differences and relationship to speech in boys and girls with nonsyndromic cleft of the lip and/or palate. *Cleft Palate Craniofac J*, **47**, 469-475.
- 32 Christensen, K., Juel, K., Herskind, A.M. and Murray, J.C. (2004) Long term follow up study of survival associated with cleft lip and palate at birth. *BMJ*, **328**, 1405.
- 33 Jones, J.L., Canady, J.W., Brookes, J.T., Wehby, G.L., L'Heureux, J., Schutte, B.C., Murray, J.C. and Dunnwald, M. (2010) Wound complications after cleft repair in children with Van der Woude syndrome. *J Craniofac Surg*, **21**, 1350-1353.
- 34 Blanton, S.H., Henry, R.R., Yuan, Q., Mulliken, J.B., Stal, S., Finnell, R.H. and Hecht, J.T. (2011) Folate pathway and nonsyndromic cleft lip and palate. *Birth Defects Res A Clin Mol Teratol*, **91**, 50-60.

- 35 Wu, T., Liang, K.Y., Hetmanski, J.B., Ruczinski, I., Fallin, M.D., Ingersoll, R.G., Wang, H., Huang, S., Ye, X., Wu-Chou, Y.H. *et al.* (2010) Evidence of gene-environment interaction for the IRF6 gene and maternal multivitamin supplementation in controlling the risk of cleft lip with/without cleft palate. *Hum Genet*, **128**, 401-410.
- 36 Aizenbud, D., Coval, M., Hazan-Molina, H. and Harari, D. (2011) Isolated soft tissue cleft lip: epidemiology and associated dental anomalies. *Oral Dis*, **17**, 221-231.
- 37 Basseri, B., Kianmahd, B.D., Roostaeian, J., Kohan, E., Wasson, K.L., Basseri, R.J. and Bradley, J.P. (2011) Current national incidence, trends, and health care resource utilization of cleft lip-cleft palate. *Plast Reconstr Surg*, **127**, 1255-1262.
- 38 Mulliken, J.B. (2004) The changing faces of children with cleft lip and palate. *N Engl J Med*, **351**, 745-747.
- 39 Furr, M.C., Larkin, E., Blakeley, R., Albert, T.W., Tsugawa, L. and Weber, S.M. (2010) Extending multidisciplinary management of cleft palate to the developing world. *J Oral Maxillofac Surg*, **69**, 237-241.
- 40 van Rooij, I.A., Ocke, M.C., Straatman, H., Zielhuis, G.A., Merkus, H.M. and Steegers-Theunissen, R.P. (2004) Periconceptional folate intake by supplement and food reduces the risk of nonsyndromic cleft lip with or without cleft palate. *Prev Med*, **39**, 689-694.
- 41 Schneider, E.L. (1973) Lip pits and congenital absence of second premolars: varied expression of the Lip Pits syndrome. *J Med Genet*, **10**, 346-349.
- 42 Eastman, J.R., Bixler, D. and Escobar, V. (1978) Linkage studies in Van der Woude syndrome. *J Med Genet*, **15**, 217-218.
- 43 Spence, M.A., Glass, L., Crandall, B.F., Stewart, R.E., Miles, J., Falk, R.E., Field, L.L. and Sparkes, R.S. (1983) Genetic linkage studies with cleft lip and palate: report of two family studies. *J Craniofac Genet Dev Biol*, **3**, 207-212.
- 44 Wienker, T.F., Hudek, G., Bissbort, S., Mayerova, A., Mauff, G. and Bender, K. (1987) Linkage studies in a pedigree with Van der Woude syndrome. *J Med Genet*, **24**, 160-162.
- 45 Bocian, M. and Walker, A.P. (1987) Lip pits and deletion 1q32----41. *Am J Med Genet*, **26**, 437-443.
- 46 Sander, A., Moser, H., Liechti-Gallati, S., Grimm, T., Zingg, M. and Raveh, J. (1993) Linkage of Van der Woude syndrome (VWS) to REN and exclusion of the candidate gene TGFB2 from the disease locus in a large pedigree. *Hum Genet*, **91**, 55-62.

- 47 Sander, A., Schmelzle, R. and Murray, J. (1994) Evidence for a microdeletion in 1q32-41 involving the gene responsible for Van der Woude syndrome. *Hum Mol Genet*, **3**, 575-578.
- 48 Houdayer, C., Soupre, V., Rosenberg-Bourgin, M., Martinez, H., Tredano, M., Feldmann, D., Feingold, J., Aymard, P., Munnich, A., Le Bouc, Y. *et al.* (1999) Linkage analysis of 5 novel van der Woude syndrome kindreds to 1q32-q41 markers further supports locus homogeneity of the disease trait. *Ann Genet*, **42**, 69-74.
- 49 Schutte, B.C., Sander, A., Malik, M. and Murray, J.C. (1996) Refinement of the Van der Woude gene location and construction of a 3.5-Mb YAC contig and STS map spanning the critical region in 1q32-q41. *Genomics*, **36**, 507-514.
- 50 Schutte, B.C., Basart, A.M., Watanabe, Y., Laffin, J.J., Coppage, K., Bjork, B.C., Daack-Hirsch, S., Patil, S., Dixon, M.J. and Murray, J.C. (1999) Microdeletions at chromosome bands 1q32-q41 as a cause of Van der Woude syndrome. *Am J Med Genet*, **84**, 145-150.
- 51 Schutte, B.C., Bjork, B.C., Coppage, K.B., Malik, M.I., Gregory, S.G., Scott, D.J., Brentzell, L.M., Watanabe, Y., Dixon, M.J. and Murray, J.C. (2000) A preliminary gene map for the Van der Woude syndrome critical region derived from 900 kb of genomic sequence at 1q32-q41. *Genome Res*, **10**, 81-94.
- 52 Wong, F.K., Karsten, A., Larson, O., Huggare, J., Hagberg, C., Larsson, C., Teh, B.T. and Linder-Aronson, S. (1999) Clinical and genetic studies of Van der Woude syndrome in Sweden. *Acta Odontol Scand*, **57**, 72-76.
- 53 Beiraghi, S., Miller-Chisholm, A., Kimberling, W.J., Sun, C.E., Wang, Y.F., Russell, L.J., Khoshnevisan, M., Storm, A.L., Long, R.E., Jr., Witt, P.D. *et al.* (1999) Confirmation of linkage of Van der Woude syndrome to chromosome 1q32: evidence of association with STR alleles suggests possible unique origin of the disease mutation. *J Craniofac Genet Dev Biol*, **19**, 128-134.
- 54 Neuman, Z. and Shulman, J. (1961) Congenital sinuses of the lower lip. *Oral Surg Oral Med Oral Pathol*, **14**, 1415-1420.
- 55 Hersh, J.H. and Verdi, G.D. (1992) Natal teeth in monozygotic twins with Van der Woude syndrome. *Cleft Palate Craniofac J*, **29**, 279-281.
- 56 Jobling, R., Ferrier, R.A., McLeod, R., Petrin, A.L., Murray, J.C. and Thomas, M.A. (2011) Monozygotic twins with variable expression of Van der Woude syndrome. *Am J Med Genet A*, **155A**, 2008-2010.
- 57 Tokat, C., Bilkay, U., Songur, E. and Akin, Y. (2005) Van der Woude syndrome in twins. *J Craniofac Surg*, **16**, 936-939.

- 58 Lees, M.M., Winter, R.M., Malcolm, S., Saal, H.M. and Chitty, L. (1999) Popliteal pterygium syndrome: a clinical study of three families and report of linkage to the Van der Woude syndrome locus on 1q32. *J Med Genet*, **36**, 888-892.
- 59 Wong, F.K. and Gustafsson, B. (2000) Popliteal pterygium syndrome in a Swedish family--clinical findings and genetic analysis with the van der Woude syndrome locus at 1q32-q41. *Acta Odontol Scand*, **58**, 85-88.
- 60 Bixler, D., Poland, C. and Nance, W.E. (1973) Phenotypic variation in the popliteal pterygium syndrome. *Clin Genet*, **4**, 220-228.
- 61 Escobar, V. and Weaver, D. (1978) Popliteal pterygium syndrome: a phenotypic and genetic analysis. *J Med Genet*, **15**, 35-42.
- 62 Hammer, J., Klausler, M. and Schinzel, A. (1989) The popliteal pterygium syndrome: distinct phenotypic variation in two families. *Helv Paediatr Acta*, **43**, 507-514.
- 63 Leslie, E.J., Standley, J., Compton, J., Bale, S., Schutte, B.C. and Murray, J.C. (2013) Comparative analysis of IRF6 variants in families with Van der Woude syndrome and popliteal pterygium syndrome using public whole-exome databases. *Genet Med*, **15**, 338-344.
- 64 Matsuzawa, N., Yoshiura, K., Machida, J., Nakamura, T., Niimi, T., Furukawa, H., Toyoda, T., Natsume, N., Shimozato, K. and Niikawa, N. (2004) Two missense mutations in the IRF6 gene in two Japanese families with Van der Woude syndrome. *Oral Surg Oral Med Oral Pathol Oral Radiol Endod*, **98**, 414-417.
- 65 Shotelersuk, V., Srichomthong, C., Yoshiura, K. and Niikawa, N. (2003) A novel mutation, 1234del(C), of the IRF6 in a Thai family with Van der Woude syndrome. *Int J Mol Med*, **11**, 505-507.
- 66 Wang, X., Liu, J., Zhang, H., Xiao, M., Li, J., Yang, C., Lin, X., Wu, Z., Hu, L. and Kong, X. (2003) Novel mutations in the IRF6 gene for Van der Woude syndrome. *Hum Genet*, **113**, 382-386.
- 67 Kim, Y., Park, J.Y., Lee, T.J. and Yoo, H.W. (2003) Identification of two novel mutations of IRF6 in Korean families affected with Van der Woude syndrome. *Int J Mol Med*, **12**, 465-468.
- 68 Kayano, S., Kure, S., Suzuki, Y., Kanno, K., Aoki, Y., Kondo, S., Schutte, B.C., Murray, J.C., Yamada, A. and Matsubara, Y. (2003) Novel IRF6 mutations in Japanese patients with Van der Woude syndrome: two missense mutations (R45Q and P396S) and a 17-kb deletion. *J Hum Genet*, **48**, 622-628.

- 69 Gatta, V., Scarciolla, O., Cupaioli, M., Palka, C., Chiesa, P.L. and Stuppia, L. (2004) A novel mutation of the IRF6 gene in an Italian family with Van der Woude syndrome. *Mutat Res*, **547**, 49-53.
- 70 Item, C.B., Turhani, D., Thurnher, D., Yerit, K., Sinko, K., Wittwer, G., Adeyemo, W.L., Frei, K., Erginel-Unaltuna, N., Watzinger, F. *et al.* (2005) Van Der Woude syndrome: variable penetrance of a novel mutation (p.Arg 84Gly) of the IRF6 gene in a Turkish family. *Int J Mol Med*, **15**, 247-251.
- 71 Wang, X.F., Xiao, M.Z., Shi, J.N., Zhang, H.B., Hu, L.D. and Kong, X.Y. (2005) [IRF6 gene mutation analysis in a van Der Woude syndrome family in Henan province]. *Shanghai Kou Qiang Yi Xue*, **14**, 234-237.
- 72 Ghassibe, M., Revencu, N., Bayet, B., Gillerot, Y., Vanwijck, R., Verellen-Dumoulin, C. and Vikkula, M. (2004) Six families with van der Woude and/or popliteal pterygium syndrome: all with a mutation in the IRF6 gene. *J Med Genet*, **41**, e15.
- 73 Ghassibe, M., Bayet, B., Revencu, N., Verellen-Dumoulin, C., Gillerot, Y., Vanwijck, R. and Vikkula, M. (2005) Interferon regulatory factor-6: a gene predisposing to isolated cleft lip with or without cleft palate in the Belgian population. *Eur J Hum Genet*, **13**, 1239-1242.
- 74 Ye, X.Q., Jin, H.X., Shi, L.S., Fan, M.W., Song, G.T., Fan, H.L. and Bian, Z. (2005) Identification of novel mutations of IRF6 gene in Chinese families with Van der Woude syndrome. *Int J Mol Med*, **16**, 851-856.
- 75 Du, X., Tang, W., Tian, W., Li, S., Li, X., Liu, L., Zheng, X., Chen, X., Lin, Y. and Tang, Y. (2006) Novel IRF6 mutations in Chinese patients with Van der Woude syndrome. *J Dent Res*, **85**, 937-940.
- 76 Du, X.Y., Tang, W., Tian, W.D., Li, X.Y., Liu, L. and Zheng, X.H. (2006) [Identification of three novel mutations of IRF6 in Chinese families with Van der Woude syndrome]. *Zhonghua Yi Xue Yi Chuan Xue Za Zhi*, **23**, 82-83.
- 77 Brosch, S., Baur, M., Blin, N., Reinert, S. and Pfister, M. (2007) A novel IRF6 nonsense mutation (Y67X) in a German family with Van der Woude syndrome. *Int J Mol Med*, **20**, 85-89.
- 78 Tan, E.C., Lim, E.C., Yap, S.H., Lee, S.T., Cheng, J., Por, Y.C. and Yeow, V. (2008) Identification of IRF6 gene variants in three families with Van der Woude syndrome. *Int J Mol Med*, **21**, 747-751.
- 79 Paranaiba, L.M., Martelli-Junior, H., Oliveira Swerts, M.S., Line, S.R. and Coletta, R.D. (2008) Novel mutations in the IRF6 gene in Brazilian families with Van der Woude syndrome. *Int J Mol Med*, **22**, 507-511.

- 80 de Lima, R.L., Hoper, S.A., Ghassibe, M., Cooper, M.E., Rorick, N.K., Kondo, S., Katz, L., Marazita, M.L., Compton, J., Bale, S. *et al.* (2009) Prevalence and nonrandom distribution of exonic mutations in interferon regulatory factor 6 in 307 families with Van der Woude syndrome and 37 families with popliteal pterygium syndrome. *Genet Med*, **11**, 241-247.
- 81 Yeetong, P., Mahatumarat, C., Siriwan, P., Rojvachiranonda, N., Suphapeetiporn, K. and Shotelersuk, V. (2009) Three novel mutations of the IRF6 gene with one associated with an unusual feature in Van der Woude syndrome. *Am J Med Genet A*, **149A**, 2489-2492.
- 82 Malik, S., Kakar, N., Hasnain, S., Ahmad, J., Wilcox, E.R. and Naz, S. (2010) Epidemiology of Van der Woude syndrome from mutational analyses in affected patients from Pakistan. *Clin Genet*, **78**, 247-256.
- 83 Scioletti, A.P., Brancati, F., Gatta, V., Antonucci, I., Peissel, B., Pizzuti, A., Mortellaro, C., Tete, S., Gherlone, E., Palka, G. *et al.* (2010) Two novel mutations affecting splicing in the IRF6 gene associated with van der Woude syndrome. *J Craniofac Surg*, **21**, 1654-1656.
- 84 Salahshourifar, I., Halim, A.S., Sulaiman, W.A., Ariffin, R., Naili Muhamad Nor, N. and Zilfalil, B.A. (2011) De novo interstitial deletion of 1q32.2-q32.3 including the entire IRF6 gene in a patient with oral cleft and other dysmorphic features. *Cytogenet Genome Res*, **134**, 83-87.
- 85 Birkeland, A.C., Larrabee, Y., Kent, D.T., Flores, C., Su, G.H., Lee, J.H. and Haddad, J., Jr. (2011) Novel IRF6 mutations in Honduran Van der Woude syndrome patients. *Mol Med Report*, **4**, 237-241.
- 86 Minones-Suarez, L., Mas-Vidal, A., Fernandez-Toral, J., Llano-Rivas, I. and Gonzalez-Garcia, M. (2011) A novel mutation in the IRF6 gene associated with facial asymmetry in a family affected with Van der Woude Syndrome. *Pediatr Dermatol*.
- 87 Koillinen, H., Wong, F.K., Rautio, J., Ollikainen, V., Karsten, A., Larson, O., Teh, B.T., Huggare, J., Lahermo, P., Larsson, C. *et al.* (2001) Mapping of the second locus for the Van der Woude syndrome to chromosome 1p34. *Eur J Hum Genet*, **9**, 747-752.
- 88 Rorick, N.K., Kinoshita, A., Weirather, J.L., Peyrard-Janvid, M., de Lima, R.L., Dunnwald, M., Shanske, A.L., Moretti-Ferreira, D., Koillinen, H., Kere, J. *et al.* (2011) Genomic strategy identifies a missense mutation in WD-repeat domain 65 (WDR65) in an individual with Van der Woude syndrome. *Am J Med Genet A*, **155A**, 1314-1321.
- 89 Zuccherro, T.M., Cooper, M.E., Maher, B.S., Daack-Hirsch, S., Nepomuceno, B., Ribeiro, L., Caprau, D., Christensen, K., Suzuki, Y., Machida, J. *et al.* (2004) Interferon

regulatory factor 6 (IRF6) gene variants and the risk of isolated cleft lip or palate. *N Engl J Med*, **351**, 769-780.

90 Beaty, T.H., Murray, J.C., Marazita, M.L., Munger, R.G., Ruczinski, I., Hetmanski, J.B., Liang, K.Y., Wu, T., Murray, T., Fallin, M.D. *et al.* (2010) A genome-wide association study of cleft lip with and without cleft palate identifies risk variants near MAFB and ABCA4. *Nat Genet*, **42**, 525-529.

91 Rahimov, F., Marazita, M.L., Visel, A., Cooper, M.E., Hitchler, M.J., Rubini, M., Domann, F.E., Govil, M., Christensen, K., Bille, C. *et al.* (2008) Disruption of an AP-2alpha binding site in an IRF6 enhancer is associated with cleft lip. *Nat Genet*, **40**, 1341-1347.

92 Fakhouri, W.D., Rhea, L., Du, T., Sweezer, E., Morrison, H., Fitzpatrick, D., Yang, B., Dunnwald, M. and Schutte, B.C. (2012) MCS9.7 enhancer activity is highly, but not completely, associated with expression of Irf6 and p63. *Dev Dyn*, **241**, 340-349.

93 Blik, J.B., Rothenberg, S.P. and Steegers-Theunissen, R.P. (2006) Maternal folate receptor autoantibodies and cleft lip and/or palate. *Int J Gynaecol Obstet*, **93**, 142-143.

94 Mills, J.L., Molloy, A.M., Parle-McDermott, A., Troendle, J.F., Brody, L.C., Conley, M.R., Cox, C., Pangilinan, F., Orr, D.J., Earley, M. *et al.* (2008) Folate-related gene polymorphisms as risk factors for cleft lip and cleft palate. *Birth Defects Res A Clin Mol Teratol*, **82**, 636-643.

95 Blanton, S.H., Henry, R.R., Yuan, Q., Mulliken, J.B., Stal, S., Finnell, R.H. and Hecht, J.T. (2010) Folate pathway and nonsyndromic cleft lip and palate. *Birth Defects Res A Clin Mol Teratol*.

96 Honda, K. and Taniguchi, T. (2006) Toll-like receptor signaling and IRF transcription factors. *IUBMB Life*, **58**, 290-295.

97 Bailey, C.M., Khalkhali-Ellis, Z., Kondo, S., Margaryan, N.V., Seftor, R.E., Wheaton, W.W., Amir, S., Pins, M.R., Schutte, B.C. and Hendrix, M.J. (2005) Mammary serine protease inhibitor (Maspin) binds directly to interferon regulatory factor 6: identification of a novel serpin partnership. *J Biol Chem*, **280**, 34210-34217.

98 Richardson, R.J., Dixon, J., Jiang, R. and Dixon, M.J. (2009) Integration of IRF6 and Jagged2 signalling is essential for controlling palatal adhesion and fusion competence. *Hum Mol Genet*, **18**, 2632-2642.

99 Knight, A.S., Schutte, B.C., Jiang, R. and Dixon, M.J. (2006) Developmental expression analysis of the mouse and chick orthologues of IRF6: the gene mutated in Van der Woude syndrome. *Dev Dyn*, **235**, 1441-1447.

- 100 Bailey, C.M., Margaryan, N.V., Abbott, D.E., Schutte, B.C., Yang, B., Khalkhali-Ellis, Z. and Hendrix, M.J. (2009) Temporal and spatial expression patterns for the tumor suppressor Maspin and its binding partner interferon regulatory factor 6 during breast development. *Dev Growth Differ*, **51**, 473-481.
- 101 Little, H.J., Rorick, N.K., Su, L.I., Baldock, C., Malhotra, S., Jowitt, T., Gakhar, L., Subramanian, R., Schutte, B.C., Dixon, M.J. *et al.* (2009) Missense mutations that cause Van der Woude syndrome and popliteal pterygium syndrome affect the DNA-binding and transcriptional activation functions of IRF6. *Hum Mol Genet*, **18**, 535-545.
- 102 Sabel, J.L., d'Alencon, C., O'Brien, E.K., Van Otterloo, E., Lutz, K., Cuykendall, T.N., Schutte, B.C., Houston, D.W. and Cornell, R.A. (2009) Maternal Interferon Regulatory Factor 6 is required for the differentiation of primary superficial epithelia in Danio and Xenopus embryos. *Dev Biol*, **325**, 249-262.
- 103 de la Garza, G., Schleiffarth, J.R., Dunnwald, M., Mankad, A., Weirather, J.L., Bonde, G., Butcher, S., Mansour, T.A., Kousa, Y.A., Fukazawa, C.F. *et al.* (2013) Interferon regulatory factor 6 promotes differentiation of the periderm by activating expression of grainyhead-like 3. *J Invest Dermatol*, **133**, 68-77.
- 104 Richardson, R.J., Dixon, J., Malhotra, S., Hardman, M.J., Knowles, L., Boot-Handford, R.P., Shore, P., Whitmarsh, A. and Dixon, M.J. (2006) Irf6 is a key determinant of the keratinocyte proliferation-differentiation switch. *Nat Genet*, **38**, 1329-1334.
- 105 Ingraham, C.R., Kinoshita, A., Kondo, S., Yang, B., Sajan, S., Trout, K.J., Malik, M.I., Dunnwald, M., Goudy, S.L., Lovett, M. *et al.* (2006) Abnormal skin, limb and craniofacial morphogenesis in mice deficient for interferon regulatory factor 6 (Irf6). *Nat Genet*, **38**, 1335-1340.
- 106 Su, L.-I. (2011), In *Faculty of Life Science*. University of Manchester, Manchester, Vol. Doctor of Philosophy, pp. 231.
- 107 Botti, E., Spallone, G., Moretti, F., Marinari, B., Pinetti, V., Galanti, S., De Meo, P.D., De Nicola, F., Ganci, F., Castrignano, T. *et al.* (2011) Developmental factor IRF6 exhibits tumor suppressor activity in squamous cell carcinomas. *Proc Natl Acad Sci U S A*, **108**, 13710-13715.
- 108 Ting, S.B., Wilanowski, T., Auden, A., Hall, M., Voss, A.K., Thomas, T., Parekh, V., Cunningham, J.M. and Jane, S.M. (2003) Inositol- and folate-resistant neural tube defects in mice lacking the epithelial-specific factor Grhl-3. *Nat Med*, **9**, 1513-1519.
- 109 McDade, S.S., Henry, A.E., Pivato, G.P., Kozarewa, I., Mitsopoulos, C., Fenwick, K., Assiotis, I., Hakas, J., Zvelebil, M., Orr, N. *et al.* (2012) Genome-wide analysis of p63 binding sites identifies AP-2 factors as co-regulators of epidermal differentiation. *Nucleic Acids Res*, **40**, 7190-7206.

- 110 Bailey, C.M., Abbott, D.E., Margaryan, N.V., Khalkhali-Ellis, Z. and Hendrix, M.J. (2008) Interferon regulatory factor 6 promotes cell cycle arrest and is regulated by the proteasome in a cell cycle-dependent manner. *Mol Cell Biol*, **28**, 2235-2243.
- 111 Moretti, F., Marinari, B., Lo Iacono, N., Botti, E., Giunta, A., Spallone, G., Garaffo, G., Vernersson-Lindahl, E., Merlo, G., Mills, A.A. *et al.* (2010) A regulatory feedback loop involving p63 and IRF6 links the pathogenesis of 2 genetically different human ectodermal dysplasias. *J Clin Invest*, **120**, 1570-1577.
- 112 Thomason, H.A., Zhou, H., Kouwenhoven, E.N., Dotto, G.P., Restivo, G., Nguyen, B.C., Little, H., Dixon, M.J., van Bokhoven, H. and Dixon, J. (2010) Cooperation between the transcription factors p63 and IRF6 is essential to prevent cleft palate in mice. *J Clin Invest*, **120**, 1561-1569.
- 113 Stransky, N., Egloff, A.M., Tward, A.D., Kostic, A.D., Cibulskis, K., Sivachenko, A., Kryukov, G.V., Lawrence, M.S., Sougnez, C., McKenna, A. *et al.* (2011) The mutational landscape of head and neck squamous cell carcinoma. *Science*, **333**, 1157-1160.
- 114 Nair, M., Teng, A., Bilanchone, V., Agrawal, A., Li, B. and Dai, X. (2006) *Ovol1* regulates the growth arrest of embryonic epidermal progenitor cells and represses c-myc transcription. *J Cell Biol*, **173**, 253-264.
- 115 Stransky, N., Egloff, A.M., Tward, A.D., Kostic, A.D., Cibulskis, K., Sivachenko, A., Kryukov, G.V., Lawrence, M.S., Sougnez, C., McKenna, A. *et al.* (2011) The mutational landscape of head and neck squamous cell carcinoma. *Science*, **333**, 1157-1160.
- 116 Chen, W., Lam, S.S., Srinath, H., Jiang, Z., Correia, J.J., Schiffer, C.A., Fitzgerald, K.A., Lin, K. and Royer, W.E., Jr. (2008) Insights into interferon regulatory factor activation from the crystal structure of dimeric IRF5. *Nat Struct Mol Biol*, **15**, 1213-1220.
- 117 Li, H., Sheridan, R. and Williams, T. (2013) Analysis of TFAP2A mutations in Branchio-Oculo-Facial Syndrome indicates functional complexity within the AP-2alpha DNA-binding domain. *Hum Mol Genet*, **22**, 3195-3206.
- 118 Zhang, J., Hagopian-Donaldson, S., Serbedzija, G., Elsemore, J., Plehn-Dujowich, D., McMahon, A.P., Flavell, R.A. and Williams, T. (1996) Neural tube, skeletal and body wall defects in mice lacking transcription factor AP-2. *Nature*, **381**, 238-241.
- 119 Schorle, H., Meier, P., Buchert, M., Jaenisch, R. and Mitchell, P.J. (1996) Transcription factor AP-2 essential for cranial closure and craniofacial development. *Nature*, **381**, 235-238.

- 120 Brewer, S., Feng, W., Huang, J., Sullivan, S. and Williams, T. (2004) Wnt1-Cre-mediated deletion of AP-2alpha causes multiple neural crest-related defects. *Dev Biol*, **267**, 135-152.
- 121 Thomason, H.A., Zhou, H., Kouwenhoven, E.N., Dotto, G.P., Restivo, G., Nguyen, B.C., Little, H., Dixon, M.J., van Bokhoven, H. and Dixon, J. (2010) Cooperation between the transcription factors p63 and IRF6 is essential to prevent cleft palate in mice. *J Clin Invest*, **120**, 1561-1569.
- 122 Restivo, G., Nguyen, B.C., Dziunycz, P., Ristorcelli, E., Ryan, R.J., Ozuysal, O.Y., Di Piazza, M., Radtke, F., Dixon, M.J., Hofbauer, G.F. *et al.* (2011) IRF6 is a mediator of Notch pro-differentiation and tumour suppressive function in keratinocytes. *EMBO J*.
- 123 Stottmann, R.W., Bjork, B.C., Doyle, J.B. and Beier, D.R. (2010) Identification of a Van der Woude syndrome mutation in the cleft palate 1 mutant mouse. *Genesis*, **48**, 303-308.
- 124 Goudy, S., Angel, P., Jacobs, B., Hill, C., Mainini, V., Smith, A.L., Kousa, Y.A., Caprioli, R., Prince, L.S., Baldwin, S. *et al.* (2013) Cell-autonomous and non-cell-autonomous roles for IRF6 during development of the tongue. *PLoS One*, **8**, e56270.
- 125 Boell, L., Pallares, L.F., Brodski, C., Chen, Y., Christian, J.L., Kousa, Y.A., Kuss, P., Nelsen, S., Novikov, O., Schutte, B.C. *et al.* (2013) Exploring the effects of gene dosage on mandible shape in mice as a model for studying the genetic basis of natural variation. *Dev Genes Evol*, **223**, 279-287.
- 126 Herron, B.J., Liddell, R.A., Parker, A., Grant, S., Kinne, J., Fisher, J.K. and Siracusa, L.D. (2005) A mutation in stratifin is responsible for the repeated epilation (Er) phenotype in mice. *Nat Genet*, **37**, 1210-1212.
- 127 Song, L., Dong, W., Gao, M., Li, J., Hu, M., Guo, N. and Huang, C. (2010) A novel role of IKKalpha in the mediation of UVB-induced G0/G1 cell cycle arrest response by suppressing Cyclin D1 expression. *Biochim Biophys Acta*, **1803**, 323-332.
- 128 Lee, S., Kong, Y. and Weatherbee, S.D. (2013) Forward genetics identifies Kdf1/1810019J16Rik as an essential regulator of the proliferation-differentiation decision in epidermal progenitor cells. *Dev Biol*, **383**, 201-213.
- 129 Rountree, R.B., Willis, C.R., Dinh, H., Blumberg, H., Bailey, K., Dean, C., Jr., Peschon, J.J. and Holland, P.M. (2010) RIP4 regulates epidermal differentiation and cutaneous inflammation. *J Invest Dermatol*, **130**, 102-112.
- 130 Yang, H.Y., Wen, Y.Y., Chen, C.H., Lozano, G. and Lee, M.H. (2003) 14-3-3 sigma positively regulates p53 and suppresses tumor growth. *Mol Cell Biol*, **23**, 7096-7107.

- 131 Hermeking, H., Lengauer, C., Polyak, K., He, T.C., Zhang, L., Thiagalingam, S., Kinzler, K.W. and Vogelstein, B. (1997) 14-3-3 sigma is a p53-regulated inhibitor of G2/M progression. *Mol Cell*, **1**, 3-11.
- 132 Dellambra, E., Patrone, M., Sparatore, B., Negri, A., Ceciliani, F., Bondanza, S., Molina, F., Cancedda, F.D. and De Luca, M. (1995) Stratifin, a keratinocyte specific 14-3-3 protein, harbors a pleckstrin homology (PH) domain and enhances protein kinase C activity. *J Cell Sci*, **108 (Pt 11)**, 3569-3579.
- 133 Yaffe, M.B., Rittinger, K., Volinia, S., Caron, P.R., Aitken, A., Leffers, H., Gamblin, S.J., Smerdon, S.J. and Cantley, L.C. (1997) The structural basis for 14-3-3:phosphopeptide binding specificity. *Cell*, **91**, 961-971.
- 134 Rittinger, K., Budman, J., Xu, J., Volinia, S., Cantley, L.C., Smerdon, S.J., Gamblin, S.J. and Yaffe, M.B. (1999) Structural analysis of 14-3-3 phosphopeptide complexes identifies a dual role for the nuclear export signal of 14-3-3 in ligand binding. *Mol Cell*, **4**, 153-166.
- 135 Ferguson, A.T., Evron, E., Umbricht, C.B., Pandita, T.K., Chan, T.A., Hermeking, H., Marks, J.R., Lambers, A.R., Futreal, P.A., Stampfer, M.R. *et al.* (2000) High frequency of hypermethylation at the 14-3-3 sigma locus leads to gene silencing in breast cancer. *Proc Natl Acad Sci U S A*, **97**, 6049-6054.
- 136 Umbricht, C.B., Evron, E., Gabrielson, E., Ferguson, A., Marks, J. and Sukumar, S. (2001) Hypermethylation of 14-3-3 sigma (stratifin) is an early event in breast cancer. *Oncogene*, **20**, 3348-3353.
- 137 Lahtela, J., Nousiainen, H.O., Stefanovic, V., Tallila, J., Viskari, H., Karikoski, R., Gentile, M., Saloranta, C., Varilo, T., Salonen, R. *et al.* (2010) Mutant CHUK and severe fetal encasement malformation. *N Engl J Med*, **363**, 1631-1637.
- 138 Hu, Y., Baud, V., Oga, T., Kim, K.I., Yoshida, K. and Karin, M. (2001) IKKalpha controls formation of the epidermis independently of NF-kappaB. *Nature*, **410**, 710-714.
- 139 Descargues, P., Sil, A.K., Sano, Y., Korchynskyi, O., Han, G., Owens, P., Wang, X.J. and Karin, M. (2008) IKKalpha is a critical coregulator of a Smad4-independent TGFbeta-Smad2/3 signaling pathway that controls keratinocyte differentiation. *Proc Natl Acad Sci U S A*, **105**, 2487-2492.
- 140 Le, M., Naridze, R., Morrison, J., Biggs, L.C., Rhea, L., Schutte, B.C., Kaartinen, V. and Dunnwald, M. (2012) Transforming growth factor Beta 3 is required for excisional wound repair in vivo. *PLoS One*, **7**, e48040.
- 141 Iwata, J., Suzuki, A., Pelikan, R.C., Ho, T.V., Sanchez-Lara, P.A., Urata, M., Dixon, M.J. and Chai, Y. (2013) Smad4-Irf6 genetic interaction and TGFbeta-mediated

IRF6 signaling cascade are crucial for palatal fusion in mice. *Development*, **140**, 1220-1230.

142 Chen, L., Haider, K., Ponda, M., Cariappa, A., Rowitch, D. and Pillai, S. (2001) Protein kinase C-associated kinase (PKK), a novel membrane-associated, ankyrin repeat-containing protein kinase. *J Biol Chem*, **276**, 21737-21744.

143 Meylan, E., Martinon, F., Thome, M., Gschwendt, M. and Tschopp, J. (2002) RIP4 (DIK/PKK), a novel member of the RIP kinase family, activates NF-kappa B and is processed during apoptosis. *EMBO Rep*, **3**, 1201-1208.

144 Holland, P., Willis, C., Kanaly, S., Glaccum, M., Warren, A., Charrier, K., Murison, J., Derry, J., Virca, G., Bird, T. *et al.* (2002) RIP4 is an ankyrin repeat-containing kinase essential for keratinocyte differentiation. *Curr Biol*, **12**, 1424-1428.

145 Mitchell, K., O'Sullivan, J., Missero, C., Blair, E., Richardson, R., Anderson, B., Antonini, D., Murray, J.C., Shanske, A.L., Schutte, B.C. *et al.* (2012) Exome sequence identifies RIPK4 as the Bartsocas-Papas syndrome locus. *Am J Hum Genet*, **90**, 69-75.

146 Kalay, E., Sezgin, O., Chellappa, V., Mutlu, M., Morsy, H., Kayserili, H., Kreiger, E., Cansu, A., Toraman, B., Abdalla, E.M. *et al.* (2012) Mutations in RIPK4 cause the autosomal-recessive form of popliteal pterygium syndrome. *Am J Hum Genet*, **90**, 76-85.

147 Sil, A.K., Maeda, S., Sano, Y., Roop, D.R. and Karin, M. (2004) IkappaB kinase-alpha acts in the epidermis to control skeletal and craniofacial morphogenesis. *Nature*, **428**, 660-664.

148 Keswani, S.G., Le, L.D., Morris, L.M., Lim, F.Y., Katz, A.B., Ghobril, N., Habli, M., Frischer, J.S. and Crombleholme, T.M. (2011) Submucosal gland development in the human fetal trachea xenograft model: implications for fetal gene therapy. *J Pediatr Surg*, **46**, 33-38.

149 Koppanati, B.M., Li, J., Reay, D.P., Wang, B., Daood, M., Zheng, H., Xiao, X., Watchko, J.F. and Clemens, P.R. (2010) Improvement of the mdx mouse dystrophic phenotype by systemic in utero AAV8 delivery of a minidystrophin gene. *Gene Ther*, **17**, 1355-1362.

150 Muhle, C., Neuner, A., Park, J., Pacho, F., Jiang, Q., Waddington, S.N. and Schneider, H. (2006) Evaluation of prenatal intra-amniotic LAMB3 gene delivery in a mouse model of Hurler disease. *Gene Ther*, **13**, 1665-1676.

151 Endo, M., Zoltick, P.W., Radu, A., Qiuji, J., Matsui, C., Marinkovich, P.M., McGrath, J., Tamai, K., Uitto, J. and Flake, A.W. (2011) Early intra-amniotic gene transfer using lentiviral vector improves skin blistering phenotype in a murine model of Hurler junctional epidermolysis bullosa. *Gene Ther*.

- 152 Niiya, M., Endo, M., Shang, D., Zoltick, P.W., Muvarak, N.E., Cao, W., Jin, S.Y., Skipwith, C.G., Motto, D.G., Flake, A.W. *et al.* (2009) Correction of ADAMTS13 deficiency by in utero gene transfer of lentiviral vector encoding ADAMTS13 genes. *Mol Ther*, **17**, 34-41.
- 153 Dejneka, N.S., Surace, E.M., Aleman, T.S., Cideciyan, A.V., Lyubarsky, A., Savchenko, A., Redmond, T.M., Tang, W., Wei, Z., Rex, T.S. *et al.* (2004) In utero gene therapy rescues vision in a murine model of congenital blindness. *Mol Ther*, **9**, 182-188.
- 154 Wu, C., Endo, M., Yang, B.H., Radecki, M.A., Davis, P.F., Zoltick, P.W., Spivak, R.M., Flake, A.W., Kirschner, R.E. and Nah, H.D. (2013) Intra-amniotic transient transduction of the periderm with a viral vector encoding TGFbeta3 prevents cleft palate in Tgfbeta3(-/-) mouse embryos. *Mol Ther*, **21**, 8-17.
- 155 Copp, A.J., Greene, N.D. and Murdoch, J.N. (2003) The genetic basis of mammalian neurulation. *Nat Rev Genet*, **4**, 784-793.

Chapter 2 -
Dominant mutations in *GRHL3* cause Van der Woude
syndrome and disrupt oral periderm development

Myriam Peyrard-Janvid,^{1,16*} Elizabeth J. Leslie,^{2,16} Youssef A. Kousa,^{3,16} Tiffany L. Smith,^{4,16}
Martine Dunnwald,^{2,16} Måns Magnusson,⁵ Brian A. Lentz,² Per Unneberg,⁶ Ingegerd Fransson,¹
Hannele K. Koillinen,⁷ Jorma Rautio,⁸ Marie Pegelow,⁹ Agneta Karsten,⁹ Lina Basel-
Vanagaite,^{10,11,12} William Gordon,¹³ Bogi Andersen,¹³ Thomas Svensson,⁵ Jeffrey C. Murray,²
Robert A. Cornell,⁴ Juha Kere,^{1,5,14**} and Brian C. Schutte,¹⁵

Affiliations:

¹Department of Biosciences and Nutrition, Karolinska Institutet, and Center for Biotechnology,
14183 Huddinge, Sweden

²Department of Pediatrics and Interdisciplinary Program in Genetics, University of Iowa, Iowa
City 52242, Iowa, USA

³Department of Biochemistry and Molecular Biology, Michigan State University, East Lansing
48824, Michigan, USA

⁴Department of Anatomy and Cell Biology, University of Iowa, Iowa City 52242, Iowa, USA

⁵Department of Biosciences and Nutrition, Science for Life Laboratory, Karolinska Institutet,
17121 Solna, Sweden

⁶Department of Biochemistry and Biophysics Science for Life Laboratory, Stockholm University,
17121 Solna, Sweden

⁷Department of Clinical Genetics, Helsinki University Hospital, 00029 Helsinki, Finland

⁸Cleft Palate and Craniofacial Center, Department of Plastic Surgery, Helsinki University
Hospital, 00029 Helsinki, Finland

⁹Department of Orthodontics, Stockholm Craniofacial Team, Institute of Odontology, Karolinska
Institutet, 17177 Stockholm, Sweden

¹⁰Pediatric Genetics Unit, Schneider Children's Medical Center of Israel and Raphael Recanati Genetic Institute, Rabin Medical Center, Petah Tikva 49100, Israel

¹¹Sackler Faculty of Medicine, Tel Aviv University, Tel Aviv 69978, Israel

¹²Felsenstein Medical Research Center, Petah Tikva, 49100, Israel

¹³Department of Biological Chemistry, University of California Irvine, Irvine 92697, California, USA

¹⁴Research Programs Unit, University of Helsinki, and Folkhälsan Institute of Genetics, 00014 Helsinki, Finland

¹⁵Department of Microbiology and Molecular Genetics, Michigan State University, East Lansing 48824, Michigan, USA

¹⁶These authors contributed equally to this work

Correspondence to:

*Myriam.Peyrard@ki.se

**Juha.Kere@ki.se

ABSTRACT

Mutations in the interferon regulatory factor 6 (*IRF6*) gene account for ~70% of cases of Van der Woude syndrome (VWS), the most common syndromic form of cleft lip and palate. In eight of 45 VWS families lacking a mutation in *IRF6*, we found coding mutations in the grainy head-like 3 (*GRHL3*) gene. Using a zebrafish-based assay, the disease-associated *GRHL3* mutations abrogated periderm development and were consistent with a dominant-negative effect, in contrast to haploinsufficiency seen in most VWS cases caused by *IRF6* mutations. In mouse, all embryos lacking *Grhl3* exhibited abnormal oral periderm and 17% developed a cleft palate. Analysis of the oral phenotype of double heterozygote (*Irf6*^{+/-};*Grhl3*^{+/-}) murine embryos failed to detect epistasis between the two genes, suggesting that they function in separate but convergent pathways during palatogenesis. Taken together, our data demonstrated that mutations in two genes, *IRF6* and *GRHL3*, can lead to nearly identical phenotypes of orofacial cleft. They supported the hypotheses that both genes are essential for the presence of a functional oral periderm and that failure of this process contributes to VWS.

INTRODUCTION

Grainy head-like 3 (*GRHL3*, MIM 608317) belongs to a family of three human genes that encode transcription factor orthologs of the *Drosophila* gene *grainy head* (*grh*). Among multiple conserved roles, this gene family is required for the development and repair of the epidermal barrier layer¹⁻³. In zebrafish, *grhl1* and *grhl3* were shown to be required for the development of the periderm⁴, the transient layer of squamous epithelial cells located on the surface of developing embryos. Interferon regulatory factor 6 (*irf6*) is also required for periderm development in zebrafish⁵, and directly regulates the expression of *grhl3*^{4;6}. In addition, over-expression of *Grhl3* partially rescued periderm development in zebrafish embryos that expressed a dominant-negative mutant form of *irf6*⁴. These data suggest that *Grhl3* is an important player in the *Irf6*-dependent pathway of periderm development.

IRF6 belongs to the IRF family of transcription factors that are known best for their roles in immune function⁷. However, *IRF6* (MIM 607199) is required for skin, limb and craniofacial development⁸⁻¹⁰. In mice, embryos that lack *Irf6* expression fail to develop the epidermal barrier^{9;10}. While reminiscent of embryos that lack *Grhl3*², the cutaneous phenotype of *Irf6* mutant embryos appears to be more severe macroscopically. In addition, *Irf6* mutant embryos have extensive oral epithelial adhesions^{9;10}, a phenotype not reported in the *Grhl3* mutant. The oral epithelial adhesions in *Irf6* knockout embryos lead to cleft palate^{9;10}, and appear to stem from periderm dysfunction^{4;11}.

In humans, mutations in *IRF6* cause Van der Woude syndrome (VWS, MIM 119300), the most common syndromic form of orofacial clefting, or popliteal pterygium syndrome (PPS, MIM 119500). Individuals with VWS can have cleft lip (CL), cleft palate (CP), or cleft lip and palate (CLP). In addition, 85% of affected individuals have pits in their lower lip¹². To date, mutations in *IRF6* have been identified in 70% of families with VWS^{8;13;14}. The possibility that locus

heterogeneity accounts for some of the remaining 30% of VWS mutations is underscored by linkage in one large pedigree from Finland to a locus on 1p33-p36 rather than to *IRF6* at 1q32-q41¹⁵. In this family, most affected individuals have an orofacial cleft and the proband has lip pits, the hallmark of VWS. Because of the autosomal dominant inheritance pattern and the presence of the lip pits, this family was diagnosed with VWS and the linked region was named the *VWS2* locus¹⁵.

Here we report disease-causing mutations in the *GRHL3* gene in the above mentioned original Finnish family as well as in seven additional families with VWS, therefore demonstrating that *GRHL3* is the second gene for which mutations lead to VWS. While we observed no consistently unique phenotypes in these families, individuals with a *GRHL3* mutation are more likely to have CP and less likely to have CL or lip pits than individuals with an *IRF6* mutation. In addition, we used zebrafish and murine models to show that *Grhl3*, like *Irf6*, has a conserved role in the development of the periderm. Our observations from all three species support the conclusion that a functional oral periderm is essential for the proper palatogenesis.

RESULTS

Grainy-head like 3 is the VWS2 gene

A single large VWS family of Finnish origin (Fig. 8) showed linkage to a ~40cM region on 1p33-36, pointing to a second VWS locus¹⁵, i.e. *VWS2* (MIM 606713). From this family, we selected eight affected individuals, including the proband who is the only one with lip pits, and three healthy individuals, for whole-exome sequencing. We searched the ~700 genes contained in the entire linkage region (~46 Mb) for variants common to all eight affected family members but not seen in any of the three healthy members. This resulted in three segregating exonic variants: in *GRHL3* (1:24666175; NM_198174.2: c.969-970insTG), *PHACTR4* (1:28806971; rs200581707;

NM_001048183.1: c.1615G>A) and *KTI12* (1:52499097-52499071; NM_138417.2: c.337_363delCCGATCGCGGGACCTCAGGTGGCGGGC). The *GRHL3* and *PHACTR4* variants were confirmed by TaqMan genotyping and the *KTI12* variant by allelic discrimination based on differential melting temperature. The *PHACTR4* variant was found in two out of 8252 European American chromosomes in the NHLBI/ESP database, and is therefore unlikely to be the causative variant for VWS. In a set of 561 Finnish controls, the *KTI12* variant was found at a frequency of 12.4%, and is therefore a common, non-causative variant. The *GRHL3* variant was not found in any of the Finnish controls nor in NHLBI/ESP, making *GRHL3* a strong candidate gene in the *VWS2* locus.

To test whether mutations in *GRHL3* accounted for VWS in other families, we screened 44 families of variable ethnicity where no causative *IRF6* mutations had been previously detected. We identified *GRHL3* variants in seven families, including four protein-truncating mutations and four missense mutations (Fig. 4). All mutations except c.1661A>G (coding for the p.Asn554Ser missense mutation) were predicted by Polyphen2 and SIFT to be damaging/deleterious and two were confirmed *de novo* events (Table 1). In one of the seven families (VWS-III), we found two variants located in *trans*. Variant c.268_278delTACTACCATGG was inherited from the proband's affected father and from the healthy paternal grandfather, while variant c.1661A>G was inherited from the proband's healthy mother (Fig S1). In addition, one family (VWS-IV) was previously determined to have a novel *IRF6* missense variant (c.239A>G) that was not conclusively determined to be causative for VWS²³, raising the possibility that variants in both *IRF6* and *GRHL3* could contribute to VWS in one family (Fig. 8).

We tested for phenotypic variation between the *VWS* and *VWS2* loci. The phenotypes observed in the individuals with mutations in *GRHL3* overlap with the classic VWS phenotype

(Fig. 8). However, individuals positive for a *GRHL3* mutation were significantly more likely to have CP (70% (*GRHL3*) vs. 27% (*IRF6*), p-value = 2.0×10^{-6}) and less likely to have CL/P (CL or CLP) (11% vs. 46%, p-value = 0.001) than individuals with *IRF6* mutations (Table 2). Lip pits were less frequent among individuals with *GRHL3* mutations (52% vs. 76%), however this difference was not statistically significant (p-value = 0.05). The presence of dental and limb anomalies did not differ significantly between the two groups.

Affect of *GRHL3* alleles on zebrafish development

To distinguish whether the human *GRHL3* alleles that cause VWS are nulls or dominant-negative, we developed an *in vivo* assay to measure the function of the gene on the development of the periderm in zebrafish⁴. The assay is based on the observation that over-expression of wild type *grhl3* in zebrafish or frog embryos (*Xenopus laevis*) is sufficient to induce, in deep cells, ectopic expression of genes whose expression is normally restricted to the periderm, e.g. *keratin 4* (*krt4*)^{4; 24}. Also, simultaneous reduction of *grhl1* and *grhl3*, or over-expression of an engineered dominant-negative variant of frog *grhl1*, prevents the expression of *krt4* in epithelial cells of the zebrafish periderm, and causes embryonic death during epiboly⁴.

Thus, we injected wild type and mutant alleles of human *GRHL3* mRNA into zebrafish embryos and scored for embryonic viability and *krt4* expression. At shield stage (6 h post fertilization, hpf), most embryos injected with a control mRNA (*lacZ*) developed normally, and *krt4* expression was confined to the periderm (Fig. 5A,E). In most embryos injected with wild type *GRHL3* epiboly was slightly delayed in comparison to *lacZ*-injected control embryos (Fig. 5B), and *krt4* was ectopically expressed in deep cells (Fig. 5F). In contrast, the majority of embryos injected with *GRHL3* mRNA carrying the c.1171C>T variant from VWS-II stalled before (4 hpf) or during epiboly stage, and then ruptured through the animal hemisphere (Fig.

5C). This phenotype resembles that of embryos injected with the dominant-negative alleles of *Xenopus grhl1* or zebrafish *irf6*^{4;5}. We tested four other VWS-associated alleles of *GRHL3* with this *in vivo* assay, including both alleles found in VWS-III. For all four alleles, embryonic development stalled and the embryo ruptured at a timepoint and frequency similar to embryos injected with the c.1171C>T variant from VWS-II (Fig 2D).

To test whether the effect of these mutations was cell-autonomous, we generated mosaic embryos by co-injecting *GRHL3* mRNA and biotin into one cell at the 16-cell stage of zebrafish development. In this assay, cells that inherited the *GRHL3* mRNA were marked by biotin staining. In embryos injected with control mRNA (*LacZ*), we observed normal *krt4* expression in all periderm cells, regardless of the biotin staining (Fig. 5G). In embryos injected with *GRHL3* mRNA containing the c.893G>A variant (from VWS-IV), the cells from the periderm inheriting the mutated mRNA (biotin-positive) lacked *krt4* expression, but biotin-negative cells expressed *krt4* (Fig. 5H). We conclude that mutant *GRHL3* variant interfered with the development of the periderm in a cell-autonomous fashion. In summary, each of the five *GRHL3* mutations appeared to encode a protein with dominant-inhibitory effect that disrupted the development of the periderm through a cell-autonomous mechanism.

***Grhl3*^{-/-} murine embryos have cleft palate at low penetrance**

To identify a potential common mechanism for orofacial clefts in individuals with VWS, we compared the oral phenotype of murine embryos that lack *Irf6* (*Irf6*^{-/-}) to embryos that lack *Grhl3* (*Grhl3*^{-/-}). Wild type embryos at E15.5 had normal oral epithelium and a fully fused palate (Fig. 6A), whereas *Irf6*^{-/-} embryos (n = 4) had extensive epithelial adhesions between the palatal shelves and the lingual, mandibular and maxillary surfaces (Fig. 6B)^{9; 10}. These adhesions prevented the palatal shelves from elevating and led to a cleft palate in all embryos. Similarly, all

Grhl3^{-/-} embryos at E15.5 had bilateral oral epithelial adhesions (n = 6) and one of these embryos had a cleft palate (Fig. 6C). Thus, *Grhl3*, like *Irf6*, is required for palatal development.

To compare the histological changes in these two mutant strains, we immunostained with keratin 6 (Krt6), a marker for the periderm²⁵ and tumor protein p63 (p63), a marker for the basal epithelial layer²⁶. We detected Krt6 in the oral periderm of wild type embryos (Fig. 6D), but Krt6 expression was strongly reduced in the epithelium superficial to the tooth germs in both *Irf6*^{-/-} and *Grhl3*^{-/-} mutant embryos (Fig. 6E,F). Similar results were observed for activated Notch1 (Act N1) (Fig. 10), another protein expressed in the periderm¹¹. Thus, we concluded that both *Irf6* and *Grhl3* were required for proper development of the oral periderm in the mouse.

In addition to its potential role in the periderm, *Irf6* regulates the differentiation of the keratinocytes in the epidermis^{9; 10} and the oral cavity¹¹. In the oral cavity, wild type embryos had a uniform, single layer of basal epithelium (Fig. 6D), whereas the basal layer in *Irf6*^{-/-} embryos was disorganized and thicker, and p63 was ectopically expressed in the cells of the suprabasal layer (Fig. 6E). In *Grhl3*^{-/-} embryos, the basal epithelial layer appeared grossly normal with normal expression of p63 (Fig. 6F). We also looked at the medial edge epithelium (MEE), the epithelium located at the medial edge of the palatal shelves that must dissolve for proper palatal fusion. In wild type embryos (Fig. 6G) and *Grhl3*^{-/-} (Fig. 6I), the MEE dissolved to form a confluent bridge of mesenchymal cells across the palate as shown by the loss of expression of p63. In contrast, while we do not know the exact location of the MEE in *Irf6*^{-/-} embryos, expression of p63 persisted throughout the epithelium of the palatal shelves (Fig. 6H)¹¹. Thus, *Irf6*^{-/-} embryos have at least two problems during palatal development: the presence of oral epithelial adhesions and the failure of the MEE to dissolve. In contrast, *Grhl3*^{-/-} embryos only have oral epithelial adhesions due to the loss of periderm. Since mutations in both these genes

cause VWS, these results are consistent with the hypothesis that abnormal periderm function contributes to CL/P in humans.

The oral phenotypes of *Irf6* and *Grhl3* heterozygous murine mutants are independent

Based on ChIP-seq experiments on a human keratinocyte cell line and epistasis experiments in zebrafish embryos, we hypothesized that *Irf6* and *Grhl3* function in a common pathway^{4;6}. To test for epistasis during murine palatogenesis, we generated embryos that were heterozygous for both *Irf6* and *Grhl3* (*Irf6*^{+/-};*Grhl3*^{+/-}). As expected, we did not observe any oral epithelial adhesions in wild-type embryos (Fig. 7A,D). In *Irf6*^{+/-} embryos we detected bilateral oral adhesions at the tooth germ sites (Fig. 7B). We also observed bilateral epithelial abnormalities in *Grhl3*^{+/-} embryos (Fig. 7E), but they differed from those seen in the *Irf6*^{+/-} embryos in three respects. First, whereas oral adhesions in *Irf6*^{+/-} embryos were more prominent at the tooth germ sites (Fig. 7B), epithelial abnormalities in *Grhl3*^{+/-} embryos were located throughout the oral cavity and most frequently posterior to the tooth germs (Fig. 7E). Second, epithelial abnormalities included oral fusions (Fig. 7E), which do not occur in *Irf6*^{+/-} embryos. Here, we distinguish oral epithelial adhesions from oral fusions histologically. Whereas adhesions have a loss of periderm that allows cell interactions between two adjacent epithelial layers, fusions have a loss of both the periderm and the basal epithelial layers that allows cell interactions between the underlying mesenchymal cells from adjacent tissues. Finally, whereas oral adhesions in *Irf6*^{+/-} occurred most frequently between the mandible and maxilla, oral fusions in *Grhl3*^{+/-} embryos occurred between the mandible and either the palate or the maxilla. In the *Irf6*^{+/-};*Grhl3*^{+/-} double heterozygous embryos, we found oral adhesions at areas superficial to the tooth germ (Fig. 7C), similar to *Irf6*^{+/-} embryos, as well as oral adhesions and fusions posterior to the tooth germ (Fig. 7F), similar to *Grhl3*^{+/-} embryos. Thus, the oral histopathology of the *Irf6*^{+/-};*Grhl3*^{+/-} double

heterozygote embryos provides no evidence for epistasis and suggests that *Irf6* and *Grhl3* function in independent but converging pathways during oral periderm development..

As previously observed in the single knockout *Irf6*^{-/-} and *Grhl3*^{-/-} embryos, we detected a reduction in expression of Krt6 in both heterozygous embryos (Fig. 7G vs 4H,I) and a more apparent reduction of Krt6 in the double heterozygous embryos (Fig. 7J). At higher magnification, the loss in Krt6 staining coincided with the loss of oral periderm cells (Fig. 7K vs 4L-N). We did not detect any change in p63 expression in the *Irf6*^{+/-} embryos (Fig. 7O vs 4P). However, in the *Grhl3*^{+/-} (Fig. 7Q) and the *Irf6*^{+/-};*Grhl3*^{+/-} (Fig. 7R) embryos, we observed a loss of expression of p63, indicating a loss of the basal epithelial cells at the sites of the oral fusions. Again, these molecular data suggest that *Irf6* and *Grhl3* function independently during palatal development.

Although we did not detect epistasis between *Irf6* and *Grhl3* during palatal development, we observed a 12% (6/51) rate of resorbing embryos (Table S3). This frequency was significantly higher than expected (3%, p-value = 0.0008) for the C57Bl/6 murine strain²⁷. In addition, while we observed a Mendelian distribution of pups at birth (postnatal day 0, P0), *Irf6*^{+/-};*Grhl3*^{+/-} pups were significantly under-represented at P21 (p-value = 0.01). Thus, pre-natal and post-natal lethality from crosses that generated the double heterozygous pups suggest positive epistasis between *Irf6* and *Grhl3* at other timepoints and/or tissues during development.

DISCUSSION

Using a combination of whole-exome and Sanger sequencing methods, we identified mutations in *GRHL3* in eight families with VWS that had no causative mutations in *IRF6*, thus demonstrating that, when mutated, *GRHL3* is the gene responsible for VWS at the *VWS2* locus. Although previous studies had found *IRF6* mutations in 70% of families with VWS, there had been very

little evidence for locus heterogeneity. Despite 15 published linkage studies on 49 families from throughout the world ²⁸, only one pedigree demonstrated linkage outside of the *IRF6* locus ¹⁵. Since this family originated from Finland, a relatively isolated population, and since, at that time, only one member of the family had lip pits, the cardinal feature of VWS, the broader impact of this family on VWS genetics was uncertain. However, the finding of causative mutations in seven additional families from broad geographic and phenotypic spectra supports the clinical and biological significance of this locus for VWS, and demonstrates that locus heterogeneity contributes to the genetic architecture of VWS.

The results from our mutation screen also suggest a complex allelic architecture for *GRHL3* in VWS. Based on the precedent of *IRF6*, we hypothesized that VWS due to mutation at the second locus (*VWS2*), would be caused by haploinsufficiency of *GRHL3*. Consistent with this hypothesis, we observed both missense and protein truncation mutations. In addition, the DECIPHER database (Database of Chromosomal Imbalance and Phenotype in Humans using Ensembl Resources) ²⁹ includes a 1.9Mb *de novo* deletion encompassing *GRHL3* in an individual with CP, club foot, developmental delay, prominent forehead, and a thin upper lip. In our small number of cases, we also observed a case of compound heterozygous alleles for *GRHL3* (proband in VWS-III) and another case with a rare variant in both *IRF6* and *GRHL3* (proband in VWS-IV). However, all five *GRHL3* variants used in the zebrafish assay, including both alleles of the compound heterozygote individual, uniformly tested as dominant-negative. If VWS-associated *GRHL3* alleles also have a dominant-negative effect in human tissues, it is not clear why they would be found in a coupled state, how the protein truncation alleles remain stable and whether *GRHL3* participates in protein complexes. Further genetic and biochemical studies will be required to understand the effects of these alleles in human tissues.

The analysis of human phenotypes suggests two clinical hypotheses. First, since individuals with *GRHL3* mutations were more likely to have CP and less likely to have CL/P than individuals with *IRF6* mutations, this association may be used to prioritize these two genes for mutation screens in VWS cases. We note that this association was made from a small number of individuals with *GRHL3* mutations (n = 27) and that 9 individuals originated from one family (VWS-I). However, when we restricted the analysis to a family-based phenotype (n = 8), we observed the same trends, although not achieving statistical significance due to low power. Second, like *IRF6*, common DNA variants in *GRHL3* may also be associated with isolated forms of orofacial clefting³⁰, especially for CP, given the increased likelihood of CP in individuals with a mutation in *GRHL3*. However, multiple genome-wide association studies for CL/P³¹ and one for CP³² have not provided strong evidence for common variants at the *GRHL3* locus. While these studies suggest that common DNA variants in *GRHL3* do not account for significant risk for CL/P or CP, *GRHL3* remains an excellent candidate gene for isolated orofacial clefts.

Finally, our analysis of phenotypes in *Irf6* and *Grhl3* mutant mice identified common and distinct oral abnormalities. Previous studies revealed that *Irf6* deficiency in mice could lead to an orofacial cleft by at least two pathophysiological mechanisms: abnormal periderm differentiation and failure of the medial edge epithelium (MEE) to dissolve^{11;33}. Since the MEE was able to dissolve normally in embryos that lack *Grhl3*, the common feature of *Irf6* and *Grhl3* mutants is failed periderm differentiation, strengthening the previously hypothesized role of periderm in development of the lip and palate.

In conclusion, these studies identify *GRHL3* as the second gene which when mutated leads to Van der Woude syndrome, thus confirming locus heterogeneity for this syndrome. Further, they strengthen the connection between cleft palate and abnormal periderm development. We

anticipate that these findings will improve the molecular diagnostic for VWS and other forms of orofacial clefting

SUPPLEMENTAL DATA DESCRIPTION

Supplemental data include three figures and three tables.

ACKNOWLEDGEMENTS

We greatly appreciate the many individuals affected with VWS, their family members and clinicians for participating in this study. We would like to thank Arianna L. Smith and Mager Scientific for technical assistance; Nicole Patel for the artistic renderings of murine embryos at E13.5 and E15.5; Päivi Lahermo for providing the Finnish controls and Dr. Pat Venta for critiques. Financial support for this research was provided by the Swedish Research Council 521-2007-3133 (MP-J) and 2009-5091 (JK), NIH grants DE021071 (RAC), DE13513 (BCS), F31DE022696 (YAK), DE08559 (JCM), GM008629 (EJL), AR061586 (MD), AR44882 (BA) and the Sigrid Jusélius Foundation (JK).

The authors do not have any conflicts of interest.

WEB RESOURCES

Online Mendelian Inheritance in Man: www.omim.org

Picard toolkit: picard.sourceforge.net

GATK: www.broadinstitute.org/gatk/

Primer3: biotools.umassmed.edu/bioapps/primer3_www.cgi

NHLBI/ESP database: evs.gs.washington.edu/EVS/

UCSC genome browser: genome-euro.ucsc.edu/cgi-bin/hgGateway

MATERIALS AND METHODS

Human DNA samples

DNA samples from 45 families of multiple ethnicities and who were completely sequenced for *IRF6* without identifying a causative mutation were used in this study. All subjects were examined by clinical geneticists or genetic counselors who made diagnoses as described previously¹⁵⁻¹⁷. Written informed consent was obtained for all subjects and all protocols were approved by the local ethical boards in Helsinki (Finland) or in Stockholm (Sweden), or by the Institutional Review Boards at the University of Iowa (U.S.A.). Three hundred and sixty unrelated individuals without a history of oral cleft from the Philippines were used as controls for the *GRHL3/c.1171C>T* Filipino variant, while 561 unrelated Finnish individuals (blood donors) were used as controls for the *GRHL3/c.969-970insTG*, the *PHACTR4/c.1615G>A/rs200581707* and the *KTH12/c.337_363delCCGATCGCGGGACCTCAGGTGGCGGGC* Finnish variants.

Targeted exome sequencing

Genomic DNA from eight affected and three healthy individuals from the *VWS2* Finnish family underwent SureSelect Target Enrichment (Agilent Technologies) in order to perform sequence capture of the exome. Enriched samples were sequenced on an Illumina HiSeq instrument. Reads were aligned to reference sequence with the bwa read mapper¹⁸. A high-quality variant call set was generated based on a best-practice workflow¹⁹, in which we utilized the Picard and Genome analysis toolkit (GATK) for data processing and analysis.

Genotyping

Genotyping of the *GRHL3* c.969-970insTG (Finnish) and c.1171C>T (Filipino) variants, the *PHACTR4*/c.1615G>A/rs200581707 (Finnish) variant, was performed using TaqMan SNP Genotyping Assays (Life Technologies, Grand Island, NY) on the ABI Prism 7900HT or ABI 7500 and analyzed with the SDS 2.3 or SDS 1.4 software (Applied Biosystems, Foster City, CA), respectively. Family relationships for apparently *de novo* variants (c.1171C>T and c.1559_1562delGGAG) were confirmed by genotyping 16 markers distributed across the genome (Table S2). The *KTH12*/c.337_363delCCGATCGCGGGACCTCAGGTGGCGGGC variant was genotyped using PCR amplification using SYBR green labelling of the wild type (100 bp) and the deleted (73 bp) alleles, and checked for their respective melting temperatures/curves.

Mutation screening by Sanger sequencing

Primers for *GRHL3* were designed to amplify the exons of all isoforms of *GRHL3* using Primer3. The exons of all four *GRHL3* transcript variants were screened in a total of 13 PCR amplicons (Table S1). PCR reactions were incubated at 94°C for 5 min followed by 35 amplification cycles (45 s at 94°C, 45 s at 60°C, 45 s at 72°C) and a final extension at 72°C for 7 min. PCR products were sent for sequencing using an ABI 3730XL (Functional Biosciences, Inc., Madison, WI). Chromatograms were transferred to a UNIX workstation, base-called with PHRED (v.0.961028), assembled with PHRAP (v. 0.960731), scanned by POLYPHRED (v. 0.970312), and viewed with the CONSED program (v. 4.0). The effects of missense variants were predicted using the Variant Effect Predictor program²⁰ which generates scores from Polyphen2 and SIFT.

Phenotype Analysis

Affected individuals with *GRHL3* mutations (n = 27) were assigned a phenotype classification of cleft lip with or without cleft palate (CL/P which includes CL and CLP cases), cleft palate (CP), lip pits only, CL/P with lip pits, or CP with lip pits based on the clinical diagnoses. Additional phenotypic classifications described the presence of dental anomalies (hypodontia, dental aplasia, or malocclusion), limb anomalies (syndactyly, polydactyly, club foot or contractures), or popliteal pterygia. From the set of families positive for *IRF6* mutations^{8; 13; 14; 17; 21}, affected individuals were also assigned to the same phenotype classifications (n = 632). Exclusion criteria for this analysis were individuals with a cleft but without identified familial mutation (i.e. potential phenocopies), and individuals diagnosed with VWS without a known *IRF6* or *GRHL3* mutation.

Transfection of human *GRHL3* mutation variants into Zebrafish embryos

Full-length, wild-type human *GRHL3* cDNA variant 4 (v4) was obtained as a cDNA clone from Open Biosystems (MHS1010-9204655) and shuttled by Gateway cloning into the CS2+ destination vector (kindly provided by Dave Turner, University of Michigan). This construct was used for *in vitro* synthesis of wild type *GRHL3* mRNA. Specific mutations from VWS-affected individuals were generated in the *GRHL3* mRNA (v4) using PCR-mediated mutagenesis and the resulting cDNAs engineered into CS2+, resulting in the truncation of the first 6 bp of 5'UTR and the last 70 bp of 3'UTR from mutant variants. These constructs were further used for *in vitro* synthesis of mutant variants of *GRHL3*. These truncations (the first 6 bp of 5'UTR and the last 70 bp of 3'UTR from mutant variants) had no functional consequence, as we tested a similarly truncated and cloned wild type *GRHL3*, and *GRHL3* mRNA synthesized from this construct behaved equivalently to full-length *GRHL3* in the zebrafish-based functional assay.

Capped mRNA was synthesized *in vitro* (mMESSAGE mMACHINE SP6 kit, Ambion Inc., Austin, TX), purified using the MEGAclean kit (Ambion Inc., Austin, TX) and approximately 1 ng of mRNA was injected into wild type zebrafish embryos (Scientific Hatcheries outbred strain, Huntington Beach, USA), at the one cell or, for mosaic injections, at the 16-cell stage. Embryos were fixed at 50% epiboly or corresponding time-point (5-6 hpf), and whole mount *in situ* hybridization for *krt4* was performed as previously described²². Plasmids used for probe synthesis are available upon request. Embryos were injected with biotinylated-dextran (Invitrogen, D-1956) and processed for visualization as previously described⁴. Animal use protocols were approved by the Public Health Service Assurance.

Murine crosses

We crossed mice heterozygous for the *Irf6* genetrap allele (*Irf6*^{+/*gt*}; here referred to as *Irf6*^{+/-})⁹ with mice heterozygous for the *Grhl3* knockout allele (*Grhl3*^{+/-})³ to generate wild type, *Irf6*^{+/-}, *Grhl3*^{+/-} and *Irf6*^{+/-};*Grhl3*^{+/-} double heterozygous embryos. *Grhl3* knockout embryos were obtained by crossing *Grhl3*^{+/-} mice. Presence of a copulation plug was denoted as E0.5. Pregnant dams were injected intraperitoneally with BrdU (Sigma) two hours before euthanization at a dose of 100 mg per gram pregnant dam body weight. Embryos were collected at indicated timepoints and genotyped for *Irf6* and *Grhl3* null alleles as described previously^{3;9}. Both alleles were maintained on a C57BL/6 background. Animal use protocols were approved by the Institutional Animal Care and Use Committees at Michigan State University and the University of California, Irvine, U.S.A.

Morphological, histological and molecular analyses of mice

Gross morphological analysis of the *Irf6*^{+/-} by *Grhl3*^{+/-} cross was done at E13.5, E17.5, P0 and P21. Embryos were then fixed in 4% paraformaldehyde, embedded in paraffin and sectioned at 7 mm intervals. Haematoxylin and Eosin staining was performed as described⁹. For immunostaining, antigen retrieval was performed in sodium citrate, followed by blocking steps in BSA and a Goat anti-mouse Fab fragment (Jackson ImmunoResearch Laboratories, 115-007-003). Primary antibody was incubated overnight at 4°C and secondary antibody was incubated for 1.5 h at room temperature. We used primary antibodies against Keratin 6 (Covance, PRB-190169P), tumor protein p63 (Santa Cruz, 4A4, SC-8431), *Irf6* (Sigma-Aldrich, SAB2102995) and Activated Notch1 (Act N1, Cell Signaling, Val1744, D3B8, 4147S). We used the following secondary antibodies: goat anti-rabbit (Molecular Probes, A21429), goat anti-mouse (Molecular Probes, A11029) and goat anti-rat (Molecular Probes, A11006). Nuclei were stained with DAPI (Invitrogen, D3571) followed by slide mounting in ProLong Gold Antifade Reagent (Invitrogen, P36930).

Imaging

Histological and immunostained sections were imaged with a Nikon Eclipse 90i upright microscope using a Plan APO 10x/0.45 DIC, a CFI Plan Apo Lambda 20x/0.75 and a Plan APO 40x/0.95 DIX M/N2 objectives. A Nikon DS-Fi1 high-definition camera head and a DigitalSight PC-use control unit were used for Haematoxylin and Eosin imaging. A X-Cite Series 120Q laser and a CoolSnap HQ2 photometric camera were used to obtain immunofluorescent images. NIS Elements Advanced Research v3.10 was used for RAW image deconvolution and Adobe Photoshop Elements v9.0 was used for figure formation.

Statistical analysis

Fisher's exact test in STATA (v12.1) was used to compare the frequencies of VWS-associated phenotypes between individuals with *GRHL3* mutations and those with *IRF6* mutations. The threshold p-value for this analysis was calculated using a Bonferroni correction ($p = 0.05; 8$ phenotypes = 0.006). We used Chi-Squared Analysis to compare the observed genotype distributions of mice with the predicted Mendelian frequencies. Previous reports show that resorption rates in C57Bl/6 mice range between 1-3%. We used a two-tailed Fisher's exact test to compare the upper limit of this range with the observed resorption rates.

APPENDIX

APPENDIX

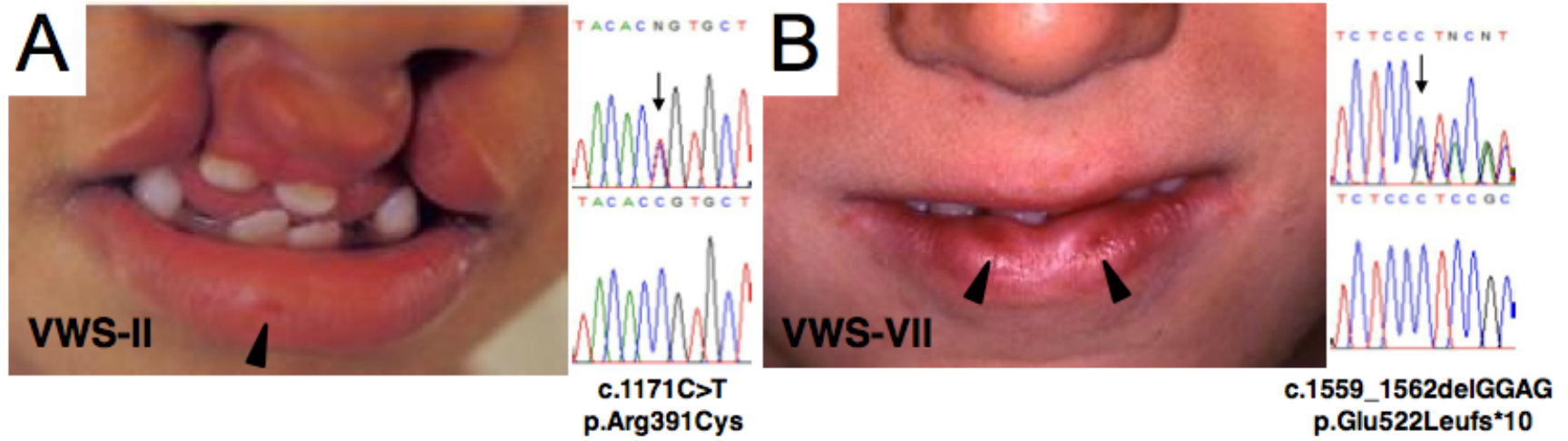


Figure 4: Mutations in *GRHL3* cause Van der Woude syndrome.

Figure 4. (cont'd)

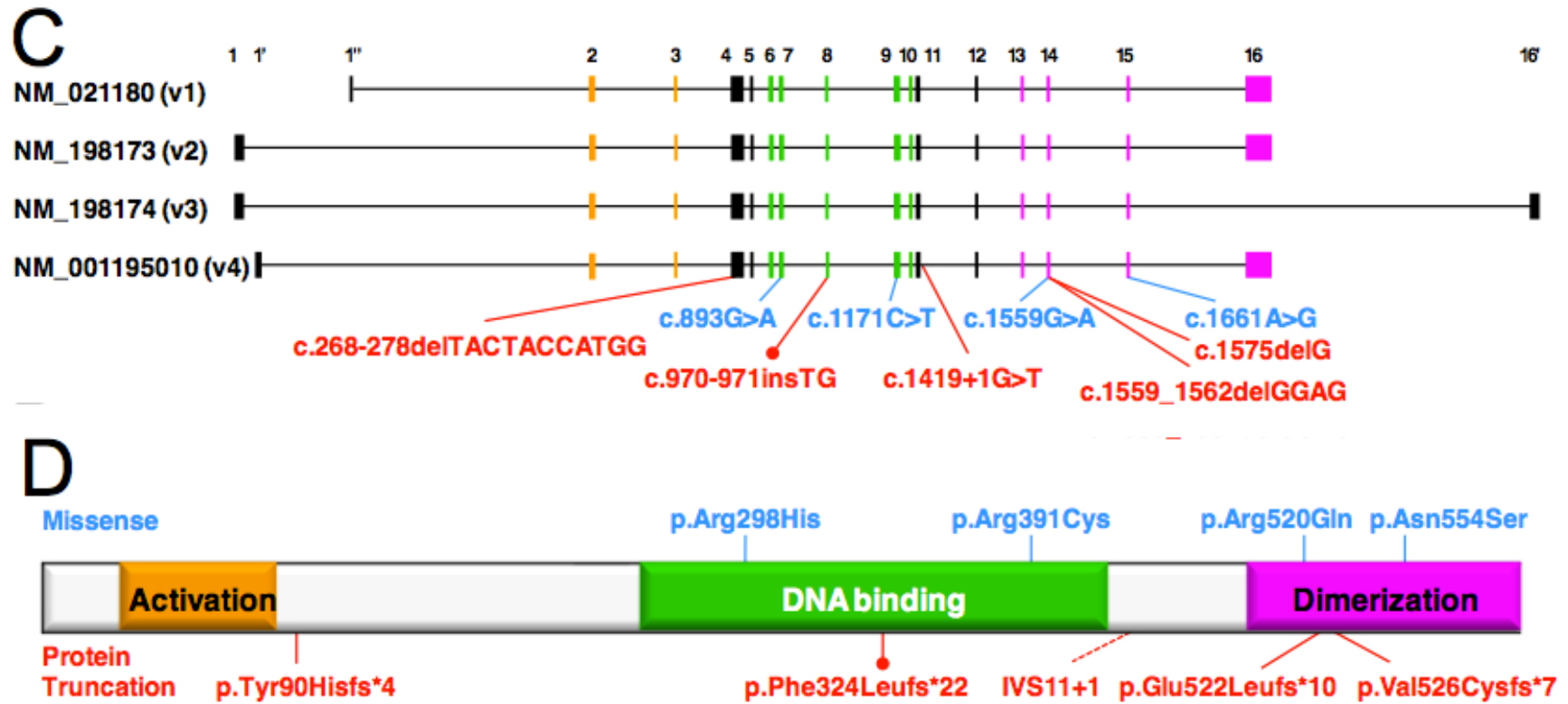


Figure 4. (cont'd)

(A,B) Clinical images of the proband from families VWS-II (A) and VWS-VII (B) display the cardinal feature of VWS, i.e. lip pits (arrowhead). Sequence tracks from each individual are shown to the right with an arrow pointing to the base affected by the mutation. Note that the sequence for c.1559_1562delGGAG is to be read from the reverse strand. (C) *GRHL3* has four alternative transcripts variants, v1 to v4 (UCSC genome browser), with three alternative first exon (1, 1' and 1'') and two alternative last exons (16 and 16'). Translation starts in the first exon of each variant except for v4 where translation starts in exon 2, and stops in the last exon of each variant. The genomic location and cDNA change of each of the nine mutations observed are indicated (according to v3, NM_198174.2). The mutation found in the original Finnish family (VWS-I) is indicated by a filled-circle. Colors for the exons are corresponding to their coding for the GRHL3 protein domains. (D) Schematic representation of the *GRHL3* protein product v2, (NP_937816) with at scale, the three known protein domains: the transactivation (orange), the DNA binding (green) and the dimerization (pink) domains. The position of each change in the protein sequence is also indicated. Please note that as no mutation was found in exon 16, the denomination for each amino acid changes is valid both in v2 and v3. More details of the v2 full protein sequence can also be found in Fig. 9.

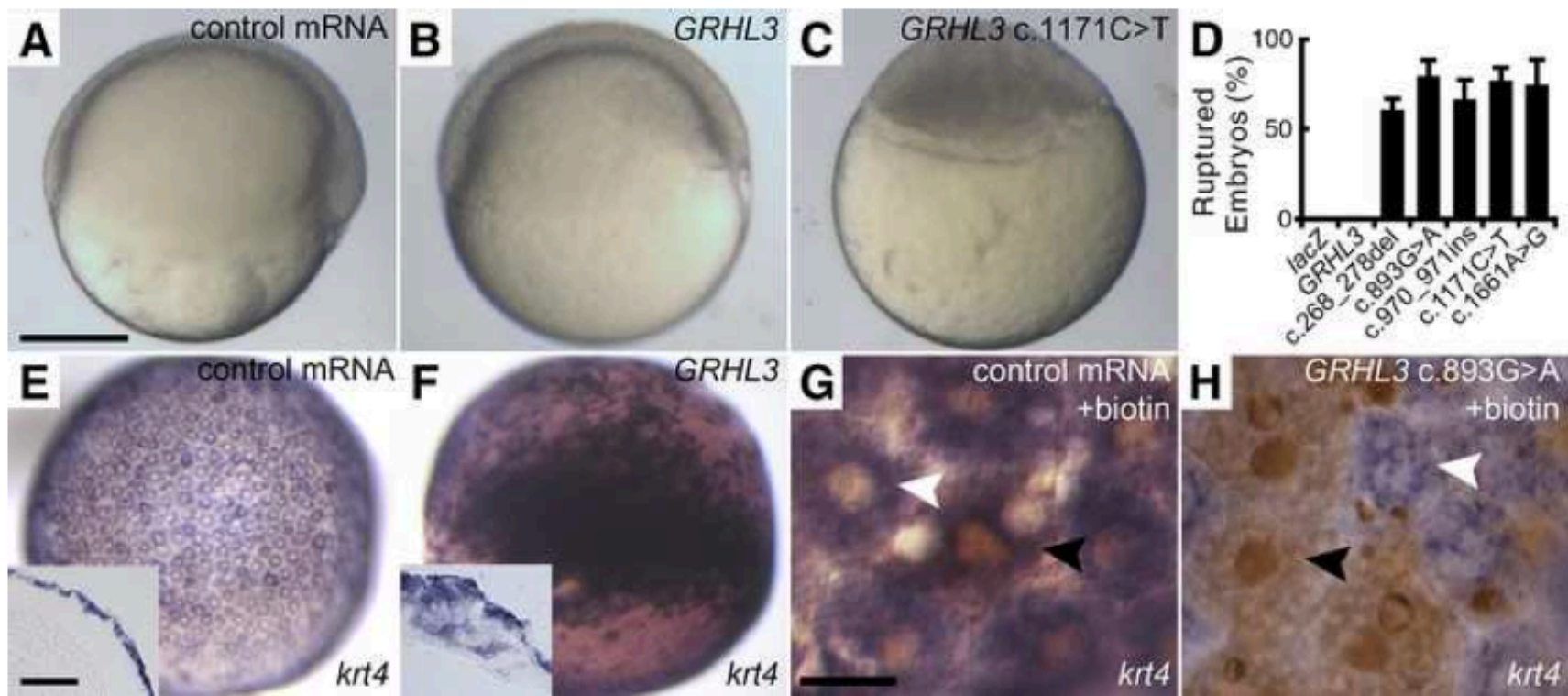


Figure 5: VWS-associated alleles of *GRHL3* disrupt the development of the periderm when expressed in zebrafish embryos.

Figure 5. (cont'd)

(A-C) Lateral views of live sibling embryos injected with indicated mRNA. Embryo shown in C, injected with the *GRHL3* mRNA carrying the c.1171C>T mutation, ruptured through the animal hemisphere shortly after the image was taken (67% [n = 48] of wild type *GRHL3*-injected embryos reached at least 50% epiboly stage, while 76% [n = 115] of mutant-injected embryos burst without initiating epiboly). (D) Histogram showing fraction of embryos that ruptured when injected with indicated mRNA. Percentage is the average from 3-4 separate experiments of 20-40 embryos each. (E,F) Animal pole views of embryos injected with indicated mRNA and processed to detect *krt4* expression. Insets, cross sections of the same embryos showing (E) *krt4* expression confined to the periderm and (F) ectopically in deep cells. (G,H) Animal pole views of mosaic embryos injected with mRNA and biotinylated-dextran at 16-cell stage, fixed at shield stage, and processed for *krt4* expression (blue) and biotin distribution (brown). Periderm cells possessed (black arrowhead) or lacked (white arrowhead) biotin stain, demonstrating that they were, or were not, derived from an RNA injected cell, respectively. Daughter cells derived from the cell injected with the c.893G>A mutant variant of *GRHL3* lack *krt4* expression. Scale bars represent 500 μm (A-C,E,F), 100 μm (E,F inset), and 20 μm (G,H).

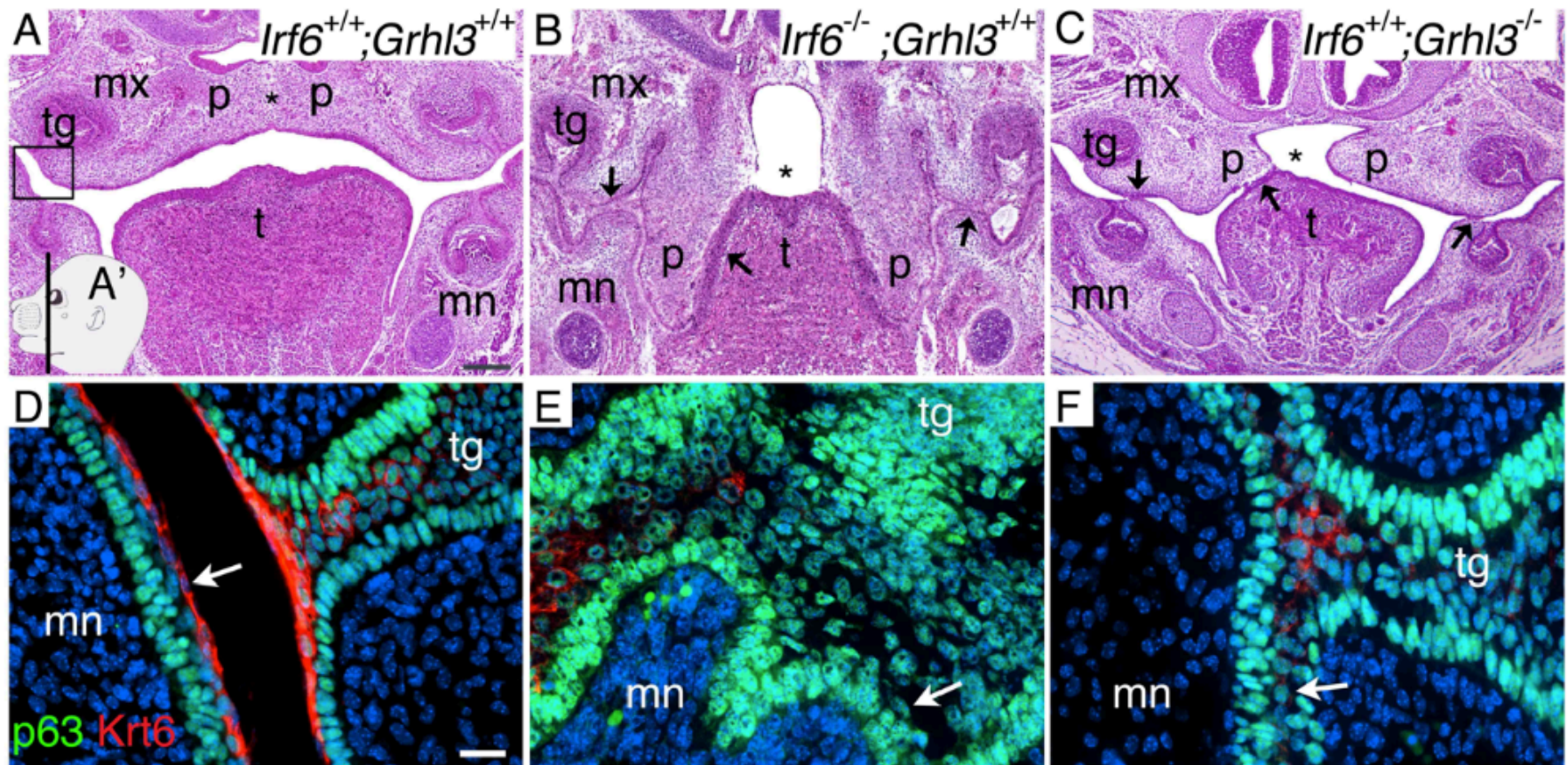


Figure 6: *Grhl3* is required for murine periderm and palatal development.

Figure 6. (cont'd)

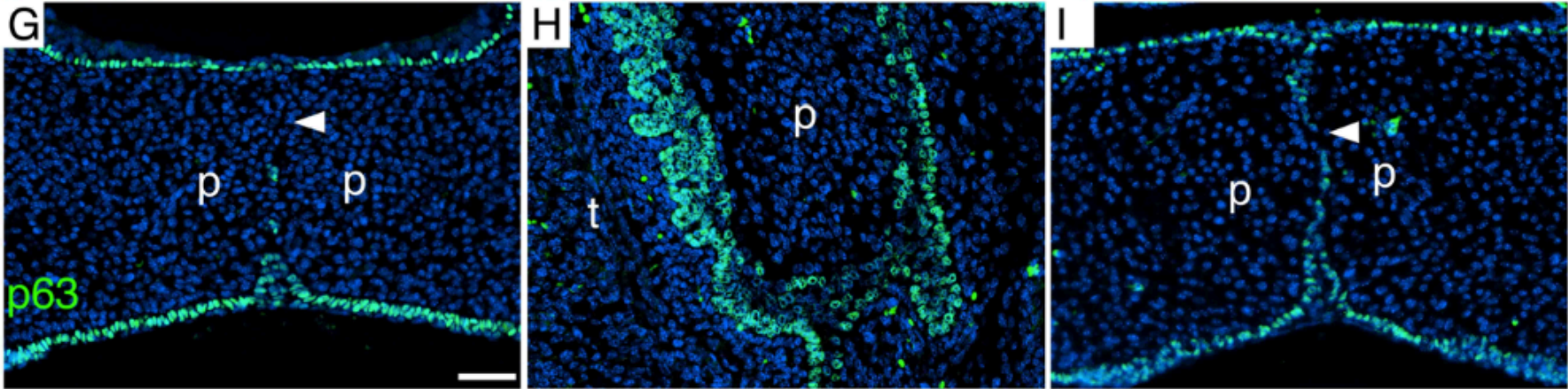


Figure 6. (cont'd)

(A-C) Haematoxylin and Eosin staining of coronal sections of posterior palate at E15.5 (A'). Wild type embryos showed complete fusion of palatal shelves (*) (A). In contrast, *Irf6*^{-/-} embryos have bilateral oral adhesions (arrows) and a fully penetrant cleft palate (*) (B). Similarly, *Grhl3*^{-/-} embryos have bilateral oral adhesions (arrows) (C). However, in *Grhl3*^{-/-} embryos, adhesions were restricted to areas superficial to the tooth germ and palatal surfaces, and a cleft palate was observed in 1 of 6 embryos (*) (C). (D-F) Immunostaining for Krt6 (red) and p63 (green). Krt6 was expressed uniformly in the periderm superficial to the tooth germ (arrow) of wild type embryos (D) (from boxed structure in A), but was very weakly expressed in *Irf6*^{-/-} (E) and *Grhl3*^{-/-} (F) embryos. P63 was expressed uniformly in the basal epithelium of wild type (D) and *Grhl3*^{-/-} (F) embryos, but was expressed ectopically in suprabasal cells in *Irf6*^{-/-} embryos (E). (G-I) Loss of p63 expression marks normal dissolution of the medial edge epithelium (MEE) (arrowhead) in wild type (G) and *Grhl3*^{-/-} (I) embryos. In contrast, p63 expression persisted around the palatal epithelium in *Irf6*^{-/-} embryos (H). Nuclei are counterstained with DAPI (blue) (D-I). Scale bars are 2 mm for images A-C; 20 mm for D-F; 50 mm for G-I. Labeled oral structures are mandible (mn), maxilla (mx), palatal shelf (p), tongue (t) and tooth germ (tg).

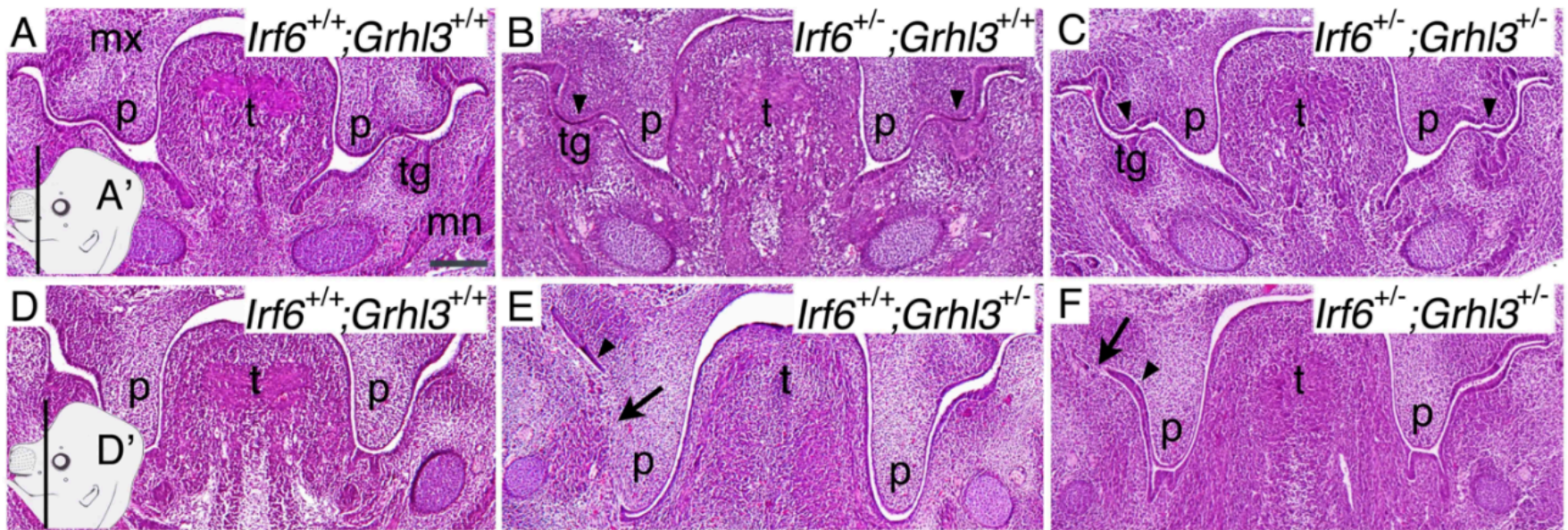


Figure 7: No evidence for genetic interaction between *Irf6* and *Grhl3* in murine palatal development.

Figure 7. (cont'd)

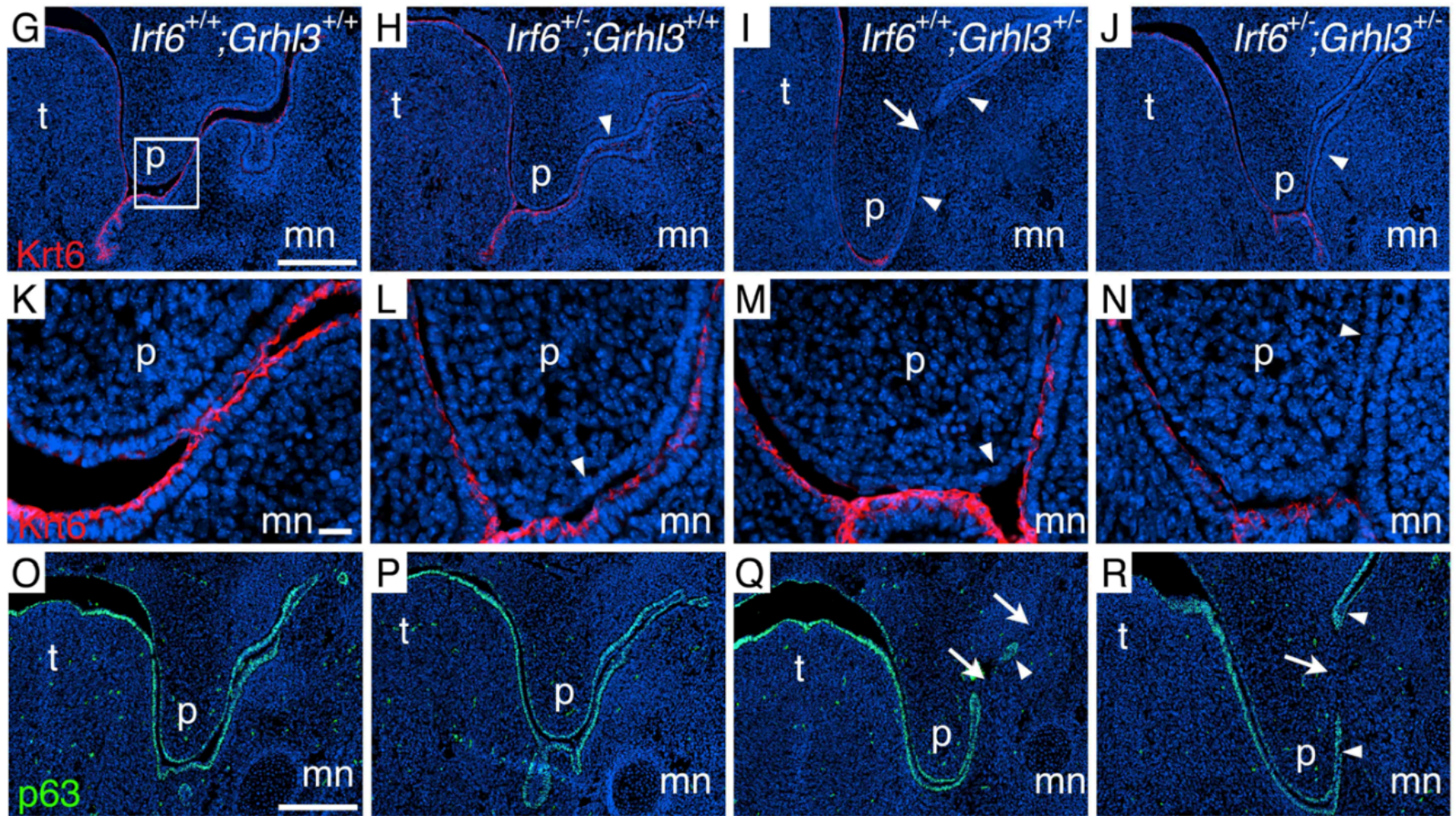


Figure 7. (cont'd)

Haematoxylin and Eosin staining of coronal sections of E13.5 palate at (A') and posterior (D') to the tooth germ. Compared to wild type embryos (A,D), *Irf6*^{+/-} embryos had bilateral oral adhesions (arrowheads) at the tooth germ site (B). In contrast, *Grhl3*^{+/-} littermates had oral adhesions (arrowheads) and fusions (arrow) located predominantly posterior to the tooth germ (E). *Irf6*^{+/-};*Grhl3*^{+/-} embryos (C,F) have oral adhesions (arrowheads) at the tooth germ (C) as well as adhesions (arrowheads) and fusions (arrow) posterior to the tooth germ (F). Krt6 immunostaining (red) of the oral periderm (G-N). Compared to wild type embryos (G and enlarged in K), Krt6 expression in *Irf6*^{+/-} (H, enlarged in L), *Grhl3*^{+/-} (I, enlarged in M), and *Irf6*^{+/-};*Grhl3*^{+/-} (J, enlarged in N) embryos was markedly reduced along the oral surface of the palatal shelves and the mandible. Loss of Krt6 expression coincides with oral adhesions (arrowheads) and fusions (arrow) (G-N). P63 immunostaining (green) of the basal epithelium was continuous in wild type (O) and *Irf6*^{+/-} (P) embryos. In contrast, p63 staining of *Grhl3*^{+/-} (Q) and *Irf6*^{+/-};*Grhl3*^{+/-} (R) embryos was discontinuous. Oral fusions are seen between surfaces of the palate and mandible with mesenchymal communication (arrows) punctuating islands of p63 positive epithelial cells (arrowheads). Scale bars are 2 mm (A-F, G-J and O-R) and 20 mm (K-N). Labeled oral structures are mandible (mn), maxilla (mx), palatal shelf (p), tongue (t) and tooth germ (tg).

Table 1: *GRHL3* mutations in eight Van der Woude syndrome families

VWS pedigree	Origin	DNA change^b	Protein change^d	Genomic position^f	Exon	<i>De novo/ Familial</i>
I^a	Finland	c.970_971insTG	p.Phe324Leufs*22	1:24666175	8	Familial
II	Philippines	c.1171C>T	p.Arg391Cys ^c	1:24668728	9	<i>De novo</i>
III	Israel	c.[268_278delTACTA CCATGG];[1661A>G] ^c	p.[Tyr90Hisfs*4];[Asn554Ser] ^c	1:24662973 -24662983; 24676579	4 15	Familial
IV	Pakistan	c.893G>A	p.Arg298His ^e	1:24664534	7	N/A
V	U.K.	c.1419+1G>T	Splice donor site IVS11+1	1:24669516	IVS11	Familial
VI	U.S.A.	c.1559G>A	p.Arg520Gln ^e	1:24673973	14	N/A
VII	Swedish	c.1559_1562delGGAG	p.Glu522Leufs*10	1:24673973 -24673976	14	<i>De novo</i>
VIII	U.S.A./ African American	c.1575delG	p.Val526Cysfs*7	1:24673989	14	Familial

Table 1. (cont'd)

^a Family originally studied by linkage analysis in ¹⁵ and presently, by exome sequencing

^b Position on *GRHL3* cDNA variant 3 (v3) NM_198174.2

^c Mutations occurring in the same family but on separate chromosomes as indicated

^d Position on *GRHL3* protein product NP_937817.3

^e Missense mutation predicted to be damaging by Polyphen2 and SIFT using the Variant Effect Predictor program

^f Position according to the human genome reference hg19

N/A Not applicable as parent DNA unavailable

Table 2: Comparison of VWS phenotypes caused by mutations in *IRF6* and *GRHL3*

	Has Phenotype?	CL/P^a	CP	Cleft only^b	Lip Pits	Lip Pits Only	Dental anomalies^c	Limb defects^d	Pterygia^e
<i>GRHL3</i> (n = 27)	Yes	3	19	12	14	5	2	2	0
	No	24	8	15	13	22	25	25	27
	%	11	70	44	52	19	7	7	0
<i>IRF6</i> (n = 632)	Yes	267	159	141	445	158	70	45	10
	No	365	473	491	187	474	562	587	622
	%	46	27	24	76	27	12	8	2
p-value		0.001	2.0×10 ⁻⁶	0.02	0.05	0.65	0.76	1	1

^a Includes cleft lip (CL) and cleft lip and palate (CLP)

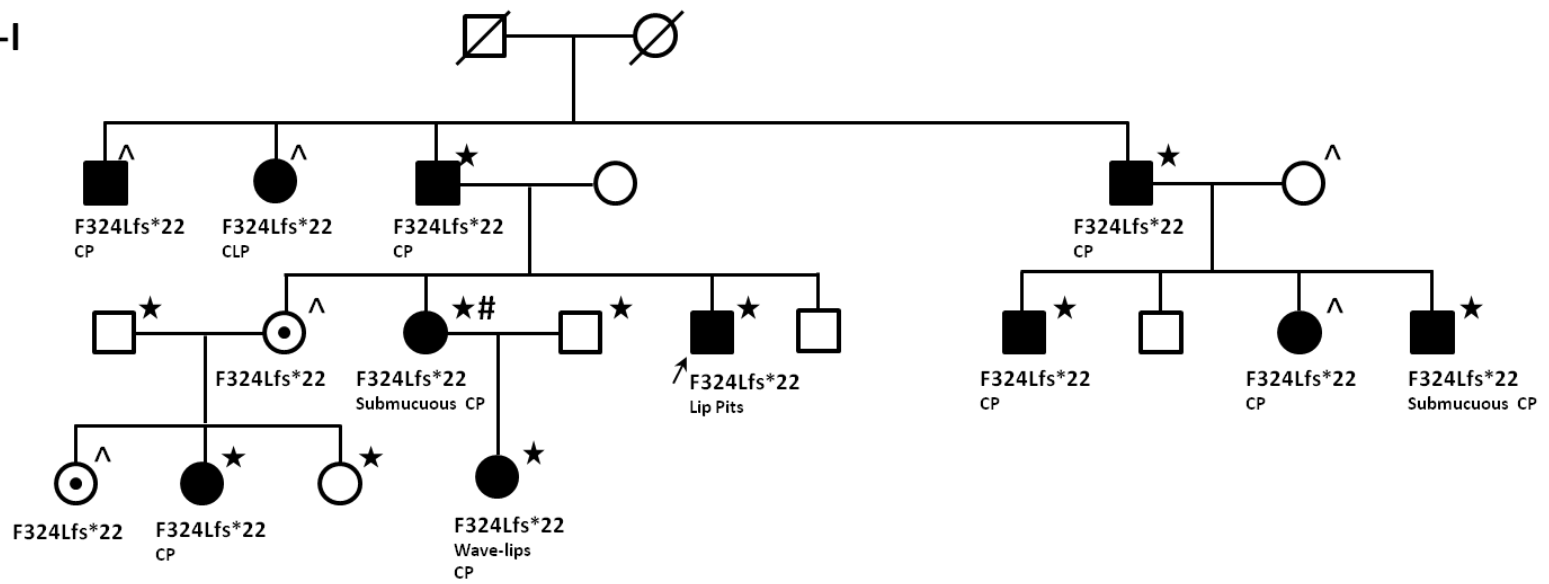
^b Includes cleft palate (CP), CL or CLP but without lip pits.

^c Dental anomalies include hypodontia, dental aplasia, and malocclusion

^d Includes syndactyly, polydactyly, club foot, contractures and pterygium

^e Only pterygia coun

VWS-I



VWS-II

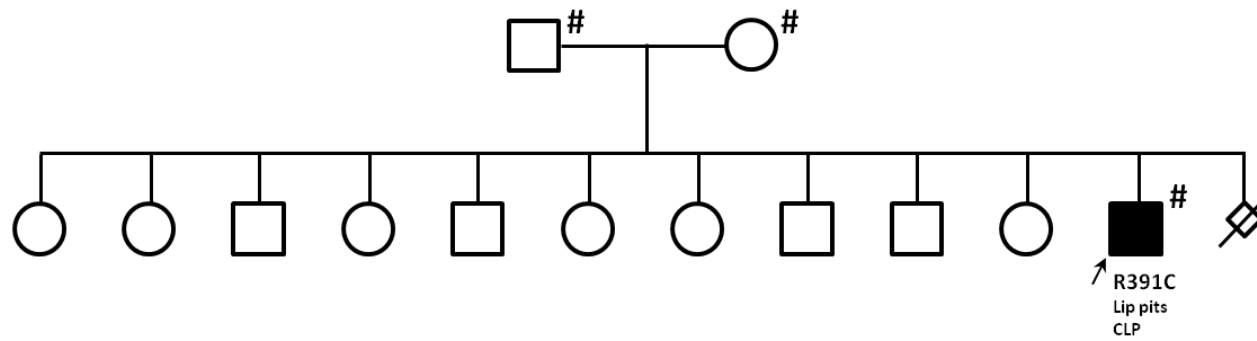
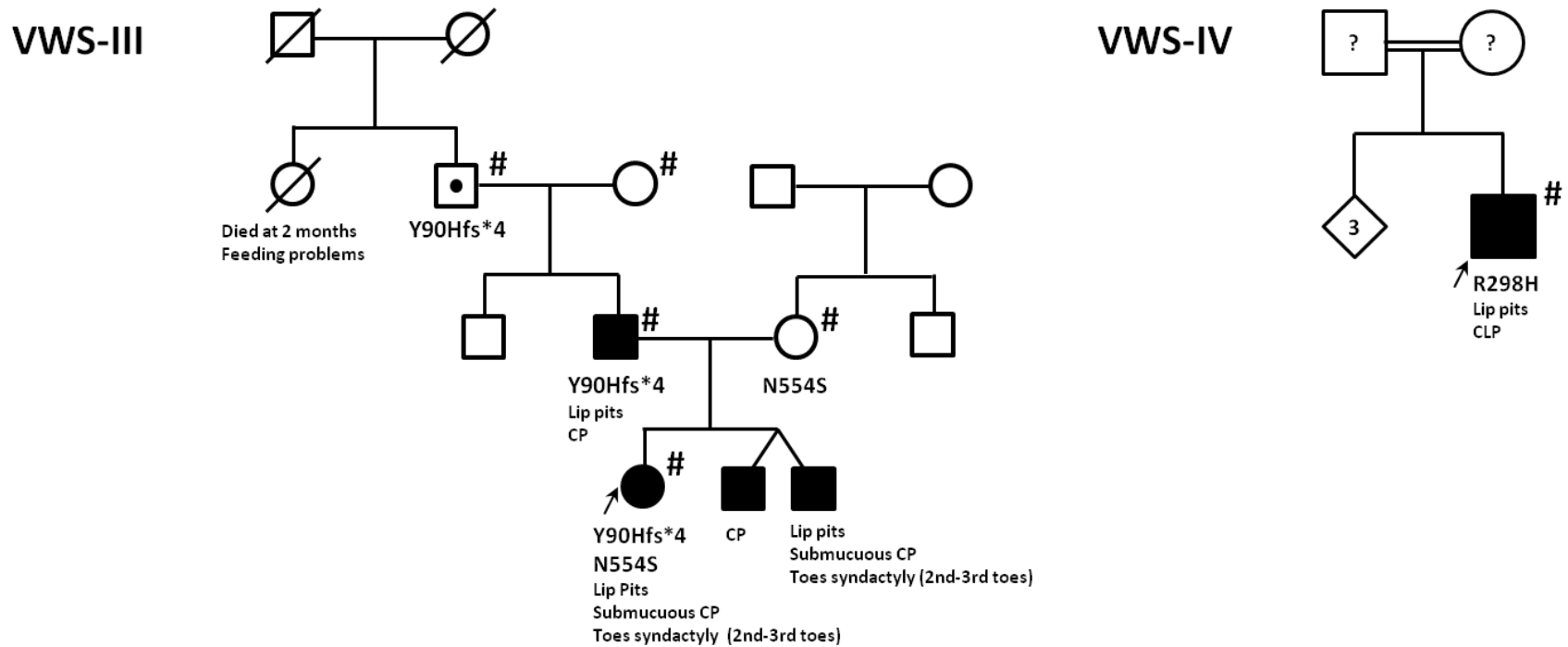


Figure 8: Pedigrees of the eight VWS families with *GRHL3* mutation.

Figure 8. (cont'd)



- ★ Exome sequenced and TaqMan verified
- ^ TaqMan genotyped
- # Sanger sequenced
- *GRHL3* mutation carrier
- ? Unknown phenotype
- ↗ Proband

- CP cleft palate
- CLP cleft lip and palate

Figure 8. (cont'd)

VWS-V

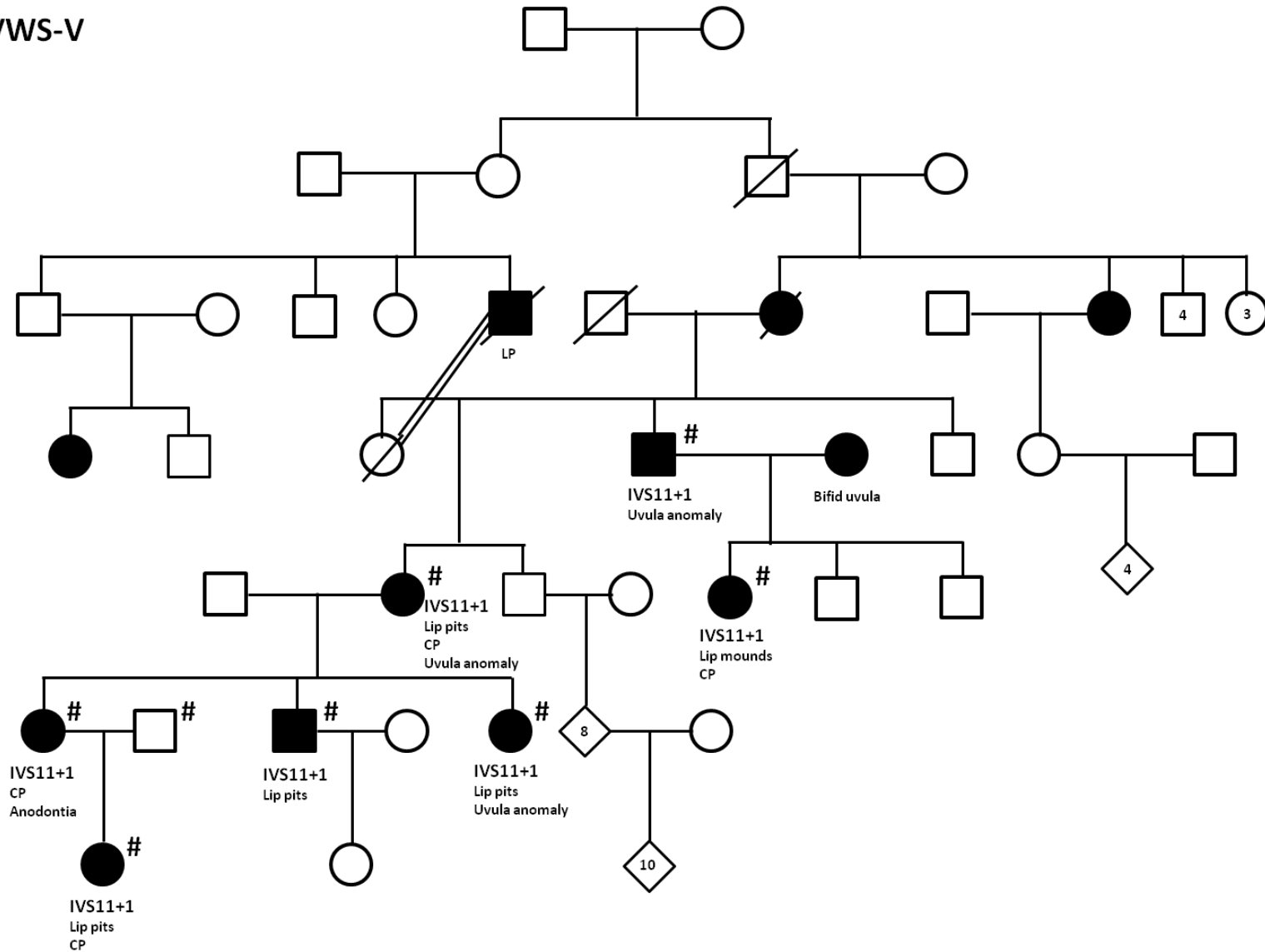
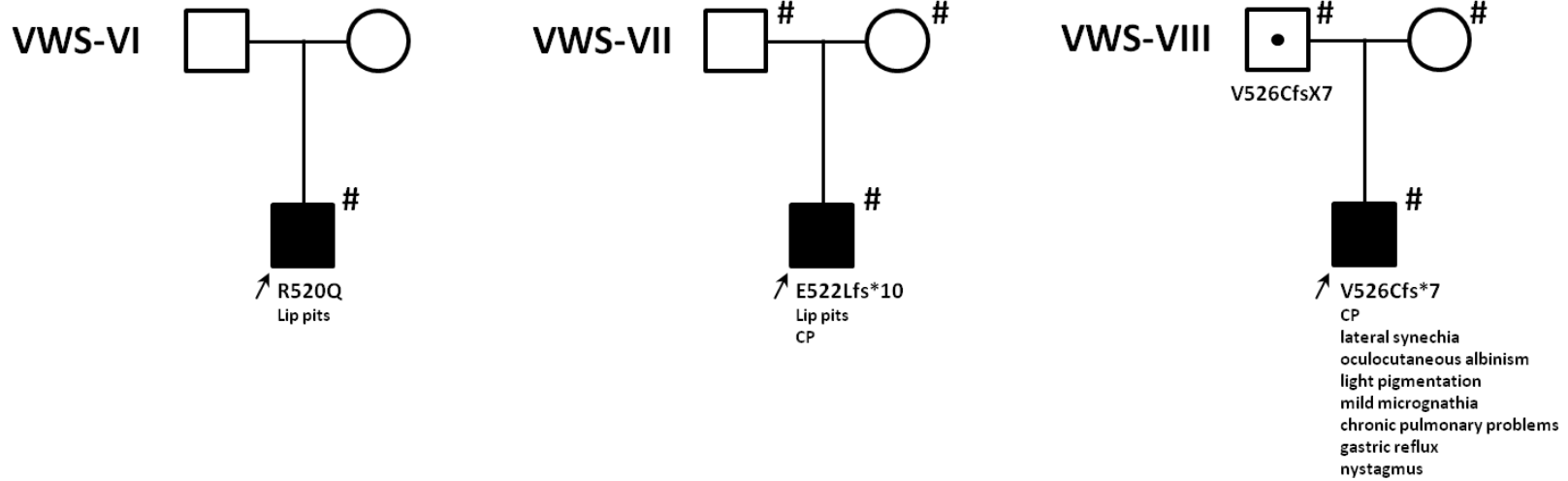


Figure 8. (cont'd)



- ★ Exome sequenced and TaqMan verified
- ^ TaqMan genotyped
- # Sanger sequenced
- *GRHL3* mutation carrier
- ? Unknown phenotype
- ↗ Proband

- CP cleft palate
- CLP cleft lip and palate

Figure 8. (cont'd)

In each family, the corresponding *GRHL3* mutation is named under each individual where it is detected. Mutations were detected by whole-exome sequencing (* in VWS-I only), TaqMan genotyping (^) or Sanger sequencing (#). Mutation carriers without any detected phenotypic characteristics of VWS are indicated with a black dot in their symbol. Phenotypical characteristics of affected individuals are cleft palate (CP), cleft lip and palate (CLP) or unknown (?). The proband in VWS-IV has been shown to be carrier of a rare variant in *IRF6* (K80R)¹. VWS-I was previously described in², VWS-IV in¹ under the denomination VWS-SM13 and VWS-VII in³ under the denomination VWS-12.

Figure 9. (cont'd)

The alignment was done with the input protein sequences from human (NP_937816 for H.s.GRHL3v2, Homo sapiens variant 2), Mouse (NP_001013778.1 for M.m.Grh13, Mus musculus) and zebrafish (XP_001332938.3 for D.r.Grh13, Danio rerio) and using Clustal Omega 1.1.0 software (www.ebi.ac.uk/Tools/msa/clustalo). Amino acids conserved in the 3 species, are denoted by a star below the alignment. In the human protein sequence, the corresponding coding exons are numbered 1 to 16 and are identifiable by a blue or a black protein sequence. Amino acids in red are encoded by two neighboring exons. In the human GRHL3 protein sequence, the three known protein domains are underlined in orange for the transactivation domain (exons 2 and 3, amino acids 25-74), in green for the DNA-binding domain (exons 6 to 10, amino acids 230-423) and in pink for the dimerization domain (exons 13 to 16, amino acids 493-602). For each of the exonic mutations/variants detected in our set of families, the first amino acid affected by the mutation is labeled in red (protein truncation) or in green (missense), and a red arrow indicates the location of the splice site mutation IVS11+1 (from VWS-V). The known repressive and activating protein domains of the murine Grh13 are underlined in the mouse sequence by a continuous line (repressive, amino acids 1-102 and 296-603) or dotted line (activating, amino acids 102-296)⁴. A blue arrow above human exon 2 indicates the start of the GRHL3 protein produced by variant 4 (v4), and used in the zebrafish experiments.

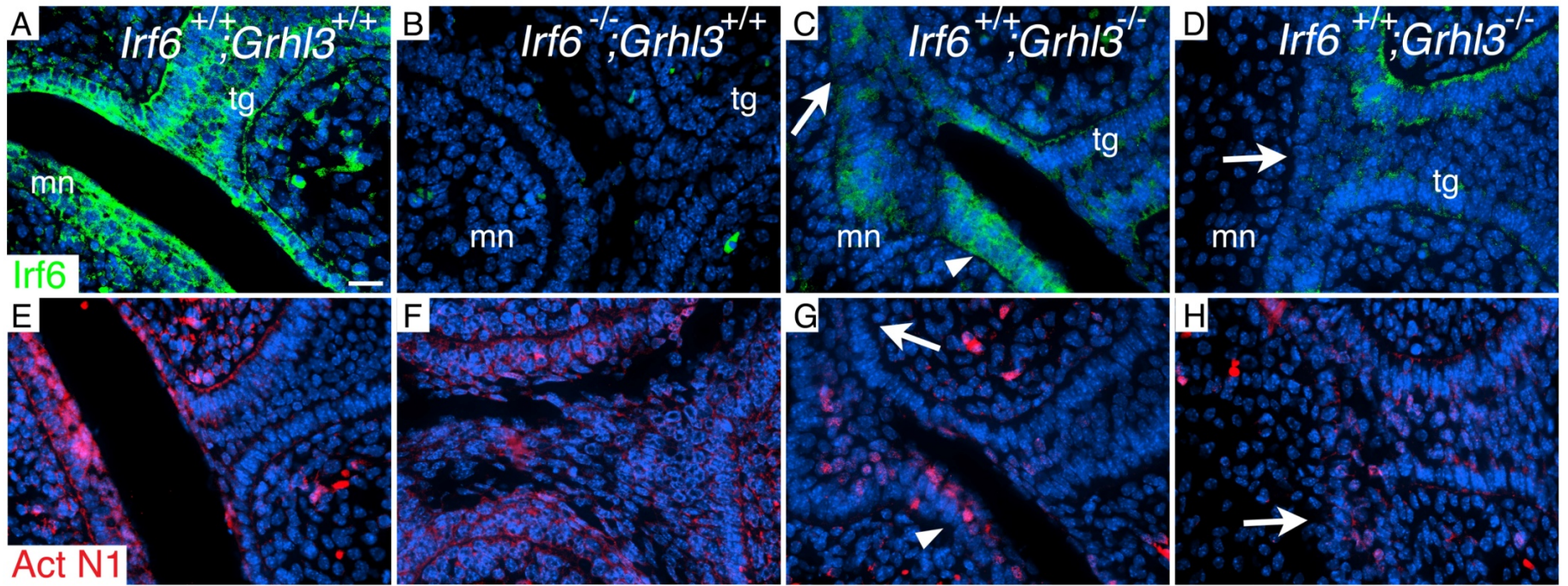


Figure 10: Molecular changes in the oral epithelium of *Irf6*^{-/-} and *Grhl3*^{-/-} embryos.

Figure 10. (cont'd)

Comparison of expression in E15.5 wild type (A,E), *Irf6*^{-/-} (B,F) and *Grhl3*^{-/-} (C,D,G,H) embryos. Images in columns 3 and 4 are taken at the tooth germs sites in two different *Grhl3*^{-/-} embryos to illustrate the dynamic changes in gene expression in areas without (C,G) and with oral adhesions (D,H), respectively. *Irf6* expression is seen in epithelial cells of the tooth germ and oral epithelium in wild type embryos (A) but absent in *Irf6*^{-/-} embryos (B). *Irf6* expression is detected in the oral epithelium (arrowhead) of *Grhl3*^{-/-} embryos, but reduced at sites of oral adhesion (arrow) (C,D). Activated Notch1 (Act N1) is seen in the oral periderm of wild type embryos (E) while it is undetectable in *Irf6*^{-/-} littermate embryos (F). *Grhl3*^{-/-} embryos (G,H) show loss of Act N1 in areas of oral adhesion (arrow) but not in adjacent healthy epithelium (arrowhead). Scale bar is 20 μm (A-H). Labeled oral structures are mandible (mn) and tooth germ (tg).

Table 3: Human *GRHL3* primers used in Sanger sequencing mutation screening

<i>GRHL3</i> exons		Primer Sequence^a
1 and 1'	F	CTCACCAAGGAAGGAATTGG
	R	TAGCTTGAGACTGGGGCTTG
1''	F	GTCTTAGCCGAGCAGCCATAG
	R	GTAGTGGATTTGGGAACCTCCT
2	F	GTGGCAGGAAGAGGCAGTTTC
	R	CAAAGGCCAGAGATGAGG
3	F	AAAGCTGCAGGAGGGGATT
	R	TCAGCACTGTGCCTCCTGT
4 and 5	F	GCATGCTGGATGGACCTAAA
	R	TTCATCCCCCACTTCTCATT
6 and 7	F	TTTTCCAAGGTCAAACAGCA
	R	GACAGAGGTCAGAGCCAGGT
8	F	GAGTGAGGCCAGTTTTTAATG
	R	CGTCGGAGCAAATGACACTA
9, 10 and 11	F	CTTGGCAGTCTAGCGGAAAC
	R	GAAGCCTCCTCTTTGTGTGC
12	F	CTGAGCAGAATGGGCTAGAA
	R	AGGCGTGTGGTTGTTTCTCT
13 and 14	F	TGATGGGCTAAGGGACTCAC
	R	GATAACATCGCAGAGGCACA
15	F	GCACACCCAGATGTTAATGG
	R	AGAGGTGACCAGTGGCTTTG
16	F	ACCACATCCCCTCTTCCATT
	R	TAGCCATCTCTTCCAGCAGAC
16'	F	TTGCTTCTGATACTCCCCACTT
	R	CAGCCCTCTGCTTTTCTCTG

^a All primers had a melting temperature of 61°C

Table 4: Genomic SNPs used for confirming *de novo* mutations

SNP	Chromosomal band
rs1051614	1q21.3
rs10204426	2p11.2
rs237887	3p26.1
rs1063499	5p13.1
rs654351	6p24.3
rs1366883	7q21.13
rs4458901	8p23.2
rs2515617	9q31.1
rs2136892	10q21.1
rs1729410	11q23.3
rs1053900	14q32.2
rs140685	15q12
rs3744262	17p13.1
rs2296241	20q13.2
rs1789953	21q22.3
rs2051616	22q13.31

Table 5: Frequency of genotypes and resorbing embryos from *Irf6*^{+/-}x*Grhl3*^{+/-} cross

	E13.5	E17.5	Embryos	P0	P21	Pups	Total
Litters	3	2	5	6	5	11	32
<i>Irf6</i> ^{+/+} ; <i>Grhl3</i> ^{+/+}	5	3	8	15	5	20	28
<i>Irf6</i> ^{+/-} ; <i>Grhl3</i> ^{+/+}	4	3	7	10	9	19	26
<i>Irf6</i> ^{+/+} ; <i>Grhl3</i> ^{+/-}	11	4	15	12	12	24	39
<i>Irf6</i> ^{+/-} ; <i>Grhl3</i> ^{+/-}	5	4	9	9	1	10	19
Resorbing	3	3	6	N/A	N/A	NA	6 (p=0.0008)
Total	25	14	45	46	27	73	118
p-value	0.18	0.96	0.34	0.60	0.01	0.12	0.06

Figure 5. (cont'd)

We intercrossed mice heterozygous for the *Irf6* genetrapped allele (*Irf6*^{+/^{gt}} here called *Irf6*^{+/⁻}) with mice heterozygous for the *Grhl3* knockout allele (*Grhl3*^{+/⁻}) to generate wild-type (*Irf6*^{+/⁺};*Grhl3*^{+/⁺}) embryos; *Irf6*^{+/⁻} or *Grhl3*^{+/⁻} single mutant embryos; and *Irf6*^{+/⁻};*Grhl3*^{+/⁻} double heterozygous embryos. We detected significant embryonic resorptions at combined E13.5 and E17.5. Furthermore, we found a significant reduction in *Irf6*^{+/⁻};*Grhl3*^{+/⁻} double heterozygous mice at weaning.

BIBLIOGRAPHY

BIBLIOGRAPHY

1. Mace KA, Pearson JC, McGinnis W (2005) An epidermal barrier wound repair pathway in *Drosophila* is mediated by grainy head. *Science* 308:381-385
2. Ting SB, Caddy J, Hislop N, Wilanowski T, Auden A, Zhao LL, Ellis S, Kaur P, Uchida Y, Holleran WM, Elias PM, Cunningham JM, Jane SM (2005) A homolog of *Drosophila* grainy head is essential for epidermal integrity in mice. *Science* 308:411-413
3. Yu Z, Lin KK, Bhandari A, Spencer JA, Xu X, Wang N, Lu Z, Gill GN, Roop DR, Wertz P, Andersen B (2006) The Grainyhead-like epithelial transactivator Get-1/Grhl3 regulates epidermal terminal differentiation and interacts functionally with LMO4. *Dev Biol* 299:122-136
4. de la Garza G, Schleiffarth JR, Dunnwald M, Mankad A, Weirather JL, Bonde G, Butcher S, Mansour TA, Kousa YA, Fukazawa CF, Houston DW, Manak JR, Schutte BC, Wagner DS, Cornell RA (2013) Interferon regulatory factor 6 promotes differentiation of the periderm by activating expression of grainyhead-like 3. *J Invest Dermatol* 133:68-77
5. Sabel JL, d'Alencon C, O'Brien EK, Van Otterloo E, Lutz K, Cuykendall TN, Schutte BC, Houston DW, Cornell RA (2009) Maternal Interferon Regulatory Factor 6 is required for the differentiation of primary superficial epithelia in *Danio* and *Xenopus* embryos. *Dev Biol* 325:249-262
6. Botti E, Spallone G, Moretti F, Marinari B, Pinetti V, Galanti S, De Meo PD, De Nicola F, Ganci F, Castrignano T, Pesole G, Chimenti S, Guerrini L, Fanciulli M, Blandino G, Karin M, Costanzo A (2011) Developmental factor IRF6 exhibits tumor suppressor activity in squamous cell carcinomas. *Proc Natl Acad Sci U S A* 108:13710-13715
7. Tamura T, Yanai H, Savitsky D, Taniguchi T (2008) The IRF family transcription factors in immunity and oncogenesis. *Annu Rev Immunol* 26:535-584
8. Kondo S, Schutte BC, Richardson RJ, Bjork BC, Knight AS, Watanabe Y, Howard E, et al. (2002) Mutations in IRF6 cause Van der Woude and popliteal pterygium syndromes. *Nat Genet* 32:285-289
9. Ingraham CR, Kinoshita A, Kondo S, Yang B, Sajan S, Trout KJ, Malik MI, Dunnwald M, Goudy SL, Lovett M, Murray JC, Schutte BC (2006) Abnormal skin, limb and craniofacial morphogenesis in mice deficient for interferon regulatory factor 6 (*Irf6*). *Nat Genet* 38:1335-1340
10. Richardson RJ, Dixon J, Malhotra S, Hardman MJ, Knowles L, Boot-Handford RP, Shore P, Whitmarsh A, Dixon MJ (2006) *Irf6* is a key determinant of the keratinocyte proliferation-differentiation switch. *Nat Genet* 38:1329-1334

11. Richardson RJ, Dixon J, Jiang R, Dixon MJ (2009) Integration of IRF6 and Jagged2 signalling is essential for controlling palatal adhesion and fusion competence. *Hum Mol Genet* 18:2632-2642
12. Burdick AB, Bixler D, Puckett CL (1985) Genetic analysis in families with van der Woude syndrome. *J Craniofac Genet Dev Biol* 5:181-208
13. de Lima RL, Hoper SA, Ghassibe M, Cooper ME, Rorick NK, Kondo S, Katz L, Marazita ML, Compton J, Bale S, Hehr U, Dixon MJ, Daack-Hirsch S, Boute O, Bayet B, Revencu N, Verellen-Dumoulin C, Vikkula M, Richieri-Costa A, Moretti-Ferreira D, Murray JC, Schutte BC (2009) Prevalence and nonrandom distribution of exonic mutations in interferon regulatory factor 6 in 307 families with Van der Woude syndrome and 37 families with popliteal pterygium syndrome. *Genet Med* 11:241-247
14. Leslie EJ, Standley J, Compton J, Bale S, Schutte BC, Murray JC (2012) Comparative analysis of IRF6 variants in families with Van der Woude syndrome and popliteal pterygium syndrome using public whole-exome databases. *Genet Med* 15:338-344
15. Koillinen H, Wong FK, Rautio J, Ollikainen V, Karsten A, Larson O, Teh BT, Huggare J, Lahermo P, Larsson C, Kere J (2001) Mapping of the second locus for the Van der Woude syndrome to chromosome 1p34. *Eur J Hum Genet* 9:747-752
16. Schutte BC, Bjork BC, Coppage KB, Malik MI, Gregory SG, Scott DJ, Brentzell LM, Watanabe Y, Dixon MJ, Murray JC (2000) A preliminary gene map for the Van der Woude syndrome critical region derived from 900 kb of genomic sequence at 1q32-q41. *Genome Res* 10:81-94
17. Peyrard-Janvid M, Pegelow M, Koillinen H, Larsson C, Fransson I, Rautio J, Hukki J, Larson O, Karsten AL, Kere J (2005) Novel and de novo mutations of the IRF6 gene detected in patients with Van der Woude or popliteal pterygium syndrome. *Eur J Hum Genet* 13:1261-1267
18. Li H, Durbin R (2010) Fast and accurate long-read alignment with Burrows-Wheeler transform. *Bioinformatics* 26:589-595
19. DePristo MA, Banks E, Poplin R, Garimella KV, Maguire JR, Hartl C, Philippakis AA, del Angel G, Rivas MA, Hanna M, McKenna A, Fennell TJ, Kernytzky AM, Sivachenko AY, Cibulskis K, Gabriel SB, Altshuler D, Daly MJ (2011) A framework for variation discovery and genotyping using next-generation DNA sequencing data. *Nat Genet* 43:491-498
20. McLaren W, Pritchard B, Rios D, Chen Y, Flicek P, Cunningham F (2010) Deriving the consequences of genomic variants with the Ensembl API and SNP Effect Predictor. *Bioinformatics* 26:2069-2070
21. Pegelow M, Koillinen H, Magnusson M, Fransson I, Unneberg P, Kere J, Karsten A, Peyrard-Janvid M (2013) Association and mutation analyses of the IRF6 gene in families with

non-syndromic and syndromic cleft lip and/or cleft palate. *Cleft Palate-Craniof J* 2013 Feb 8. [Epub ahead of print]

22. Thisse C, Thisse B (2008) High-resolution in situ hybridization to whole-mount zebrafish embryos. *Nat Protoc* 3:59-69
23. Malik S, Kakar N, Hasnain S, Ahmad J, Wilcox ER, Naz S (2010) Epidemiology of Van der Woude syndrome from mutational analyses in affected patients from Pakistan. *Clin Genet* 78:247-256
24. Chalmers AD, Lachani K, Shin Y, Sherwood V, Cho KW, Papalopulu N (2006) Grainyhead-like 3, a transcription factor identified in a microarray screen, promotes the specification of the superficial layer of the embryonic epidermis. *Mech Dev* 123:702-718
25. Mazzalupo S, Coulombe PA (2001) A reporter transgene based on a human keratin 6 gene promoter is specifically expressed in the periderm of mouse embryos. *Mech Dev* 100:65-69
26. Koster MI, Kim S, Mills AA, DeMayo FJ, Roop DR (2004) p63 is the molecular switch for initiation of an epithelial stratification program. *Genes Dev* 18:126-131
27. Krishnan L, Guilbert LJ, Wegmann TG, Belosevic M, Mosmann TR (1996) T helper 1 response against *Leishmania major* in pregnant C57BL/6 mice increases implantation failure and fetal resorptions. Correlation with increased IFN-gamma and TNF and reduced IL-10 production by placental cells. *J Immunol* 156:653-662
28. Schutte BC, Dixon MJ, Murray JC (2008) Interferon Regulatory Factor 6 (IRF6) is causal in Van der Woude and popliteal pterygium syndromes and contributes to the risk for non-syndromic cleft lip and palate. In: Epstein C (ed) *Inborn Errors of Metabolism* Oxford University Press
29. Firth HV, Richards SM, Bevan AP, Clayton S, Corpas M, Rajan D, Van Vooren S, Moreau Y, Pettett RM, Carter NP (2009) DECIPHER: Database of Chromosomal Imbalance and Phenotype in Humans Using Ensembl Resources. *Am J Hum Genet* 84:524-533
30. Zuccherro TM, Cooper ME, Maher BS, Daack-Hirsch S, Nepomuceno B, Ribeiro L, Caprau D, et al. (2004) Interferon regulatory factor 6 (IRF6) gene variants and the risk of isolated cleft lip or palate. *N Engl J Med* 351:769-780
31. Ludwig KU, Mangold E, Herms S, Nowak S, Reutter H, Paul A, Becker J, et al. (2012) Genome-wide meta-analyses of nonsyndromic cleft lip with or without cleft palate identify six new risk loci. *Nat Genet* 44:968-971
32. Beaty TH, Ruczinski I, Murray JC, Marazita ML, Munger RG, Hetmanski JB, Murray T, et al. (2011) Evidence for gene-environment interaction in a genome wide study of nonsyndromic cleft palate. *Genet Epidemiol* 35:469-478

33. Knight AS, Schutte BC, Jiang R, Dixon MJ (2006) Developmental expression analysis of the mouse and chick orthologues of IRF6: the gene mutated in Van der Woude syndrome. *Dev Dyn* 235:1441-1447
34. Malik S, Kakar N, Hasnain S, Ahmad J, Wilcox ER, Naz S (2010) Epidemiology of Van der Woude syndrome from mutational analyses in affected patients from Pakistan. *Clin Genet* 78:247-256
35. Koillinen H, Wong FK, Rautio J, Ollikainen V, Karsten A, Larson O, Teh BT, Huggare J, Lahermo P, Larsson C, Kere J (2001) Mapping of the second locus for the Van der Woude syndrome to chromosome 1p34. *Eur J Hum Genet* 9:747-752
36. Peyrard-Janvid M, Pegelow M, Koillinen H, Larsson C, Fransson I, Rautio J, Hukki J, Larson O, Karsten AL, Kere J (2005) Novel and de novo mutations of the IRF6 gene detected in patients with Van der Woude or popliteal pterygium syndrome. *Eur J Hum Genet* 13:1261-1267
37. Kudryavtseva EI, Sugihara TM, Wang N, Lasso RJ, Gudnason JF, Lipkin SM, Andersen B (2003) Identification and characterization of Grainyhead-like epithelial transactivator (GET-1), a novel mammalian Grainyhead-like factor. *Dev Dyn* 226:604-617

Chapter 3 -

***Irf6* regulates *Tfap2α* and *Grhl3* in neurulation**

Youssef A. Kousa¹, Huiping Zhu², Allison Ashley-Koch³, Tamara D. Busch⁴, Akira Kinoshita⁵, Walid D. Fakhouri⁶, Raeuf R. Roushangar¹, Trevor J. Williams⁷, Yang Chai⁸, Brad A. Amendt⁹, Jeffrey C. Murray⁴, Simon Gregory³, Gary M. Shaw¹⁰, Alexander G. Bassuk⁴, Richard H. Finnell², Brian C. Schutte¹¹

¹Biochemistry and Molecular Biology Department, Michigan State University, 48824 East Lansing, Michigan, USA

²Dell Pediatric Research Institute, Department of Nutritional Sciences, University of Texas at Austin, 78723 Austin, Texas, USA

³Duke Molecular Physiology Institute, Department of Medicine and Molecular Genetics and Microbiology, Duke University, 27701 Durham, NC, USA

⁴Department of Pediatrics, University of Iowa, 52242 Iowa City, Iowa, USA

⁵Department of Human Genetics, Nagasaki University, Nagasaki, Japan

⁶Department of Diagnostic & Biomedical Sciences, School of Dentistry, University of Texas at Houston, 77054 Houston, Texas, USA

⁷Department of Craniofacial Biology, University of Colorado Denver at Anschutz Medical Campus, 80045 Aurora, Colorado, USA

⁸Center for Craniofacial Molecular Biology, Ostrow School of Dentistry, University of Southern California, 90033 Los Angeles, California, USA

⁹Department of Anatomy and Cell Biology, University of Iowa, 52242 Iowa City, Iowa, USA

¹⁰Department of Pediatrics, Stanford University School of Medicine, 94305 Stanford, California, USA

¹¹Department of Microbiology and Molecular Genetics, Michigan State University, 48824 East Lansing, Michigan, USA

Abstract

Mutations in *IRF6* cause orofacial clefting. A DNA variant in the *IRF6* enhancer *MCS9.7* is present in 30% of the world's population, disrupts a *TFAP2α* binding site and contributes 12% of all orofacial clefting risk. Here, we show that *Tfap2α* positively regulates *Irf6* through *MCS9.7* and that *Irf6* regulates *Tfap2α*. Moreover, we show that a null allele of *Irf6* completely rescues haploinsufficiency of *Tfap2α* and that both over and under-expressing *Irf6* causes defects in neurulation. We also show that *Tfap2α* interacts with *Grhl3* through *Irf6* in caudal neurulation. Finally, we sequence *IRF6* in patients with spina bifida and find a rare coding mutation previously identified in orofacial clefting. This discovery illuminates a novel pathway that regulates orofacial and neural tube defects and may contribute to our understanding of a common, derived *IRF6* regulatory variant that increases risk for orofacial clefting.

Introduction

IRF6 encodes a member of the Interferon Regulatory Factor of transcription factors. While the *IRF* family widely regulates immunity¹, *IRF6* is required for craniofacial, skin and limb development². Mutations in *IRF6* cause two Mendelian orofacial clefting disorders, Van der Woude syndrome (VWS; OMIM#119300) and Popliteal Pterygium Syndrome (PPS; OMIM#119500)². Furthermore, a DNA variant (rs642961) within the *IRF6* locus is found in 30% of the world's population and contributes 12% of all non-

syndromic orofacial clefting risk³. The variant is located 9.7 Kb upstream of *IRF6* within a multi-species conserved enhancer sequence (*MCS9.7*). *MCS9.7* recapitulates endogenous *Irf6* expression^{3,4}. Interestingly, the variant abrogates one of four binding sites for Transcription Factor Activating Protein 2 α (TFAP2 α)³. Mutations in *TFAP2 α* can lead to Branchio-oculo-facial syndrome (BOFS; OMIM#113620) which, like VWS and PPS, can include orofacial clefting, lip pits and cutaneous abnormalities⁵⁻⁷. Prior work in primary keratinocytes shows that both TFAP2 α and TP63 co-regulate IRF6 expression via *MCS9.7*⁸. However, *in vivo* regulation of *MCS9.7* by TFAP2 α has not been demonstrated.

Considering developmental defects in VWS, PPS and BOFS, both *Irf6* and *Tfap2 α* murine models illuminate pathophysiological mechanisms. In the mouse, loss of *Irf6* leads to a hyperproliferative epidermis, craniofacial defects that include a cleft palate and appendage deformities considered secondary to skin adhesions^{9,10}. While the phenotype is dissimilar to *Irf6*, loss of *Tfap2 α* also leads to skin, limb and craniofacial defects^{11,12}. However, loss of *Tfap2 α* also leads to multiple neurulation defects.

Indeed, the *Tfap2 α* knockout mouse is unique in the biomedical literature for what can be considered whole-body clefting. Neurulation defects span the entire neural tube and include kinked tail (closure point 1/posterior neuropore, caudal), bilateral outgrowth of unfused mandibular bones and a bifurcated tongue (split-face malformation) and anencephaly (closure point 2/3, rostral). Strikingly, loss of *Tfap2 α* leads to schisis, or extrusion, of both thoracic and abdominal cavity contents (thoraco-abdomino-schisis). A

role for *Irf6* in neurulation or abdomino-thoracic wall closure has not been shown in mouse or man, even in cases where disrupted gene function leads to VWS and PPS. Also, a role for *TFAP2α* in human neural tube development has not been in BOFS or isolated spina bifida.

Many of the biological functions attributed to *Tfap2α* and *Irf6* are derived from their function in skin, an abundant and accessible tissue. Among epidermal transcription factors, *Irf6* is unique because it has been reported to have both transcriptional and post-translational regulation of down-stream targets. One prominent transcriptional target of *Irf6* in zebrafish is *Grhl3*¹³. Like *Tfap2α*, loss of *Grhl3* leads to skin, limb, craniofacial and both rostral and caudal neural tube defects¹⁴. Significantly, we recently showed that mutations in GRHL3 can also lead to Van der Woude Syndrome (VWSII; OMIM# 606713) (Peyrard, 2013). On the other hand, *TP63* drives *Irf6* expression via *MCS9.7*¹⁵ and *IRF6* down-regulate *TP63* via the proteasome¹⁶. Importantly, mutation in *TP63* also lead to dominantly inherited orofacial clefting in Ectrodactyly, Ectodermal Dysplasia (EEC; OMIM#604292)¹⁷.

In this work, we dissect the nature of *Tfap2α-Irf6-Grhl3* genetic interaction *in vivo*. We show that *Tfap2α* is necessary for *MCS9.7* enhancer activity in the mouse, a genetic relationship that may explain orofacial clefting risk within the *IRF6* locus. We titer *Irf6* dose *in vivo* and find that reducing *Irf6* expression leads to a curly tail, a caudal neural tube defect, through regulation of *Tfap2α* and *Grhl3*. Furthermore, we find that 11% of embryos over-expressing *Irf6* have craniofacial and neural tube defects (NTD) that

phenocopy *Tfap2α* heterozygous and knockout embryos. Moreover, while loss of *Irf6* has multiple pathophysiological consequences, we report here that a null allele of *Irf6* completely rescues craniofacial and neural tube defects in *Tfap2α* haploinsufficiency. Finally, to assess the role of *IRF6* in human neurulation, we sequenced 92 individuals with spina bifida. We found a rare missense mutation at a highly conserved amino acid in exon 9 of *IRF6* (D427Y), previously reported in orofacial clefting but not in any control database. However, sequencing of the *IRF6* 3'UTR shows no association with spina bifida risk. Our discovery illuminates *Tfap2α-Irf6-Grhl3* as a novel gene regulatory network in both orofacial and neural tube development.

Results

***Tfap2α* is necessary for *MCS9.7* activity and *Irf6* expression**

We previously showed that *Tfap2α* binds *MCS9.7* *in vitro*. Additional work in primary keratinocytes shows that *Tfap2α* and *Trp63* co-regulate *Irf6* expression via *MCS9.7*. Here, we predict that *Tfap2α* is necessary for *MCS9.7* expression *in vivo*. We analyzed changes in *MCS9.7* activity with a *LacZ* reporter construct crossed into the *Tfap2α* knockout mouse (N=66; genotype distribution based on Mendelian genetics, not statistically significant, p-value = 0.71; Supp Table 9). At E17.5, we found gross changes in β-Gal staining, most prominently differing from wildtype littermates in limb, skin and craniofacial structures (Fig. 11a,b). At E13.5, we detected more subtle differences in β-Gal activity (Fig. 11c,d). Specifically, as opposed to the linear, evenly stained tail of Wt embryos, *Tfap2α*^{-/-} embryos either lacked or had punctuate staining near the distal segments of the closed posterior neuropore. Unlike E17.5 embryos, the intensity of the

LacZ stain at E13.5 did not differ in cutaneous and limb structures. Combined, these results suggest that *Tfap2α* is necessary for *MCS9.7* activity *in vivo*.

We predict that loss of *Tfap2α* trans-activation at *MCS9.7* would result in altered *Irf6* expression. As shown previously, *MCS9.7* is active and *Tfap2α*, *Irf6* are co-expressed in the spinous layer. Histologically, loss of *Tfap2α* leads to a disorganized basal cell layer with a hypertrophic epidermis at E17.5 (Fig. 11e-g). We marked the basal cell layer with *Tfap2α* and *Trp63* (Fig. 11i,j), the spinous layer with *Krt1* (Fig. 11m,n), the cornified and granular layer with *Loricrin* (Fig. 11o,p) in wild type and *Tfap2α* knockout embryos. Despite morphological changes, we detected the epidermal cell layer *Tfap2α*^{-/-} embryos. In wildtype skin, *Trp63* is restricted to the basal cell layer and *Tfap2α* is expressed in both the basal and spinous cells. Conversely, *Irf6* is expressed in the basal layer but emerges more robustly in the spinous and granular cells. Consistent with our prediction, we did not detect *Irf6* expression in the spinous layer of *Tfap2α* knockout embryos. This pattern is in direct contrast with the adjacent granular and cornified layers, where a different cohort of *Irf6* trans-factors are active^{18,19}. Loss of *Tfap2α* also lead to persistence of *Krt6* (Fig. 11u,v), a marker of stress, and altered desmocolin expression, perhaps contributing to epidermal folding(Fig. 11w,x).

We previously found that *Irf6* restricts *Krt14*, *Trp63*, and proliferation to the basal cell layer¹⁰. We predict here that loss of *Irf6* in the spinous layer would lead to ectopic *Krt14*, *Trp63* and, as a measure of cellular proliferation, *Ki-67*. Importantly, previous work shows that loss of *Tfap2α* was not sufficient to alter *Trp63* expression⁸. Consistent with

our prediction, loss of *Irf6* expression in the spinous layer coincided with ectopic cellular proliferation (Fig. 11h,i) and spinous-cell expression of both *Trp63* and *Krt14* (Fig. 11s,t). This data suggests that loss of *Irf6* can uniquely contribute to the pathophysiology of *Tfap2α* knockout embryos. Considering *TFAP2α* mutations in the DNA binding domain, reduced *IRF6* expression may contribute to BOFS pathology.

In addition to qualitative, localized changes in *Irf6* gene expression, we also wanted to assess if *Irf6* transcript level might be reduced in *Tfap2α* knockout skin. However, in comparing *Tfap2α*^{+/+}, *Tfap2α*^{+/-} and knockout embryos, we did not find quantitative changes in *Irf6* mRNA level despite a significant reduction in *Krt1* transcript, a marker for the cell layer where *Irf6* is expressed (Fig. 11y). Consistent ectopic expression of *Trp63*, we found a significant increase in *Trp63* transcript level. An analogous change in *Krt14* expression was not observed.

Furthermore, previous reports have shown that *Tfap2α* and *Tfap2c*²⁰ play redundant roles in skin, limb and craniofacial development and share cis-acting regulator elements.

Therefore, loss of *MCS9.7* expression in *Tfap2α* knockout mice may also result from changes in *Tfap2c* expression that is co-incident with loss of *Tfap2α*. However, in *Tfap2α* knockout mice, *Tfap2c* is significantly increased (Fig. 11y). Taken together, these data suggest that *Tfap2α* is necessary for *MCS9.7* activation and *Irf6* expression. Moreover, as rs642961 abrogates one of four *Tfap2* binding sites within *MCS9.7*, this data suggests that rs642961 is a functional variant.

Irf6* regulates *Tfap2α

Seeing that *Tfap2α* is a critical trans-acting factor for *Irf6* expression, we wanted to assess if *Irf6* also regulates *Tfap2α*, as previously suggested for *Trp63*. At E14.5 we find that *Tfap2α* is expressed in both the periderm, as marked by *Krt6*, and basal cell layer, as marked by *Krt14* and *Lef1* (Fig. 12a,b). In *Irf6*^{-/-} embryos, we found an expanded epidermis. While *Lef1* continues to mark the basal cell layer in *Irf6*^{-/-} embryos, we found ectopic expression of *Krt14* and *Tfap2α* (Fig. 12c,d). Similarly, at E17.5, *Irf6* restricts *Tfap2α* expression to the basal and spinous layer whereas loss of *Irf6* leads to expression of *Tfap2α* throughout the epidermis, as previously shown for *Trp63* (Fig. 12e,f).

Transcriptionally, we find that loss of *Irf6* in the epidermis leads to over-expression of *Trp63*, *Krt14*, *Tfap2α* and *Tfap2c* (Fig. 12g). We hypothesized that an expanded epidermis with more *Trp63* and *Tfap2α* positive cells would lead to a quantitative increase in their relative protein content. Consistent with the transcriptional changes and prior reports¹⁶, we find a significant increase of *Trp63* in *Irf6* knockout embryos (Fig. 12h). Unexpectedly, despite the 4-fold increase of *Tfap2α* mRNA, we found a reduction in *Tfap2α* protein. Therefore, loss of *Irf6* leads to diverging quantitative changes in *Tfap2α* mRNA and protein. These results suggest that multiple regulatory mechanisms link *Irf6* and *Tfap2α* expression. These mechanisms may have arisen as a result of important roles in pleiotropic developmental disease.

***Irf6* homeostasis is required for neurulation and *Tfap2α* expression in epidermis**

To determine the gene regulatory network between *Irf6* and *Tfap2α* *in vivo*, we modulated *Irf6* expression *in vivo*. To reduce *Irf6* expression, we created a hypomorphic

allele (*Irf6^{ey}*, Supp Fig. 17) and examined embryos at E13.5 and E17.5 (N=47, Mendel's p-value = 0.5; Supp Table 10). To create an allelic series, we combined the *Irf6* hypomorphemic allele (*Irf6^{ey}*) with a genetrap (functionally null) allele (*Irf6*). At E17.5, *Irf6^{ey/+}* (n=17) heterozygotes appeared grossly normal (Fig. 13a). Unexpectedly, compound heterozygous embryos (*Irf6^{ey/-}*, n=18) had a completely penetrant curled tail. At E13.5, tail abnormalities were not grossly visible in either *Irf6^{ey/+}* (n=3) or *Irf6^{ey/-}* (n=6) embryos (data not shown). These results are striking because while *Irf6* knockout embryos have a shortened, dysmorphic tail, we presumed that severe skin adhesions led to tail anomalies.

To over-express *Irf6*, we used the *KRT14* promoter to drive ectopic expression (*Tg^{KRT14-Irf6}*)²¹. As a basal keratin, we predict over-expression would begin at E9.5, as previously described²². The genotypic distribution from this mating did not differ from the predict (N=246; Mendel's p-value = 0.7; Supp Table 11). Surprisingly, while 89% of transgenic embryos appeared grossly normal (*Irf6^{tg-wt}*), we found that 11% (N=14) of transgenic embryos (*Irf6^{tg-mut}*) showed severe rostral and caudal neural tube defects. Of those, eight embryos (6%, *Irf6^{tg-ex}*) presented with exencephaly (Fig. 13a). The rest, six embryos (5%), presented with anencephaly, thoracoabdominoschisis and a kinked tail, a phenotype highly analogous but not identical to *Tfap2a* knockout embryos (*Irf6^{tg-an}*). This data suggests that over-expressing *Irf6* could repress *Tfap2a*. However, considering that ectodermal loss of *Tfap2a* leads to pathology as early as E9.5, this data also suggests that the *KRT14* promoter is driving *Irf6* earlier than previously recognized for either gene.

Developmentally, palate and neural tube closure occur in highly analogous process. Essentially, a flat epithelium and underlying mesenchyme rapidly expand, pivot toward midline, appose, adhere and fuse. However, neural tube development is a more complex process, involving multiple independent closure or fusion points. Defects in the rostral closure points can lead to exencephaly and anencephaly, which are highly analogous in mouse and humans. Defects in the caudal closure point can result in curled or kinked tail in the mouse and spina bifida in humans. The incidence of both rostral and caudal closure defects is 1/1000, perhaps constituting the most severe and least treatable cohort of developmental anomalies. While more than 200 mouse models of neural tube defects have been reported, few of these have been conclusively tested for a conserved role in human disease and fewer still have shown an association.

We wanted to understand how altering endogenous *Irf6* expression can lead to five grossly different developmental phenotypes. We hypothesized that differing phenotypes resulted from different levels of *Irf6* expression. Transcriptionally in skin, we found five different levels of *Irf6* expression across five different phenotypes tested (Fig. 13b).

Remarkably, variable transgene expression accounts for two of these levels.

Transcriptionally, we found a dose-dependent negative correlation between *Irf6* and *Tfap2 α* across five different murine models. Strikingly, the most severely affected transgenic embryo had the greatest amount of *Irf6* and the least amount of *Tfap2 α* .

Furthermore, while *Irf6* expression is necessary to restrict *Trp63* mRNA level, over-expression of *Irf6* was not sufficient to further reduce *Trp63* transcript. A similar relationship is also observed for *Krt14* and *Tfap2c*. Paradoxically, while *Irf6* expression

was not necessary to maintain *Tgm1* and *Krt1* levels, over-expression was sufficient for repression (Supp Fig 18).

Having observed that more severely affected transgenic embryos expressed more *Irf6*, we asked if both the penetrance and variable expressivity of the transgene could be modified *in vivo*. To test this hypothesis, we intercrossed *Irf6*^{tg-wt} mice. We found that 36% of transgene positive embryos are affected (*Irf6*^{tg-mut}, N=33; Mandel's p-value = 0.35; Supp Table 12). While 10% of transgenic embryos had exencephaly, 26% of the embryos had anencephaly. Therefore, by intercrossing *Irf6*^{tg-wt} mice, we increased the penetrance of murine neural tube defects (11% vs. 36% affected) and the severity (5% vs. 26% anencephaly). These findings suggest that murine development is highly sensitive to *Irf6* dose.

Our data suggests that *Irf6* transcriptionally represses *Tfap2α*. However, the protein level, loss of *Irf6* lead to a reduction of *Tfap2α*. Therefore, we hypothesized that both over- and under-expressing *Irf6* would reduce *Tfap2α*. Consistent with transcriptional changes, we found that over-expressing *Irf6* lead to a reduction in *Tfap2α* (Fig. 13c). However, consistent with post-translational stabilization, we found that lowering *Irf6* expression also lead to reduction in *Tfap2α* in a dose-dependent manner despite a relative increase in *Tfap2α* mRNA. Thus, both over and under-expressing *Irf6* leads to reductions in *Tfap2α* protein.

To further characterize how changes in *Irf6* expression affect skin development and *Tfap2a* localization, we examined five different murine phenotypes and *Irf6* doses histologically and molecularly at E17.5. We found that over-expression of *Irf6* leads to epidermal hyperplasia, with a disorganized basal cell layer and vacuolated superficial cells (Supp Fig 19). Loss of *Irf6* expression resulted in a hypotrophic epidermis that also included vacuolated cells. Epidermal thickness positively correlated with changes in the spinous cell layer, as marked by *Krt1* and *Krt14* (Fig. 13d,e), suggesting that *Irf6* expression is both necessary and sufficient for spinous layer development and epidermal thickness. Reducing *Irf6* expression lead to the stratification of *Tfap2a* into the granular layer and *Trp63* into the spinous cell layer. Conversely, over-expression of *Irf6* leads to a loss of *Tfap2a* but not *Trp63* (Fig. 13f,g).

In skin, like the neural tube, both over and under expression of *Irf6* lead to pathology, including ectopic expression of *Krt6*, *Krt14*, and *Ki-67* (Supp Fig 19). No appreciable change in Activated Caspase 3 expression was noted despite *Irf6* function in tumor suppression. Instead, *Irf6* expression correlated with *Tgm1* and Loricin immunostaining, suggesting necessity. In viewing serial sections, we found well-circumscribed foci of highly proliferative, *Krt14* positive foci in the epidermis resulting from dermal projections. These included hair follicles and basal cells, but were engulfed by more superficial epidermal cells. These epidermal plumes seem to result from binding of non-contiguous adjacent basal cell layers and altered desmosome expression, as seen in *Tfap2a* knockout embryos (Fig. 11w,x).

Endogenous and transgenic *Irf6* expression regulate *Tfap2α* in neurulation

Seeing cross-regulation of *Irf6* and *Tfap2α*, we hypothesized that *Irf6* and *Tfap2α* interact genetically. We tested the genetic interaction *in vivo* by interbreeding mice that are heterozygous for the *Irf6* genetrapp (*Irf6*^{+/-}) and *Tfap2α* LacZ knockin (*Tfap2α*^{LacZ/+}) alleles. The distribution of embryonic genotypes was not different from the Mendelian prediction (N = 300 embryos; Mandel's p-value = 0.30; Supp Table 13). We found that 10.3% of embryos are resorbing, a significant number relative to the expected rate of 1-3%²³(p-value = 0.0007, Fisher's Exact, two-tail, t-test). Whereas *Tfap2α*^{LacZ/LacZ} knockin mice have completely penetrant neural tube and abdominal wall defects, we found that 10.3% of *Tfap2α*^{LacZ/+} embryos have exencephaly, frontonasal hypoplasia, low-set unattached pinna, and disproportionately short upper and lower limbs (Fig. 14a,b) (N=68, 7 affected). We replicated this finding in embryos heterozygous for the *Tfap2α* knockout allele (*Tfap2α*^{+/-}) (N=69, 3 affected, 7%; Mandel's p-value = 0.02; Supp Table 14). Strikingly, and consistent with our allelic series, a null allele of *Irf6* completely rescues haploinsufficiency of *Tfap2α* in *Irf6*^{+/-};*Tfap2α*^{LacZ/+} embryos (Fig. 14c,d) (N=69, 0 affected, p-value = 0.0063, Fisher's Exact Test, two-tail t-test). We conclude that intergenic suppression of *Irf6* rescues *Tfap2α* haploinsufficiency. These results are consistent with our findings, which suggest that embryonic development is exquisitely sensitive to *Irf6* and *Tfap2α* dose and that endogenous *Irf6* expression regulates *Tfap2α*.

As noted above, the transgenic phenotype suggested *Irf6* and *KRT14* expression prior to E9.5. As such, we asked if *Irf6* and *Krt14* are expressed in at E8.75, prior to neural tube development. Consistent with intergenic suppression, we detected *Irf6* in the neural plate,

neural plate border and non-neural ectoderm with two different antibodies (Fig. 14e',f'). Further, we found co-localization of *Irf6* and *Tfap2α* in the neural folds and non-neural ectoderm.

At E9.0, we dual-stained for *Irf6* and *RhoB*, a marker of early migrating neural crest cells. We found *Irf6* expression in the neural tube and co-localization with *RhoB*²⁴ in delaminating neural crest cells (Fig. 14g). Consistently, dual staining for *Irf6* and *Krt14* shows co-expression in the neural tube (Fig. 14h). We did not detect *Irf6* expression in migratory neural crest cells (Fig. 14k). Molecular staining for *Irf6* and *RhoB* in transgenic embryos shows ectopic *Irf6* expression in the neural tube, non-neural ectoderm and cephalic mesenchyme (Fig. 14l). *Irf6* and *Tfap2α* co-localized in the neural tube, non-neural ectoderm and delaminating neural crest cells (Fig. 14m). Significantly, in embryos over-expressing *Irf6* we did not detect *Tfap2α* in the neural tube and delaminating neural crest cells (Fig. 14n). Consistently, embryos over-expressing *Irf6* had neural tube closure defects rostrally and caudally, including defects in the optic cup and disordered cephalic mesenchymal tissue (Fig. 14i,j).

Given our immuno-staining, which suggested co-localization of *Irf6*, *Krt14* and *Tfap2α* in the neural tube and delaminating neural crest cells, we wanted to test the hypothesis that endogenous and transgenic *Irf6* expression cooperatively antagonize *Tfap2α* expression *in vivo*. Considering co-localization and intergenic suppression of *Tfap2α* by reducing *Irf6*, we reasoned that over-expressing *Irf6* via the *KRT14* promoter in *Tfap2α* heterozygous embryos (*Tg*^{*KRT14-Irf6*}; *Tfap2α*^{*LacZ/+*}) would increase the penetrance and the

severity of neural tube defects. Importantly, genotypic distribution did not differ from Mendel's prediction (N=63, Mendel's p-value = 0.18; Supp Table 15). In total, 16 embryos genotyped as $Tg^{KRT14-Irf6};Tfap2\alpha^{LacZ/+}$. While half of these embryos appeared grossly normal, the other half is more severely affected than *Tfap2 α* knockout embryos (Fig. 14o). We further hypothesized that if transgene and endogenous *Irf6* expression co-antagonize *Tfap2 α* , than $Tg^{KRT14-Irf6};Irf6^{+/-};Tfap2\alpha^{LacZ/+}$ embryos would be less severely affected than $Tg^{KRT14-Irf6};Tfap2\alpha^{LacZ/+}$ littermates because it would reduce total endogenous *Irf6* expression. The *Irf6* null allele did not affect the genotypic distribution (N=66, Mendel's p-value = 0.07; Supp Table 16). Significantly, as predict, reducing endogenous *Irf6* expression ($Tg^{KRT14-Irf6};Irf6^{+/-};Tfap2\alpha^{LacZ/+}$, n=11) partially rescued all affected tissues relative to $Tg^{KRT14-Irf6};Tfap2\alpha^{LacZ/+}$ littermates (Fig. 14o). Strikingly, $Tg^{KRT14-Irf6};Irf6^{+/-};Tfap2\alpha^{LacZ/+}$ phenocopied *Tfap2 α* ^{-/-}, further supporting the role of *Irf6* in regulating endogenous *Tfap2 α* levels.

***Tfap2 α* and *Grhl3* interact in caudal neurulation**

We wanted to determine how lowering *Irf6* expression in *Irf6*^{ey/-} embryos could lead to a curly tail. Significantly, we showed that *Irf6* binds to and transcriptionally activates *Grhl3* and that *irf6* is epistatic to *grhl3* in zebrafish¹³. In primary human keratinocytes, IRF6 binds to and positively regulates GRHL3²⁵. This association is significant because in mouse, a spontaneous mutation in *Grhl3* leads to a hypomorphic allele and the curly tail mouse (ct/ct), one the oldest and best-described murine neural tube defect phenotypes. Furthermore, knocking out *Grhl3* leads to exencephaly, a defective epidermis, an open lumbosacral neural tube defect and a curly tail¹⁴. A genetic cross

between *Irf6* and *Grhl3* heterozygous mice suggested epistasis via early embryonic resorptions and post-natal lethality of double heterozygous pups, but gross phenotypic anomalies were not observed (Peyrard, xx).

Considering epidermal expression data and analogous tail phenotypes, we predict that *Irf6* regulates *Grhl3* in neural tube development. To test our hypothesis, we compared *Grhl3* in grossly normal (*Irf6^{ey/+}*) and abnormal (*Irf6^{ey/-}*) tail tissue. We predict that reducing *Irf6* would lead to a reduction in *Grhl3*. Consistently, reducing *Irf6* leads to a reduction in *Grhl3* at E17.5 (Fig. 15a). Considering kinked tail in the knockout and interaction with *Irf6*, we also examined *Tfap2α* levels. Remarkably, and in direct contrast to the skin, reducing *Irf6* expression in the tail also lead to a reduction in *Tfap2α*. Prior genomic screen also showed that *Irf6* binds within *Tfap2c*²⁵ and that tissue-specific deletion of *Tfap2c* leads to a curled tail²⁶. As predict, reducing *Irf6* expression lead to a reduction in *Tfap2c* at E17.5 (Supp Fig. 20). Consistent with onset of tail dysmorphology, molecular changes in *Irf6*, *Tfap2α*, *Grhl3* and *Tfap2c* occurred at E17.5. Considering changes in *MCS9.7* enhancer activity in the tail of *Tfap2α* knockout embryos (Fig. 11c,d), this work shows that *Irf6*, *Tfap2α*, *Tfap2c* and *Grhl3* constitute a gene regulatory network in caudal neurulation.

Our model (Fig. 15c) suggests that *Irf6* is an intermediate node between *Tfap2α* more proximally and *Grhl3* more distally. Based on our model, we further predict that *Tfap2α* and *Grhl3* interact in caudal neural tube development. Consistent with our prediction, we find that of 15% *Tfap2α^{+/-};Grhl3^{+/-}* double heterozygous embryos have a curly tail (Fig.

15b) (N=20, 3 affected; Mandel's p-value = 0.11, Supp Table17). Consistent with the curly tail mouse, we find incomplete penetrance. However, our prior work shows that *Grhl3* and *Irf6* double heterozygous embryos do not have a curly tail. Absence of a curly tail in *Irf6*^{+/-};*Grhl3*^{+/-} double heterozygous embryos suggests that additional targets, including *Tfap2c*, may be playing a redundant role with *Grhl3* downstream of *Irf6* in caudal neurulation.

Shared *IRF6* mutation in Spina Bifida and VWS

Considering the role of *Irf6* in murine neural tube development, we hypothesized that common and rare variants in *IRF6* could contribute risk to neural tube defects in humans. To test our hypothesis in the caudal neural tube, we sequenced *IRF6* protein coding sequence in 96 patients with Spina Bifida. Consistent with our hypothesis, we found a non-synonymous substitution in exon 9 that alters a highly conserved amino acid residue, D427Y (Fig. 16). The variant, previously reported in patient with Van der Woude Syndrome²⁷, is predict to be damaging and probably deleterious by PolyPhen2.0 and SIFT, and is not found in nearly 7000 control samples (EVS and 1000 genomes). Most strikingly, structural analysis reveals that D427Y occurs at the junction of the c-terminal alpha helix of *IRF6*. Prior work on *IRF6* paralogs has shown that mutations in this region may affect the c-terminal domain and prevent activation and dimerization²⁸.

Considering detection of rare variants, we further predict that common and rare non-coding variants within *IRF6* may be associated with spina bifida risk. Our analysis suggests no association with three *IRF6* variants, rs642961 (MAF 17%), rs17371411

(MAF 8%), rs75012801 (MAF 0.8%) (Tables 6-8). Additional analysis has also shown that rs17371411 is not associated with anencephaly in humans. While we did not detect an association, these three variants only account for 28% of the genetic variation at *IRF6*. As such, the role of *IRF6* in human neurulation remains largely unanswered.

DISCUSSION

Our data show that *Irf6*, *Tfap2α* and *Grhl3* interact in the development of multiple ectodermal lineages, including skin, craniofacial and the neural tube. Mechanistically, while *Tfap2α* regulates *Irf6* enhancer activity and expression in skin and tail, we found that *Irf6* regulates *Tfap2α* through both transcriptional repression and post-translational stabilization. These data may provide a molecular rationale that underpins common co-occurring orofacial clefting, lip pits and skin defects in VWS, PPS and BOFS. More broadly, this pathway provides a functional link that may be perturbed in 30% of the world's population who have rs642961, a DNA variant that alters *Tfap2α* binding at MCS9.7 and is associated with 12% of all orofacial clefting.

Evolutionarily, rs642961 is perplexing because it is a derived, common variant and yet increases risk for orofacial clefting in multiple, ethnically diverse populations.

Considering that increasing *Irf6* expression increased risk for rostral neural tube defects, uniformly lethal events in mouse and humans, a variant that dampens *Irf6* expression may provide a selective survival advantage during development. In support of this hypothesis, we also show here that a null *Irf6* allele rescues perinatal lethal neural tube defects in *Tfap2α* haploinsufficient embryos, a seldom-described biological relationship in the

mouse^{29,30}. Similar to the heterozygous advantage provided by sickle cell trait in the context of endemic malaria risk, we provide evidence here that dampening *Irf6* expression may confer a developmental advantage.

In addition, recent evidence suggests that IRF6 and TFAP2 α function is critical in preventing post-embryonic disease. For example, previous work shows that IRF6 functions as a tumor suppressor in breast cancer and more recent work shows that mutations in IRF6 can lead to squamous cell carcinoma^{31,32}. Furthermore, a variant within TFAP2 α modifies BRCA2 breast cancer risk³³. Therefore, if this pathway is conserved in other tissues, additional biological and or novel therapeutic applications may be explored.

Interestingly, D427Y was previously identified in a patient with Van der Woude Syndrome. While neural tube defects have not been reported in VWS, these results suggest that common IRF6 function is perturbed in orofacial clefting and neural tube defects. Furthermore, considering a common *Tfap2 α -Irf6-Grhl3* pathway in neural tube and orofacial development in mouse and man, we suggest a novel category of genes that are mutually involved in both biological processes. While underpinned by strikingly different cellular processes, both neural tube and palate formation essentially occurs through analogous tissue processes, including proliferation, growth, pivot toward midline, adhesion and fusion of apposing surfaces. Considering analogous genetic and morphological pathways, we suggest use of ‘orofacial and neural tube clefting’ genes.

Strikingly, we found that over-expression of *Irf6* leads to anencephaly and a kinked tail and that reductions in *Irf6* expression leads to a curly tail. While posterior neuropore dysfunction has been blended together, differences in the molecular etiology suggested here support their phenotypic distinctions. Biologically, *Irf6* joins PTEN as a tumor suppressor genes that when under-expressed leads to loss-of-function and when over-expressed leads to gain-of-function *in vivo*³⁴. Surprisingly, few studies have examined *in vivo* over-expression of tumor suppressors. However, as we have shown here, over-expressing this important class of genes may provide insight into novel pathways, targets or tissue-specific functions.

To date, the only known murine alleles that display both anencephaly and a thoracoabdominoschesis are *Tfap2a* knockout embryos and those that over-express *Irf6*. However, *Palladin* and *Grhl2* knockout embryos also display anencephaly and abdominal-schesis but have an intact thoracic wall. Considering the morphological similarity, future work should address if these genes are part of the same pathway as *Irf6* and *Tfap2a*, although prior work suggested that *Tfap2a* did not interact with *Grhl2*³⁵. Similarly, knocking out *Ikka*³⁶, *14-3-3 sigma*⁹, *Ripk4*³⁷ and *Kdf1*³⁸ produced murine embryos that phenocopy the *Irf6* knockout. Considering the shortened abnormal tail in *Irf6* knockout embryos was consistent with a role in neural tube development, future work may uncover analogous roles for *Ikka*, *14-3-3sigma*, *Ripk4* and *Kdf1*. Consistent with this hypothesis, homozygous recessive mutations in *IKKa* lead to Cacoon Syndrome, which includes an abdomino-schesis and neural tube defects, as evidenced by brain anomalies and exencephaly in both reported fetuses. Taken together, neural tube

biology may gain a new pathway that originated in skin and palate development and human genetics may consider a new cohort of candidate genes.

Like the complex genetics of human neural tube defects, many inbred murine neural tube defects models display variable penetrance and expressivity. To that end, we discovered that variable expressivity and penetrance in our mouse models stems from exquisite sensitivity to *Irf6* dose. As such, genes upstream and downstream of *Irf6* in neural tube development may provide novel candidate genes.

Epidemiological data has suggested a common pathway for orofacial and neural tube development as evidenced by reduced risk for either defect with folate supplementation³⁹. One line of reasoning suggests that folate supplementation affects methylation of target genes and as such buffers gene transcription to fine-tune development (methylation hypothesis). Consistently, previous work has shown that the IRF6 promoter is methylated to suppress transcription²⁵. If folate supplementation affects this promoter, IRF6, and this core-network, could provide a molecular rationale that integrates folate epidemiology but not the folate pathway specifically for both oral and neural tube development.

Considering multiple mechanisms that dynamically dampen *Irf6* expression, including a negative feedback loop reported here in the rostral neural tube, IRF6 promoter methylation as an end target of folate supplementation provides an attractive target for future study.

SUPPLEMENTAL DATA DESCRIPTION

Supplemental data include four figures and eleven tables.

AUTHOR CONTRIBUTIONS

YAK and BCS conceived of the work. YAK designed in vitro, cell culture and murine crosses, performed all murine crosses and experiments, completed statistical analyses, analyzed all data, prepared the figures and tables and wrote the manuscript. BCS and YAK designed human sequencing with RHF and HZ. HZ and TDB performed human sequencing and statistical analysis. YAK performed comparative sequence analysis. BCS designed and AK made the *Irf6^{ey}* hypomorphic allele. WDF performed and analyzed in vitro experiments and RRR performed mouse genotyping and statistical analyses. TJW and YC contributed critical reagents. RHF, GMS, AGB and JCM carried out patient recruitment. YAK, BAA, JCM, AGB and RHF supervised experiments. BCS established and maintained key collaborations and supervised the project. All co-authors reviewed the manuscript and edits were reviewed/incorporated by YAK and BCS.

ACKNOWLEDGEMENTS

Financial support to YAK (#F31DE022696-01) came from the NIH National Institute of Dental and Craniofacial Research.

WEB RESOURCES

Online Mendelian Inheritance in Man: www.omim.org

PolyPhen-2: <http://genetics.bwh.harvard.edu/pph2/>

Primer3: biotools.umassmed.edu/bioapps/primer3_www.cgi

NHLBI/ESP database: evs.gs.washington.edu/EVS/

UCSC genome browser: genome-euro.ucsc.edu/cgi-bin/hgGateway

MATERIALS AND METHODS

Murine crosses

All animal use protocols and procedures are approved by the Institutional Animal Care and Use Committees, AUF Number 05/12-093-00, at Michigan State University. In all matings, presence of a copulation plug is denoted as E0.5. $Tfap2\alpha^{-/-}; Tg^{MCS9.7-LacZ}$: We used a recently characterized $Tg^{MCS9.7-LacZ}$ allele, a transgene with the *Irf6* enhancer *MCS9.7* fused to the *LacZ* gene, to assess the necessity of *Tfap2\alpha* in the function of this *Irf6* enhancer. We crossed $Tg^{MCS9.7-LacZ}$ with $Tfap2\alpha^{+/-}$ mice, a knockout allele via homologous recombination, to produce $Tfap2\alpha^{+/-}; Tg^{MCS9.7-LacZ}$ mice. We then crossed $Tfap2\alpha^{+/-}; Tg^{MCS9.7-LacZ}$ males with $Tfap2\alpha^{+/-}$ female littermates to obtain $Tfap2\alpha^{-/-}; Tg^{MCS9.7-LacZ}$ embryos at E13.5 and E17.5. $Irf6^{+/-}; Tfap2\alpha^{LacZ/+}$: To test the genetic interaction between *Irf6* and *Tfap2\alpha*, we intercrossed $Irf6^{+/-}$ mice, heterozygous for a gstrap allele knocked into the first intron of *Irf6*, with $Tfap2\alpha^{LacZ/+}$ mice, *LacZ* knocked into exon 7 of *Tfap2\alpha*. We generated single heterozygous mice for each genotype by intermating $Irf6^{+/-}$ and $Tfap2\alpha^{LacZ/+}$ and the cross is done with both males and females carrying each of the respective alleles to generate $Irf6^{+/-}; Tfap2\alpha^{LacZ/+}$ embryos at timepoints spanning E13.5-E18.5. $Tg^{KRT14-Irf6}$: We characterized $tg^{KRT14-Irf6}$ allele by first intercrossing transgene positive mice with littermates that are transgene negative. As with the $Irf6^{+/-}$ and $Tfap2\alpha^{LacZ/+}$ cross, we controlled for differential parent-of-origin

transmission by conducting the crosses with either males or females carrying the transgene. To test the affect of *Irf6* dose, we intercrossed $Tg^{KRT14-Irf6}$ mice. To test the relevance of *Irf6* expression from the transgene relative to endogenous *Irf6* expression, we first generated $Tg^{KRT14-Irf6};Irf6^{+/-}$ mice by intercrossing transgene positive embryos with those heterozygous for the *Irf6* genetrapp allele. In the second generation, we intercrossed $Tg^{KRT14-Irf6};Irf6^{+/-}$ with $Tfap2\alpha^{LacZ/+}$ mice.

***Irf6* hypomorphic allele**

We generated the *Irf6* hypomorphic allele by creating a targeting vector from a mouse BAC clone (RPC122-516G1) digested with restriction enzymes. The targeting vectors spanned *Irf6* genomic sequence from Intron 2 through Intron 6. We placed a P_{gk}-Neo cassette within a BamHI site within Intron 4. Specifically, a 1.8 kb of *KpnI/BamHI* fragment for 5'-arm and 3.9 kb of *BamHI/HindIII* fragment for 3'-arm were cloned into pBluescript II SK(-) (Agilent Technologies). 3 kb of *BamHI* fragment containing exons 3 and 4, coding DNA binding (IRF) domain, was cloned into ploxP3-Neo-pA vector (kind gift from Professor Takeshi Yagi, Osaka University). 5.8 kb of *XhoI* fragment which contains floxed exons and *Pgk-Neo* cassette was subcloned into *BamHI* site between 5'- and 3'- arms. *NotI* digested targeting construct was electroporated into mouse R1 ES cells. After G418 selection, ES cells were screened by PCR. Primer set of 5'- GAGAAATAGGGCCTTCACGGTG-3' (sense) and 5'- TGTGCCCTCTGATGCTGGAACAG-3' (antisense) for 5'-side, 5'- TCGCCTTCTTGACGAGTTCTTCTG-3' (sense, in *Pgk-Neo* cassette) and 5'- GCTCAACTCCCTTTGTGACTGTCC-3' (antisense) for 3' side were used.

Positive ES clones were used for establishment of *Irf6* hypomorphic mouse (*neo*).

Murine genotyping

Both embryos and pups were euthanized before tissue collection. We extracted DNA from each individual embryos/yolk sac or pup. We obtained genomic DNA by first incubating the tissue in lysis buffer with proteinase K (03115887001, Roche) and then isolated the DNA using ethanol precipitation. We performed PCR to identify genotype. PCR protocols for the *Irf6* genetrapped allele, *Tfap2a* neomycin and LacZ knockin alleles and MCS9.7 were completed as described previously. Genotyping for the transgenic *Tg^{KRT14-Irf6}* was done using newly designed *KRT14* forward primer 5' TTACAAAACCCTTTCACATACATTGTCGCATTGG3' and *KRT14* reverse primer 5' TTGGGGTGGGAACCACGATACACCT3' to yield an expected amplicon of 328 bp. Genotyping for the *Irf6* hypomorphic allele was complete with primers that flank the LoxP recombined sites with forward primer 5'-GCAGAGTGGAGCACACTTCA-3' and reverse primer 5'-AAGCATGTCTATTTGGGGGTTA-3'. Expected amplicon sizes were 283 bp for the wildtype allele and 592 bp for the hypomorphic allele. PCR protocols included a 4 min denaturation step at 94°C. Following denaturation, 30-35 amplification cycles (94°C for 30 sec, 60°C for 30 sec, 72°C for 40 sec) were completed before a final 5 min extension step.

Morphological, histological and molecular analyses of murine tissue

Gross morphological assessment of all embryos was complete upon dissection. Embryos are placed in freshly-prepared 4% paraformaldehyde, paraffin embedded and sectioned at

7 μm intervals. Hematoxylin (GHS332, Sigma) and Eosin (E511-25, Fisher Chemical) staining was performed using a series of hydration and dehydration steps.

Immunostaining is performed with an initial set of hydration steps and followed by antigen retrieval in sodium citrate (pH6.0) on a hot plate and than Triton X-100 (VWR) permeabilization for 30 minutes. To reduce background, we undertake two blocking steps, each lasting 1 hour. The first is in BSA (A7906, Sigma) diluted in PBS at 10mg/ml and the second is in a Goat anti-mouse Fab fragment (Jackson ImmunoResearch Laboratories, 115-007-003) also diluted in PBS as a function of the embryonic timepoint tested (20ug/ml for E13.5, 30ug/ml for E15.5, and 40ug/ml for E17.5). Primary antibody is incubated for 16 to 19 hours at 4°C. Primary Antibodies tested are as follows: Irf6 (Sigma-Aldrich, SAB2102995), Tfp2 α (3B5, sc-12726, Santa Cruz), TTrp63 (Santa Cruz, 4A4, sc-8431), Keratin 6 (Covance, PRB-169P), Keratin 14 (Novocastra, NCL-L-LL002), Keratin 1 (NCL-CK1, Novocastra), Loricrin (PRB-145P, Covance), RhoB (56.4H7, University of Iowa Hybridoma Facility)²⁴, Activated Caspase 3 (Abcam, Ab13847), Ki-67 (ab15580, Abcam), BrdU (Abcam, Ab6326). Secondary antibodies are incubated for 1.5 hr at room temperature. Secondary Antibodies tested are as follows: goat anti-mouse (Molecular Probes, A11029), goat anti-rat (Molecular Probes, A11006), goat anti-rabbit (Molecular Probes, A21429 and O-6381). We labeled nuclei with DAPI (Invitrogen, D3571). Finally, to prevent loss of signal over time and protect the sections, we mount slides in ProLong Gold Antifade Reagent (Invitrogen, P36930).

Skeletal prep

Embryos were fixed in formalin at 4°C until time of processing. Once genotyped, embryos were placed in 70% Ethanol for 24 hours at 4°C, partially dissected to remove skin and subcutaneous fat, and then transferred into 95% Ethanol for at least 48 hours also at 4°C, at which point dehydration was grossly apparent. We then removed the 95% Ethanol and placed in the embryos in 2% KOH for approximately 72 hours at room temperature, at which point skeletal structures become clearly visible. We replaced the 2% KOH with Alcian blue solution (Sigma, A5268-10G), which stains cartilage. The embryos began to once again dehydrate and in the process absorbed the stain. This process took about 72 hours and was followed by a de-staining step in 95% Ethanol for 6 – 24 hours at room temperature. At this point, we removed the Ethanol and added Alizarin Red Solution (Sigma-Aldrich, A5533-25G) for 24-36 hours at room temperature. To perform a final clearing step, we placed the skeleton in a 1%KOH/20% Glycerol solution until it become totally clear. Final specimens were kept in a 1:1 glycerol:95% Ethanol solution until imaging. All incubations performed at room temperature were done on an elliptical rocker.

Bioimaging upright/fluorescent microscope

Imaging was completed with a Nikon Eclipse 90i upright microscope. The two objectives used for this work are the Plan APO 10x/0.45 DIC and Plan APO 40x/0.95 DIC M/N2. For light microscope imaging of Hematoxylin and Eosin sections we used the Nikon DS-Fi1-U2 5 mega-pixel color digital camera. Fluorescent imaging is complete using a HQ2 photometric CoolSnap camera and an X-Cite 120Q illuminator. We used NIS Elements

Advanced Research v3.10 imaging software to capture the images in RAW format. Image processing is limited to sharpening and deconvolution with Gauss-Laplace Sharpening on the NIS-Elements AR software. Adobe Photoshop Elements v9.0 is used for plate configuration and enhancement of color and contrast. *Stereomicroscope*. We used a Nikon SMZ800 with a motorized stage, a Nikon DS-Fi2 high-definition camera and a Nikon Digital Sight DS-U3 control unit for high-magnification imaging of whole-mount embryos. For whole-mount, 1x imaging of embryos we used a SMZ1000 Nikon microscope. A Fiber Optic Light Ring is used for both microscopes. We use NIS-Elements Basic Research software version 4.11 to process the embryonic images and Adobe Photoshop Elements v9.0 for plate configuration

Transcriptional profiling using quantitative-PCR

Skin is collected from embryos directly after harvesting at the timepoint specified. Skin sample is snap frozen in liquid nitrogen and stored in -80°C until time of RNA extraction. TRIzol RNA extraction (15596-026, Ambion) is used with minor modifications to the manufacturers protocol. Briefly, we homogenize the tissue manually, add 200 μ l of chloroform and shake vigorously for 15 seconds. After a brief incubation at room temperature, we centrifuge for 15 minutes at 4°C and transfer the aqueous phase to a new vial. To prevent DNA contamination we add 30 units of RNase-Free DNase (79254, Qiagen) for 45 minutes at 37°C and we inactivate the enzyme at 65°C for 5 minutes. To extract the RNA, we then add 50 μ l NaAcetate (3M, pH4.0), 500 μ l acidic phenol and 200 μ l chloroform and finally centrifuge for 15 minutes at 12,000 RPM at 4°C. The aqueous phase is transferred to a new vial and 20 μ l NaAcetate, 500 μ l of propanol and

yeast-tRNA (15401-029, Invitrogen) are added for RNA precipitation. To pellet the RNA, we centrifuge the sample at 14,000 RPM at 4°C for 20 minutes. The supernatant is removed and the RNA pellet is washed with 75% ethanol, centrifuged and resuspended in RNase-free H₂O and incubated at 55°C for 10 minutes. RNA is quantified and stored at -70°C until preparation of cDNA. *cDNA*. We use a total of 440ng of RNA in addition to Oligo dT primers (18418-012, Invitrogen) and dNTP mix (18427-013, Invitrogen) plus water for a total volume of 13µl for an initial heat mixture step at 65°C for 5 minutes. Furthermore, we added SuperScriptIII Reverse Transcriptase (18080-093, Invitrogen) and reaction components as per the manufacturers protocol. Including Recombinant RNasin Ribonuclease Inhibitor (N2511, Promega) and RNA-Free H₂O, total cDNA reaction volume was 20µl. We performed quantification using SYBR Green (4309155, Applied Biosystems) as recommended in a total reaction volume of 10µl, including 5.5 ng of cDNA and 0.31 picomoles for each of the primer pair. A complete list of primers is included in Supp table xx. We performed all reactions with three technical replicates per biological replicate. Negative controls for the cDNA did not include Reverse transcriptase and RNaseOut. qPCR data was collected during the extension step of each cycle and melting curves were generated for each reaction. We used the cycle threshold (Ct), set within the linear range of amplification, to analyze the data. We obtained the delta-Ct relative to Beta-Actin and the delta-delta Ct and the fold change, relative to wildtype embryo levels for the gene of interest. A complete list of qPCR primer sequences is in Supp Table 18.

Western blotting

We performed protein extraction on murine skin at E17.5. First, we used a mortar and pestle to ground the tissue in liquid nitrogen. The samples were then placed in RIPA buffer with a cocktail of protease inhibitors (11836153011, Roche Diagnostics). After a brief incubation, samples were sonicated on ice to prevent overheating. Finally, we centrifuged the samples for 15 min using 14,000 RPM at 4°C, collected the supernatant and determined protein concentration. We loaded 50 µg of protein per sample.

Membranes were blocked in 5% milk and washed in TBST. Irf6 (SPEA, Schutte Lab) and Tfp2α (3B5, sc-12726, Santa Cruz) antibodies were diluted in 5% milk at a concentration of 1:750.

Human sequencing and genotyping

A complete list of qPCR primer sequences is in Supp Table 19.

Statistical analysis

We used GraphPad Prism software, version 5, for data analysis. A Student's t-test is used to determine significance based on the variance between the two sample populations with an f-test. For this analysis, a p-value of 0.05 is considered to be significant.

APPENDIX

APPENDIX

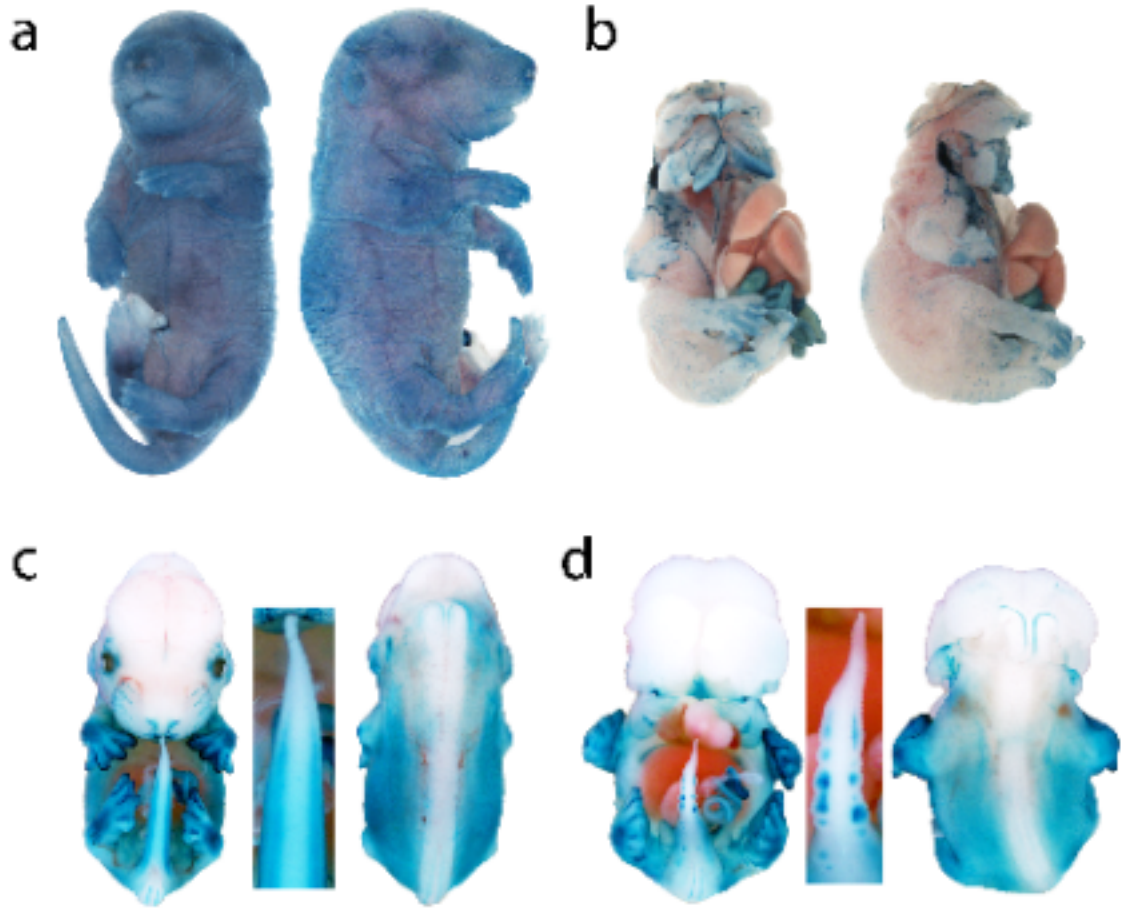


Figure 11: *Tfp2α* is necessary for *MCS9.7* activity and *Irf6* expression.

Figure 11. (cont'd)

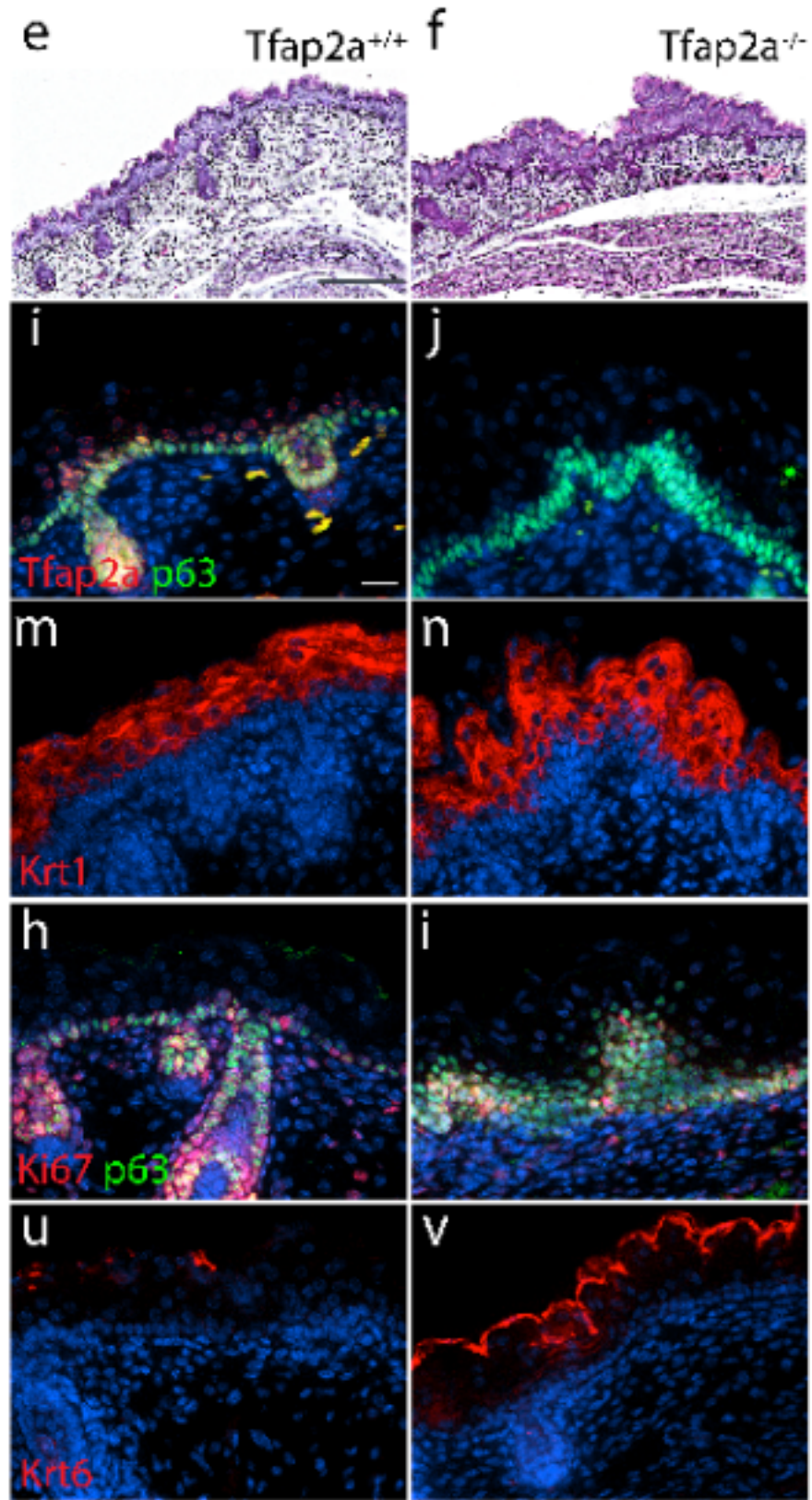


Figure 11. (cont'd)

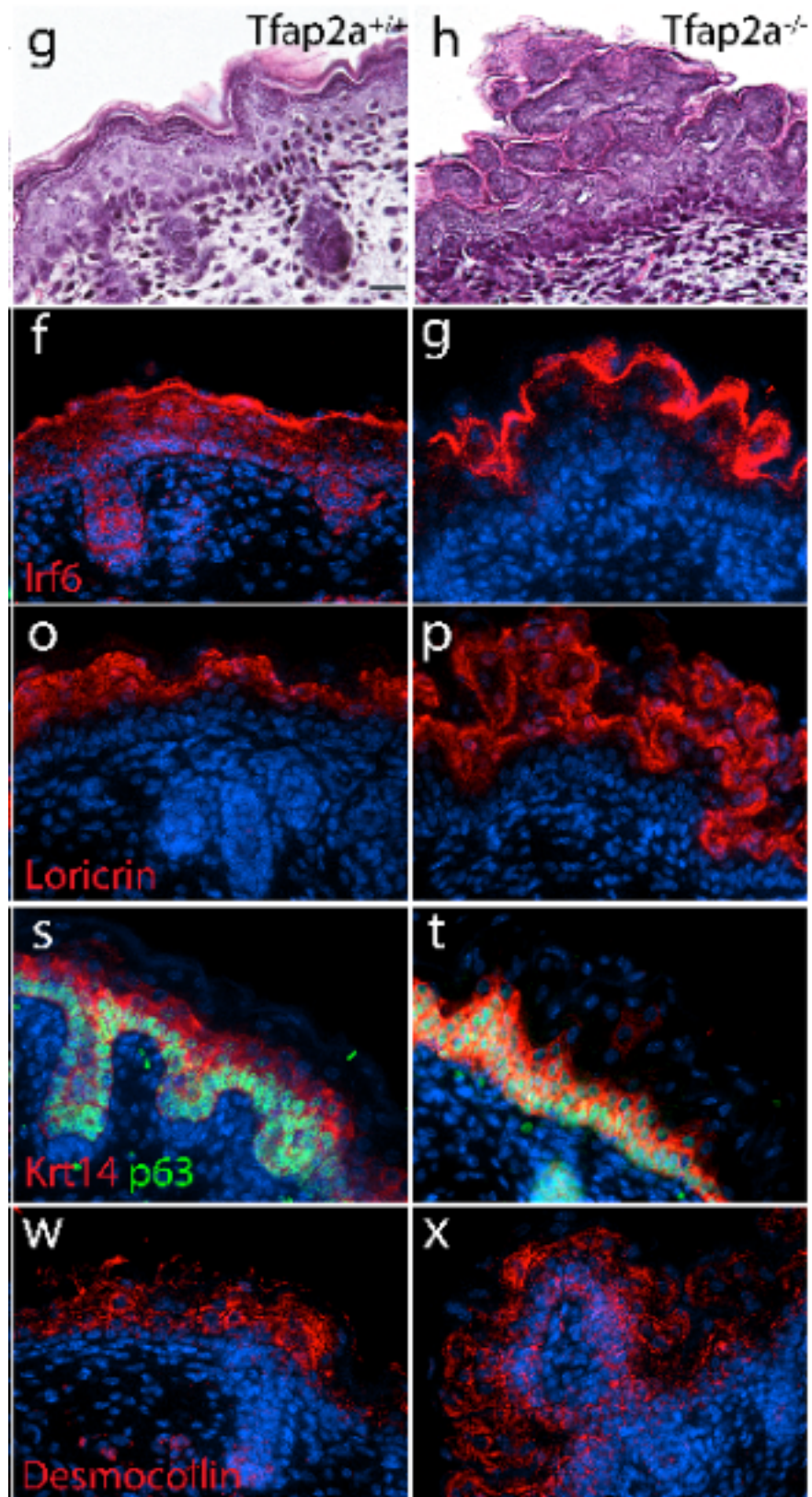


Figure 11. (cont'd)

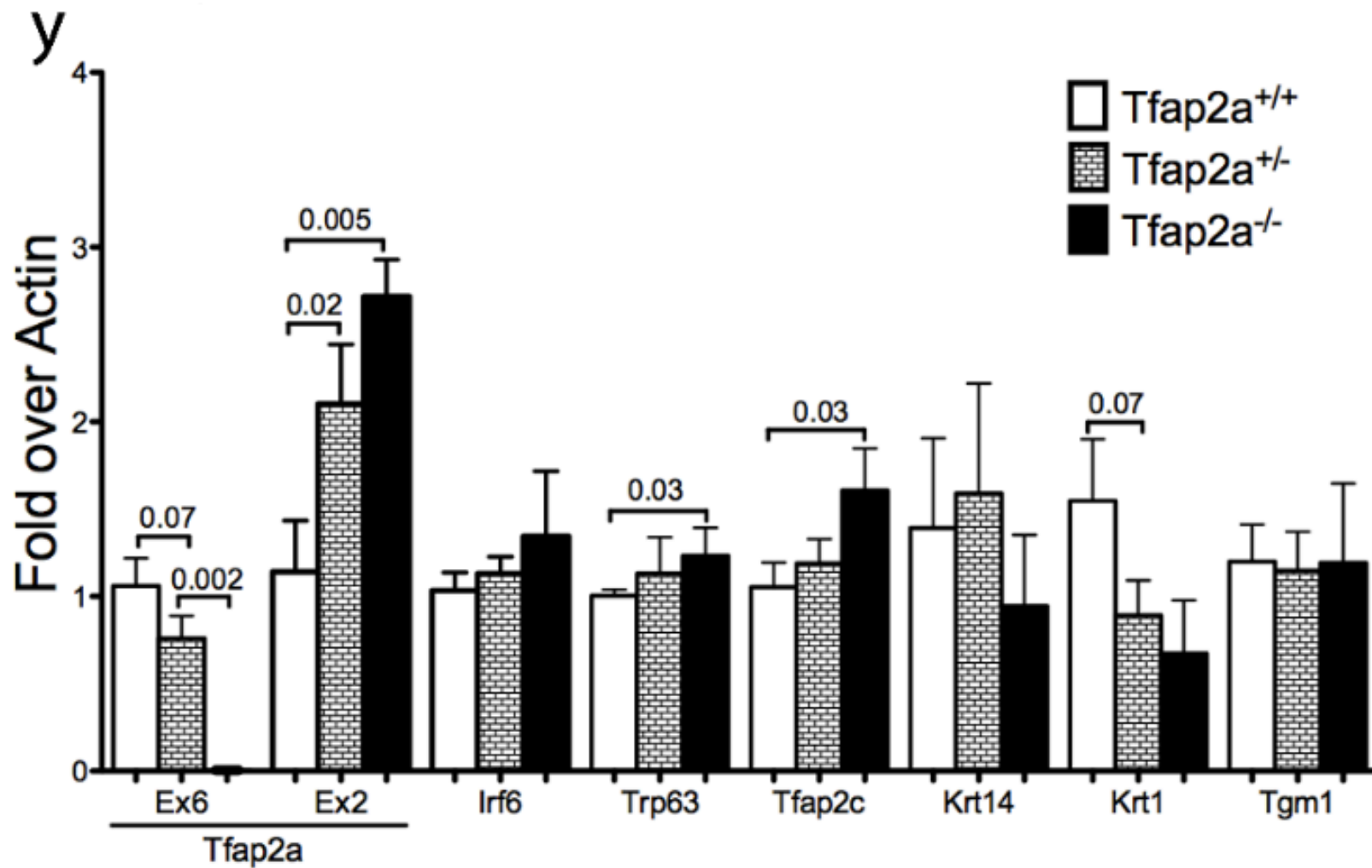


Figure 11. (cont'd)

(a-d) Loss of *Tfap2α* alters MCS9.7 enhancer activity during two different developmental time points and in different tissue. (a,b) Representative images of transgene positive (*Tg^{MCS9.7-LacZ}*) *Tfap2α^{+/-}* (n=20) (a) and *Tfap2α^{-/-}* (n=4) embryos at E17.5 (b). (c,d) Representative images of *Tfap2α^{+/-};Tg^{MCS9.7-LacZ}* (n=4) and *Tfap2α^{-/-};Tg^{MCS9.7-LacZ}* (n=7) embryos at E14.0. We did not detect differences in *MCS9.7* activity between *Tfap2α^{+/-}* (n=16) and *Tfap2α^{+/+}* (n=3) at either time point (data not shown). (e-x) Loss of *Tfap2α* leads to loss of *Irf6* expression in spinous cells of the epidermis. (e-g) Hematoxylin and Eosin staining of *Tfap2α^{+/+}* and *Tfap2α^{-/-}* skin at E17.5. Scale bars - e,f: 200μm; g-h: 20μm; (i-x) Immunofluorescence comparing *Tfap2α^{+/+}* and *Tfap2α^{-/-}* skin at E17.5, with molecular markers as indicated. In all sections, DAPI staining of nuclei (blue). *Tfap2α* (red) and *Trp63* (green) (i-j); *Irf6* (red) (f-g); *Krt1* (red) (m-n); *Loricrin* (red) (o-p); *Ki-67* (red) and *Trp63* (green) (h-i); *Krt14* (red) and *Trp63* (s-t); *Krt6* (red) (u-v); *Desmocollin* (red) (w-x). Scale bars - i-x: 20μm. (y) Quantitative PCR comparing skin transcriptional profiles in *Tfap2α^{+/+}* (n=7, white), *Tfap2α^{+/-}* (n=6, checker) and *Tfap2α^{-/-}* (n=3, black). Bar graphs presented as a mean ± SEM. A Student's t-test is used to analyze significance and a p-value is shown above the groups being compared.

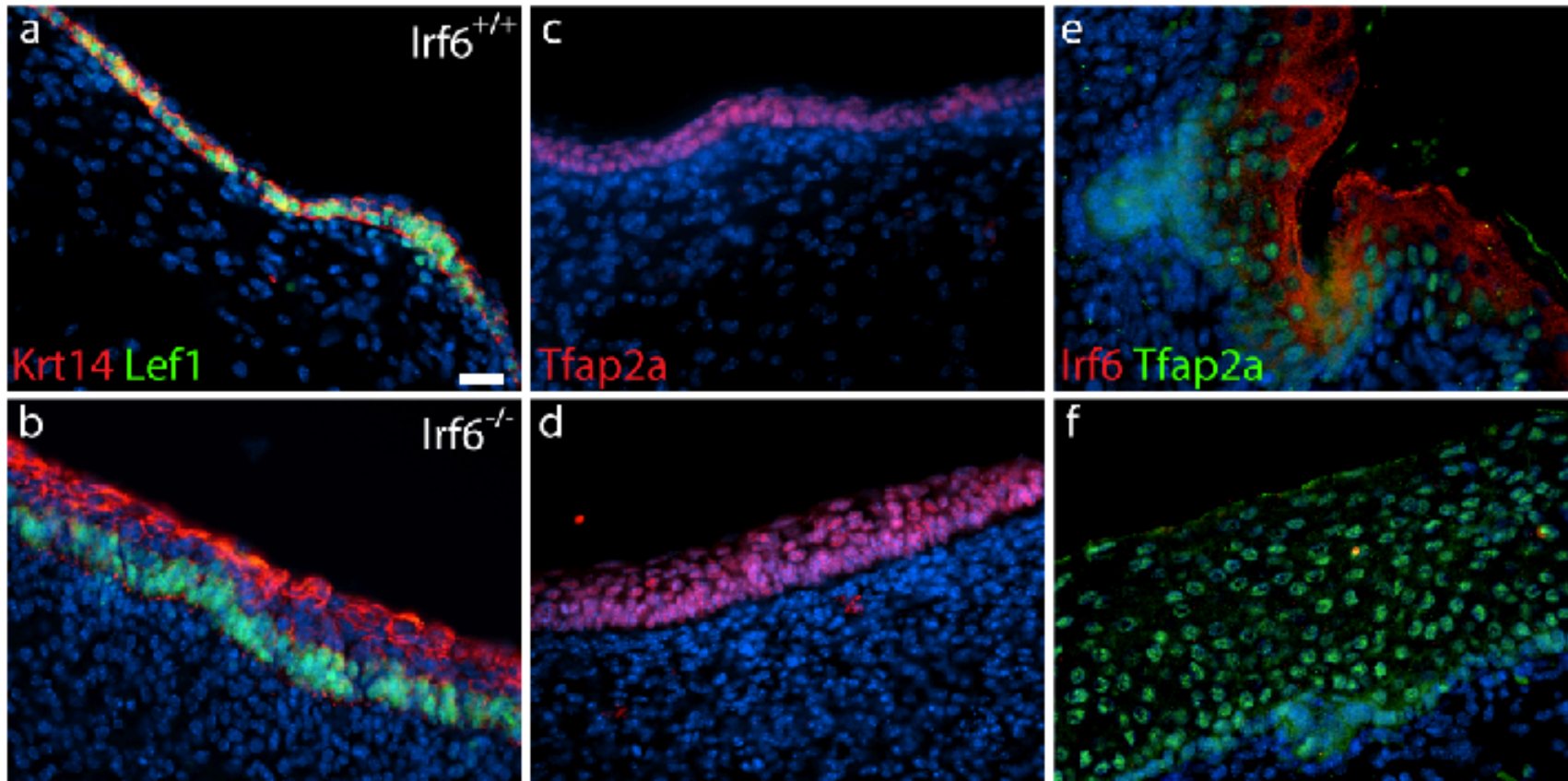


Figure 12: *Irf6* regulates Tfap2 α .

Figure 12. (cont'd)

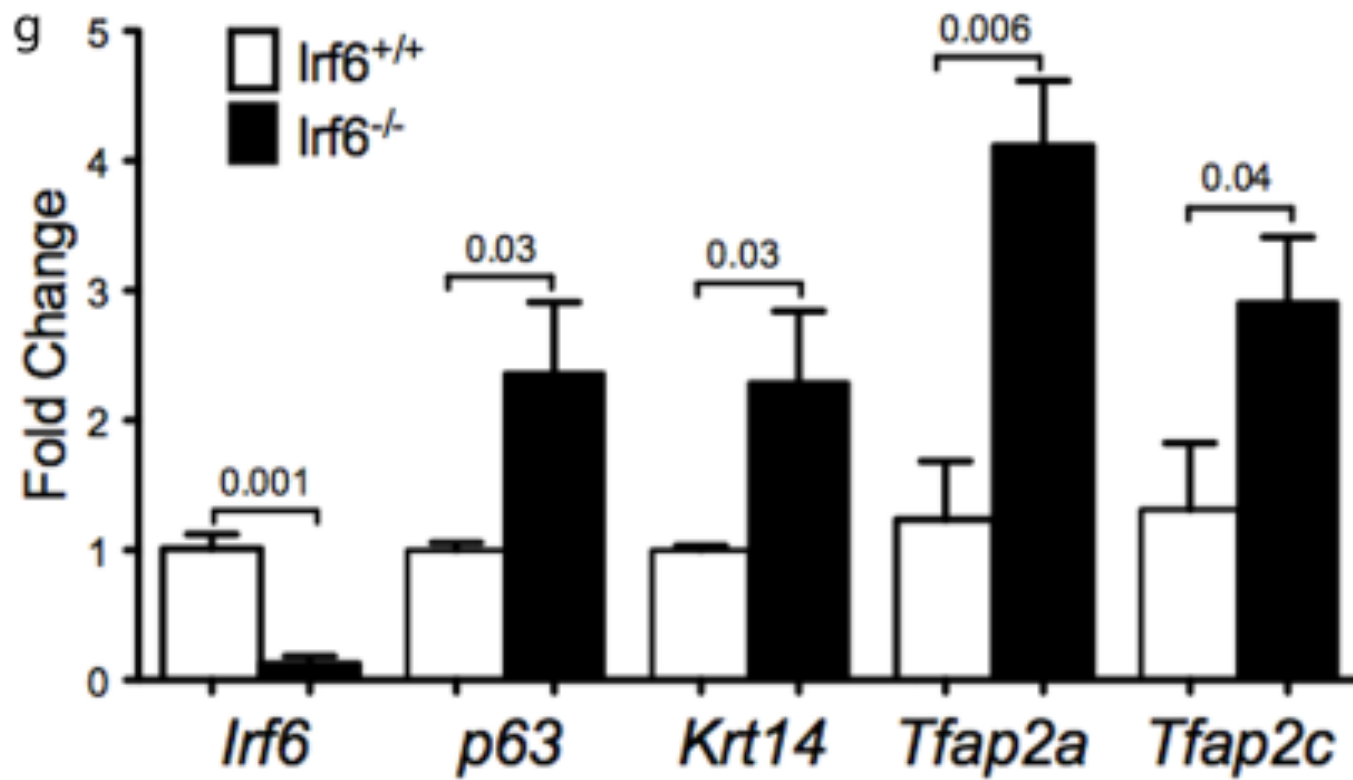


Figure 12. (cont'd)

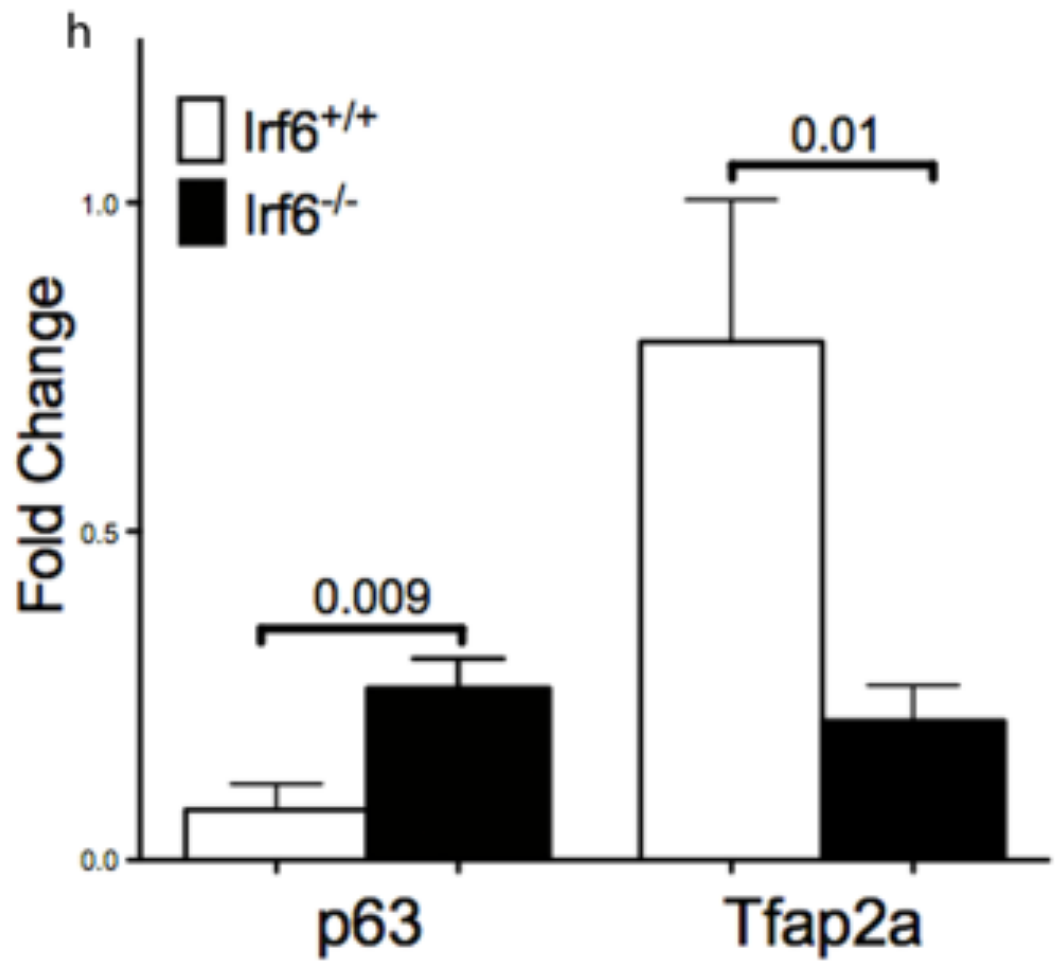


Figure 12. (cont'd)

(a-f) Loss of *Irf6* leads to ectopic *Tfap2α* expression at two different developmental time points. (a-d) Representative images of wildtype (a,c) (*Irf6*^{+/+}, n=4, white) and *Irf6*^{-/-} (b,d) embryos (n=4, black) at E14.5, immunostained for (a-b) *Krt14* (red) and *Lef1* (green) and (c-d) *Tfap2α* (red). In all sections, DAPI marks the nuclei (blue). In *Irf6*^{-/-} (b, d), while *Lef1* expression remains restricted to the basal cell layer, *Tfap2α* is ectopically expressed. (e-f) Immunostaining of *Tfap2α* (green) and *Irf6* (red) in wildtype (n=3) (e) and *Irf6*^{-/-} (b,d) embryos (n=5) at E17.5, when murine skin has embryonic reached maturation. In wildtype embryos *Tfap2α* is restricted to basal and spinous cells (e) while *Irf6* expression is more robustly seen superiorly. In wildtype embryos *Tfap2α* is restricted to basal and spinous cells (e) while *Irf6* expression is more robustly seen superiorly. In contrast, loss of *Irf6* leads to ectopic *Tfap2α* expression (b). Scale bars a-f: 20μm. (g) Loss of *Irf6* in skin leads to ectopic *Tfap2α* expression. Quantitative PCR comparing skin transcriptional profiles in *Irf6*^{+/+} (n=3) and *Irf6*^{-/-} embryos (n=3) at E18.5. Consistent with previous microarray data at E17.5, loss of *Irf6* leads to transcriptional increase in *Trp63*, *Krt14*, *Tfap2α* and *Tfap2c*. (h) Loss of *Irf6* in skin leads to reduction in *Tfap2α* expression, in contrast to *Trp63* at E18.5. Quantitative analysis of western blot data from *Irf6*^{+/+} (n=4) and *Irf6*^{-/-} (n=5) embryonically mature skin given as a ratio relative to *Gapdh* loading control. Consistent with an increase in *Trp63* mRNA level, *Trp63* protein levels increases in *Irf6*^{-/-} skin. In contrast to *Tfap2α* mRNA level, *Tfap2α* protein level is reduced. Bar graphs presented as a mean ± SEM. A Student's t-test is used to analyze significance and a p-value is shown above the groups being compared.

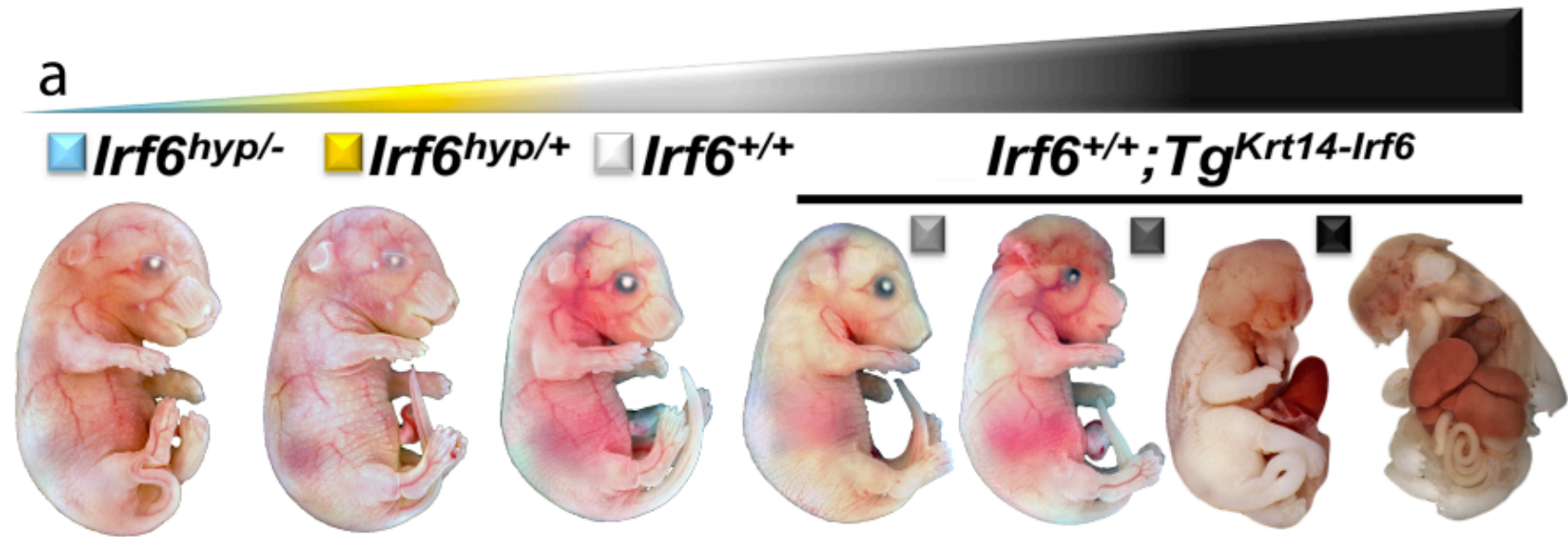


Figure 13: *Irf6* homeostasis is required for neurulation and *Tfap2α* expression in epidermis.

Figure 13. (cont'd)

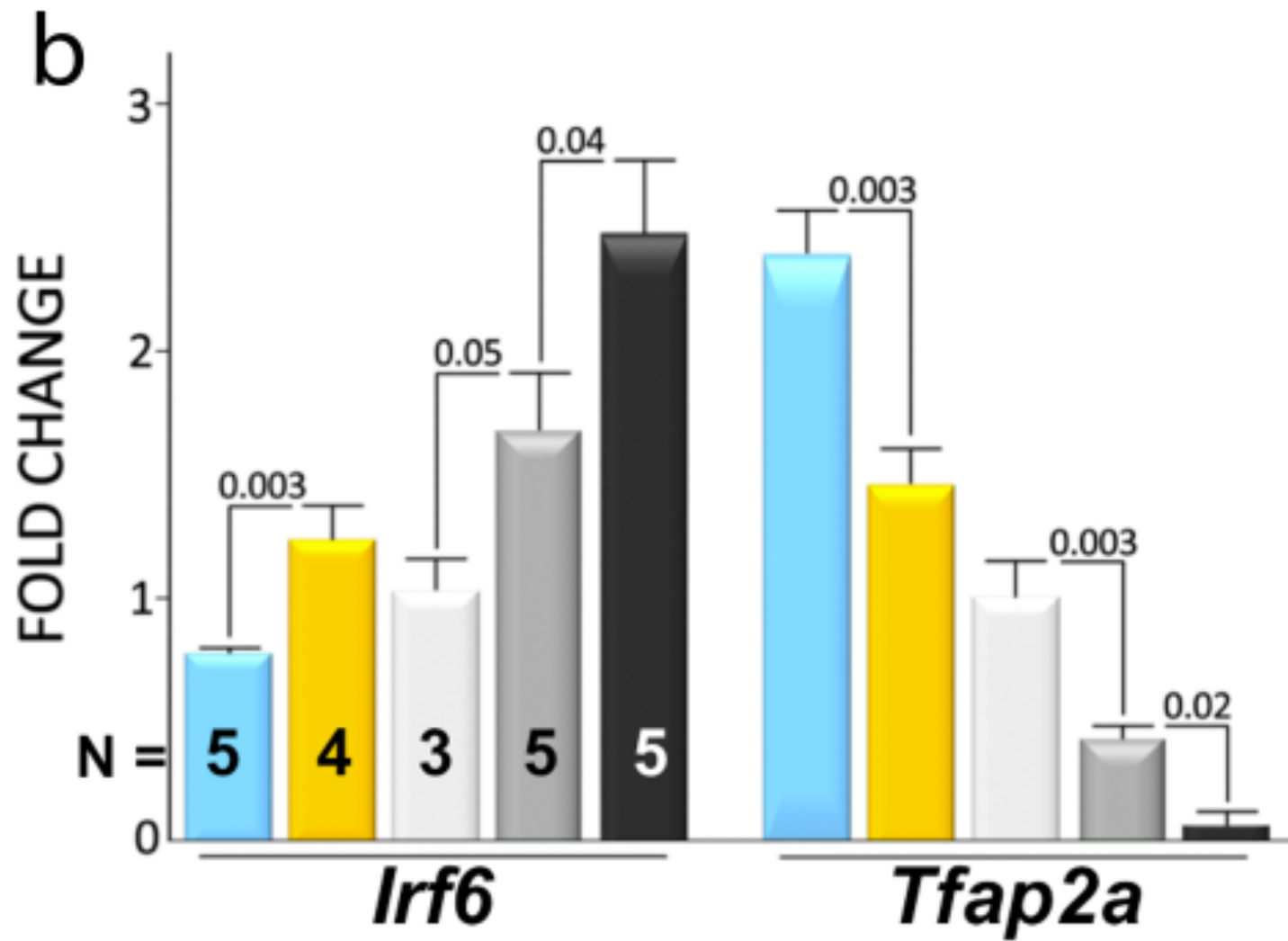


Figure 13. (cont'd)

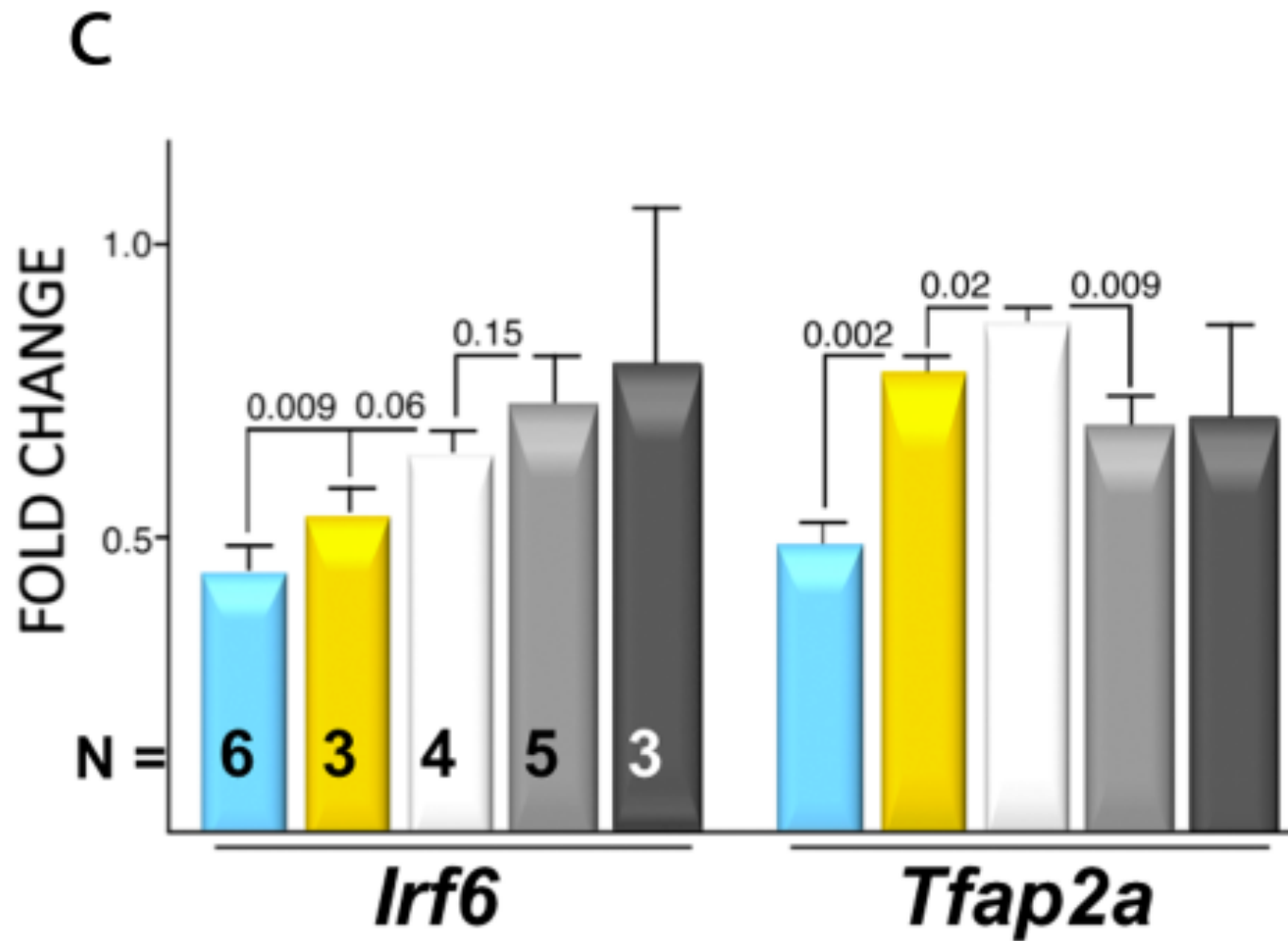


Figure 13. (cont'd)

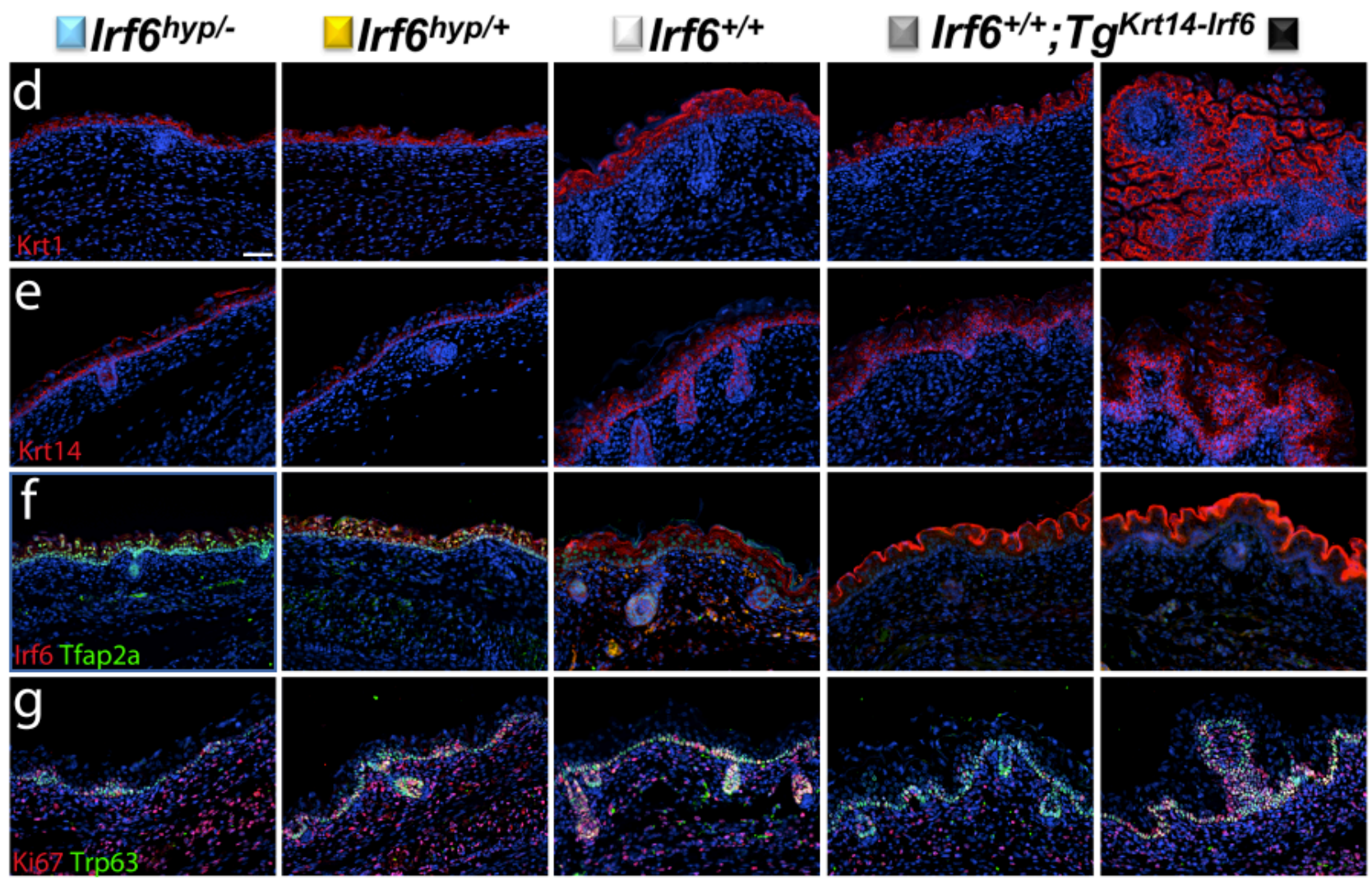


Figure 13. (cont'd)

(a) Neural tube development is exquisitely sensitive to *Irf6* dose. Representative whole-mount of an *Irf6* allelic series at E17.5. (b,c) qPCR and Western blot data shows direct correlation between *Irf6* expression in skin and severity of neural tube defect at E17.5. Transcriptional profiling (b) for *Irf6* and *Tfap2α* shows a direct negative correlation embryos with 5 grossly different phenotype, including *Irf6*^{ey/-} (n=5, blue), *Irf6*^{ey/+} (n=4, orange), *Irf6*^{+/+} (n=3, white), *Irf6*^{tg-wt} (n=5, gray), *Irf6*^{tg-an} (n=5, black). Quantification of western blots from skin at E17.5 (c) for proteins of interests was calculated relative to an internal *Gapdh* loading control. Values on the y-axis represent absolute ratio. Pattern of transcriptional changes in *Irf6* expression highly correlate with *Irf6* protein quantity. However, both over-expression and under-expression of *Irf6* leads to a reduction in *Tfap2α* among 5 grossly different phenotypes, including *Irf6*^{ey/-} (n=6), *Irf6*^{ey/+} (n=3), *Irf6*^{+/+} (n=4), *Irf6*^{tg-wt} (n=5), *Irf6*^{tg-ex} (n=3). (d-g) Skin immunofluorescence at E17.5. In all sections, DAPI marks the nuclei (blue). In a manner analogous to neural tube development, both over and under-expression of *Irf6* leads to skin pathology in *Irf6*^{ey/-}, *Irf6*^{ey/+}, *Irf6*^{+/+}, *Irf6*^{tg-wt} and *Irf6*^{tg-an}. (d) Krt1 (red); (e) Krt14 (red); (f) *Irf6* (red) and *Tfap2α* (green); (g) Ki-67 (red) and Trp63 (green).

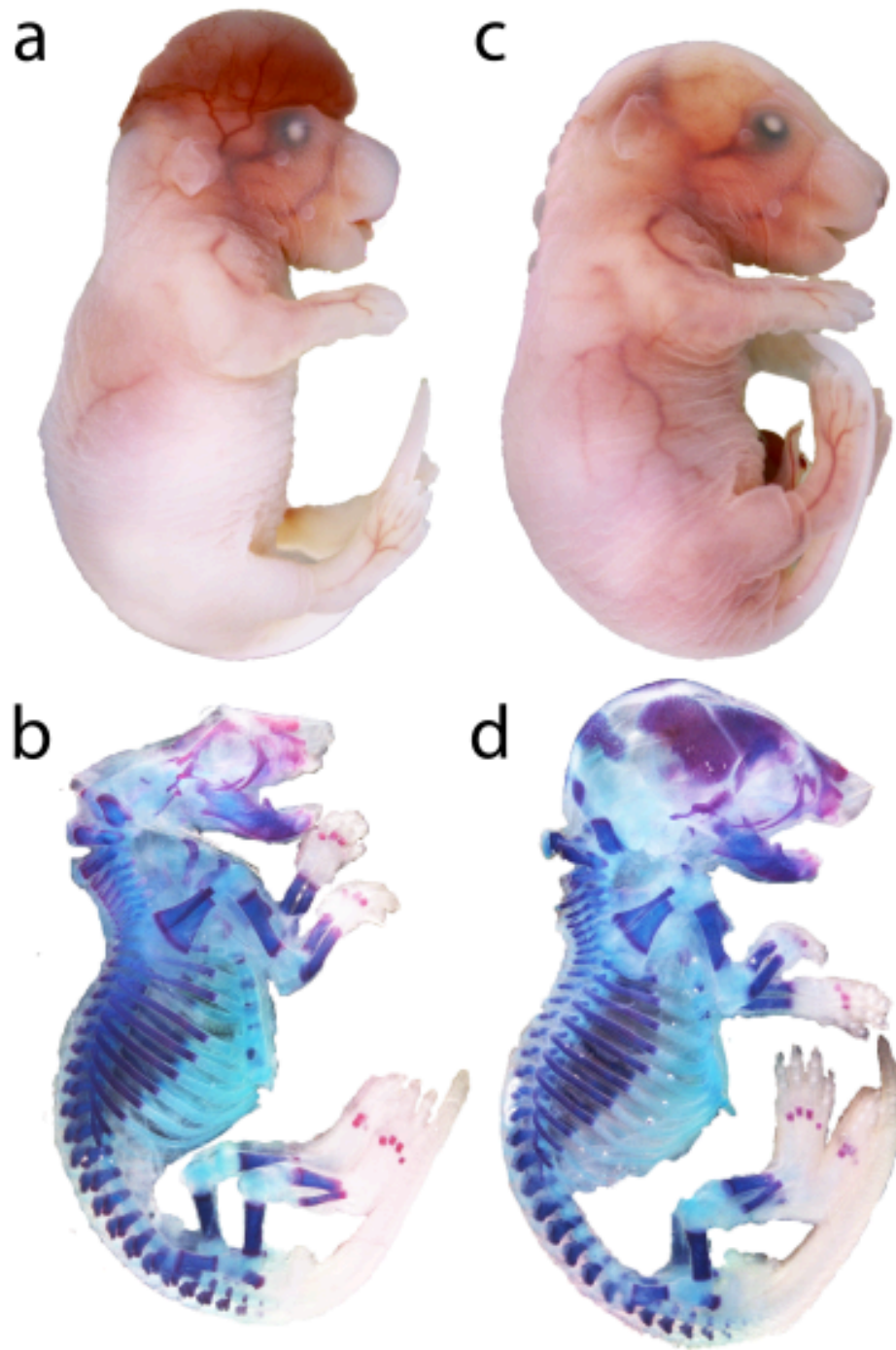


Figure 14: Endogenous and Transgenic *Irf6* expression regulates *Tfap2 α* in neurulation.

Figure 14. (cont'd)

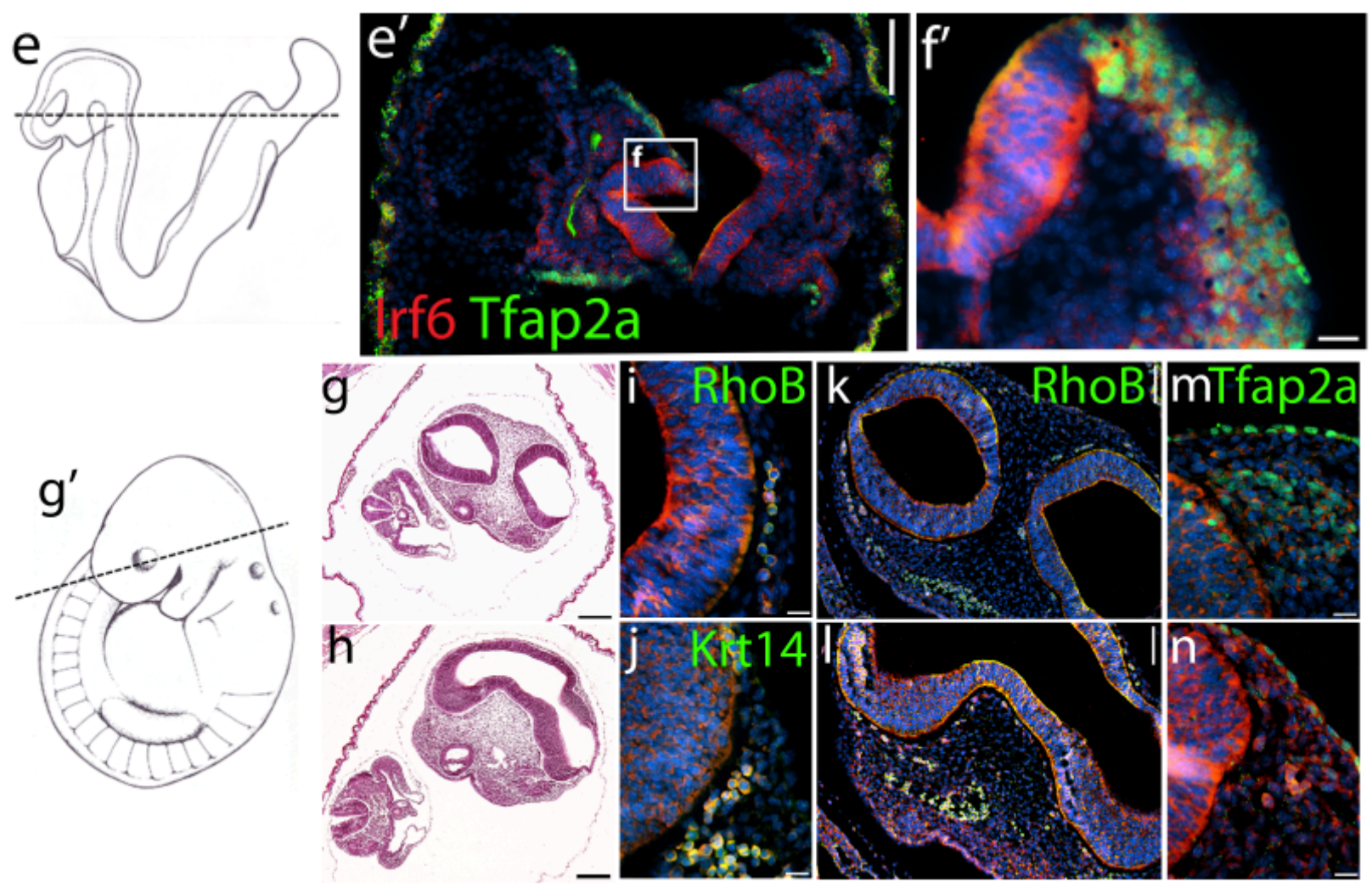


Figure 14. (cont'd)

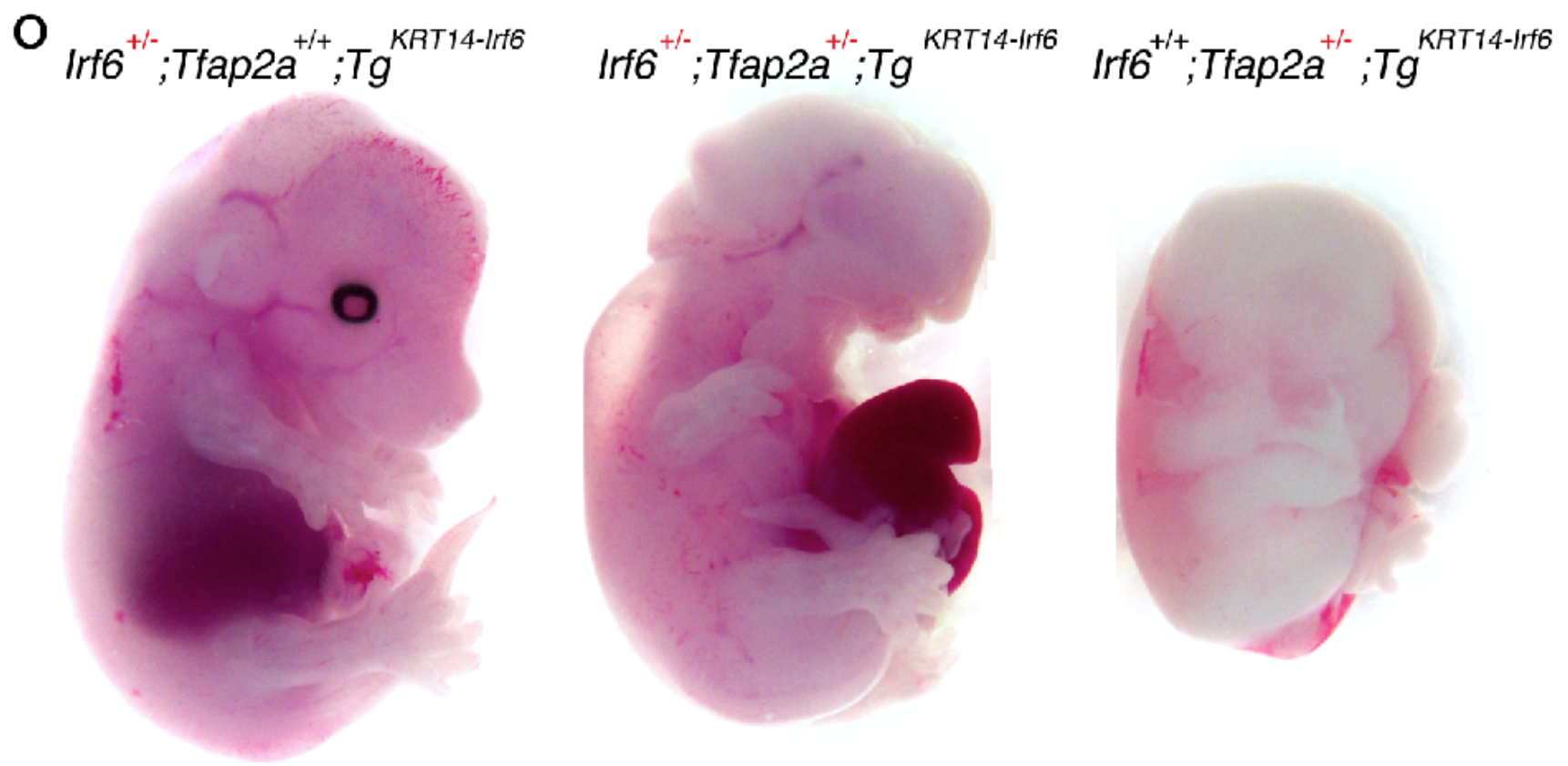


Figure 14. (cont'd)

Intergenic suppression of *Irf6* rescues *Tfap2a* haploinsufficiency. (a-b) Representative whole-mount images *Tfap2a*^{LacZ/+} haploinsufficient embryos E17.5 (n=7 affected from 68 *Tfap2a*^{LacZ/+} heterozygous embryos examined). These results were completely reproducible with the *Tfap2a* knockout allele. (a) 10% of *Tfap2a*^{+/-} embryos have exencephaly, limb defects, frontonasal hypoplasia with a protruding tongue, abnormally folded pinna and low-set ears and abnormal limbs and digits. (b) Skeletal prep of *Tfap2a*^{LacZ/+} haploinsufficient embryos show absence of the skull bones, including the frontal, parietal and intra-parietal bones. (c-d) Representative whole-mount images *Tfap2a*^{LacZ/+};*Irf6*^{+/-} embryos E17.5 (n=69, 0 affected, p=0.0063). (c) 100% of *Tfap2a*^{LacZ/+};*Irf6*^{+/-} embryos have grossly normal craniofacial and limb. (d) Skeletal prep of *Tfap2a*^{LacZ/+};*Irf6*^{+/-} embryos shows complete rescue of neural tube development, including craniofacial and limb structures. (e-n) Representative images are shown for all histological and immunostained data. (e-f) Immunostaining at E8.5 shows *Irf6* and *Tfap2a* co-localization in neural tube, superficial ectoderm and neural crest cells. (e') Plane of section at E8.5, for images e-f. In all sections, DAPI marks the nuclei (blue). (e) *Irf6* (red) and *Tfap2a* (green) are co-expressed in the neural plates, non-neural superficial ectoderm, and neural folds. (f') magnified view of white box (f) in (e) showing *Irf6* (red) and *Tfap2a* (green) co-localization. (g-n) Histological analysis and immuno-staining reveals neural tube defects and loss of *Tfap2a* cells in embryos over-expressing *Irf6* as early as E9.5. (g') marks the plane of the section for (g-n). (g-h) histological analysis of wildtype (g) and mutant embryos over-expressing *Irf6* (h). Wild type embryos have both rostral and caudal neural tube closure, with intact facial mesenchyme (g).

Figure 14. (cont'd)

In contrast, littermate mutant embryos show severe neural tube closure defects rostrally and closure delay caudally, abnormal optic vesicle and disorganized facial mesenchyme (h). (i-n) Immunostaining of wildtype (i-j,k,m) and mutant littermates (l,n). (i-n), *Irf6* (red) and DAPI (blue). (i) RhoB (green), marks neural crest cells, co-localizes with *Irf6*. (j) *Krt14* (green), co-expressed with *Irf6*, stains both the neural tube and neural crest cells. (k-l) RhoB (green). Compared to wildtype embryos (k), mutant littermates have ectopic *Irf6* expression and abnormal rostral neural tube closure and neural crest cell migration (l). (m-n) *Tfap2α* (green). Wildtype embryos (m) have *Irf6* (red) and *Tfap2α* co-localization in neural tube and pre-migratory neural crest cells whereas mutant littermates have ectopic *Irf6* expression and loss of *Tfap2α* staining in the neural tube and neural crest but not non-neural epithelium (n). (o) Endogenous and transgenic *Irf6* expression cooperate to functionally antagonize *Tfap2α* in skin, limb craniofacial and body-wall development. While *Irf6*^{+/-};*Tfap2α*^{+/+};*Tg*^{KRT14-Irf6} (n=12) do not develop neural tube defects, 10% of *Irf6*^{+/-};*Tfap2α*^{+/-};*Tg*^{KRT14-Irf6} (n=10, 1 affected) develop anencephaly and an abdominal wall defect. In contrast, 55% of *Irf6*^{+/+};*Tfap2α*^{+/-};*Tg*^{KRT14-Irf6} (n=18, 10 affected, 8 grossly normal) developed more severe neural tube, limb and abdominal wall defects (p-value = 0.02).

a

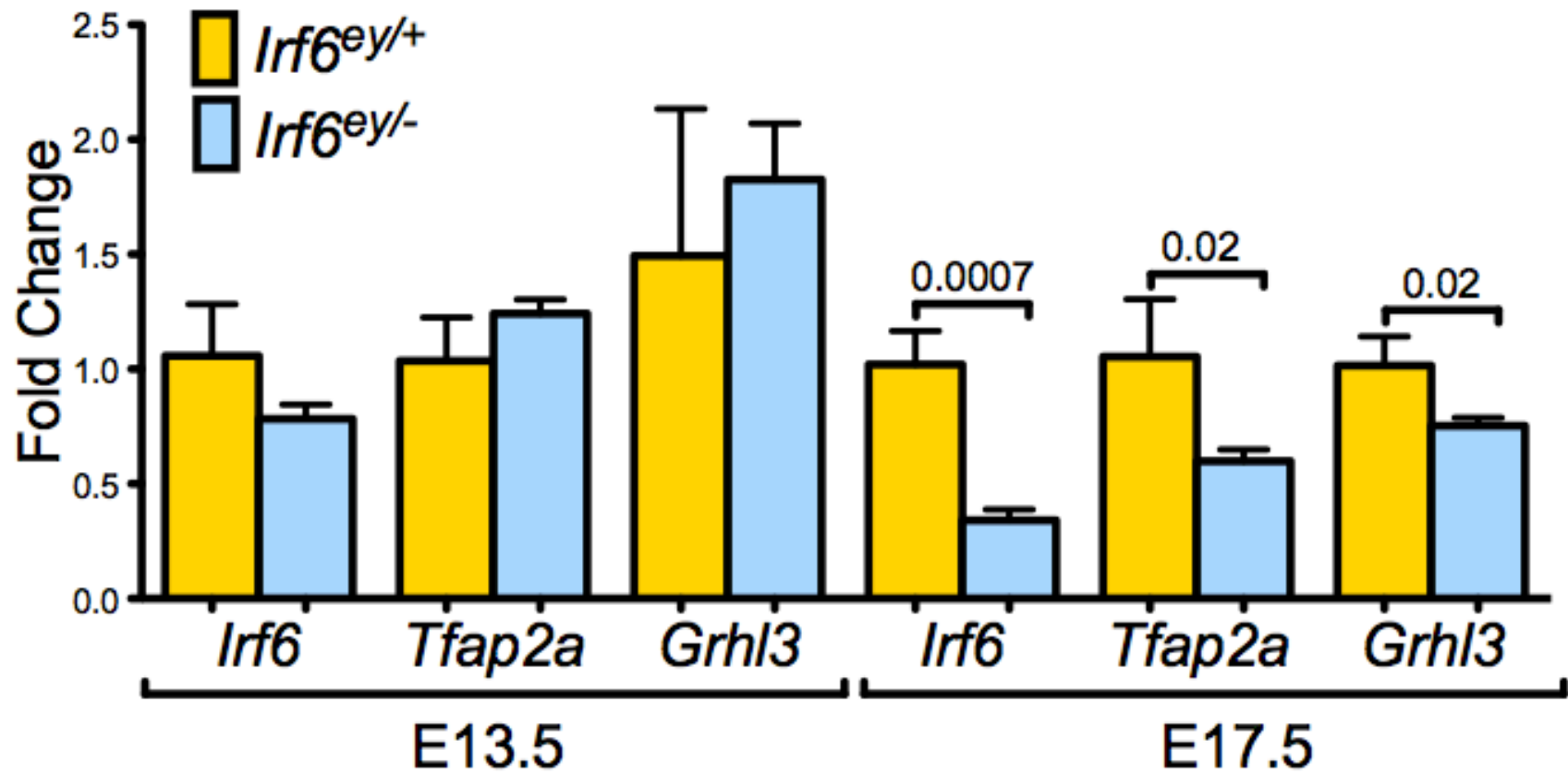


Figure 15: *Tfap2a* and *Grhl3* interact in caudal neurulation.

Figure 15. (cont'd)

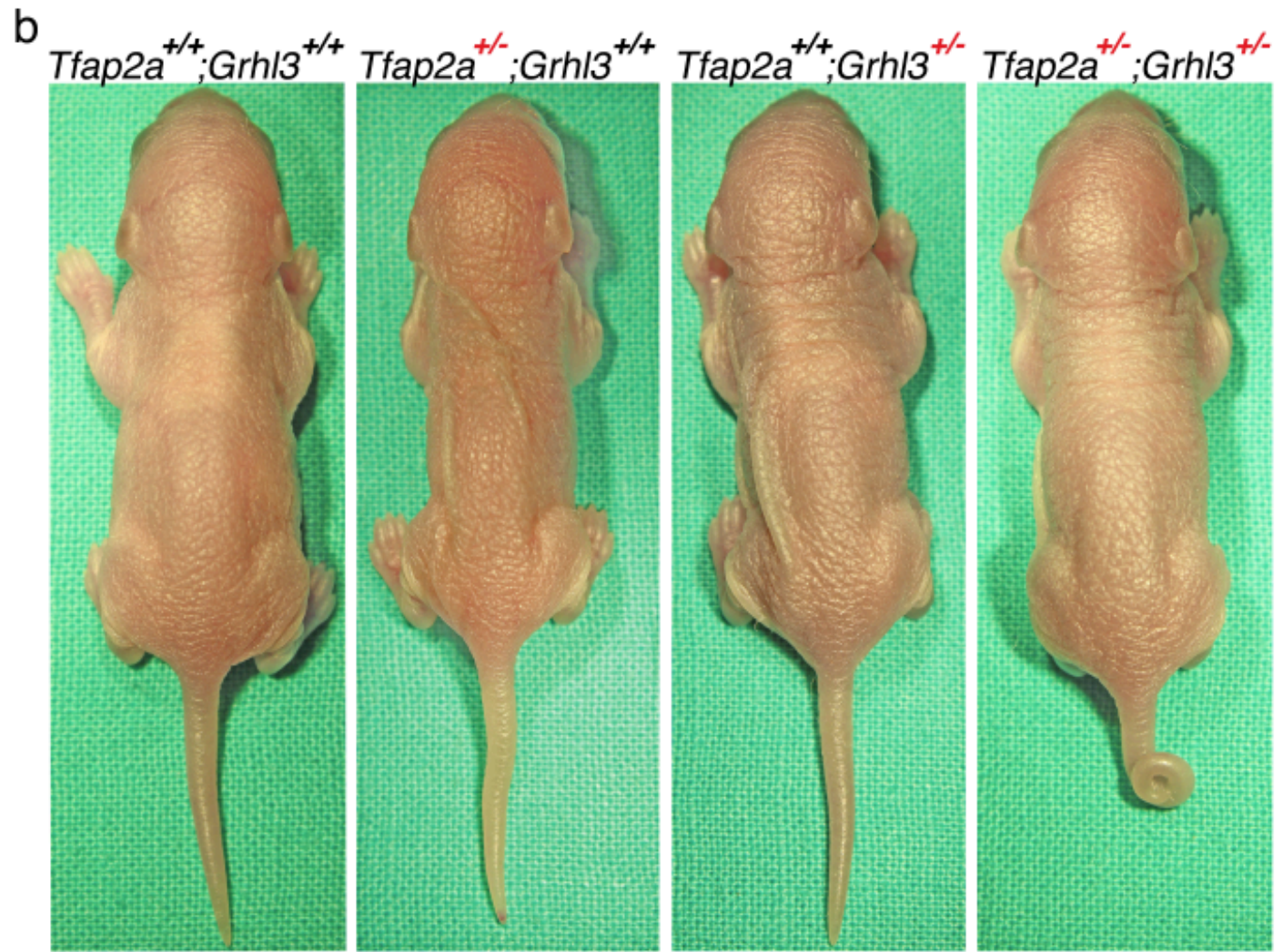


Figure 15. (cont'd)

(a) In contrast to skin, reducing *Irf6* expression in tail leads to reduction in *Tfap2α* and *Grhl3*. (a) qPCR data at E13.5 and E17.5 from whole-tail RNA extraction. Transcriptional profiling shows that reducing *Irf6* in *Irf6^{ey/-}* (n=5, blue) as compared to littermates with the wildtype allele, *Irf6^{ey/+}* (n=3, orange), leads to a reduction of *Irf6* and a corresponding reduction in *Tfap2α* and *Grhl3* at E17.5 but not E13.5, when tail abnormalities are not yet obvious (data not shown). (b) While wildtype, and singly heterozygous pups and embryos for *Grhl3* and *Tfap2α* have a grossly normal tail, 15% of double heterozygous, *Tfap2α^{+/-};Grhl3^{+/-}*, embryos and pups (n=20, 3 affected) have a grossly curled tail, defined as >90° change in tail angle from base to tip.

a

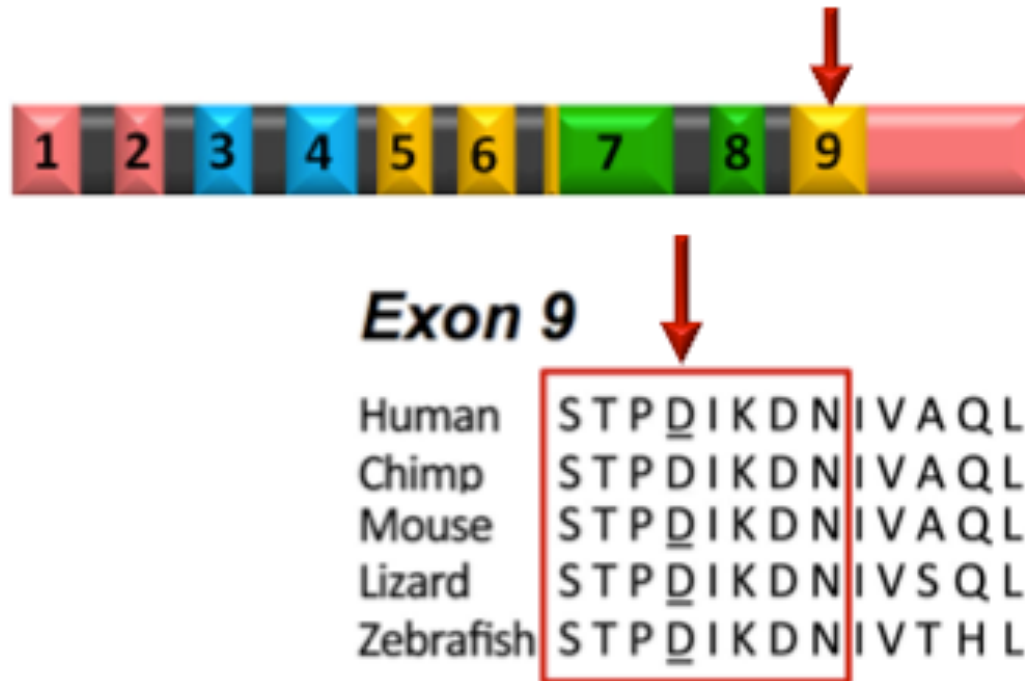
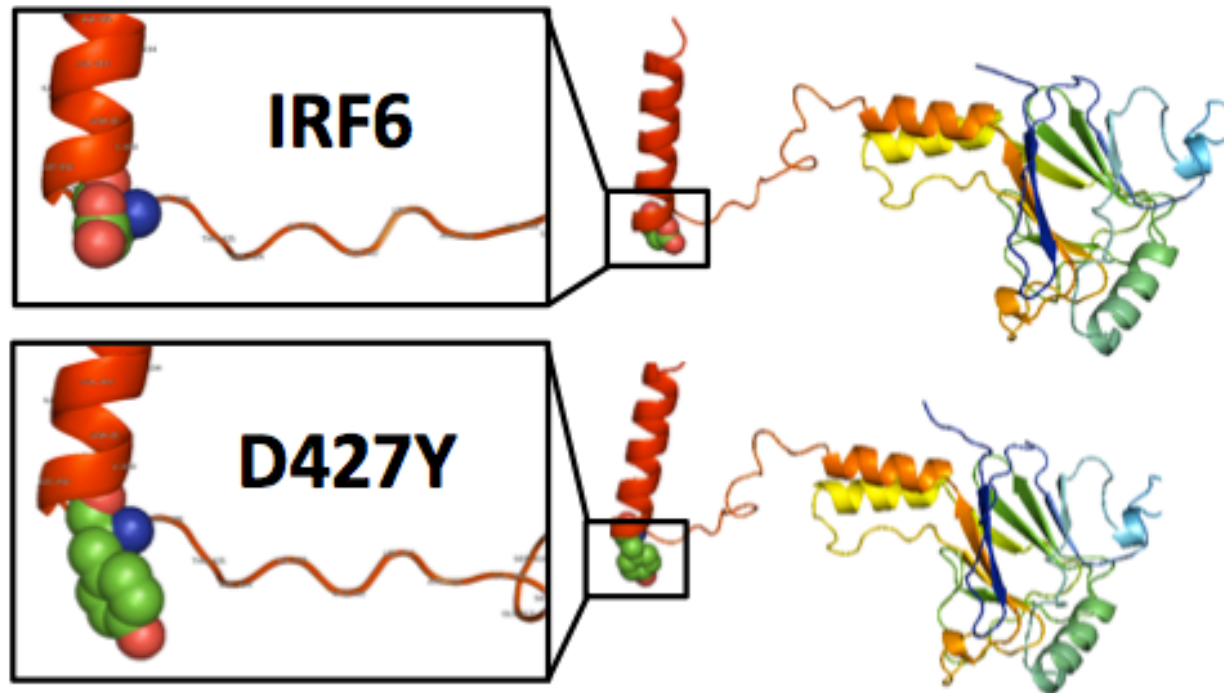


Figure 16: Shared IRF6 mutation in Spina Bifida and VWS.

Figure 16. (cont'd)



Sequencing of 96 patients with Spina Bifida reveals shared mutation in orofacial clefting and neural tube defects. The mutation, D427Y, occurs at a highly conserved amino acid within exon 9. Structural analysis shows that the mutation is found at the junction of a non-ordered linker region and a the c-terminal alpha-helix of IRF.

Table 6: Association between IRF6 (rs642961) and risk of NTDs

rs642961 Genotype	Case	Control	OR (%95 CI)	Adjusted OR* (95% CI)
<u>Among All</u>				
AA	53	42	1.3 (0.8-2.0)	1.3 (0.8-2.0)
GA	89	113	0.8 (0.6-1.1)	0.8 (0.6-1.2)
GG	283	292	Reference	
<u>Among white</u>				
AA	6	8	1.0 (0.3-2.9)	
GA	33	49	0.9 (0.5-1.4)	
GG	85	108	Reference	
<u>Among HISP-NB</u>				
AA	13	10	1.3 (0.5-3.3)	
GA	14	20	0.7 (0.3-1.6)	
GG	44	44	Reference	
<u>Among HISP-FB</u>				
AA	30	18	1.3 (0.7-2.6)	
GA	36	35	0.8 (0.5-1.4)	
GG	124	100	Reference	
<u>Among Black</u>				
AA	0	0	---	
GA	3	4	0.8 (0.2-4.2)	
GG	15	16	Reference	
<u>Among Asian</u>				
AA	3	6	1.0 (0.2-5.0)	
GA	3	5	1.3 (0.3-6.2)	
GG	11	23	Reference	

* Adjusted for race/ethnicity.

Table 7: Association between IRF6 (rs75012801) and risk of NTDs

rs75012801 Genotype	Case	Control	OR (%95 CI)	Adjusted OR* (95% CI)
<u>Among ALL</u>				
TG	5	7	0.7 (0.2-2.4)	0.7 (0.2-2.1)
TT	420	438	Reference	
<u>Among White</u>				
TG	1	2	0.7 (0.1-7.4)	
TT	122	161	Reference	
<u>Among HISP-NB</u>				
TG	1	1	1.0 (0.1-16.8)	
TT	70	72	Reference	
<u>Among HISP-FB</u>				
TG	3	4	0.6 (0.1-2.7)	
TT	188	149	Reference	
<u>Among Black</u>				
TG	0	0	---	
TT	18	20	Reference	
<u>Among Asian</u>				
TG	0	0	---	
TT	17	35	Reference	

Table 8: Association between IRF6 (rs17317411) and risk of NTDs

rs17317411 Genotype	Case	Control	OR (%95 CI)	Adjusted OR* (95% CI)
<u>Among ALL</u>				
CC	1	3	0.4 (0.04-3.5)	0.5 (0.05-4.6)
TC	73	66	1.2 (0.8-1.7)	1.2 (0.9-1.8)
TT	351	382	Reference	
<u>Among White</u>				
CC	1	3	0.5 (0.1-4.8)	
TC	34	32	1.6 (0.9-2.7)	
TT	89	132	Reference	
<u>Among HISP-NB</u>				
CC	0	0	---	
TC	6	13	0.4 (0.2-1.2)	
TT	64	61	Reference	
<u>Among HISP-FB</u>				
CC	0	0	---	
TC	27	16	1.4 (0.7-2.7)	
TT	164	138	Reference	
<u>Among Black</u>				
CC	0	0	---	
TC	2	3	0.7 (0.1-4.8)	
TT	16	17	Reference	
<u>Among Asian</u>				
CC	0	0	---	
TC	2	1	4.5 (0.4-53.9)	
TT	15	34	Reference	

* Adjusted for race/ethnicity.

Tables 6 – 8 show sequencing results from our examination of an association between *IRF6* variants and Spina Bifida. While sequencing is currently on-going, we have examined three variants, including rs642961 (MAF 17%), rs17371411 (MAF 8%), rs75012801 (MAF 0.8%). At this point, these three *IRF6* variants do not appear to be associated with spina bifida.

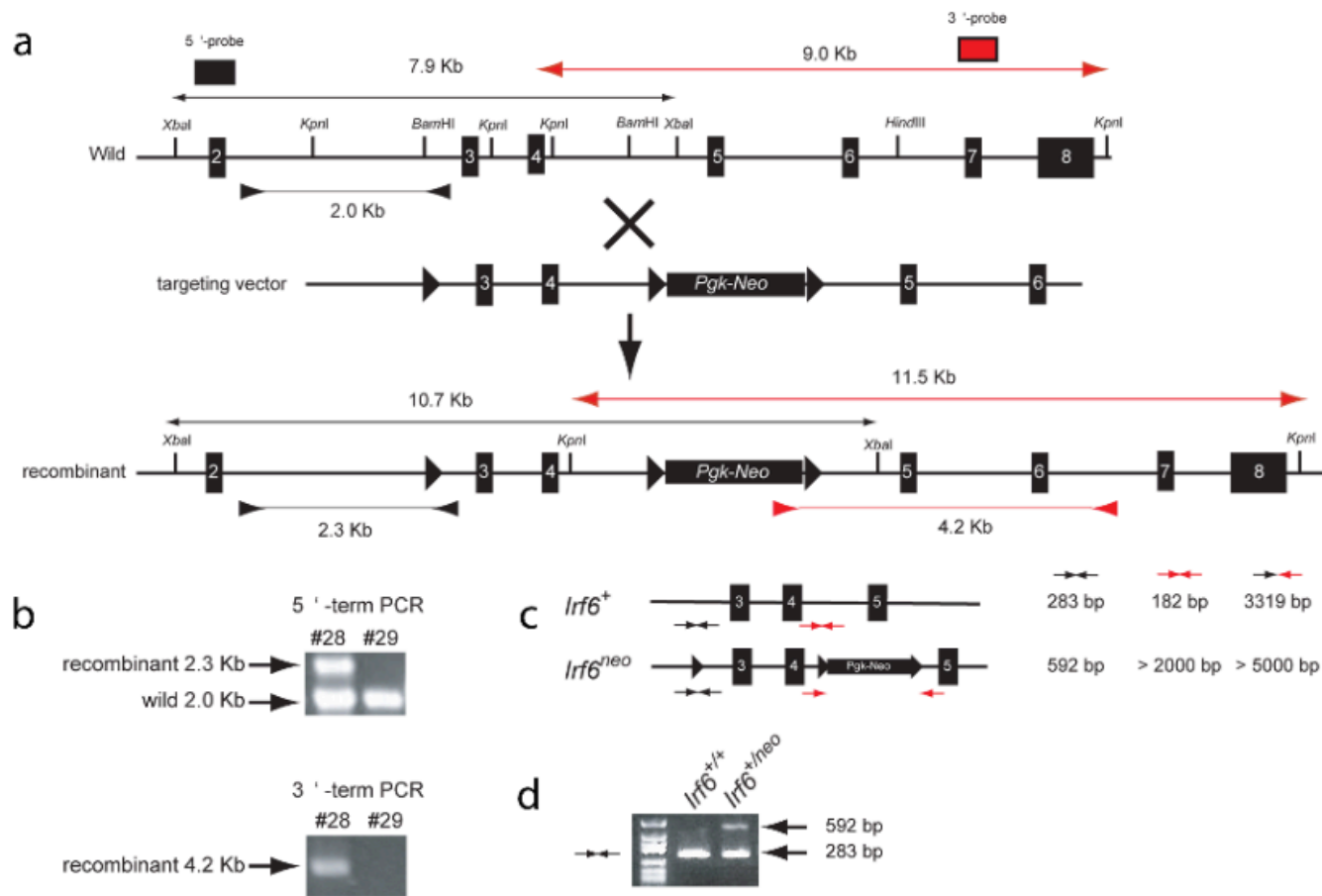


Figure 17: Generation of *Irf6* hypomorphic allele.

Figure 17. (cont'd)

(a) We inserted a neomycin cassette, bracketed with LoxP sites (black triangles within intron), into intron 4 of a *Irf6* BAC clone. Spanning introns two-six, we inserted a Pgk-Neo cassette into intron 4. (b) 5 and 3 prime PCR was used to confirm wildtype (#29) and recombinant clones (#28). (c) For genotyping, two primer sets were designed. In intron two, one set is designed to bracket a LoxP site in the recombined clone (black arrows). In intron four, an additional primer set brackets the Pgk-Neo cassette (red). Primer combinations and fragment sizes are also shown. (d) PCR confirms genotypes of *Irf6* wildtype and hypomorphic (*Irf6^{neo}* or *Irf6^{ey}*) embryos.

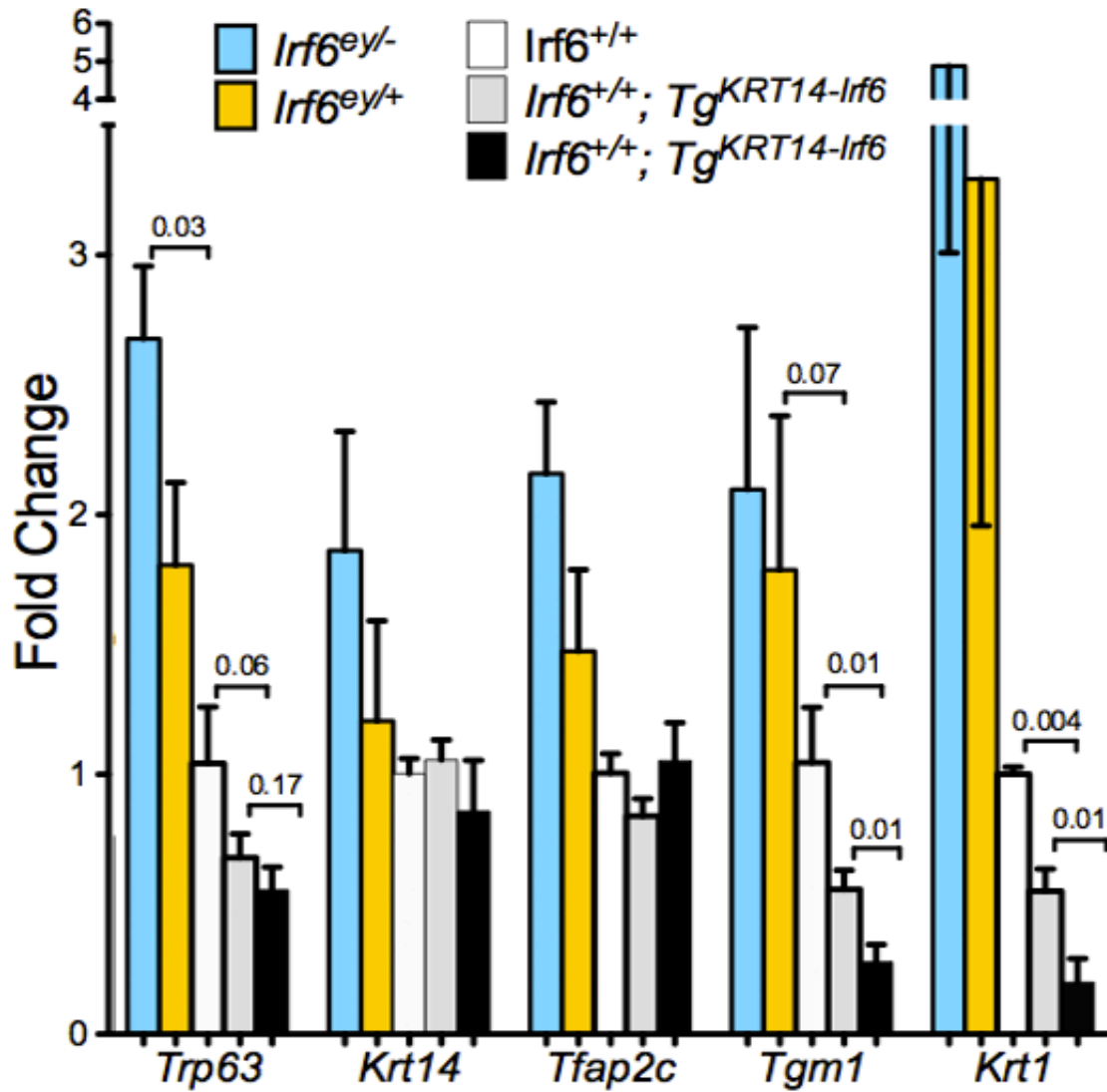


Figure 18: *Irf6* transcriptionally regulates *Trp63*, *Tgm1* and *Krt1* but not *Krt14* and *Tfp2c* in skin.

Figure 18. (cont'd)

Genotypes and biological replites include $Irf6^{ey/-}$ (n=5, blue), $Irf6^{ey/+}$ (n=4, orange), $Irf6^{+/+}$ (n=3, white), $Irf6^{tg-wt}$ (n=5, gray), $Irf6^{tg-an}$ (n=5, black). In addition to post-translational degradation, we found that reducing *Irf6* lead to an increase in *TrTrp63* mRNA. While over-expressing *Irf6* was associated with reduction in *TrTrp63* mRNA, this was not statistically significant. While loss of *Irf6* leads to ectopic *Krt14* and *Tfap2c*, modulation of *Irf6* dose did not alter *Krt14* or *Tfap2c* transcript. In contrast, over-expressing *Irf6* lead to reduction in *Krt1* and *Tgm1*, consistent with *Irf6* driving differentiation in epidermis.

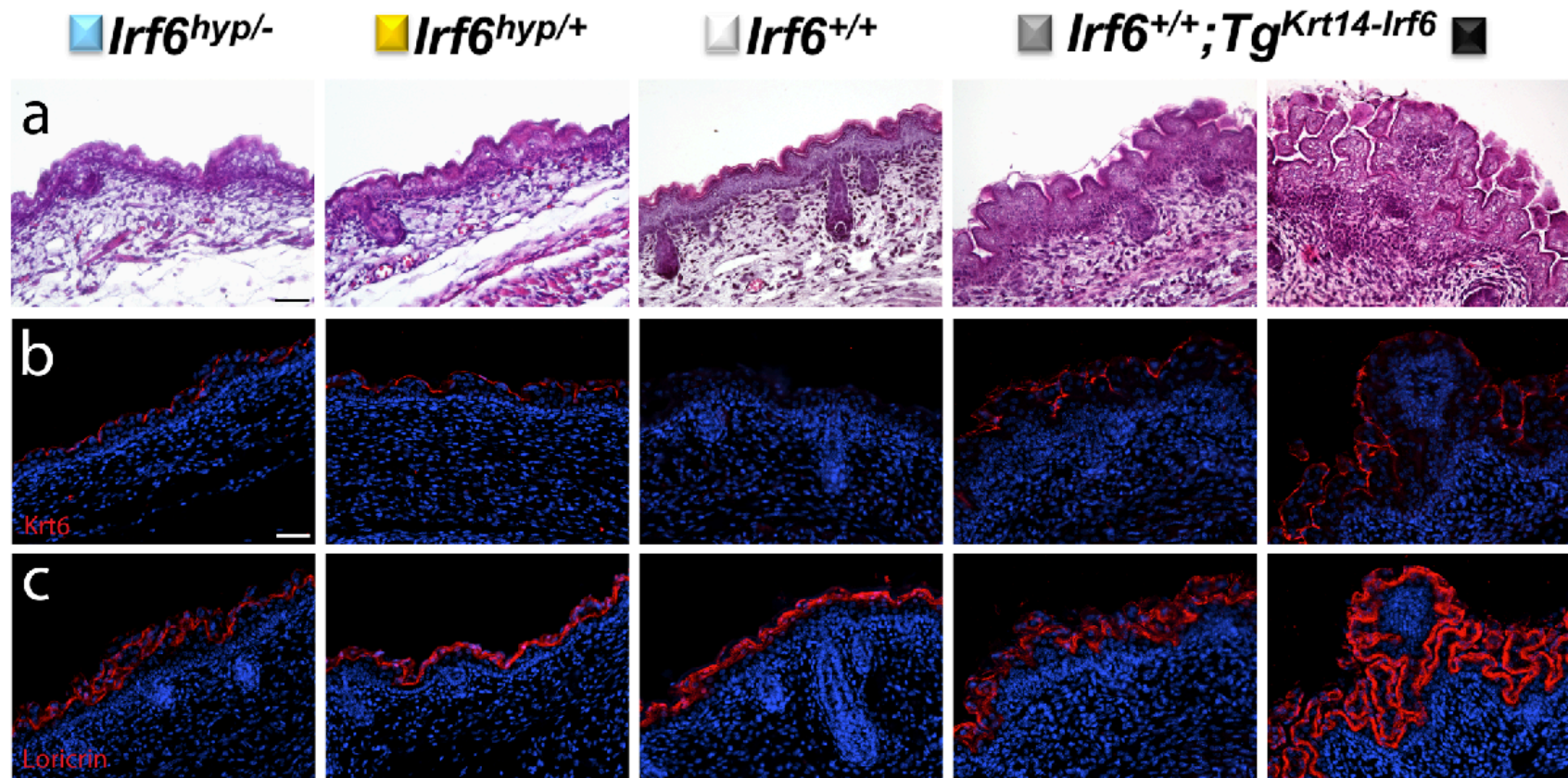


Figure 19: *Irf6* homeostasis is required for epidermal development.

Figure 19. (cont'd)

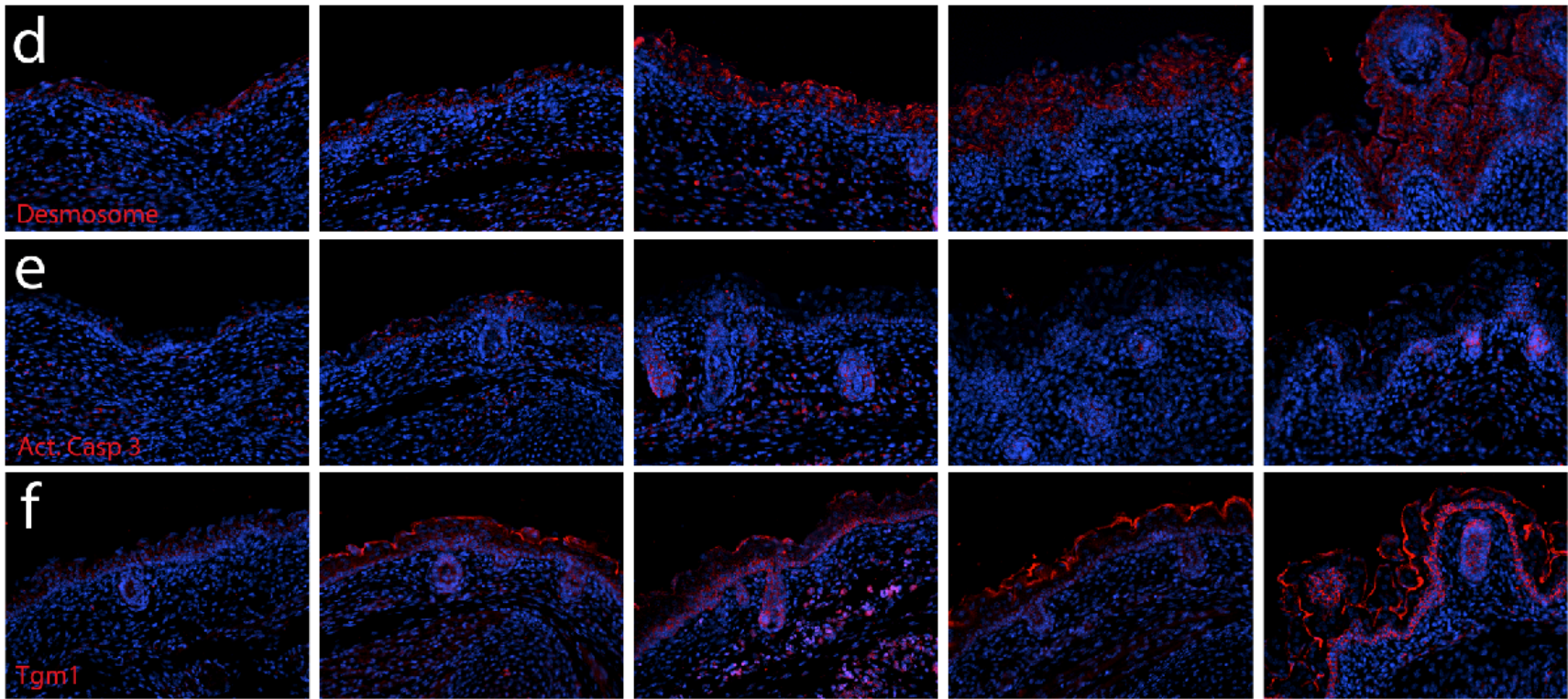


Figure 19. (cont'd)

(a-f) Skin development is exquisitely sensitive to *Irf6* dose. (a) Representative skin histology of an *Irf6* allelic series at E17.5, stained with Hematoxylin and Eosin. *Irf6* regulates epidermal thickness, with reductions leading to hypotrophic and over-expression leading to hypertrophic skin. (b-f) Skin immunofluorescence of an *Irf6* allelic series at E17.5. In manner highly analogous to neural tube development, both over and under-expression of *Irf6* leads to skin pathology in *Irf6*^{ey/-}, *Irf6*^{ey/+}, *Irf6*^{+/+}, *Irf6*^{tg-wt} and *Irf6*^{tg-an}. Counter-staining of nuclei with DAPI (blue) is seen in all sections. (b) Krt6 (red); (c) Loricrin (red); (d) desmosome; (e) Activated Caspase 3 (red); (f) Tgm1 (red).

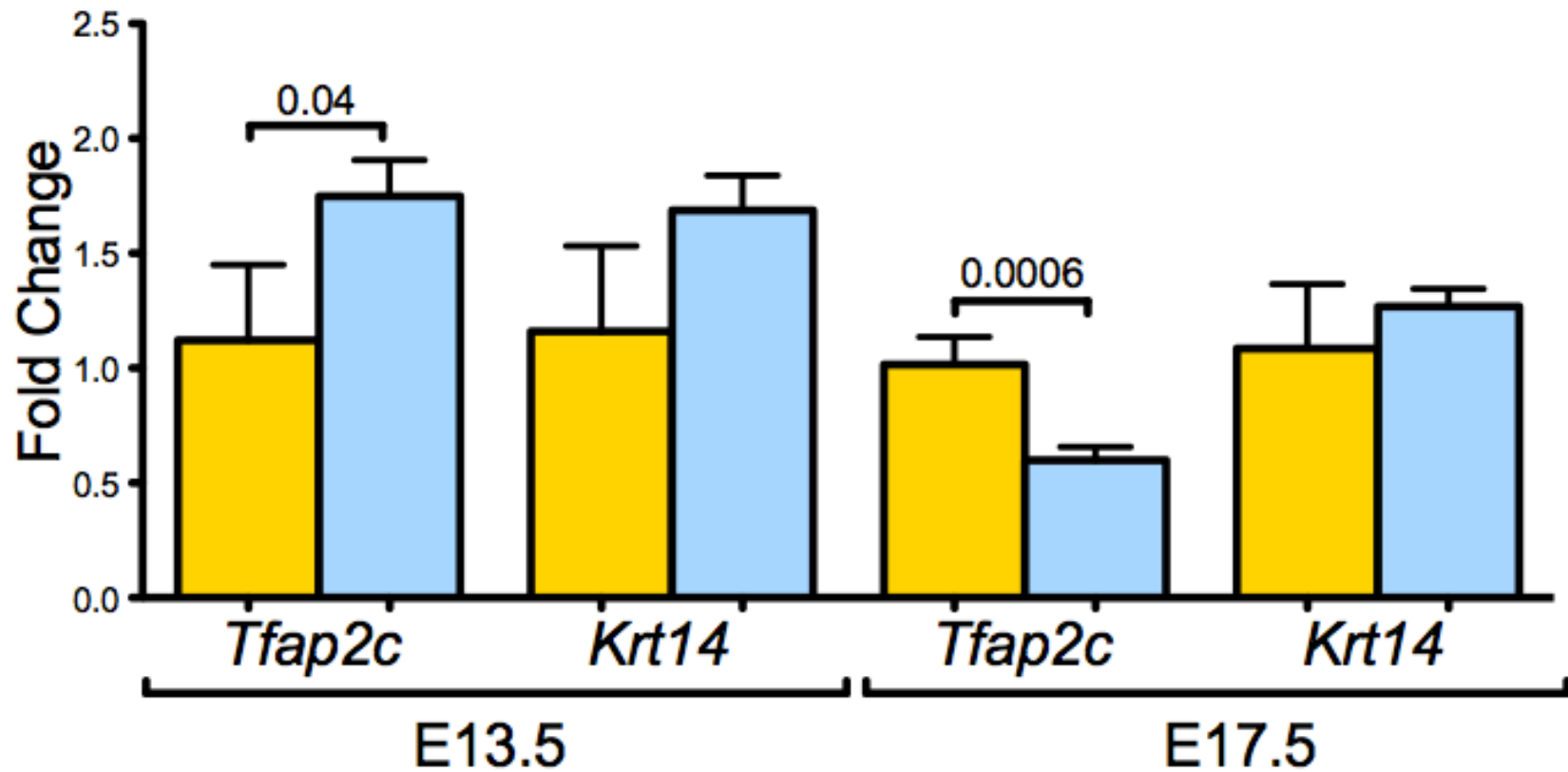


Figure 20: *Irf6* Transcriptionally regulates *Tfap2c* but not *Krt14* in tail development. Reducing *Irf6* in tail tissue leads to an increase of *Tfap2c* at E13.5 but a decrease at E17.5, in direct contrast to skin tissue. *Irf6* does not regulate *Krt14* in the tail at either timepoint.

Table 9: $Tfap2\alpha^{+/-};Tg^{MCS9.7-LacZ}$

	E13.5	E17.5	Total
Litters	3	8	11
$Tfap2\alpha^{+/+}$	4	4	8
$Tfap2\alpha^{+/-}$	3	13	16
$Tfap2\alpha^{-/-}$	3	5	8
$Tfap2\alpha^{+/+};Tg^{MCS9.7-LacZ}$	1	6	7
$Tfap2\alpha^{+/-};Tg^{MCS9.7-LacZ}$	4	20	24
$Tfap2\alpha^{-/-};Tg^{MCS9.7-LacZ}$	7	4	11
Total	19	47	66
p-value	0.36	0.29	0.71
Resorbing	3	8	11 (p=0.0086)

We intercrossed mice hemizygous for the $Tg^{MCS9.7-LacZ}$ transgene with mice heterozygous for the $Tfap2\alpha$ knockout allele. To produce the F2 progeny that were $Tfap2\alpha^{-/-};Tg^{MCS9.7-LacZ}$, we intercrossed $Tfap2\alpha^{+/-};Tg^{MCS9.7-LacZ}$ with $Tfap2\alpha^{+/-}$ mice. We examined embryos at E13.5 and E17.5 and found no differences from the predict distribution. We did find a significant number of resorptions. We also found that one $Tfap2\alpha^{+/-}$ had exencephaly.

Table 10: $Irf6^{ey/-}$ vs. $Irf6^{ey/+}$

	E13.5	E17.5	Total
Litters	1	4	5
$Irf6^{ey/+}$	3	17	20
$Irf6^{ey/-}$	6	18	24
Total	9	35	47
p-value	0.32	.87	.51
Resorbing	0	2	2 (p=0.51)

We intercrossed mice homozygous for the *Irf6* hypomorphic allele ($Irf6^{ey/ey}$) with mice heterozygous for the *Irf6* genetrapped allele ($Irf6^{+/-}$). We examined embryos at E13.5 and E17.5 and found no differences from predicted genotype distribution.

Table 11: *Irf6*^{+/+}; *Tg*^{*KRT14-Irf6*}

	E13.5-E15.5	E16.5 – 18.5	Total
Litters	4	30	34
<i>Irf6</i> ^{+/+}	16	104	120
<i>Irf6</i> ^{+/+} ; <i>Tg</i> ^{<i>KRT14-Irf6</i>}	12	114	126
Total	28	218	246
p-value	.44	.49	0.70
Resorbing	4	19	23 (p=0.0086)

We intercrossed mice hemizygous for the *Tg*^{*KRT14::Irf6*} transgene with either wild type littermates or *Tg*^{*MCS9.7-LacZ*} mice . We examined embryos between E13.5-E15.5 and E16.5-E18.5 and the embryonic distribution did differ from the expected ratios with or without the *MCS9.7-LacZ* transgene. However, we found a significant number of resorbing embryos in either case.

Table 12: $Tg^{KRT14-Irf6}$; $Tg^{KRT14-Irf6}$

	E17.5 – P0	Total
Litters	5	5
$Irf6^{+/+}$	8	8
$Irf6^{+/+}$; $Tg^{KRT14-Irf6}$	32	32
Total	40	40
p-value	.35	0.35
Resorbing	4	4 (p=0.18)

We intercrossed mice hemizygous for the $Tg^{KRT14::Irf6}$. Genotyping protocol does not differentiate between hemizygous and homozygous embryos for the $Tg^{KRT14::Irf6}$ transgene. We calculated the expected ratio as 3:1, $Tg^{KRT14::Irf6}$, to wildtype embryos. We examined embryos at E17.5 and not detect differences from predict distribution. We did not have a sufficiently large sample size to assay resorptions differences.

Table 13: $Tfap2\alpha^{+/-};Irf6^{+/-}$

	E13.5	E15.0	E17.5 – P0	Total
Litters	8	7	23	38
$Tfap2\alpha^{+/+};Irf6^{+/+}$	18	13	34	65
$Tfap2\alpha^{+/-};Irf6^{+/+}$	16	10	41	66
$Tfap2\alpha^{+/+};Irf6^{+/-}$	16	12	38	67
$Tfap2\alpha^{+/-};Irf6^{+/-}$	17	9	43	69
Total	69	45	157	299
p-value	0.98	.25	.43	0.34
Resorbing	1	14	17	32 (p=0.0006)

We intercrossed mice heterozygous for the *Irf6* genetrapped allele ($Irf6^{+/-}$) and the $Tfap2\alpha^{+/-}$ to generate $Tfap2\alpha^{+/-};Irf6^{+/-}$ embryos and pups. We examined embryos at all time points and found no significant difference in embryonic distributions. However, we found a significant number of embryonic resorptions that did not affect any one genotype.

Table 14: $Tfap2\alpha^{-/-}$

	E17.5 – P0	Total
Litters	9	9
$Tfap2\alpha^{+/+}$	16	16
$Tfap2\alpha^{+/-}$	29	29
$Tfap2\alpha^{-/-}$	4	4
Total	49	49
p-value	0.02	0.02
Resorbing	8	8 (p=0.047)

We intercrossed mice heterozygous for $Tfap2\alpha^{+/-}$ allele. In this cross, we found that three $Tfap2\alpha^{+/-}$ had exencephaly.

Table 15: $Tfap2\alpha^{+/-};Tg^{KRT14-Irf6}$

	E16.5-17.5	Total
Litters	8	8
$Tfap2\alpha^{+/+}$	19	19
$Tfap2\alpha^{+/-}$	19	19
$Tfap2\alpha^{+/+}; Tg^{KRT14-Irf6}$	9	9
$Tfap2\alpha^{+/-}; Tg^{KRT14-Irf6}$	16	16
Total	63	63
p-value	0.24	0.24
Resorbing	9	9 (p=0.03)

We intercrossed mice heterozygous for the $Tfap2\alpha^{+/-}$ with mice hemizygous for the $Tg^{KRT14::Irf6}$ to generate $Tfap2\alpha^{+/-}; Tg^{KRT14::Irf6}$ embryos. We found no significant difference in the distribution of embryonic genotypes but found a significant increase in the number of resorptions.

Table 16: $Tfap2\alpha^{+/-};Irf6^{+/-};Tg^{KRT14-Irf6}$

	E17.5 – P0
Litters	9
$Tfap2\alpha^{+/+};Irf6^{+/+}$	12
$Tfap2\alpha^{+/-};Irf6^{+/+}$	5
$Tfap2\alpha^{+/+};Irf6^{+/-}$	7
$Tfap2\alpha^{+/-};Irf6^{+/-}$	5
$Tfap2\alpha^{+/+};Irf6^{+/+};Tg^{KRT14-Irf6}$	7
$Tfap2\alpha^{+/-};Irf6^{+/+};Tg^{KRT14-Irf6}$	2
$Tfap2\alpha^{+/+};Irf6^{+/-};Tg^{KRT14-Irf6}$	12
$Tfap2\alpha^{+/-};Irf6^{+/-};Tg^{KRT14-Irf6}$	11
Total	66
p-value	0.07
Resorbing	5 (p-value =0.44)

We intercrossed mice hemizygous for the $Tg^{KRT14::Irf6}$ (over-expressing *Irf6* under the control of the *KRT14* promoter) with mice heterozygous for the *Irf6* genetrapped allele ($Irf6^{+/-}$) and the $Tfap2\alpha^{+/-}$ generate $Tfap2\alpha^{+/-};Irf6^{+/-};Tg^{KRT14-Irf6}$ and $Tfap2\alpha^{+/-};Irf6^{+/+};Tg^{KRT14-Irf6}$. We examined embryos at E17.5 and P0, shown are the combined genotypic distribution. While $Tfap2\alpha^{+/-};Irf6^{+/+};Tg^{KRT14-Irf6}$ were under-represented, the genotype distribution did not differ from the predict value.

Table 17: $Tfap2\alpha^{+/-};Grhl3^{+/-}$

	E15.5- P0
Litters	7
$Tfap2\alpha^{+/+};Grhl3^{+/+}$	8
$Tfap2\alpha^{+/-};Grhl3^{+/+}$	14
$Tfap2\alpha^{+/+};Grhl3^{+/-}$	19
$Tfap2\alpha^{+/-};Grhl3^{+/-}$	20
Total	61
p-value	0.11
Resorbing	3 (p=1.0)

We intercrossed mice heterozygous the $Tfap2\alpha^{+/-}$ and $Grhl3^{+/-}$ alleles to generate $Tfap2\alpha^{+/-};Grhl3^{+/-}$ embryos and pups. Both the number of resorptions and the genotype distribution did not differ from the predict values.

Table 18: Murine qPCR primers sequences

Gene	Primer name	Primer Sequence (5' to 3')
Irf6	4938 mIrf6 F	AGTGTGGCCCAAAACAGAAC
	4939 mIrf6 R	GGGTTGCTCACCGTCATAGT
Beta Actin	4588 Actb F	TCTGGCTCCTAGCACCAT
	4589 Actb R	GGGCCGACTCATCGTAC
Grhl3 set 1	4994 Grhl3-197F	GAACCTCGGAGAAGGAAGAT
	4995 Grhl3-240R	TTCTTCAGCAACCGCACAGA
Grhl3 set 2	4996 mGrhl3-1779F	TTGACGCGCTCATGTTGAAG
	4997 mGrhl3-1848R	AGGCCGTA CTCTCAGAGAT
<i>Trp63</i>	4781 mTr <i>Trp63</i> -707F	GAAGGCAGAGCGTGCTGGTC
	4782 mTr <i>Trp63</i> -811R	TCATTCCTCCGACGCAGCTG
<i>Krt14</i>	5121 CK14 F	AGCGGCAAGAGTGAGATTCT
	5122 CK14 R	CCTCCAGGTTATTCTCCAGGG
Tgm1	5109 Tgm1F	GCGGAGGGCTGTGGAGAAGG
	5110 Tgm1R	GGGTGCGCAAACGGAAGGTG
Krt1	5103 Krt1 F	GACACCACAACCCGGACCCAAA ACTTAGAC
	5104 Krt1 R	ATACTGGGCCTTGACTTCCGAGATGATG
Tfap2c	5125 Tfap2c F	ATCCCTCACCTCTCTCTCC
	5126 Tfap2c R	CCAGATGCGAGTAATGGTCCG
Tfap2 α set 1	5127 Tfapa F	GAAGACTGCGAGGACCGTC
	5128 Tfapa R	GAAGTCGGCATTAGGGGTGTG
Tfap2 α set 2	5191 - Tfap2 α F	CGCCCTACCAGCCTATCTAC
	5192 - Tfap2 α R	GGGAGTAAGGATCTTGC GACT

Primers for *Krt14*, Tfap2c and Tfap2 α set 1 were previously published in Qiao et al, 2012, Cell Research; doi:10.1038/cr.2012.122. Primers for Tgm1 and Krt1 were previously published in Wang et al, 2008, JCB; doi/10.1083/jcb.200804030

Table 19: *IRF6* sequencing primers

	Forward Primer		Forward Primer
IRF6_1F	ttagaagcggaggagtaggg	IRF6_1R	accccaaacacacagatgc
IRF6_2F	caaagctgtctcatgactgct	IRF6_2R	gggctttggaagagaaggaa
IRF6_3F	tggcacagcttattccata	IRF6_3R	ttcaaccattgcagacatgc
IRF6_4F	tgtgtgtttgtctatgagaaagg	IRF6_4R	tcaggctgtttcaagtgactat
IRF6_5F	ggaggtccttccatgagaga	IRF6_5R	caggagttcctcacctctg
IRF6_6F	caggagcaggggaaccttat	IRF6_6R	gaggatgcctctgagacagg
IRF6_7F	tgaatgctggtgaaaggtg	IRF6_7R	gcaggaaggtgaaagacagg
IRF6_8F	tgactaatgtgaccaggaact	IRF6_8R	aagatctccactaaatcaatcacc
IRF6_9F	gtcttctcagggectttt	IRF6_9R	AAACTCCCAGGCCAAATCTC
IRF6_10F	TGGAAAAATCACCCCTTCAGA	IRF6_10R	TCCCTAGGCTTTCTGTGTCAA
IRF6_11F	GCTGGCTGGTTGCTTAGAA	IRF6_11R	TGAAAGGGTTAGAGACTCAGCA
IRF6_12F	GCTGGGCAGTACTCTTCTGG	IRF6_12R	GTTGGAGATGGCCTGGTTTA
IRF6_13F	AAGCCCCAGTCCTCTTGAAT	IRF6_13R	TTGGCACTTTTCCAATACCC
IRF6_14F	CTCTTGAATCTGGGCCAGTC	IRF6_14R	TTTTATGGGAAAGGGACCAG
IRF6_15F	TCACTGTGTACCCACCAAA	IRF6_15R	tgggaggaggaccagcttat

BIBLIOGRAPHY

BIBLIOGRAPHY

1. Taniguchi T, Ogasawara K, Takaoka A, Tanaka N. (2001) IRF family of transcription factors as regulators of host defense. *Annu Rev Immunol*;19:623-55.
2. Kondo S, Schutte BC, Richardson RJ, et al. (2002) Mutations in IRF6 cause Van der Woude and popliteal pterygium syndromes. *Nat Genet*;32:285-9.
3. Rahimov F, Marazita ML, Visel A, et al. (2008) Disruption of an AP-2alpha binding site in an IRF6 enhancer is associated with cleft lip. *Nat Genet*;40:1341-7.
4. Fakhouri WD, Rhea L, Du T, et al. (2012) MCS9.7 enhancer activity is highly, but not completely, associated with expression of Irf6 and p63. *Dev Dyn*;241:340-9.
5. Milunsky JM, Maher TA, Zhao G, et al. (2008) TFAP2A mutations result in branchio-oculo-facial syndrome. *Am J Hum Genet*;82:1171-7.
6. Stoetzel C, Riehm S, Bennouna Greene V, et al. (2009) Confirmation of TFAP2A gene involvement in branchio-oculo-facial syndrome (BOFS) and report of temporal bone anomalies. *Am J Med Genet A*;149A:2141-6.
7. Li H, Sheridan R, Williams T. (2013) Analysis of TFAP2A mutations in Branchio-Oculo-Facial Syndrome indicates functional complexity within the AP-2alpha DNA-binding domain. *Hum Mol Genet*;22:3195-206.
8. McDade SS, Henry AE, Pivato GP, et al. (2012) Genome-wide analysis of p63 binding sites identifies AP-2 factors as co-regulators of epidermal differentiation. *Nucleic Acids Res*;40:7190-206.
9. Richardson RJ, Dixon J, Malhotra S, et al. (2006) Irf6 is a key determinant of the keratinocyte proliferation-differentiation switch. *Nat Genet*;38:1329-34.
10. Ingraham CR, Kinoshita A, Kondo S, et al. (2006) Abnormal skin, limb and craniofacial morphogenesis in mice deficient for interferon regulatory factor 6 (Irf6). *Nat Genet*;38:1335-40.
11. Schorle H, Meier P, Buchert M, Jaenisch R, Mitchell PJ. (1996) Transcription factor AP-2 essential for cranial closure and craniofacial development. *Nature*;381:235-8.
12. Zhang J, Hagopian-Donaldson S, Serbedzija G, et al. (1996) Neural tube, skeletal and body wall defects in mice lacking transcription factor AP-2. *Nature*;381:238-41.

13. de la Garza G, Schleiffarth JR, Dunnwald M, et al. (2013) Interferon regulatory factor 6 promotes differentiation of the periderm by activating expression of grainyhead-like 3. *J Invest Dermatol*;133:68-77.
14. Ting SB, Wilanowski T, Auden A, et al. (2003) Inositol- and folate-resistant neural tube defects in mice lacking the epithelial-specific factor Grhl-3. *Nat Med*;9:1513-9.
15. Thomason HA, Zhou H, Kouwenhoven EN, et al. (2010) Cooperation between the transcription factors p63 and IRF6 is essential to prevent cleft palate in mice. *J Clin Invest*;120:1561-9.
16. Moretti F, Marinari B, Lo Iacono N, et al. (2010) A regulatory feedback loop involving p63 and IRF6 links the pathogenesis of 2 genetically different human ectodermal dysplasias. *J Clin Invest*;120:1570-7.
17. Celli J, Duijf P, Hamel BC, et al. (1999) Heterozygous germline mutations in the p53 homolog p63 are the cause of EEC syndrome. *Cell* 1999;99:143-53.
18. Le M, Naridze R, Morrison J, et al. (2012) Transforming growth factor Beta 3 is required for excisional wound repair in vivo. *PLoS One*;7:e48040.
19. Restivo G, Nguyen BC, Dziunycz P, et al. (2011) IRF6 is a mediator of Notch pro-differentiation and tumour suppressive function in keratinocytes. *EMBO J*.
20. Li W, Cornell RA. (2007) Redundant activities of Tfap2a and Tfap2c are required for neural crest induction and development of other non-neural ectoderm derivatives in zebrafish embryos. *Dev Biol*;304:338-54.
21. Iwata J, Suzuki A, Pelikan RC, et al. (2013) Smad4-Irf6 genetic interaction and TGFbeta-mediated IRF6 signaling cascade are crucial for palatal fusion in mice. *Development*;140:1220-30.
22. Byrne C, Tainsky M, Fuchs E. (1994) Programming gene expression in developing epidermis. *Development*;120:2369-83.
23. Krishnan L, Guilbert LJ, Wegmann TG, Belosevic M, Mosmann TR. (1996) T helper 1 response against *Leishmania major* in pregnant C57BL/6 mice increases implantation failure and fetal resorptions. Correlation with increased IFN-gamma and TNF and reduced IL-10 production by placental cells. *J Immunol*;156:653-62.
24. Liu JP, Jessell TM. (1998) A role for rhoB in the delamination of neural crest cells from the dorsal neural tube. *Development*;125:5055-67.

25. Botti E, Spallone G, Moretti F, et al. (2011) Developmental factor IRF6 exhibits tumor suppressor activity in squamous cell carcinomas. *Proc Natl Acad Sci U S A*;108:13710-5.
26. Guttormsen J, Koster MI, Stevens JR, Roop DR, Williams T, Winger QA. (2008) Disruption of epidermal specific gene expression and delayed skin development in AP-2 gamma mutant mice. *Dev Biol*;317:187-95.
27. Leslie EJ, Standley J, Compton J, Bale S, Schutte BC, Murray JC. (2013) Comparative analysis of IRF6 variants in families with Van der Woude syndrome and popliteal pterygium syndrome using public whole-exome databases. *Genet Med*;15:338-44.
28. Chen W, Lam SS, Srinath H, et al. (2008) Insights into interferon regulatory factor activation from the crystal structure of dimeric IRF5. *Nat Struct Mol Biol*;15:1213-20.
29. Jones NC, Lynn ML, Gaudenz K, et al. (2008) Prevention of the neurocristopathy Treacher Collins syndrome through inhibition of p53 function. *Nat Med*;14:125-33.
30. Laue K, Janicke M, Plaster N, Sonntag C, Hammerschmidt M. (2008) Restriction of retinoic acid activity by Cyp26b1 is required for proper timing and patterning of osteogenesis during zebrafish development. *Development*;135:3775-87.
31. Bailey CM, Khalkhali-Ellis Z, Kondo S, et al. (2005) Mammary serine protease inhibitor (Maspin) binds directly to interferon regulatory factor 6: identification of a novel serpin partnership. *J Biol Chem*;280:34210-7.
32. Stransky N, Egloff AM, Tward AD, et al. (2011) The mutational landscape of head and neck squamous cell carcinoma. *Science*;333:1157-60.
33. Couch FJ, Wang X, McGuffog L, et al. (2013) Genome-wide association study in BRCA1 mutation carriers identifies novel loci associated with breast and ovarian cancer risk. *PLoS Genet*;9:e1003212.
34. Garcia-Cao I, Song MS, Hobbs RM, et al. (2012) Systemic elevation of PTEN induces a tumor-suppressive metabolic state. *Cell*;149:49-62.
35. Pyrgaki C, Liu A, Niswander L. (2011) Grainyhead-like 2 regulates neural tube closure and adhesion molecule expression during neural fold fusion. *Dev Biol*;353:38-49.
36. Takeda K, Takeuchi O, Tsujimura T, et al. (1999) Limb and skin abnormalities in mice lacking IKKalpha. *Science*;284:313-6.
37. Holland P, Willis C, Kanaly S, et al. (2002) RIP4 is an ankyrin repeat-containing kinase essential for keratinocyte differentiation. *Curr Biol*;12:1424-8.

38. Lee S, Kong Y, Weatherbee SD. (2013) Forward genetics identifies Kdf1/1810019J16Rik as an essential regulator of the proliferation-differentiation decision in epidermal progenitor cells. *Dev Biol*;383:201-13.
39. Shaw GM, Lammer EJ, Wasserman CR, O'Malley CD, Tolarova MM. (1995) Risks of orofacial clefts in children born to women using multivitamins containing folic acid periconceptionally. *Lancet*;346:393-6.

Chapter 4 -
Epithelial *Irf6* rescues lethality but not craniofacial and
limb development

Youssef A. Kousa¹, Dina Moussa², Brian C. Schutte²

¹Biochemistry and Molecular Biology Department, Michigan State University, 48824

East Lansing, Michigan, USA

²Department of Microbiology and Molecular Genetics, Michigan State University, 48824

East Lansing, Michigan, USA

Abstract

IRF6 regulates epithelial development and differentiation. Inherited *IRF6* alleles cause and contribute risk for orofacial clefting and somatic mutations are associated with skin tumorigenesis. In human and mouse, perturbing *IRF6* function also leads to limb, digit and craniofacial defects. However, the critical dose, cell autonomy and tissue-type by which *IRF6* mutations confer pleiotropic disease are unknown. To delineate the critical dose at which disease occurs, we use an allelic series to titrate *Irf6* expression in the mouse. We find that compound heterozygous embryos for the *Irf6* null and hypomorphic alleles display completely penetrant bilateral oral adhesions and abnormal periderm. To test the role of epithelium in the human-mouse disease spectrum, we drive an *Irf6* transgene in the basal epithelium of embryos lacking endogenous expression. Rescue embryos appear to have a normal epidermis and, remarkably, survive parturition and early post-natal development. Despite epidermal rescue, limb clubbing and a curled tail persist. Strikingly, palatal elevation is obstructed by oral adhesions between the palatal shelves and the tongue, leading to a cleft palate in 100% of rescue embryos (N = 23). Despite *Irf6* expression in the basal cell layer, we find an abnormal periderm at oral adhesion sites. Therefore, while sufficient for a functional epidermal barrier and post-

natal survival, basal *Irf6* expression is not sufficient for palate, limb and tail development. Together, this work suggests that inherited *IRF6* alleles can contribute to pleiotropic disease through dosage sensitivity (heterozygous vs. compound hypomorph), involvement in multiple developmental pathways (skin vs. limb clubbing and tail) and cell-autonomous expression (basal vs. periderm expression in palate).

Introduction

Mutations in Interferon regulators factor 6 (*IRF6*) lead to Van der Woude Syndrome (VWS, # 119300) and Popliteal Pytergium Syndrome (PPS, # 119500), two dominantly inherited orofacial clefting disorders (1). Moreover, DNA variants within the *IRF6* locus also increase risk for isolated or nonsyndromic orofacial clefting (iCLP), accounting for 12% of world-wide risk (2). Loss of *IRF6* expression in epithelial tissue has also been linked to skin and head and neck squamous cell carcinoma (3, 4). Furthermore, we recently showed that *IRF6* is required for neurulation (Kousa, Chapter 3). Therefore, understanding the dose, cell-type and cell autonomy by which *IRF6* exerts its function may provide important insight into human development and disease.

In the mouse, loss of *Irf6* leads to skin, limb, craniofacial and neural tube defects (5) (Kousa, Chapter 3). While the range of affected tissues in *Irf6* knockout embryos has provided numerous insights, a murine phenotype that models iCLP, VWS and PPS pathophysiology is lacking. For instance, while haploinsufficiency of *IRF6* leads to VWS, mice heterozygous for either a null *Irf6* allele or a dominant negative *Irf6* allele do not develop a cleft palate (5, 6). By contrast, *Irf6* knockout embryos have severe, bilateral

oral adhesions that involve all epithelial surfaces in the oral cavity. While this pathology thought to lead to cleft palate in the mouse, oral epithelial adhesions are not common in patients with VWS. Therefore, a dynamic murine model that illuminates human orofacial clefting has not been developed.

In the oral cavity, *Irf6* function appears to be essential during early palatogenesis. In *Irf6* knockout embryos, pervasive oral adhesions result in vertically oriented palatal shelves from E13.5 – P0 (5, 6). Oral adhesions are thought to result from loss or dysfunction of the periderm (7), a squamous epithelium that covers the oral cavity. More broadly, epithelial adhesions in *Irf6* knockout embryos obliterate the esophageal lumen and fasten appendages to the body wall (5). However, the periderm remains an enigmatic cell type with a poorly understood role in palatal development. In addition, it is not known what role, if any, IRF6 plays in the development of non-epithelial tissues. As such, the pathophysiological mechanisms leading to limb, digit and craniofacial defects in VWS and PPS remain opaque.

In the mouse, loss of *Irf6* is highly similar to loss of *Ikka* (8, 9), *14-3-3 sigma* (Stratifin) (6), *Kdfl* (10) and, to a lesser extent, *Ripk4* (11). Invariably, a prominent phenotypic feature in these murine models is a taut, shiny epidermis that encases the organism. As a result, prior work has sought to rescue the knockout embryo by rescuing the epidermis. For example, driving *Ikka* with an epithelial specific promoter (*KRT14*) leads to complete rescue of the skin, limb and digits, suggesting both cell-autonomous and non-cell autonomous function (12). An analogous experiment using the *KRT5* promoter, co-

expressed with *KRT14* in the basal cell layer, leads to complete rescue with over-expression of *Ikka* (13). While *Ripk4* knockout embryos are less severely affected, *Ripk4* expression under the *KRT14* promoter more fully rescues skin and limb defects (14). Interestingly, *Ikka* and *14-3-3sigma* knockout embryos could not be rescued by epithelial *Ripk4* expression.

In this study, we set out to understand the dose and tissue by which *Irf6* exerts *in vivo* function. We titrate *Irf6* dose and find that compound heterozygotes for the *Irf6* null and hypomorphic alleles have completely penetrant, bilateral mandible-maxilla oral adhesions but not clefting. To test how epithelial *Irf6* expression contributes to craniofacial, limb and digit anomalies in knockout embryos, we attempt to rescue the epidermis. We find *Irf6* transgene expression in basal epithelium using the *KRT14* promoter rescues epidermal development and perinatal lethality but not limb, tail and craniofacial defects. Unexpectedly, we find that basal *Irf6* expression is not sufficient to rescue oral adhesions and palatal clefting. Furthermore, we find that oral adhesions between the palatal shelves and the tongue are completely associated with CLP, suggesting a key role in pathogenesis.

Results

Titration of *Irf6* dose shows that mandible-maxilla oral adhesions are not sufficient for clefting

To investigate how endogenous *Irf6* expression alters palatal development, we examined craniofacial tissue from embryos with a recently characterized hypomorphic allele

(*Irf6^{neo}*) (Kousa, Chapter 3). To reduce endogenous expression further, we combined the hypomorphic allele with the *Irf6* genetrapp allele ((5); herein referred to as *Irf6*). Based on previous work, we predict that reducing endogenous *Irf6* expression would lead to oral adhesions and palatal clefting. In examining *Irf6^{neo/+}* (N=3), we found no evidence for oral adhesions or palatal clefting at E17.5. In contrast, *Irf6^{neo/-}* (N=6) had completely penetrant, bilateral oral adhesions between the mandible-maxilla most frequently and severely involving the mandibular tooth germ (Fig. 21A). However, despite the severity of these oral adhesions, we did not detect palatal clefting in *Irf6^{neo/-}* embryos. To understand this process, we marked the oral epithelium using Krt6 for the periderm (Fig. 21B,C) and Krt14 and Trp63 (Fig. 21B-E) for the basal cell layer. We previously showed that loss of *Irf6* expression between the mandible and maxilla at the tooth germ is associated with loss of Krt6 and oral adhesions (15). Here, we predicted that reducing *Irf6* expression would lead to a loss of Krt6 expression and oral adhesions. However, oral adhesions were present between the mandible and maxilla despite Krt6 expression (Fig. 21B). Together, these results suggest that oral adhesions between the mandible and maxilla are not sufficient for palatal clefting and that loss of Krt6 expression is not required for oral adhesions at the tooth germ.

Assuming that periderm is required in preventing oral adhesions, these results suggest that Krt6 is an unreliable periderm marker in pathological states. An alternative explanation is that we have perturbed the periderm but that periderm function is not associated with oral adhesions. To delineate between these two models, we sought to identify a novel molecular signature for the periderm. We previously showed that Grhl3

is downstream of *Irf6* in periderm (16). Here, we predict that attenuating *Irf6* dose would affect *Grhl3* expression in periderm. Consistently, *Grhl3* expression is lost almost exclusively in adherent oral epithelium, including periderm (Fig. 21F,G). As *Grhl3* marks non-adherent periderm, we conclude that *Krt6*, an intermediate filament, may also be a marking stress in mutant oral epithelium. Analysis of proliferation using Ki-67 did not reveal qualitative changes in *Irf6*^{neo/-} embryos (Fig. 21H,I).

***Irf6* expression using the *KRT14* promoter completely rescues cutaneous defects**

To test how epithelial development contributes to pleiotropic dysmorphology in *Irf6*^{-/-} embryos, we used a basal epithelial-specific promoter (*KRT14*) to drive *Irf6* expression. In a manner analogous to *Ikka* rescue using the *KRT14* promoter (12), we predicted that epithelial *Irf6* expression would cell-autonomously rescue epidermal defects. We considered limb, skeletal, craniofacial and tail defects to be secondary to epidermal pathology. As such, we predicted that epidermal rescue would lead to limb, craniofacial and tail rescue. Genotyping of embryos from the experimental cross (*Irf6*^{+/-}; *Tg*^{Krt14::Irf6} x *Irf6*^{+/-}) revealed a significant difference between the expected and predicted Mendelian distribution (Table 20; N=168, p-value = 9.67 x 10⁻⁶). Distribution differences were primarily driven by under-representation of *Irf6*^{-/-} (predicted 22; actual 9) and *Irf6*^{+/-} (predicted 44; actual 22). At E15.5, under-representation of the *Irf6*^{-/-} genotype by approximately 13 co-occurred with 11 embryonic resorptions (p-value = 0.048, Fisher's exact, two-tailed T-Test, based on 1-3% spontaneous resorptions in C57BL/6 mice, tested against the maximum 3% rate) (17). However, *Irf6*^{-/-}; *Tg*^{Krt14::Irf6} embryos did not differ from the expected Mendelian prediction (predicted 22; actual 23). Therefore, embryonic

lethality did not contribute to a skewed production of experimental embryos (*Irf6*^{-/-}; *Tg*^{*Krt14::Irf6*}).

In the epidermis, loss of *Irf6* leads to an expanded, hyper-proliferative super-basal layer that lacks stratification and differentiation. First, we analyzed skin mRNA to quantify *Irf6* expression by the *KRT14* promoter. We find that *Irf6*^{-/-}; *Tg*^{*Krt14::Irf6*} skin expresses significantly more *Irf6* relative to knockout embryos (p-value = 0.001) (Fig. 22A). Importantly, *Irf6* expression in *Irf6*^{+/+} and *Irf6*^{-/-}; *Tg*^{*Krt14::Irf6*} was not statistically different (p-value = 0.32). Histologically, we find that *Irf6* expression using the *KRT14* promoter is sufficient to rescue epidermal morphology (Fig. 22B). Molecularly, *Irf6* expression restricts *Krt1* and *Krt14* expression in *Irf6*^{-/-}; *Tg*^{*Krt14::Irf6*}, leading to a molecular profile highly analogous to *Irf6*^{+/+} pups (Fig. 22C-D). *Irf6* expression also lead to epidermal stratification and differentiation, as seen with expression of the differentiation marker *Loricrin* in *Irf6*^{-/-}; *Tg*^{*Krt14::Irf6*} but not *Irf6*^{-/-} embryos (Fig. 22E). Furthermore, we did not detect *Krt6*, a cutaneous marker of stress, in *Irf6*^{-/-}; *Tg*^{*Krt14::Irf6*} at P0 (Fig. 22F).

Epithelial *Irf6* rescues perinatal lethality

Examination of *Irf6*^{-/-}; *Tg*^{*Krt14::Irf6*} pups (N=12) revealed dramatic differences in morphology as compared to both wild-type and *Irf6*^{-/-} littermates. Most strikingly, while *Irf6*^{-/-} pups died shortly after birth, *Irf6*^{-/-}; *Tg*^{*Krt14::Irf6*} did not (Supp movie). Instead, *Irf6*^{-/-}; *Tg*^{*Krt14::Irf6*} pups appeared to be active and responsive to environmental stimuli. However, after periods of mild activity, highly comparable to wild type littermates, *Irf6*^{-/-}; *Tg*^{*Krt14::Irf6*} demonstrated labored breathing with marked abdominal retractions. Unexpectedly, this

data suggests a novel role for *Irf6* in respiration. Despite perinatal survival, *Irf6*^{-/-}; *Tg*^{Krt14::Irf6} did not live until weaning. We did not observe gross phenotypic variation in *Irf6*^{-/-}; *Tg*^{Krt14::Irf6} experimental pups.

Grossly, *Irf6*^{-/-}; *Tg*^{Krt14::Irf6} pups had normal skin that appeared more taut than wildtype littermates (Fig. 23A-B). Importantly, cutaneous rescue led to loss of adhesions between the body wall and appendages, including the tail and limbs. Unlike littermates, *Irf6*^{-/-}; *Tg*^{Krt14::Irf6} pups did not have a milk spot, suggesting dysfunction in the digestive tract. Furthermore, despite rescue of appendage-body wall adhesions, clubbing of both upper and lower limbs persisted. Furthermore, loss of adhesions around the tail reveals a completely penetrant curl in *Irf6*^{-/-}; *Tg*^{Krt14::Irf6} pups. We analyzed the skeletons of these pups to determine cartilage and bony dysfunction. Importantly, the appendicular skeleton appeared different in two ways (Fig. 23C). First, consistent with above data, loss of skin adhesions in *Irf6*^{-/-}; *Tg*^{Krt14::Irf6} permitted limb movement away from the axial skeleton. Secondly, like knockout littermates, *Irf6*^{-/-}; *Tg*^{Krt14::Irf6} pups exhibited fully penetrate syndactyly of both upper and lower limbs (Fig. 23C, top inset). Ossification of tail vertebra did not appear to differ. In the axial skeleton, we found that *Irf6*^{-/-}; *Tg*^{Krt14::Irf6}, like *Irf6*^{-/-} pups, had a bifid xiphoid (Fig. 23C, bottom inset). This data suggests that appendage-body wall adhesions result from *Irf6* expression in the epidermis. Interestingly, these data also suggest that limb defects, including clubbing and syndactyly, do not result from loss of epithelial *Irf6* expression.

Completely penetrant clefting and esophageal adhesions despite basal *Irf6* expression

Prior work shows that *Irf6*^{-/-} pups have uniformly penetrant oral clefting with ubiquitous oral and esophageal adhesions. As we did not detect a milk spot, we further predict that oral clefting and esophageal adhesions contribute to uniform postnatal lethality of *Irf6*^{-/-}; *Tg*^{*Krt14::Irf6*} pups. Despite *Irf6* expression in basal epithelium, *Irf6*^{-/-}; *Tg*^{*Krt14::Irf6*} embryos (N=12) display completely penetrant palatal clefting at P0 (Fig. 24). However, in contrast to *Irf6*^{-/-} pups, *Irf6*^{-/-}; *Tg*^{*Krt14::Irf6*} have less extensive oral adhesions. In the anterior (Fig. 24A) and middle palate (Fig. 24B), oral adhesions are primarily found between the mandible and maxilla. More posteriorly, oral adhesions are seen between the tongue and palate but not between the mandible and maxilla (Fig. 24C). Unexpectedly, we also observe tongue-palate oral fusions in the posterior palate.

Histological examination of the thoracic cavity also reveals fully penetrant esophageal adhesions in *Irf6*^{-/-}; *Tg*^{*Krt14::Irf6*} pups (Fig. 25). Surprisingly, these adhesions are highly similar to but morphologically distinct from *Irf6* knockout embryos (“M” vs. “S” shape) (Fig. 25A). However, previous reports show that skin *KRT14* promoter activity is 1000-fold greater than the esophageal epithelium (14). Consistently, we find that Krt14 immunostaining in the esophagus requires 10-fold more exposure time relative to skin (Fig. 25B). Therefore, in direct contrast to epidermal rescue, *Irf6* expression via the *KRT14* promoter is not sufficient to rescue esophageal adhesions. Together, these data suggest that morphological change in the esophagus of *Irf6*^{-/-}; *Tg*^{*Krt14::Irf6*} pups represent an intermediate phenotype.

Palate-tongue oral adhesions prevent palatal elevation

Considering analysis of *Irf6*^{-/-}; *Tg*^{Krt14::Irf6} pups, we concluded that *Irf6* expression in basal epithelium is not sufficient to rescue palatal adhesions and clefting. To examine the pathophysiological mechanism and cell types leading to oral clefts in *Irf6*^{-/-}; *Tg*^{Krt14::Irf6} pups, we examined embryos at E15.5 (N=11). We examined three types of oral adhesions based on the surfaces they approximate: 1) mandible and maxilla, 2) palate and mandible and 3) palate and tongue. Between the mandible-maxilla, we found completely penetrant, bilateral oral adhesions throughout the palate that did not differ from *Irf6*^{-/-} embryos (Fig. 26A-C). At the palate-mandible interface, oral adhesions are completely rescued in the anterior and middle palate (Fig. 26A,B). However, oral adhesions persisted between the palate and mandible in the posterior palate (Fig. 26C). Palate-tongue oral adhesions are found throughout the palate but are limited in severity in contrast to *Irf6*^{-/-} (Fig. 26A-C). Palate-tongue oral adhesions in the anterior and middle palate obstructed elevation and stymied horizontal growth. Critically, these palate-tongue adhesions interfered with contact between the palatal shelves (Fig. 27A). As a result, fusion between the palatal shelves did not take place, leading to a frank cleft as the head enlarges progressively until birth.

To investigate the molecular mechanism underlying this highly complex process, we analyze markers of oral epithelium in mid-palate at E15.5. First, we mark the periderm with Krt6 (Fig. 27B) and basal cells with Trp63 and Krt14 (Fig. 27B-C). As expected, immunostaining for *Irf6* shows expression in the basal cell layer. Considering that basal

cells differentiate into periderm cells, we also expect and find *Irf6* expression in the periderm (Fig. 27D). Importantly, and consistent with results in *Irf6*^{-/-} and *Irf6*^{neo/-} embryos, Krt6 expression in the periderm of *Irf6*^{-/-};Tg^{Krt14::Irf6} embryos is not sufficient to alter palate-tongue oral adhesions (Fig. 27, middle panel). Furthermore, we find that re-expression of *Irf6* rescues Krt6 expression but does not attenuate adhesions at the tooth germ (data not shown). Based on results in *Irf6*^{neo/-} embryos, we predict that re-expression of *Irf6* would rescue *Grhl3* expression in periderm. Consistently, *Grhl3* expression is observed non-adherent oral epithelium bordering palate-tongue oral adhesions (Fig. 27E). Unlike Krt6, these results suggest that *Grhl3* expression in periderm is both necessary and sufficient in marking oral adhesions. Furthermore, consistent with previous findings, re-introduction of *Irf6* led to a wildtype pattern of Activated Caspase 3 expression in the nasal epithelium (Fig. 27F) and Ki-67 expression in palatal mesenchyme (Fig. 27G). Importantly, Ki-67 positive cells in palatal mesenchyme of *Irf6*^{-/-};Tg^{Krt14::Irf6} embryos suggests non-cell autonomous *Irf6* regulation of mesenchymal proliferation.

DISCUSSION

We report an *Irf6* dose-dependent model of orofacial clefting. We further provide an animal model that decouples skin development from limb, tail, skeletal and craniofacial defects in *Irf6* knockout embryos. Together, these results suggest that pleiotropic *IRF6* disease can result from the cell-type, tissue and dose. Our previous reports shows that compound heterozygous embryos for the *Irf6* null and hypomorphic alleles have completely penetrant caudal neural tube defects. Here, we report completely penetrant

mandible-maxilla oral adhesions without clefting. Taken together, these data suggests that the neural tube is more sensitive to *Irf6* dose than palatal clefting in the mouse. Presence of oral adhesions and a normal tail in *Irf6*^{+/-} heterozygous embryos suggests that oral epithelium is most sensitive to *Irf6* dose.

The preponderance of evidence, in this and previous reports, partially illuminates the mechanistic gap between oral adhesions and clefting. First, data from compound heterozygous embryos, shown here, suggests that oral adhesions between the maxilla and mandible are not sufficient for palatal clefting. In contrast, *Irf6*^{-/-}; *Tg*^{Krt14::Irf6} also have palate-tongue oral adhesions and completely penetrant palatal clefting. As seen at E15.5 in *Irf6*^{-/-}; *Tg*^{Krt14::Irf6}, palate-tongue oral adhesions may be directly interfering with the coordinated maneuvers required for palatal closure, including palatal re-orientation and adhesions. In support of this model, we recently showed that *Grhl3*^{-/-} embryos have completely penetrant bilateral mandible-maxilla oral adhesions but that clefting only results when tongue-palate adhesions are also present. Taken together, these data support a more prominent role for functional oral adhesions between the tongue and the palatal shelves.

These data are critical because it suggests that common and rare DNA variants in *Irf6* can lead to orofacial clefting secondary to oral epithelial adhesions. As such, clefting in patients with VWS, PPS and isolated orofacial clefting may result from a process that is analogous to a Pierre Robin Sequence, whereby tongue-mediated clefting results from physical attachment to the palatal shelves (adhesion) as opposed to obstruction

(micrognathia). Thus, modulating the molecular and physical properties of adhesive Pierre Robin Sequence may be a clinical target for future preventative strategies. While we don't believe that mandible-maxilla oral adhesions are playing a role in palatal development, they may be interfering with odontogenesis and contributing to hypodontia, a common finding in patients with VWS and PPS patients.. First, if oral adhesions persist, breakdown of epithelial cells may allow mesenchymal confluence, i.e. fusions. Oral fusions are found in VWS and PPS as syngnathia and may physically obstruct dental eruption. Second, considering presence at P0, suckling or mastication may obliterate oral adhesions and epithelial integrity. Obliteration of adhered dental epithelium during odontogenesis may predispose to hypodontia. These models are not exclusive of a cell-autonomous affect of *Irf6* on odontogenesis.

Oral adhesions involving the oral and nasal surfaces of the palatal shelves provide a striking contrast between *Irf6*^{-/-} and *Irf6*^{-/-};*Tg*^{Krt14::Irf6} embryos. Importantly, basal *Irf6* expression completely rescues palate-mandible but not palate-tongue oral adhesions. These results suggest that basal *Irf6* expression plays an important role in palatal development. While palate-tongue oral adhesions are also less severe, localizing to distal aspects of the palate, important developmental implications are proposed. Strikingly, palate-tongue oral adhesions physically prevent horizontal reorientation of the palatal shelves. Despite the physical constraints, medial surfaces of the palatal shelves approximate toward midline. These data suggest that palatal reorientation, rather than elevation, plays a prominent role in palatogenesis (18, 20). Furthermore, while palatal nasal epithelium adheres to the tongue, horizontal outgrowth supports a more fluid

determination of the Medial Edge Epithelium rather than a single cohort of cells along the palate. Importantly we observed this pattern in the anterior and middle sections of the palatal shelves. In the posterior palate, palatal elevation is not observed, perhaps as function of palate-mandible oral adhesions.

As compared to *Irf6*^{neo/-} (Kousa, Chapter 3), *Irf6*^{-/-}; *Tg*^{Krt14::Irf6} embryos have a comparable level of epidermal *Irf6* expression but more severe limb clubbing, syndactyly and tail anomalies. These data suggest that limb, tail and digit defects in *Irf6*^{-/-}; *Tg*^{Krt14::Irf6} are due to non-epithelial *Irf6* expression and function.. Consistent with this finding, we previously found that *Irf6* is expressed in the hindlimbs, cartilage primordium of the humerus (forelimb) and metacarpals (digits) (19). Interestingly, MCS9.7, an *Irf6* enhancer classically associated with epithelial expression, is also active in these tissues. As such, these data suggest an important conceptual shift in our understanding of *Irf6* and disease mechanism.

Unlike the cohort of alleles previously reported to phenocopy the *Irf6* knockout, use of *KRT14* promoter to drive epithelial specific *Irf6* expression did not rescue limb defects, despite skin rescue. These results suggest non-epithelial *Irf6* expression and function in limb development. Furthermore, this work suggests that the common knockout phenotype for these alleles is not through a single molecular pathway but rather an endpoint achieved through multiple cellular and molecular means. In support of this model, *Ikka* limb defects were fully rescued with the *KRT5* and *KRT14* driver while *Irf6* defects persisted. In support of this model, a test for a genetic interaction between *Ikka* and *Irf6*

did not reveal epistasis (6). In contrast, considering epistasis between *14-3-3 sigma* and both *Irf6* and *Kdfl* in skin, limb and craniofacial tissues(6), we would predict that a similar rescue with the *KRT14* promoter for *14-3-3sigma* would lead to incomplete limb rescue, as shown here for *Irf6*. As opposed to incomplete rescue, an alternative model is that phenotypes described in the rescue embryos are gain-of-function from ectopic or over-expression of *Irf6* in the basal cell layer. However, we do not prefer this model because the phenotypes are similar to *Irf6* knockout embryos than they are to embryos over-expressing *Irf6*. Furthermore, this constellation of anomalies is not seen *Irf6*^{+/+};Tg^{Krt14::Irf6}, which have higher levels of *Irf6* expression than *Irf6*^{-/-};Tg^{Krt14::Irf6}.

In that context, the results for *Ripk4* offer a striking contrast. While epithelial expression of *Ripk4* rescued limb defects, in manner analogous to *Ikka*, ectopic expression of the gene did not rescue either *Ikka* or *14-3-3sigma*. Together, these results suggest that *Ripk4* is 1) involved in an independent parallel pathway 2) requires *Ikka* and *14-3-3sigma* for activation or 3) is a peripheral player in this pathway and could be either upstream or downstream. However, in comparing the phenotypes, *Ripk4* knockouts are the least severely affected of the five alleles. Analogous rescue experiments for *14-3-3sigma* knockout and epithelial *14-3-3sigma* expression or over-expression of *Irf6*, *Ikka* and *Ripk4* has not been reported.

Author Contributions

YAK and BCS conceived of the work. YAK designed and performed all murine crosses, completed statistical analyses, analyzed all data, prepared the figures and tables and

wrote the manuscript. YAK performed and analyzed morphological phenotyping and histological analysis, immunostaining, qPCR, skeletal preps and captured images. DM performed histological stains and analysis, conducted and analyzed immunostaining, captured and collected images. YAK supervised all mouse genotyping and statistical analyses. BCS supervised the project. All co-authors reviewed the manuscript and edits were reviewed/incorporated by YAK and BCS.

ACKNOWLEDGEMENTS

Financial support to YAK (#F31DE022696-01) came from the NIH National Institute of Dental and Craniofacial Research.

WEB RESOURCES

Online Mendelian Inheritance in Man: www.omim.org

PolyPhen-2: <http://genetics.bwh.harvard.edu/pph2/>

Primer3: biotools.umassmed.edu/bioapps/primer3_www.cgi

NHLBI/ESP database: evs.gs.washington.edu/EVS/

UCSC genome browser: genome-euro.ucsc.edu/cgi-bin/hgGateway

MATERIALS AND METHODS

Murine crosses

Use, husbandry and procedures involving research animals was approved by the Michigan State University Institutional Animal Care and Use Committee (AUF # 05/12-093-00). Harem matings (4 females with a single breeder male) were used to enhance

pregnancy rates and presence of a copulation plug was denoted at E0.5. We used a recently characterized transgene that drives *Irf6* expression under the control of the *KRT14* promoter to rescue *Irf6* knockout embryos. We first inter-crossed *Irf6*^{+/-} and *Tg*^{*Krt14::Irf6*} (*Irf6*^{tg}) to produce *Irf6*^{+/-}; *Tg*^{*Krt14::Irf6*}. We then inter-crossed *Irf6*^{+/-}; *Tg*^{*Krt14::Irf6*} with *Irf6*^{+/-}. Rescue embryos (*Irf6*^{-/-}; *Tg*^{*Krt14::Irf6*}) had an expected yield of 12.5%. We examined embryos at two developmental time points, E15.5 and just upon birth (P0). To test the effect of *Irf6* dose in the development of oral epithelium, we used a recently characterized hypomorphic allele. We then combined the hypomorphic allele with a null *Irf6* allele in the compound heterozygous embryos to reduce endogenous expression further. Genotyping was complete as described previously.

Morphological and histological analysis

All embryos and pups were grossly examined upon dam euthanasia or parturition. After initial inspection, embryos and pups were placed into freshly prepared 4% paraformaldehyde (245-684, Protocol). Upon fixation at 4°C for 16-24 hours, embryos and pups were dehydrated in 50-80% ethanol until time of embedding. Paraffin embedded material was sectioned at 7 µm intervals for both craniofacial tissue and thoracic cavities. Hematoxylin (GHS332, Sigma) and Eosin (E511-25, Fisher Chemical) staining was complete essentially as described previously (Chapter 3). Briefly, we removed the paraffin with a series of short Xylene incubations. We then hydrated the tissues using a series of increasingly diluted ethanol solutions. Following short incubations in Eosin (90 seconds) and Hematoxylin (90 seconds), we dehydrated the tissue using a series of decreasingly diluted ethanol solutions. Following Xylene

incubations, the tissue was mounted (Permount, SP15-100, Fisher Scientific) and visualized. At both E15.5 and P0 we used the eyes to determine anterior (anterior to eyes), middle (at eyes) and posterior palate (posterior to eyes).

Molecular analyses of murine tissue

Immunostaining was complete with the protocol and reagents described previously (Chapter 3). Briefly, we performed a similar series of tissue incubations in Xylene and ethanol to remove paraffin and hydrate the tissue, in a manner highly analogous to Hematoxylin and Eosin staining. Following this step, we performed antigen retrieval in sodium citrate (pH6.0) and permeabilization in Triton X-100 (VWR). We then performed a series of washing steps to remove the detergent. After this step, we incubated the slides in blocking reagents, including 10% BSA in PBS for one hour and 40 µg/ml of Goat anti-mouse Fab fragment in PBS (Jackson ImmunoResearch Laboratories, 115-007-003) also for one hour. Primary antibodies were incubated for 18-24 hours at 4°C. Primary antibodies include Tp63 (Santa Cruz, 4A4, sc-8431), Keratin 6 (Covance, PRB-169P), Keratin 14 (Novocastra, NCL-L-LL002), Keratin 1 (NCL-CK1, Novocastra), Loricrin (PRB-145P, Covance), Activated Caspase 3 (Abcam, Ab13847), Ki-67 (ab15580, Abcam).

Skeletal prep

Skeletal preps were processed as described previously (Chapter 3). Briefly, after fixing as described above, we removed skin and subcutaneous fat from embryos and then incubated in 70% and 95% ethanol for 24 hours in per solution. After 72 hours incubation

in 2% KOH, we stained the cartilage in Alcian blue (Sigma, A5268-10G). De-staining of Alcian blue in 95% ethanol was followed by Alizarin Red staining (Sigma-Aldrich, A5533-25G) for 24-36 hours. Skeletal tissue was then placed in 1%KOH/20% Glycerol solution before images were taken.

Bioimaging upright/fluorescent microscope and stereomicroscope

We image tissue on an upright microscope (Nikon Eclipse 90i upright) with a 4x, 10x and 40x objectives, as described previously (Chapter 3). NIS Elements Advanced Research v3.10 imaging software was used to obtain and to analyze images. Enhancement was limited to program algorithms, applied evenly to all samples, and only included deconvolution and sharpening with Gauss-Laplace. To capture whole mount embryo images we used a SMZ1000 Nikon microscope with both Fiber Optic Gooseneck and Ring Light sources, NIS-Elements Software 4.11. We used Adobe Photoshop Elements v9.0 to construct and produce the figures.

Transcriptional profiling using quantitative-PCR

We analyzed mRNA levels using methods and protocol essentially as described previously, (Chapter 3). Briefly, dorsal skin is collected from embryos at the time point indicated. We snap freeze the tissue in liquid nitrogen and use TRIzol RNA extraction kit (15596-026, Ambion). To prevent DNA contamination we treated the samples with RNase-Free DNase (79254, Qiagen) for 30 minutes, which is followed by heat inactivation at 65°C. To purify the RNA, we used acidic phenol and chloroform. After purification, we resuspended the RNA in RNase-free H₂O and incubated at 55°C for 10

minutes. To make cDNA, we used Oligo dT primers (18418-012, Invitrogen), dNTP mix (18427-013, Invitrogen), SuperScriptIII Reverse Transcriptase (18080-093, Invitrogen) and Recombinant RNasin Ribonuclease Inhibitor (N2511, Promega). The negative control for this reaction did not include either the SuperScriptIII Reverse Transcriptase or the Recombinant RNasin Ribonuclease Inhibitor. We used SYBER Green (4309155, Applied Biosystems) to quantify transcript levels from total starting material of 5.5 ng of cDNA. We quantified fold change using the delta-delta Ct-method relative to Beta-Actin. All reactions were performed with three technical replicates per biological sample. Murine primers as shown previously (Chapter 3, Table 18).

Statistical analysis

We used both Excel, v. 2010, and GraphPad Prism Software, version 5, to analyze data. All tables and histograms were constructed within GraphPad. We used a Student's t-test to determine significance and rejected the null hypothesis with a p-value equal to or below 0.05.

APPENDIX

APPENDIX

A

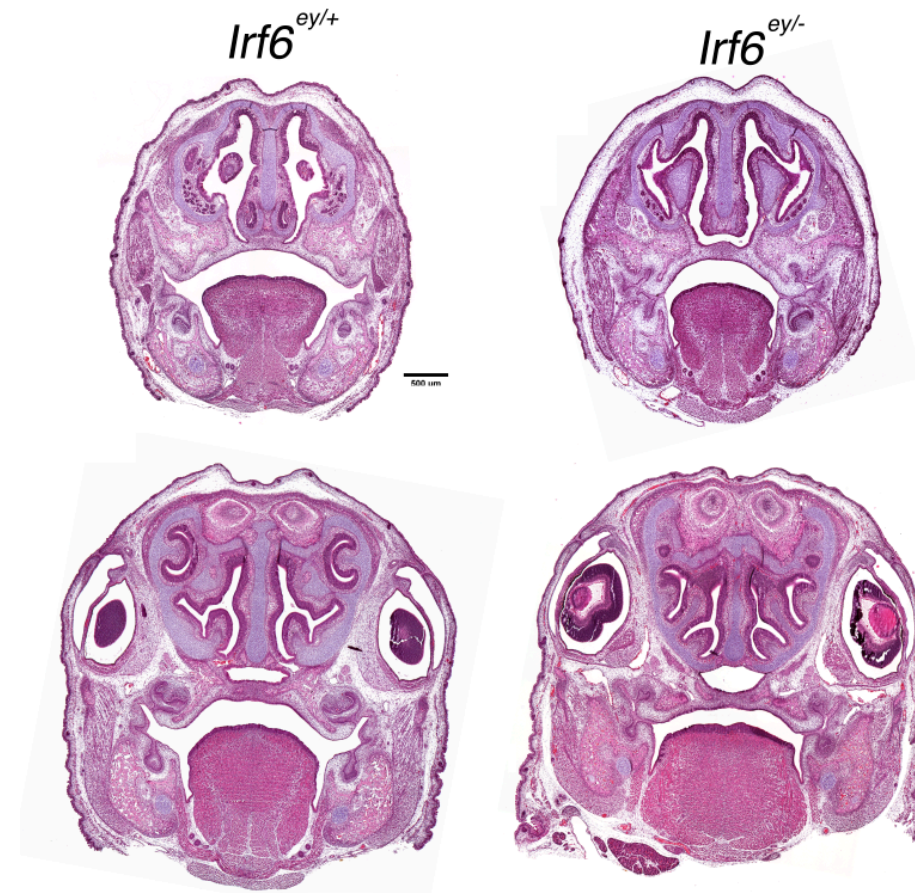


Figure 21: *Irf6* compound heterozygosity causes completely penetrant oral adhesions but not clefting.

Figure 21. (cont'd)

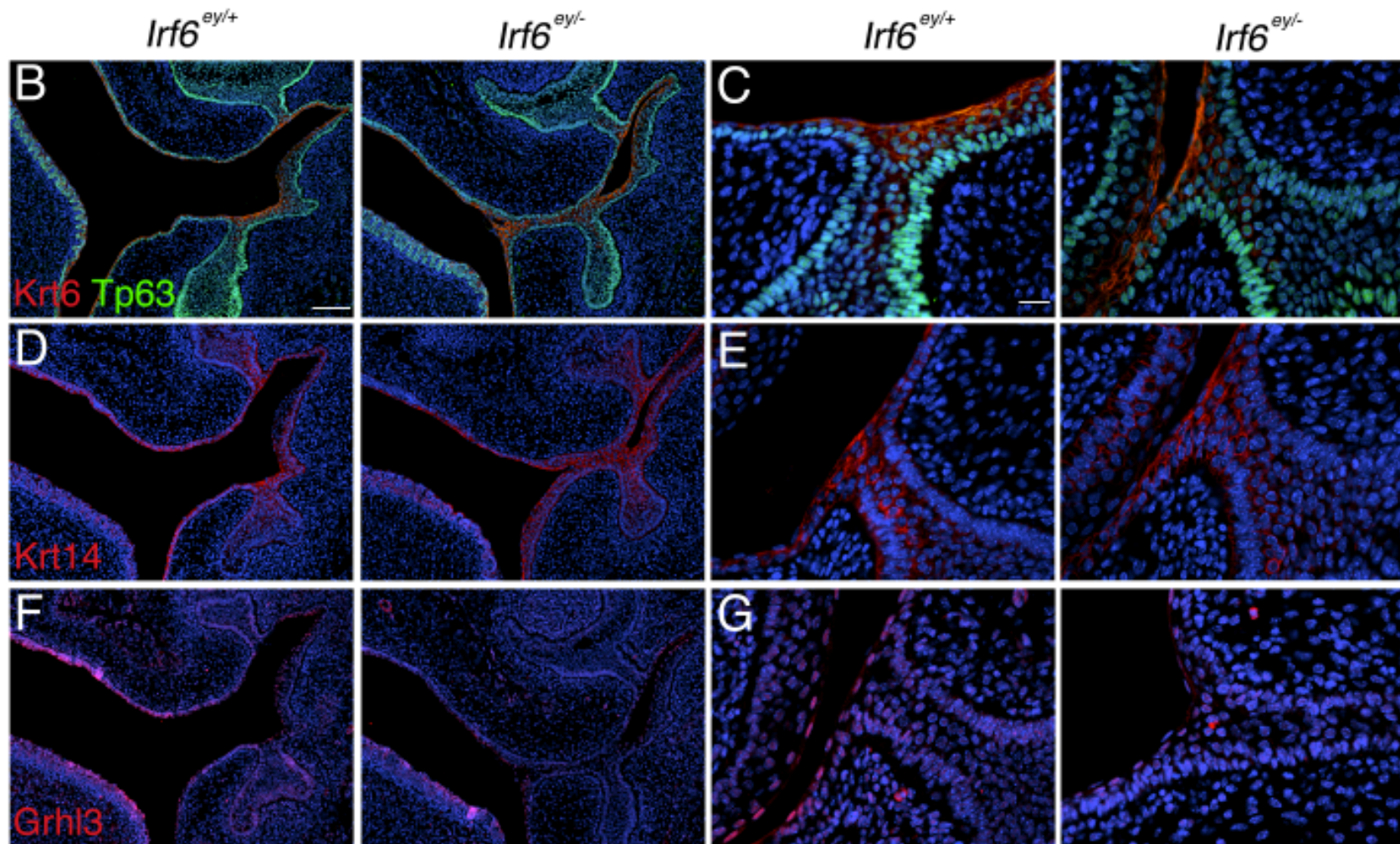


Figure 21. (cont'd)

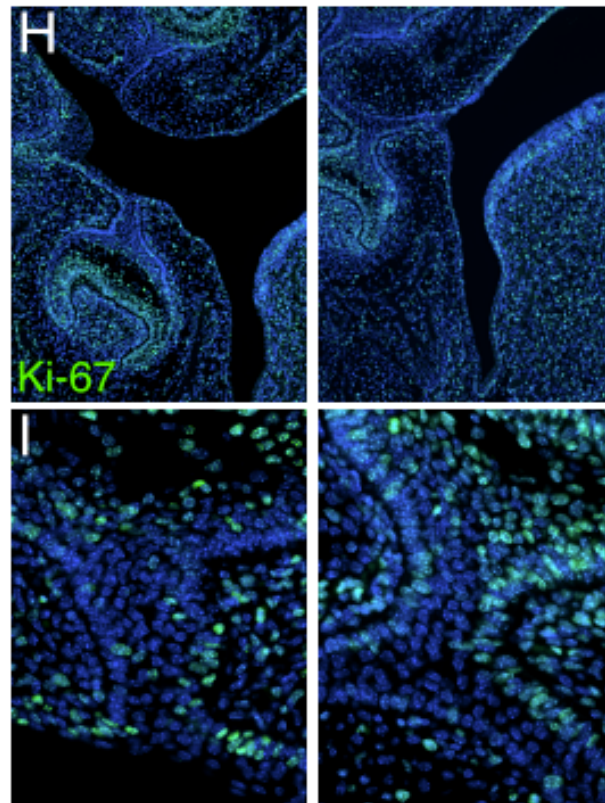


Figure 21. (cont'd)

Head coronal section stained with Hematoxylin and Eosin of E17.5 embryos examining A) anterior (top) and mid palates (bottom). Compared to *Irf6^{neo/+}*, *Irf6^{neo/-}* embryos have completely penetrant mandible-maxilla oral adhesions but not clefting. Immunostaining for Krt6 (red)/p63 (green) (B, tooth germ magnified in C), Krt14 (red) (D, E), Grhl3 (red) (F, G) and Ki-67 (green) (H, I). Krt6 expression is not sufficient to rescue oral adhesions *Irf6^{neo/-}*. DAPI (blue) marks nuclei (B-I). In contrast to Krt6, Grhl3 expression is reduced in areas of oral adhesions. Scale bar (A) 500 um; (B, D, F, H) 100 um; (C, E, G, I) 20 um.

A

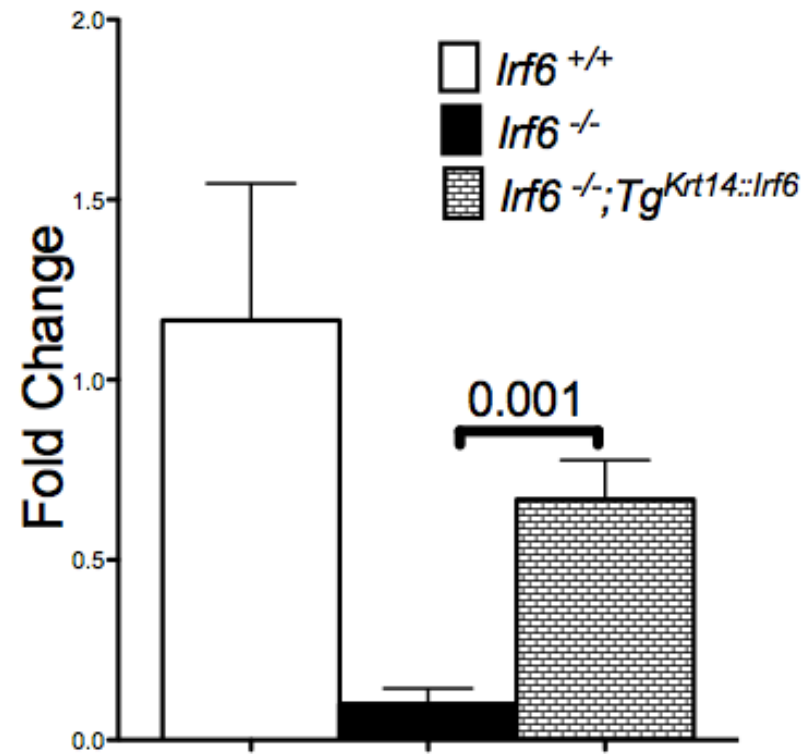


Figure 22: *Irf6* expression using the *KRT14* promoter rescues cutaneous defects in knockout embryos.

Figure 22. (cont'd)

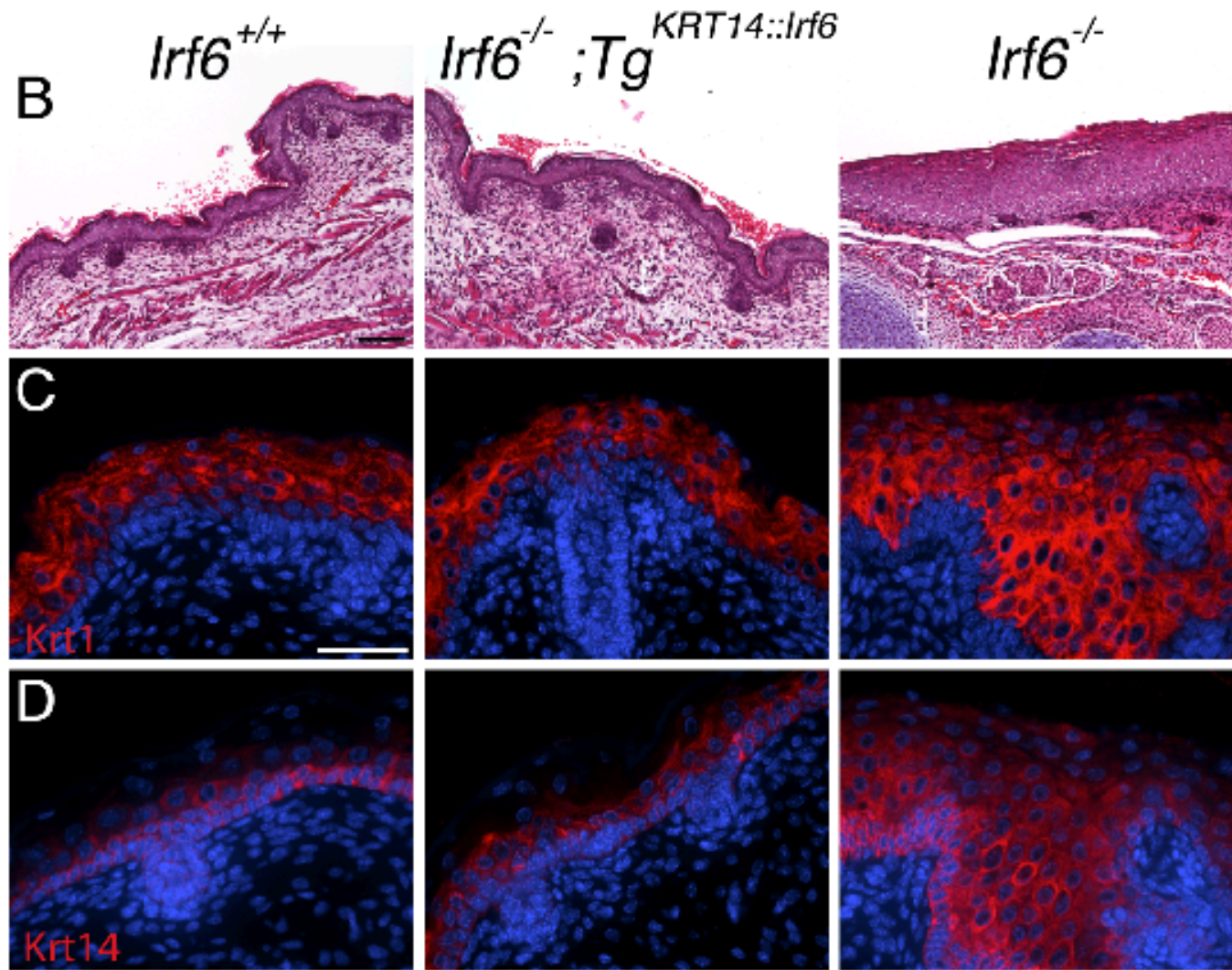


Figure 22. (cont'd)

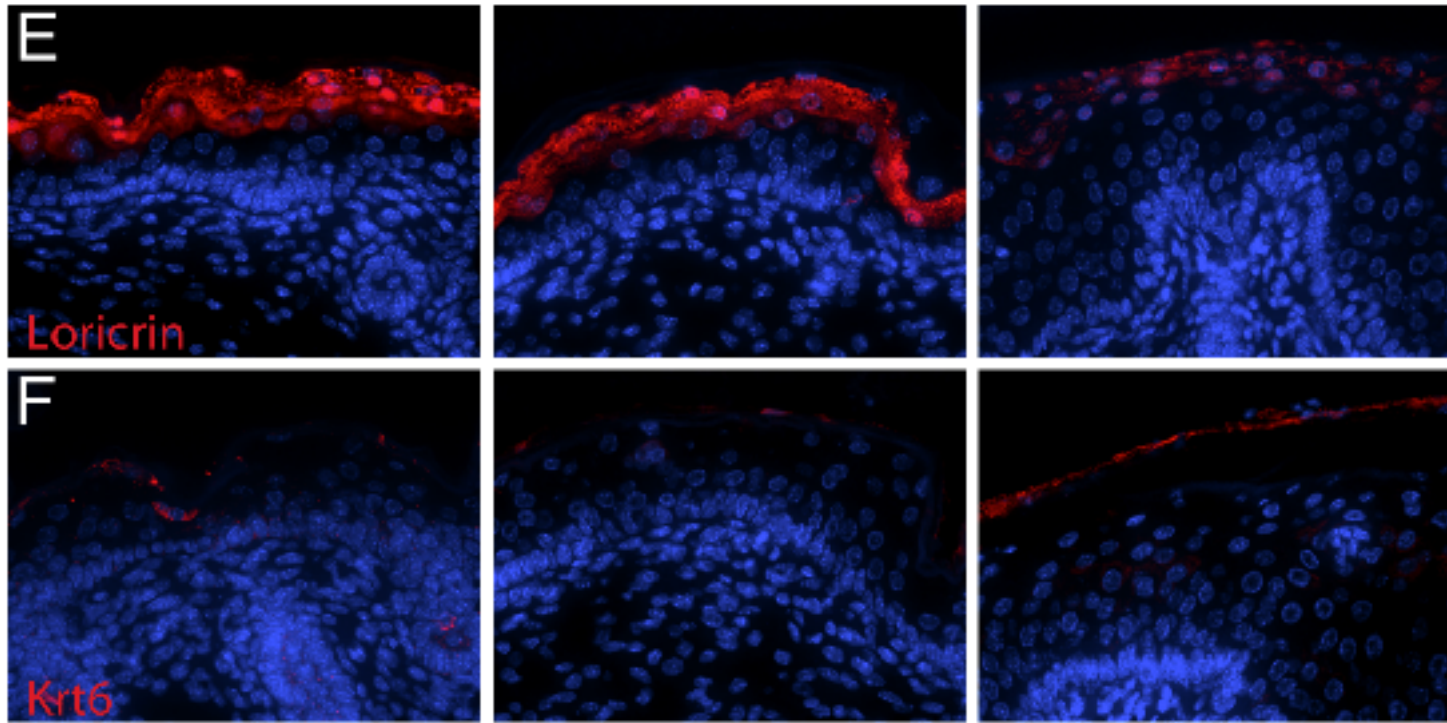


Figure 22. (cont'd)

qPCR analysis of RNA levels in perinatal murine skin (A). Transcriptional analysis reveals a significant increase in *Irf6* expression in $Tg^{KRT14::Irf6}$ (n=3) compared to $Irf6^{-/-}$ (n=4). No statistical significant differences are detected between $Tg^{KRT14::Irf6}$ and $Irf6^{+/+}$ (n=4). Skin histological analysis with Hematoxylin and Eosin reveals epidermal hypertrophy in $Irf6^{-/-}$ but not $Tg^{KRT14::Irf6}$ and $Irf6^{+/+}$ pups (B). Immunostaining of Krt1, Krt14, Loricrin and Krt6 (C-F). $Tg^{KRT14::Irf6}$ have epithelial stratification and loss of ectopic Krt1 and Krt14 expression (C-D). $Tg^{KRT14::Irf6}$ demonstrate epithelial differentiation (Loricrin) and loss cell stress markers in mature skin (Krt6) (E-F). Scale bars (A) 100 μ m, (B) 50 μ m.

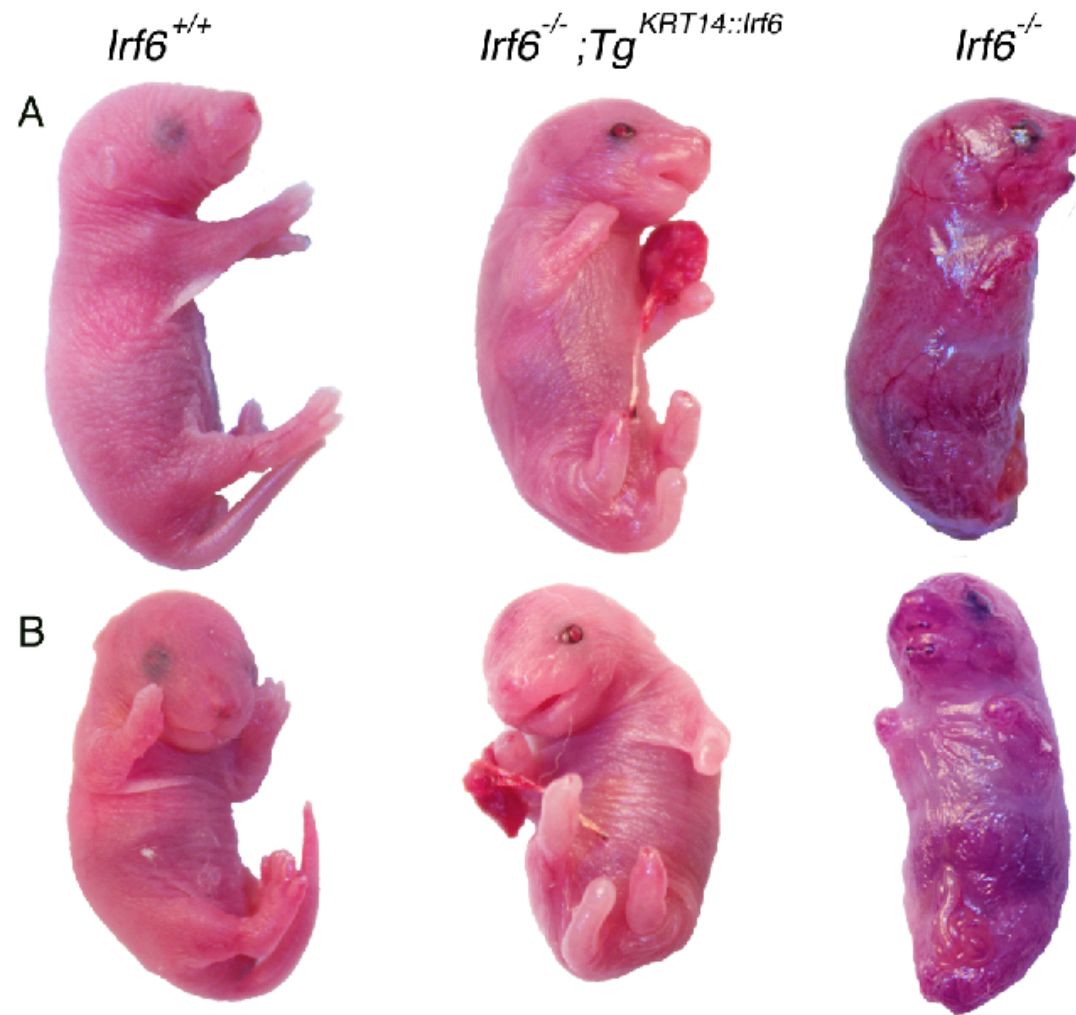


Figure 23: Epidermal expression of *Irf6* rescues perinatal lethality without altering skeletal defects, limb clubbing or syndactyly.

Figure 23. (cont'd)

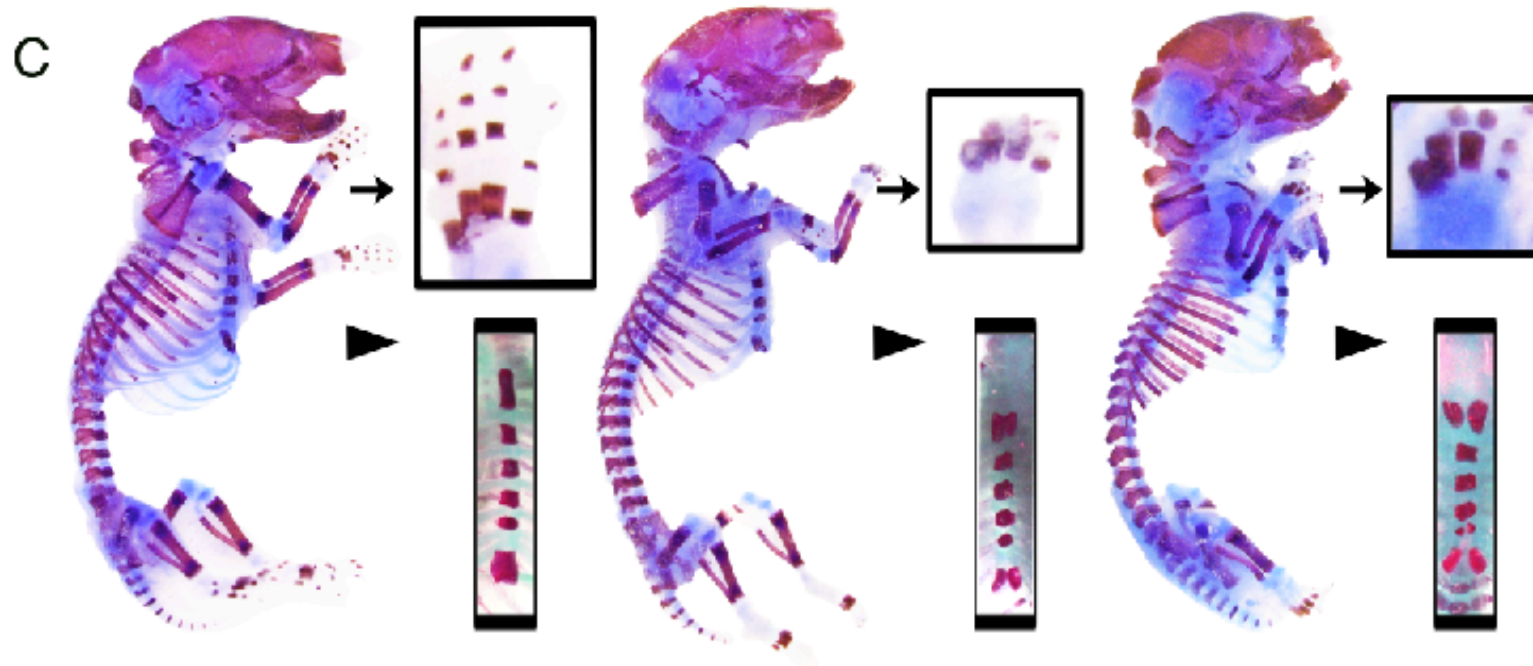


Figure 23. (cont'd)

Profile (A) and Frontal (B) views of representative P0 pups with the following genotypes; Left: $Irf6^{+/+}$; Center: $Irf6^{-/-}; Tg^{KRT14::Irf6}$; Right: $Irf6^{-/-}$. Gross analysis of $Irf6^{-/-}; Tg^{KRT14::Irf6}$ reveals perinatal survival, limb clubbing and syndactyly, a curled tail and a somewhat taut, shiny skin compared to wildtype littermates. Unlike $Irf6^{-/-}$ littermates, $Irf6^{-/-}; Tg^{KRT14::Irf6}$ appendages are not attached to the body wall and an open oral cavity is visible. Fig. 1.2. Profile views (C) of skeletal preparations of P0. Analysis of $Irf6^{-/-}; Tg^{KRT14::Irf6}$ reveals limb clubbing and syndactyly, in a manner highly analogous to $Irf6^{-/-}$ (arrow, top inset). In contrast, the sternum (arrow head, bottom inset) and in particular the xiphoid process appear to be modulated in $Irf6^{-/-}; Tg^{KRT14::Irf6}$ pups.

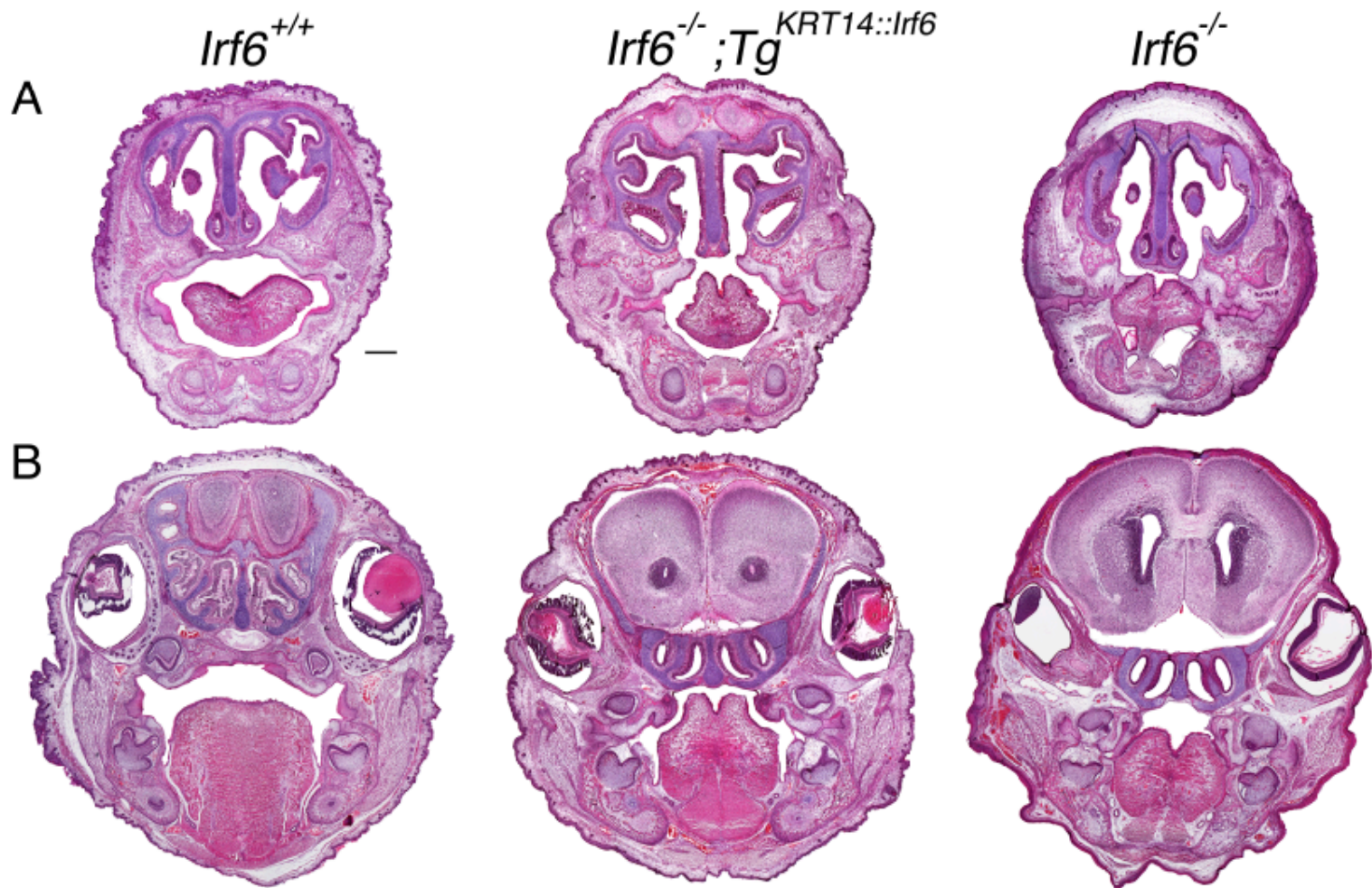
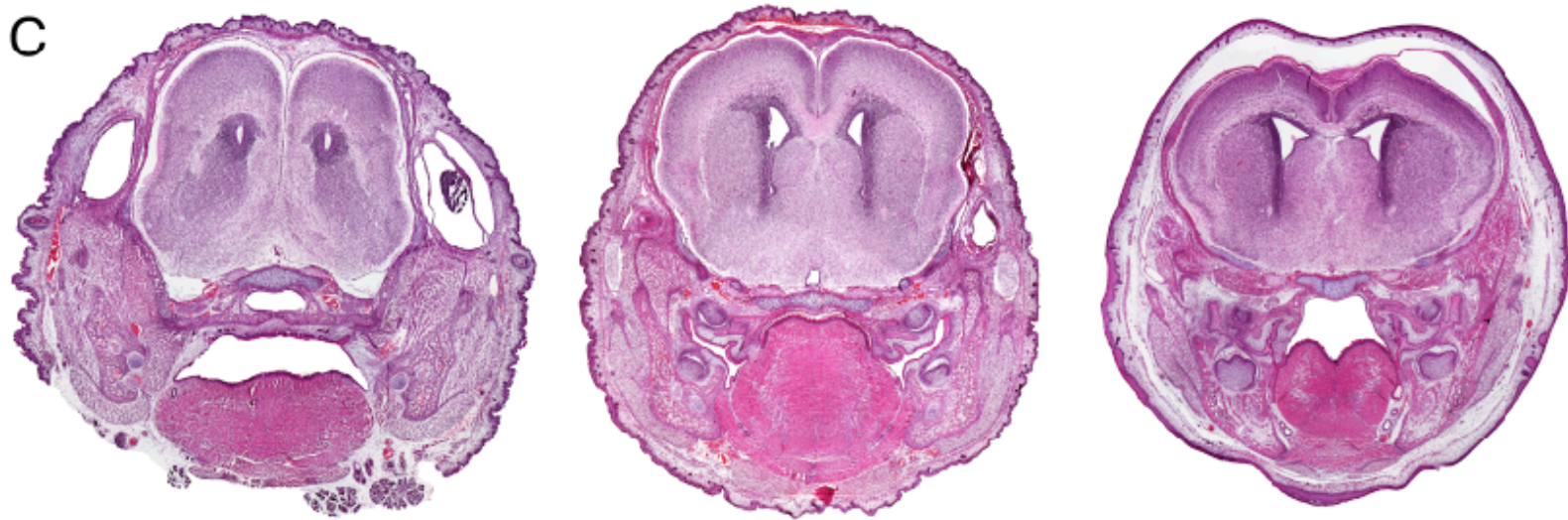


Figure 24: Rescued pups have completely penetrant palatal clefting and oral adhesions

Figure 24. (cont'd)



Head coronal section stained with Hematoxylin and Eosin of perinatal pups examining A) anterior, B) middle C) posterior soft palates. While the oral cavity is uniformly less severely affected, oral adhesions persist bilaterally. In anterior (A) and middle (B) palates, oral adhesions are prominently found between the mandible and maxilla. In the posterior palate (C), adhesions are not found between the mandible and maxilla. Scale bar (A) 500 um.

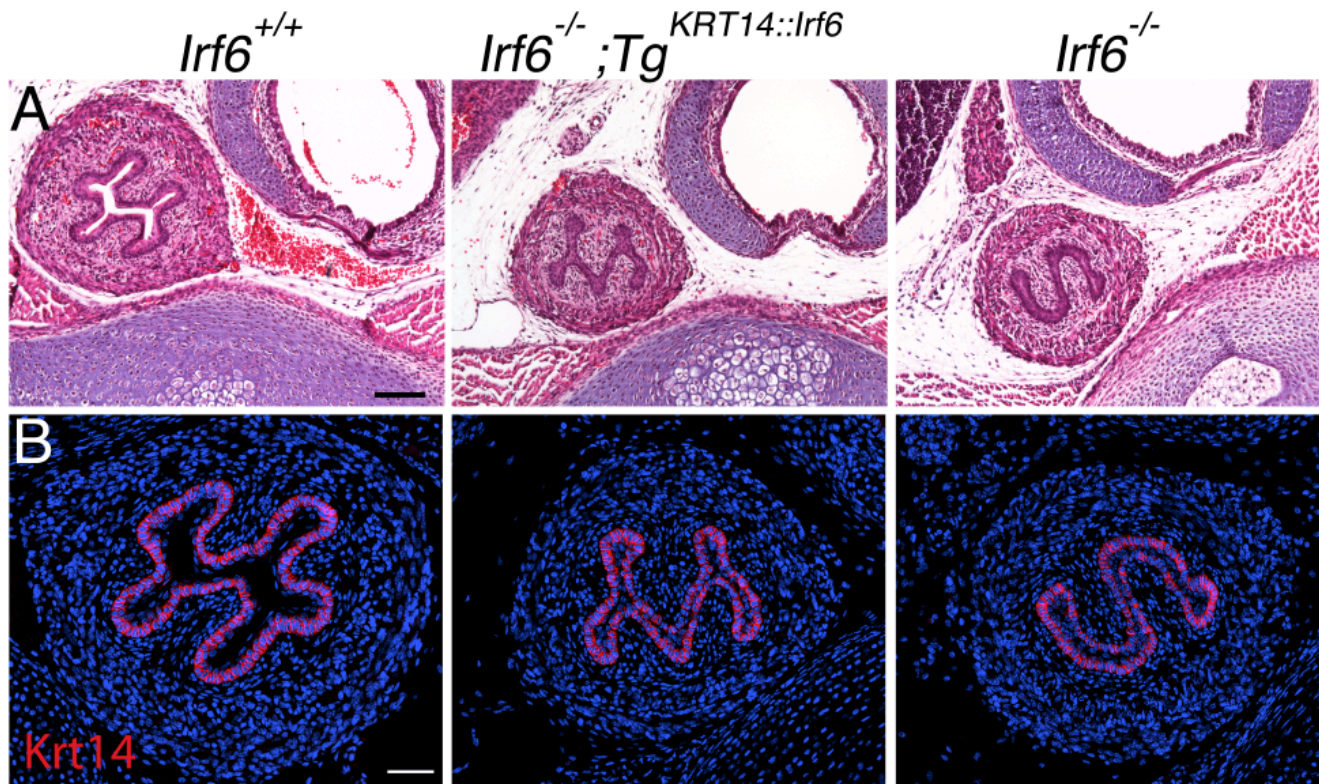


Figure 25: Obliteration of the esophageal lumen contributes to postnatal lethality.

Figure 23. (cont'd)

A) Histological analysis (Hematoxylin and Eosin) staining in transverse sections of P0 thoracic cavities. In stark contrast to the open lumen in *Irf6*^{+/+} pups, both *Tg*^{*KRT14::Irf6*}, like *Irf6*^{-/-} pups have completely penetrant esophageal adhesions. However, there was a distinct difference in the shape of the tissue, with *Tg*^{*KRT14::Irf6*} having an “M” while *Irf6*^{-/-} had an “S” shape. B) Immunostaining of Krt14. Staining for Krt14, whose highly conserved promoter is used to drive expression, showed a signal but required a 10-fold increase in exposure for detection. Scale bars (A) 100 um, (B) 50 um.

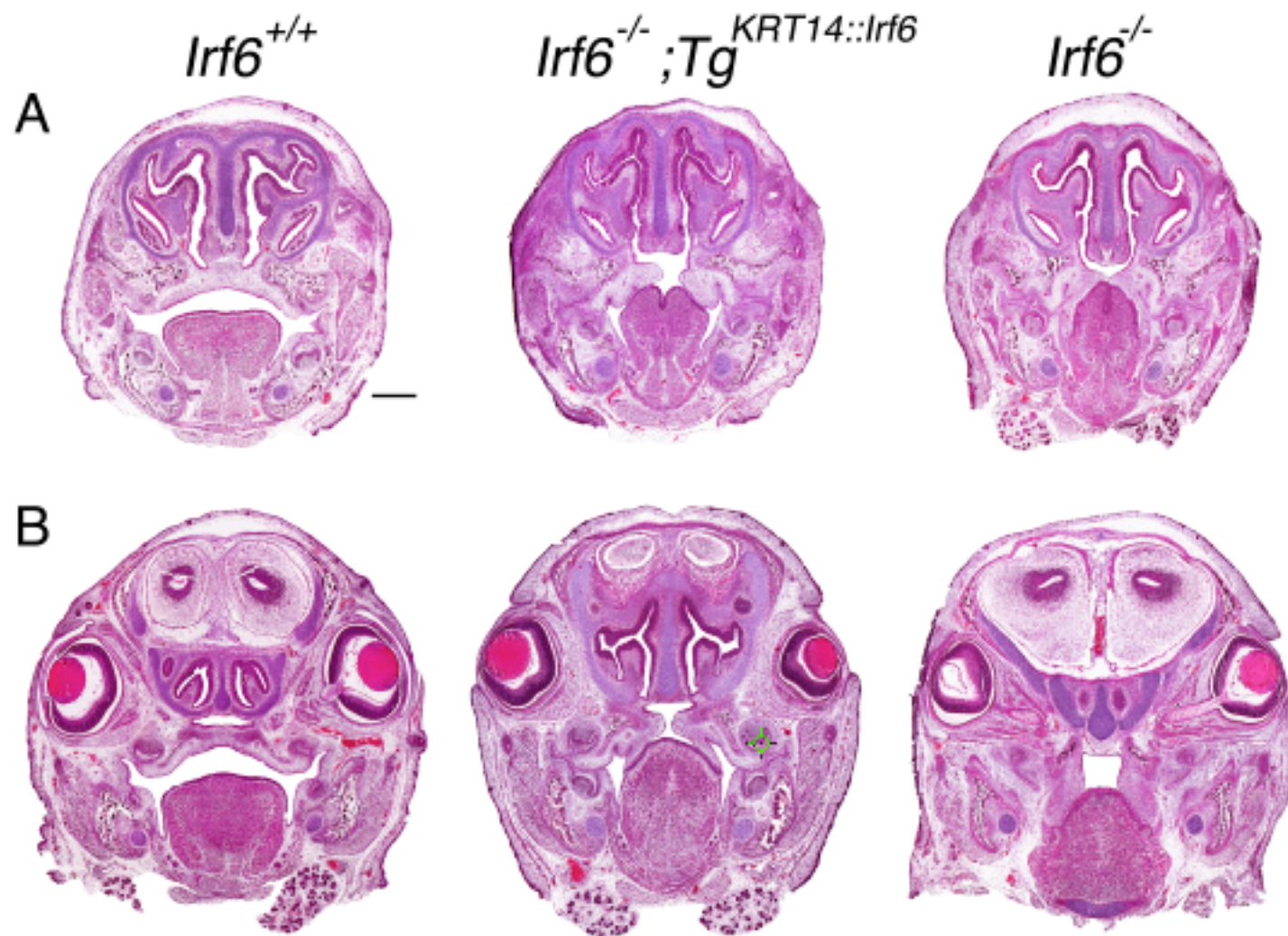


Figure 26: Tongue-palate oral adhesions obstruct palatal development

Figure 26. (cont'd)



A-C Histological analysis of *Irf6*^{+/+}, *Irf6*^{-/-}; *Tg*^{KRT14::Irf6} and *Irf6*^{-/-} head coronal sections using Hematoxylin and Eosin; A) anterior, B) middle, C) posterior soft palate. *Irf6*^{-/-}; *Tg*^{KRT14::Irf6} embryos show completely penetrant clefting at E15.5. A-B) In the anterior and middle palate, we did not find differences mandible-maxilla oral adhesions. In contrast, we found that palate (nasal epithelium)-tongue oral adhesions in *Irf6*^{-/-}; *Tg*^{KRT14::Irf6} were markedly less severe, i.e. partially rescued, compared to *Irf6*^{-/-} embryos. In addition, we found complete rescue of palatal adhesions between the oral surface of the palatal shelves and the mandible. C) In posterior palate, we found that palate-tongue oral adhesions were less severe but the palatal shelves were not re-orienting toward midline. Scale bar (A) 500 μ m.

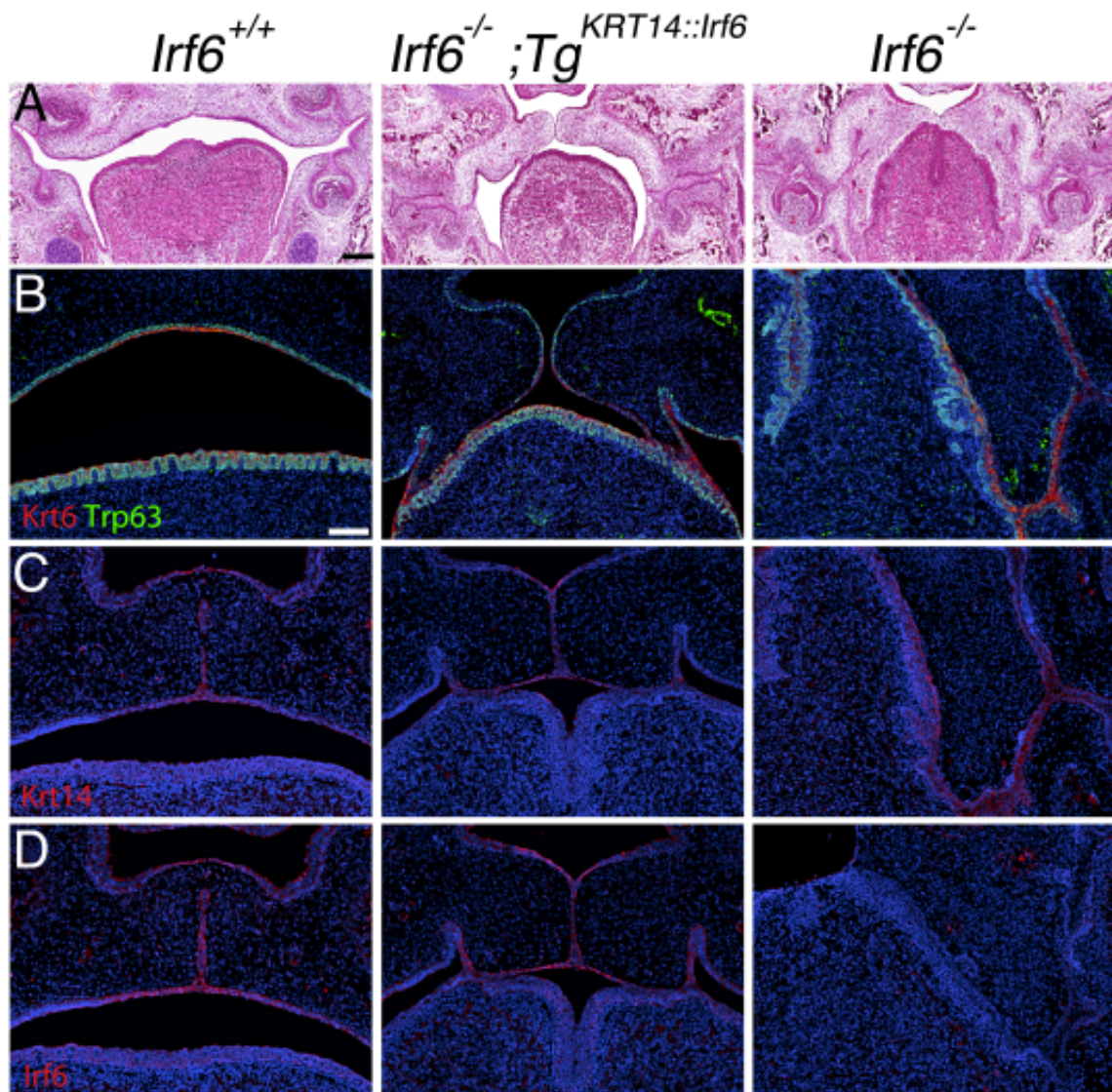
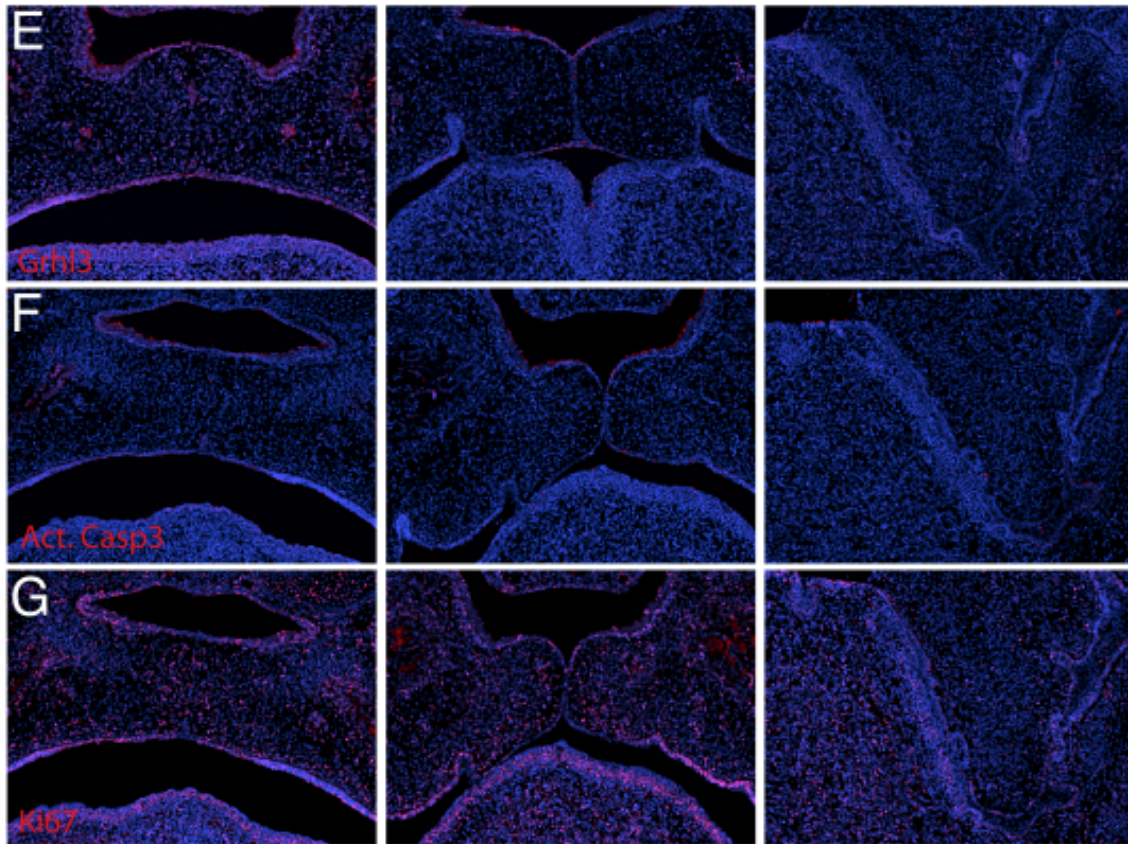


Figure 27: Oral adhesions to the tongue prevent re-orientation and apposition of palatal shelves

Figure 27. (cont'd)



Coronal section of E15.5 mid-palate histology, examined with Hematoxylin and Eosin staining (A). *Irf6*^{-/-};*Tg*^{KRT14::Irf6} embryos have marked reduction in oral adhesions and palatal shelves elevate to reach midline. Immunostaining of Krt6 (red)/p63 (green) (B), Krt14 (red) (C), *Irf6* (red) (D), *Grhl3* (red) (E), Activated Caspase 3 (red) (F), Ki-67 (red) (G). We marked the basal cell layer with Trp63/Krt14 and the periderm with Krt6. Remarkably, oral adhesions contained Krt6 expression and prevented palatal shelf reorientation in rescue embryos. Furthermore, *Irf6* expression rescued *Grhl3* expression in oral epithelium. Palatal shelves in rescue embryos exhibited Act Casp 3 and Ki-67 expression highly analogous to wild type littermates. Scale bar (A) 200 um, (B) 100 um.

Table 20: $Irf6^{-/-}$; $Tg^{KRT14::Irf6}$

	E15.5	P0	Total
Litters	13	13	26
$Irf6^{+/+}$	12	10	22
$Irf6^{+/-}$	8	17	25
$Irf6^{-/-}$	1	8	9
$Irf6^{+/+}; Tg^{KRT14::Irf6}$	26	13	39
$Irf6^{+/-}; Tg^{KRT14::Irf6}$	31	19	50
$Irf6^{-/-}; Tg^{KRT14::Irf6}$	11	12	23
Total	89	79	168
p-value	6.6×10^{-8}	0.82	9.67×10^{-6}
Resorbing	11	N/A	11 (p-value 0.049)

We intercrossed mice hemizygous for the $Tg^{KRT14::Irf6}$ (over-expressing *Irf6* under the control of the KRT14 promoter) with mice heterozygous for the *Irf6* genetrapped allele ($Irf6^{+/gt}$ from here on referred to as $Irf6^{+/-}$) to generate $Irf6^{+/-}; Tg^{KRT14::Irf6}$ mice, allowed to reach sexual maturity. We then intercrossed $Irf6^{+/-}; Tg^{KRT14::Irf6}$ with littermates that are heterozygous for the genetrapped allele ($Irf6^{+/-}$). We examined two timepoints, one during embryonic development (E15.5) and another around parturition (P0). We detected significant embryonic resorptions at E15.5. Furthermore, we found a significant under-representation of $Irf6^{-/-}$ genotypes and corresponding phenotypes.

BIBLIOGRAPHY

BIBLIOGRAPHY

- 1 Kondo, S., Schutte, B.C., Richardson, R.J., Bjork, B.C., Knight, A.S., Watanabe, Y., Howard, E., de Lima, R.L., Daack-Hirsch, S., Sander, A. *et al.* (2002) Mutations in IRF6 cause Van der Woude and popliteal pterygium syndromes. *Nat Genet*, **32**, 285-289.
- 2 Zuccherro, T.M., Cooper, M.E., Maher, B.S., Daack-Hirsch, S., Nepomuceno, B., Ribeiro, L., Caprau, D., Christensen, K., Suzuki, Y., Machida, J. *et al.* (2004) Interferon regulatory factor 6 (IRF6) gene variants and the risk of isolated cleft lip or palate. *N Engl J Med*, **351**, 769-780.
- 3 Botti, E., Spallone, G., Moretti, F., Marinari, B., Pinetti, V., Galanti, S., De Meo, P.D., De Nicola, F., Ganci, F., Castrignano, T. *et al.* (2011) Developmental factor IRF6 exhibits tumor suppressor activity in squamous cell carcinomas. *Proc Natl Acad Sci U S A*, **108**, 13710-13715.
- 4 Stransky, N., Egloff, A.M., Tward, A.D., Kostic, A.D., Cibulskis, K., Sivachenko, A., Kryukov, G.V., Lawrence, M.S., Sougnez, C., McKenna, A. *et al.* (2011) The mutational landscape of head and neck squamous cell carcinoma. *Science*, **333**, 1157-1160.
- 5 Ingraham, C.R., Kinoshita, A., Kondo, S., Yang, B., Sajan, S., Trout, K.J., Malik, M.I., Dunnwald, M., Goudy, S.L., Lovett, M. *et al.* (2006) Abnormal skin, limb and craniofacial morphogenesis in mice deficient for interferon regulatory factor 6 (Irf6). *Nat Genet*, **38**, 1335-1340.
- 6 Richardson, R.J., Dixon, J., Malhotra, S., Hardman, M.J., Knowles, L., Boot-Handford, R.P., Shore, P., Whitmarsh, A. and Dixon, M.J. (2006) Irf6 is a key determinant of the keratinocyte proliferation-differentiation switch. *Nat Genet*, **38**, 1329-1334.
- 7 Richardson, R.J., Dixon, J., Jiang, R. and Dixon, M.J. (2009) Integration of IRF6 and Jagged2 signalling is essential for controlling palatal adhesion and fusion competence. *Hum Mol Genet*, **18**, 2632-2642.
- 8 Takeda, K., Takeuchi, O., Tsujimura, T., Itami, S., Adachi, O., Kawai, T., Sanjo, H., Yoshikawa, K., Terada, N. and Akira, S. (1999) Limb and skin abnormalities in mice lacking IKK α . *Science*, **284**, 313-316.
- 9 Hu, Y., Baud, V., Delhase, M., Zhang, P., Deerinck, T., Ellisman, M., Johnson, R. and Karin, M. (1999) Abnormal morphogenesis but intact IKK activation in mice lacking the IKK α subunit of IkappaB kinase. *Science*, **284**, 316-320.

- 10 Lee, S., Kong, Y. and Weatherbee, S.D. (2013) Forward genetics identifies Kdf1/1810019J16Rik as an essential regulator of the proliferation-differentiation decision in epidermal progenitor cells. *Dev Biol*, **383**, 201-213.
- 11 Holland, P., Willis, C., Kanaly, S., Glaccum, M., Warren, A., Charrier, K., Murison, J., Derry, J., Virca, G., Bird, T. *et al.* (2002) RIP4 is an ankyrin repeat-containing kinase essential for keratinocyte differentiation. *Curr Biol*, **12**, 1424-1428.
- 12 Sil, A.K., Maeda, S., Sano, Y., Roop, D.R. and Karin, M. (2004) IkappaB kinase-alpha acts in the epidermis to control skeletal and craniofacial morphogenesis. *Nature*, **428**, 660-664.
- 13 Liu, B., Willette-Brown, J., Liu, S., Chen, X., Fischer, S.M. and Hu, Y. (2011) IKKalpha represses a network of inflammation and proliferation pathways and elevates c-Myc antagonists and differentiation in a dose-dependent manner in the skin. *Cell Death Differ*, **18**, 1854-1864.
- 14 Rountree, R.B., Willis, C.R., Dinh, H., Blumberg, H., Bailey, K., Dean, C., Jr., Peschon, J.J. and Holland, P.M. (2010) RIP4 regulates epidermal differentiation and cutaneous inflammation. *J Invest Dermatol*, **130**, 102-112.
- 15 Peyrard-Janvid, M., Leslie, E.J., Kousa, Y.A., Smith, T.L., Dunnwald, M., Magnusson, M., Lentz, B.A., Unneberg, P., Fransson, I., Koillinen, H.K. *et al.* (2014) Dominant mutations in GRHL3 cause Van der Woude Syndrome and disrupt oral periderm development. *Am J Hum Genet*, **94**, 23-32.
- 16 de la Garza, G., Schleiffarth, J.R., Dunnwald, M., Mankad, A., Weirather, J.L., Bonde, G., Butcher, S., Mansour, T.A., Kousa, Y.A., Fukazawa, C.F. *et al.* (2013) Interferon regulatory factor 6 promotes differentiation of the periderm by activating expression of grainyhead-like 3. *J Invest Dermatol*, **133**, 68-77.
- 17 Krishnan, L., Guilbert, L.J., Russell, A.S., Wegmann, T.G., Mosmann, T.R. and Belosevic, M. (1996) Pregnancy impairs resistance of C57BL/6 mice to Leishmania major infection and causes decreased antigen-specific IFN-gamma response and increased production of T helper 2 cytokines. *J Immunol*, **156**, 644-652.
- 18 Bush, J.O. and Jiang, R. (2012) Palatogenesis: morphogenetic and molecular mechanisms of secondary palate development. *Development*, **139**, 231-243.
- 19 Fakhouri, W.D., Rhea, L., Du, T., Sweezer, E., Morrison, H., Fitzpatrick, D., Yang, B., Dunnwald, M. and Schutte, B.C. (2012) MCS9.7 enhancer activity is highly, but not completely, associated with expression of Irf6 and p63. *Dev Dyn*, **241**, 340-349.
- 20 Walker, B.E., Fraser, F. C. (1956) Closure of the Secondary Palate in Three Strains of Mice. *J. Embryol. Exp. Morphol.*, **4**, 176-189.

Chapter 5 -
Conclusions and Future Directions

Major Themes: Orofacial Clefting

We previously identified *IRF6* protein-coding mutations in 70% of families with VWS (1). While etiology in the remaining 30% of VWS cases is unknown, linkage studies suggest locus heterogeneity (VWSII, # 606713) (2). Our work, using exome sequencing, targeted prevalence detection and functional studies shows that mutations in *GRHL3* can also lead to Van der Woude Syndrome (VWS). Considering interaction in zebrafish (3), we ask if *Irf6* interacts with *Grhl3* in the mouse. We find that embryos heterozygous for the *Irf6* null allele have oral adhesions at the tooth germ. Embryos heterozygous for *Grhl3* have oral adhesions and fusions posterior to the tooth germ. Double heterozygous embryos had a combination of both phenotypes. Qualitatively, we conclude an additive relationship between *Irf6* and *Grhl3* in oral epithelium. Considering our sample size of double het embryos was fairly small, we did not quantitatively analyze changes in the extent (anterior-posterior axis) or pervasiveness (length of adhesions relative to free surface) of this phenotype. As such, our conclusion is that we did not detect epistasis and conclude an additive interaction. However, an additive interaction suggests that *Grhl3* and *Irf6* have overlapping roles in murine oral epithelium, if not in the same pathway (Chapter 2). Considering multiple, highly complex gene regulatory networks, absence of epistasis should not be misconstrued for proof of absence. In fact, murine epistasis experiments are highly specific but not sensitive. More importantly, we find that *Irf6* expression is both necessary and sufficient for *Grhl3* in the periderm (Chapter 4). Consistently, we find that *Irf6* is required for *Grhl3* expression in caudal neurulation (Chapter 3). In light of this and our previous work (3), it is plausible to conclude that *Grhl3* and *Irf6* are part of the same gene regulator network in oral epithelium.

At least two additional clues suggest that *Grhl3* and *Irf6* interact in the mouse. First, we found a significant number of embryonic resorptions. Second, at weaning, we found significantly less *Irf6*^{+/-};*Grhl3*^{+/-} mice than expected. While many systemic diseases can cause lethality, prior work shows that both *Irf6* and *Grhl3* regulate development of the gastrointestinal system (4, 5). While loss of *Irf6* leads to esophageal adhesions, loss of *Grhl3* leads to a shortened digestive track. However, we did not find esophageal adhesions in *Irf6*^{+/-};*Grhl3*^{+/-} pups. Analysis of more distal aspects of the digestive track in pups or older mice has not been undertaken. Furthermore, in the epithelium of both mouse and zebrafish, *Grhl1* and *Grhl2* interact with *Grhl3*, providing redundant function (3, 6, 7). Therefore, in the oral epithelium of *Irf6*^{+/-};*Grhl3*^{+/-} embryos, *Grhl1* and *Grhl2* may be providing partially redundant, regulatory function and activation of more distal factors. A test for epistasis between *Irf6* and *Grhl2* is currently underway with a collaborator. A similar experiment for *Irf6* and *Grhl1* is not currently being pursued but this analysis is warranted. Considering redundant roles in epithelium, *Grhl1* and *Grhl2* may play a role in human orofacial clefting. Sequencing of *Grhl1* and *Grhl2* in families with VWS is also currently being pursued.

Major Themes: Neural Tube Defects

In addition to novel insights into orofacial clefting, this work also outlines novel roles for *Irf6* in ectoderm development. Importantly, we show that *Tfap2a*, *Irf6* and *Grhl3*, human orofacial clefting genes, also regulate epithelial and neural tube development in the mouse via a complex gene regulatory network (Fig. 1). In addition, our preliminary

sequencing data from individuals with Spina Bifida suggests that *IRF6* is also involved in human neurulation. Considering that we found one mutation in 96 individuals, the impact of *IRF6* function in human neurulation is not yet clear. More significant impact from this work comes from clinical and epidemiological research showing that orofacial clefting and neural tube defects share common environmental risk (smoking), iatrogenic compounds (valproic acid) and preventative factors (folic acid). Here, we describe a shared molecular network that might be perturbed in both developmental diseases. It is not yet clear if such shared pathways are common in neural tube and orofacial clefting. Examination of orofacial clefting genes in neurulation and neurulation genes in orofacial clefting may provide novel shared gene regulatory networks.

Biologically, few studies have reported over-expression of a tumor suppresser transcription factor leading to gain-of-function phenotypes (Chapter 3). One prominent example, although not a transcription factor, is *PTEN* (8). Importantly, *IRF6*, *TFAP2A* and *GRHL3* are tumor suppressor genes and transcription factors. Considering gain-of-function phenotypes for *IRF6*, future work may seek to over-express *TFAP2A* and *GRHL3* in orofacial and neural tube development. Whatever the mechanism of perturbation, exploring this gene regulatory network may provide additional candidate genes, risk loci and environmental preventative strategies to reduce the risk of two congenital diseases associated with significant morbidity and mortality.

Genetic risk for orofacial and neural tube defects

VWS and PPS are monogenic diseases, with as yet inconclusive evidence for genetic modifiers (9). In contrast, nonsyndromic cleft palate, cleft lip and cleft lip and palate constitute three different congenital diseases each with multiple genetic and environmental risk factors. Likewise, neural tube defects are a highly heterogeneous cohort of anomalies involving at least three different types of developmental defects, each with an array of presentations. For example, spina bifida, a type of neural tube defect, has four different presentations, including occulta, closed, meningocele and myelomeningocele. Each of these, in turn, has multiple genetic and environmental modifiers. Therefore, upon examination, spina bifida, a type of neural tube defects, may be as genetically complex as orofacial clefting. This reasoning provides important considerations for identifying additional candidate genes in human neural tube defects, including sample size, power, effect size and heterogeneity of populations.

Considering this genetic complexity, can spina bifida co-occur with orofacial clefting? From our murine studies, we found that under-expressing *Irf6* can lead to a curled tail (Chapter 3) and oral adhesions (Chapter 5). Consistently, a review of the literature reveals that the phenotypic spectrum of Popliteal Ptyergium Syndrome (PPS) can include spina bifida (10). In addition, Multiple Ptyergium Syndrome, which has a phenotypic spectrum highly similar to but more severe than PPS, includes multiple examples of spina bifida (11-13). Considering murine studies and multiple clinical examples of orofacial clefting with spina bifida, families with VWS and PPS may be at increased risk of developing neural tube defects. Understanding and managing risk in these families can

therefore prevent significant co-morbidity. In that context, murine models with both orofacial clefting and neural tube defects (*Irf6*^{neo/-}) provide a tractable system to assess patient risk.

This work supports two important questions about risk. First, is there a common cohort of genes that ‘stack the deck’ for all neural tube defects? Second, what is the architecture of genetic risk, i.e. involving a single or multiple biological pathways? I would predict that a cohort of genes in a single or multiple pathways contribute baseline risk but that an environmental or additional genetic insult tips the balance toward pathology. From that vantage point, it is difficult to contextualize a highly complex disease like spina bifida in the “common disease, common allele” model. Similarly, gene discovery efforts in diabetes (14) have shown that common alleles contribute a paucity of the risk toward common disease.

Expanding the gene regulatory network: *Tfap2* and *Grhl* paralogs

Expanding the Gene Regulatory Network (GRN) is critical in determining and then modifying clinical risk for isolated orofacial clefting and neural tube defects. Initially, we discovered an association between orofacial clefting and a *TFAP2* binding site within an *IRF6* enhancer sequence (15). Mutations in *TFAP2α* can lead to Branchio-Oculo-Facial Syndrome, which like VWS, is associated with orofacial clefting and lip pits.

Significantly, we find that *Tfap2α* regulates *Irf6* expression in multiple time points and tissues (Chapter 3). However, we also realize that *TFAP2* family members, α , β , γ , δ and ϵ , share an identical cis-binding motif. In fact, functional redundancy for *Tfap2* paralogs

is observed in different tissues and species (16, 17). Therefore, are *TFAP2* paralogs co-regulating *IRF6* in the same or different spatiotemporal contexts? In particular, *TFAP2 γ* and *TFAP2 β* are highly expressed in the epidermis, in the same cell types as *IRF6* (18). Exploring the relationship between *IRF6*, *TFAP2 γ* and *TFAP2 β* may provide additional nodes in this GRN.

In support of additional feedback loops, genome-wide analysis of *IRF6* binding sites also shows a signal within *TFAP2 γ* (19). Consistently, we find that *Irf6* regulates *Tfap2 γ* in the skin (Chapter 3). This interaction seems to be evolutionarily conserved in zebrafish, where *irf6* is necessary for *tfap2c* expression in the periderm (20). Considering this, our collaborators are currently sequencing *TFAP2 γ* in individuals with VWS. In addition, tissue specific deletion of *Tfap2 γ* using *Sox2* leads to caudal neural tube defects that are highly analogous to *Irf6* compound heterozygous embryos (21). Thus, we ask if *Irf6* regulates *Tfap2 γ* in caudal neurulation. Importantly, we find that *Irf6* is required for *Tfap2 γ* in murine tail development. Considering that *Irf6*, *Tfap2 α* , *Tfap2 γ* and *Grhl3* seem to be co-regulating mouse neural tube development, sequencing additional individuals with spina bifida is plausible.

Similarly, previous work shows that *Grhl* paralogs, 1, 2 and 3, have both independent and overlapping function in epidermal development (6). Like *tfap2a* and *tfap2c*, *grhl1* and *grhl2* are expressed in zebrafish periderm. Furthermore, injecting dominant negative *irf6* also perturbs *grhl1* and *grhl2* expression. Remarkably, knocking out *Grhl2* in the mouse leads to anencephaly and abdominal wall defects that are highly analogous to *Tfap2 α*

knockout embryos. While the phenotypic similarity suggests interaction, a test for epistasis between *Grhl2* and *Tfap2α* did not reveal novel phenotypes in eight double heterozygous embryos (22). Our work, with incomplete penetrance (*Tfap2α-Grhl3* and *Tfap2α-Irf6*) and variable expressivity (*Tg^{KRT14::Irf6}*), would suggest that a larger sample size is required to examine this gene regulator network (Chapter 3). Furthermore, considering zebrafish work, *Tfap2a* and *Grhl2* may be interacting indirectly through *Irf6*. Examining the *Grhl2* locus for *Irf6* cis-binding elements would provide additional mechanistic insights. Considering that *Irf6* post-translationally regulates *Trp63* and *Tfap2α*, protein-protein interactions are also plausible (Chapter 3). If experimental work is consistent, these paralogs may be excellent candidate genes for human orofacial clefting and neural tube defects.

Novel implications for *Irf6* knockout phenotype

Currently, knockout of five murine alleles produces a phenotype highly analogous to loss *Irf6*. This phenotype include craniofacial defects, orofacial clefting, a hyperproliferative epidermis, defective permeability barrier, limb clubbing, syndactyly. In addition to *Irf6* (4, 23), these genes are *Ikka* (24), *14-3-3σ* (23), *Ripk4* (25) and *Kdfl* (26). Considering five genes, 10 possible genetic interactions can be done. Currently, we know that 1) *Irf6* and *14-3-3σ* interact, 2) *Irf6* and *Ikka* do not appear to interact, 3) *14-3-3σ* and *Kdfl* interact. However, we also know that both *Irf6* and *Kdfl* interact with *Trp63* (26, 27). Furthermore, while the nature of these interactions is not yet clear, a genome-wide scan shows that *IRF6* binds within *14-3-3σ* (19). Testing all additional combinations may provide novel phenotypes and expand our understanding of this gene regulator network.

Further, lack of interaction (e.g. *Irf6* and *Ikka*) can be queried further by the addition of other null alleles from this cohort (*14-3-3σ*) to create triple heterozygous embryos (*Irf6*^{+/-}; *Ikka*^{+/-}; *14-3-3σ*^{+/-}). Considering that 1) *Irf6* interacts with *Trp63*, *Grhl3* and *Tfap2α* and 2) *Kdfl* interacts with *Trp63*, additional work can delineate how *Grhl3* and *Tfap2α* interact with this cohort of alleles.

Considering that over-expressing *Irf6* partially rescues the *Irf6* knockout, another way to pursue epistasis would be through heterologous genetic rescue using the *Tg*^{KRT14::Irf6} transgene in *14-3-3σ*, *Ikka*, *Ripk4* and *Kdfl* knockout embryos. Rescue, partial or complete, would suggest that *Irf6* is downstream, which is plausible considering transcriptional regulation. Considering that we have multiple positive controls for a genetic interaction in this pathway (*Irf6-14-3-3σ* (4), *14-3-3σ-Kdfl* (26)), negative results in multiple assays are more informative, assuming a sufficiently large sample size.

As *IRF6* plays an important role in orofacial clefting, the role of *Ikka*, *14-3-3σ*, *Ripk4* and *Kdfl* in isolated and syndromic orofacial clefting should be examined. Similarly, considering phenotypic overlap, our finding that *Irf6* regulates murine neurulation suggests that these four genes have analogous role. Consistent with this rationale, a test for epistasis between *Irf6* and *14-3-3σ* (23) showed a caudal neural tube defect. Further, while *14-3-3σ* and *Kdfl* were epistatic in skin, they did not interact in the neural tube. However, *Kdfl* and *Trp63* did interact in the caudal neural tube (26). Interestingly, *Trp63* interacts with *Irf6* in palate development but an impact on the neural tube was not reported in the pertinent study (27). Together, this data suggests that a novel cohort of

murine alleles might be playing a role in the pathogenesis of spina bifida. Therefore, a comprehensive examination of gene-gene interactions, as mentioned above, would also be informative for this phenotype.

Proposed gene regulatory network

Considering that we discovered a shared gene regulator network in orofacial and neural tube development by examining regulatory elements in multiple tissues, a comprehensive interactome irrespective of cell type, tissue or timepoint may provide candidate regulatory elements in future studies (Fig. 2). Importantly, this regulatory network is involved in multiple tissues and cell lines, providing multiple orthogonal views of function and regulation. In addition to the data presented in this thesis, prior work shows that *Tfap2 α* regulates *p21* (CDKN1A) via co-regulation with *Smad2/3* in keratinocytes (28, 29). Likewise, in Medial Edge Epithelium (MEE), *Irf6* regulates *p21* expression through repression of *Trp63* (30). Considering that *Irf6* stabilizes *Tfap2 α* protein, *Irf6* seems to be regulating *p21* expression in at least two different indirect mechanisms. Furthermore, *Smad2/3* associates with *Ikk α* to regulate *Ovo11* and *Mad1* (31, 32). Likewise, *Irf6* also regulates *Ovo11* (19). While *Ovo11* transcriptionally represses c-Myc (33), *Mad1* antagonizes Myc-Max dimmers (34, 35). Importantly, prior work shows that *Trp63* positively regulates *IKK α* expression (36). *IKK α* in turn positively regulates 14-3-3 σ by inhibiting promoter hypermethylation (37). In addition, Notch signaling regulates *Irf6* expression in epithelium (38). Consistently, a test for epistasis in the mouse shows that *Irf6* interacts with *Jagged2*, a transmembrane receptor that regulates Notch signaling (39). In oral epithelium, *Irf6* is required for *Mmp13* (39) and in breast epithelium it

stabilizes Maspin (40). While *Irf6* is regulated via the proteasome (41), the E3 ubiquitin ligase that mediates this interaction has not been identified. Considering the function of these genes, the balance of this signaling cascade, activation of p21 and repression of cMyc, is stopping cellular proliferation and driving differentiation. This molecular rationale provides insight into murine knockout phenotypes of *Irf6*, *Ikkα* and *14-3-3σ*. At this point, it is not clear how *Ripk4* and *Kdf1* regulate proliferation and differentiation or how they might interact in this gene regulator network.

Therapeutic considerations in congenital disease

In order to treat genetic disease, we must first understand what tissues are affected. For VWS and PPS, previous work shows that *Irf6* is expressed in epithelium and *Irf6*^{-/-} mice have an abnormal epidermis and oral epithelium (4, 23, 39). As such, many of the syndromic anomalies seen in VWS and PPS were thought to result from epithelial defects. However, the phenotypic spectrum of VWS and PPS also includes musculoskeletal, digit, limb and genital anomalies. Therefore, we ask if epithelial rescue is sufficient to modify associated developmental defects in the mouse. Strikingly, epithelial rescue enables perinatal survival and the limbs are no longer adherent to the body wall but upper and lower limb pterygium persist. Similarly, expression of *Irf6* in oral basal epithelium dramatically reduces adhesions around the palatal shelves but does not prevent palatal clefting. Moreover, limb clubbing, craniofacial defects and a curled tail persist. Therefore, unlike complete rescue of *Ikkα* using the *KRT14* promoter (42), *Irf6* is cell-autonomously required in epithelial and non-epithelial tissues. Using tissue specific promoters to over-express or delete *Irf6* in cartilage, bone, neural tube and

periderm (a cell type that is thought to regulate oral adhesions) will allow further dissection of this important molecular pathway. Most importantly, this work will inform which tissues we need to target to reduce disease burden in utero.

Importantly, while palate-mandible adhesions are rescued anteriorly, palate-tongue adhesions persist. Technically, this may result from regulating *Irf6* expression with the *KRT14* promoter, leading to a spatiotemporal expression program that is inconsistent with endogenous expression. Biologically, this may suggest that nasal periderm is more sensitive to *Irf6* dose. Considering the histology, it appears that palate-tongue oral adhesions play an important role in palatal clefting. Considering attachment of the palatal shelves to the tongue and ensuing physical obstruction, we propose an adhesive Pierre Robin Sequence. As opposed to micrognathia limiting the volume of the oral cavity, this process involves physical restraints on movement of the palatal shelves with a normal oral cavity volume (Chapter 4).

Preventative strategies in orofacial clefting and neural tube defects

If GRHL3 is downstream of IRF6 in human neural tube development, can we design rationale preventative strategies for further exploration? Considering current data suggesting that *Grhl3* is downstream of *Irf6* in periderm (Chapter 2) and caudal neural tube development (Chapter 3), mutually advantageous translational and clinical modalities seem feasible. Epidemiological data has shown that folate supplementation reduces 45-70% of neural tube defect risk. However, a significant portion of neural tube defects are resistant to folate supplementation. What accounts, if anything, for this

unresponsive cohort? Critically, mouse data suggests that neural tube defects in *Grhl3* knockout embryos are not responsive to folate but do respond to inositol (43). If *TFAP2α-IRF6-GRHL3* regulate a pathway in human neural tube, then targeted supplementation with inositol may further lower the incidence of neural tube defects. Determining the distal node by which inositol exerts its function may provide important insight in designing and expanding the pool of patients who are eligible for targeted therapy. Alternatively, like folate, fortification in essential foods may be possible. Furthermore, inositol is used to treat patients with depression, suggesting safety or minimal side effects.

Can inositol also be a therapy in human orofacial clefting? In humans, we show that mutations in *IRF6* and *GRHL3* lead to Van der Woude Syndrome. In the mouse, *Irf6* and *Grhl3* regulate oral epithelium and palatal development (Chapter 2). If inositol can rescue *Grhl3* function in the oral cavity in a manner analogous to the neural tube then supplementation may also be indicated to prevent orofacial clefting. However, prior work examining inositol modulation of neural tube defects did not examine the palate and oral epithelium. As such, examining these embryos would provide critical information for feasibility. Ideally, one would pursue a co-clinical trial, i.e. mouse and human, for the prevention orofacial and neural tube defects using inositol and folate relative to historical epidemiological data.

While drug targets are not currently being explored, an epithelial specific factor that regulates proliferation and differentiation, like *Ikka*, *Kdfl*, *Ripk4* $14-3-3\sigma$, *Irf6*, *Grhl3*,

may provide a robust clinical application. To test many potential targets, we would need tissue. To test for specificity, we would need both epithelial and non-epithelial cell types. To test for efficacy, we would need a cell type that is particularly affected. These three requirements are uniquely found in murine skin, which contains both epidermis (affected epithelium) and dermis (unaffected adipocytes, mesenchyme, vasculature, etc). Putative targets could be tested in murine palate cultures, which would provide a robust *ex vivo* model for further screening. Highly attractive targets could then be tested *in vivo* using multiple murine alleles (gene trap, hypomorphic, mutated, etc) for the affected genes. Because clefting also occurs in canine and feline, larger animal models may also be tested. These approaches would require substantial funding and a pipeline for tissue processing.

Another approach is gene therapy, that is replacing missing or defective gene in the cell type(s) that contribute(s) to disease. This would truly achieve the pinnacle of personalized therapeutic approaches and limit side effects. Toward that end, we have begun to perform *in utero* gene delivery of *Irf6* using an adenoviral vector. In addition to a report showing gene deliver to the oral cavity and developing epidermis (44), we find that a [E1,E3-]Ad-LacZ vector can transduce oral periderm and developing epidermis of both wildtype and *Irf6* knockout embryos when injected at E12.5 (unpublished results). We also find that Ad-LacZ vectors can transduce cells along the medial edge of the palatal shelves. As such, our approach is feasible and we predict that *Irf6* gene delivery to the periderm of *Irf6* compound heterozygous (*Irf6^{neo/-}*) and knockout embryos (*Irf6^{-/-}*) (4) will reduce the severity of oral adhesion as seen with genetic rescue. Targeting of the

developing epidermis may also ameliorate skin anomalies, leading to a reduction in proliferating cells and an increase in terminal differentiation (Chapter 4). Having characterized multiple murine models with varying amounts of *Irf6* expression, we can attempt to complement the endogenous deficit with exogenous vector dose. This approach would provide a unique test of translational feasibility because different Van der Woude families have different types of *IRF6* mutations with dramatically different phenotypic presentations. In that respect, finding the dose-disease ratio relative to mutation type would be extremely valuable. At this point, the feasibility of adenoviral vector transduction during neurulation is unknown. Finally, considering that replacing *Irf6* expression in epithelium did not rescue limb, digit and skeletal defects, epithelial rescue will not be a panacea.

APPENDIX

APPENDIX

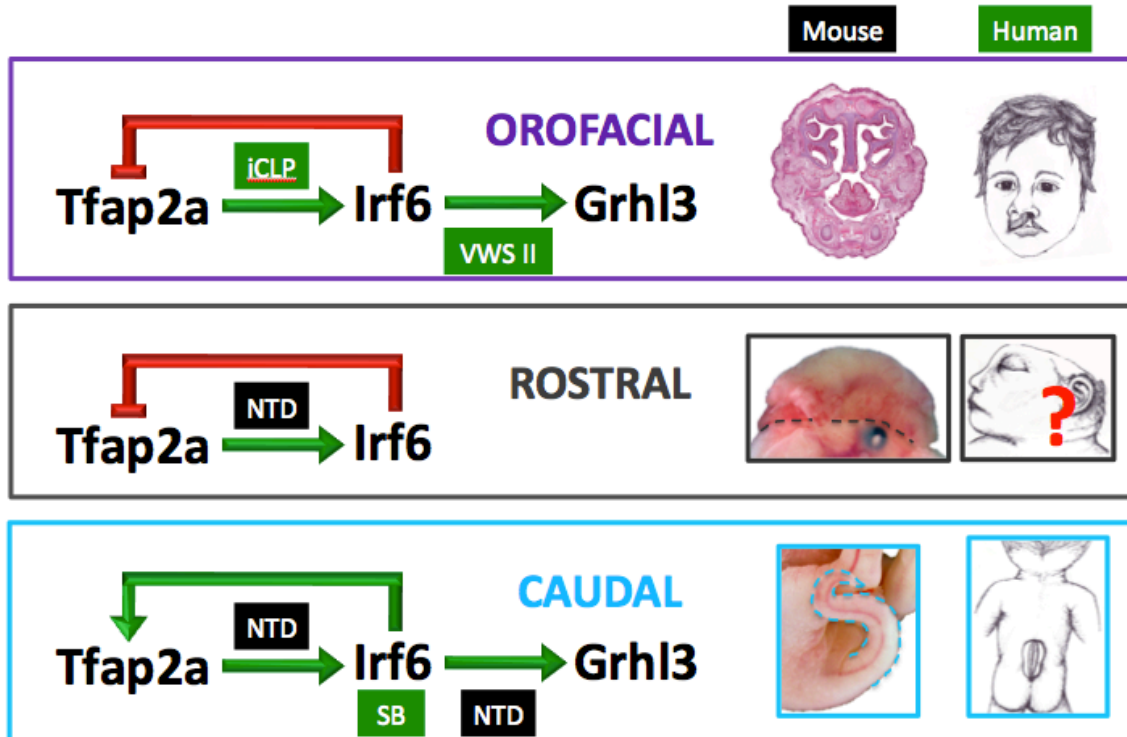


Figure 28: Summary of genetic network for orofacial and neural tube development.

We find that three human orofacial clefting genes are involved in murine neural tube development. Data from human sequencing (green boxes: iCLP, isolated cleft lip and palate; VWS, Van der Woude Syndrome; SB, Spina Bifida) and murine models (black boxes: NTD, Neural Tube Defects) suggest a shared molecular network. Top: From orofacial and epidermal tissue, we find that *Tfap2a* regulates *Irf6*, which in turn regulates *Grhl3*. We also find that *Irf6* negatively regulates *Tfap2a* transcriptionally. Middle: In rostral neurulation, *Irf6* negatively regulates *Tfap2a*. As this point, it is not clear if *Grhl3* is downstream of *Irf6* in rostral neural tube development. It is also not clear if this molecular network plays a role in anencephaly. Bottom: In caudal neurulation, we find that *Tfap2a* and *Irf6* positively regulate each other and that *Irf6* is required for *Grhl3* expression.

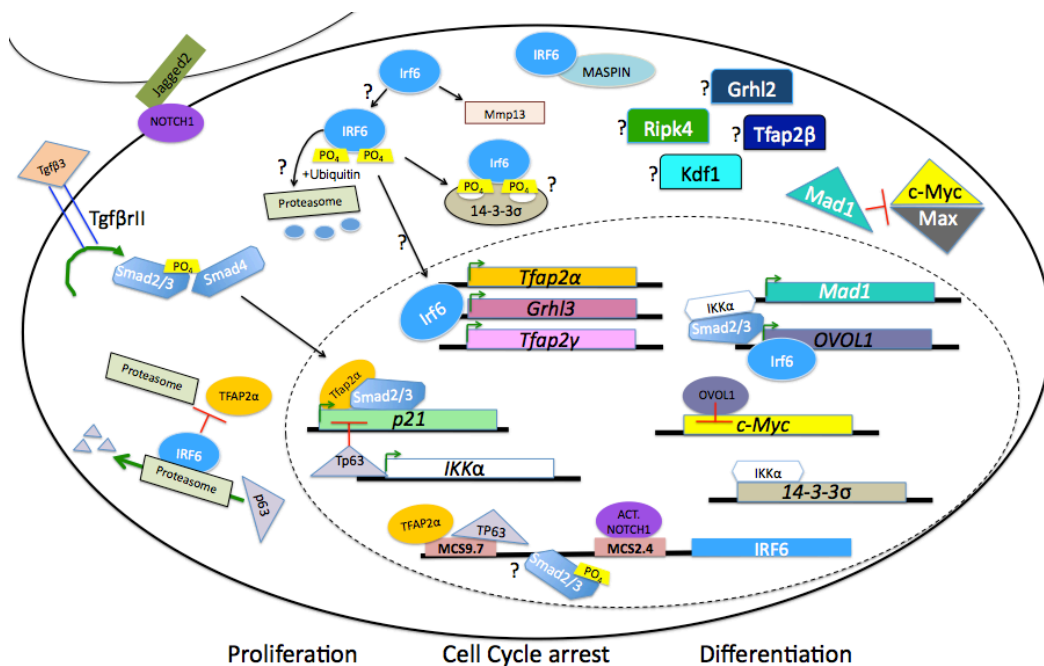


Figure 29: Proposed IRF6 gene regulator network. A proposed gene regulatory network for *Irf6* and associated molecules. Proposed interactions, molecular processes or function of related genes that are at this point minimally elucidated are highlighted (?). The balance of this gene regulatory network is aimed at stopping proliferation (repressing c-Myc), initiating cell cycle arrest (induction of p21) and driving differentiation (Grhl3, which drives *Tgm1*). While Smad2/3 is required for *Irf6* expression in the medial edge epithelium, it is not yet clear which enhancer mediates this activation. Additional questions include: 1) Mechanism by which *Irf6* is targeted to the proteasome; 2) E3 ubiquitin ligase for IRF6; 3) How and under what conditions *Irf6* is phosphorylated (PO₄); 4) Function of *Ripk4*, *Kdf1*, *Grhl2* and other *Tfp2* family members in this gene regulatory network; 5) Mechanism by which *Irf6* translocates into the nucleus to mediate transcriptional activity. We propose that 1) *Irf6* is bound to 14-3-3σ when phosphorylated; 2) *Irf6* stabilizes *Tfap2α* by inhibiting proteasome-mediated degradation.

BIBLIOGRAPHY

BIBLIOGRAPHY

- 1 de Lima, R.L., Hoper, S.A., Ghassibe, M., Cooper, M.E., Rorick, N.K., Kondo, S., Katz, L., Marazita, M.L., Compton, J., Bale, S. *et al.* (2009) Prevalence and nonrandom distribution of exonic mutations in interferon regulatory factor 6 in 307 families with Van der Woude syndrome and 37 families with popliteal pterygium syndrome. *Genet Med*, **11**, 241-247.
- 2 Koillinen, H., Wong, F.K., Rautio, J., Ollikainen, V., Karsten, A., Larson, O., Teh, B.T., Huggare, J., Lahermo, P., Larsson, C. *et al.* (2001) Mapping of the second locus for the Van der Woude syndrome to chromosome 1p34. *Eur J Hum Genet*, **9**, 747-752.
- 3 de la Garza, G., Schleiffarth, J.R., Dunnwald, M., Mankad, A., Weirather, J.L., Bonde, G., Butcher, S., Mansour, T.A., Kousa, Y.A., Fukazawa, C.F. *et al.* (2013) Interferon regulatory factor 6 promotes differentiation of the periderm by activating expression of grainyhead-like 3. *J Invest Dermatol*, **133**, 68-77.
- 4 Ingraham, C.R., Kinoshita, A., Kondo, S., Yang, B., Sajan, S., Trout, K.J., Malik, M.I., Dunnwald, M., Goudy, S.L., Lovett, M. *et al.* (2006) Abnormal skin, limb and craniofacial morphogenesis in mice deficient for interferon regulatory factor 6 (Irf6). *Nat Genet*, **38**, 1335-1340.
- 5 Yu, Z., Bhandari, A., Mannik, J., Pham, T., Xu, X. and Andersen, B. (2008) Grainyhead-like factor Get1/Grhl3 regulates formation of the epidermal leading edge during eyelid closure. *Dev Biol*, **319**, 56-67.
- 6 Boglev, Y., Wilanowski, T., Caddy, J., Parekh, V., Auden, A., Darido, C., Hislop, N.R., Cangkrama, M., Ting, S.B. and Jane, S.M. (2011) The unique and cooperative roles of the Grainy head-like transcription factors in epidermal development reflect unexpected target gene specificity. *Dev Biol*, **349**, 512-522.
- 7 Auden, A., Caddy, J., Wilanowski, T., Ting, S.B., Cunningham, J.M. and Jane, S.M. (2006) Spatial and temporal expression of the Grainyhead-like transcription factor family during murine development. *Gene Expr Patterns*, **6**, 964-970.
- 8 Garcia-Cao, I., Song, M.S., Hobbs, R.M., Laurent, G., Giorgi, C., de Boer, V.C., Anastasiou, D., Ito, K., Sasaki, A.T., Rameh, L. *et al.* (2012) Systemic elevation of PTEN induces a tumor-suppressive metabolic state. *Cell*, **149**, 49-62.
- 9 Leslie, E.J., Mancuso, J.L., Schutte, B.C., Cooper, M.E., Durda, K.M., L'Heureux, J., Zuccherro, T.M., Marazita, M.L. and Murray, J.C. (2013) Search for genetic modifiers of IRF6 and genotype-phenotype correlations in Van der Woude and popliteal pterygium syndromes. *Am J Med Genet A*, **161**, 2535-2544.

- 10 Froster-Iskenius, U.G. (1990) Popliteal pterygium syndrome. *J Med Genet*, **27**, 320-326.
- 11 McKeown, C.M. and Harris, R. (1988) An autosomal dominant multiple pterygium syndrome. *J Med Genet*, **25**, 96-103.
- 12 Srivastava, R.N. (1968) Arthrogryposis multiplex congenita. Case report of two siblings. *Clin Pediatr (Phila)*, **7**, 691-694.
- 13 Srivastava, R.N. (1969) Arthrogryposis or a new syndrome? *J Pediatr*, **74**, 840-841.
- 14 Clee, S.M. and Attie, A.D. (2007) The genetic landscape of type 2 diabetes in mice. *Endocr Rev*, **28**, 48-83.
- 15 Rahimov, F., Marazita, M.L., Visel, A., Cooper, M.E., Hitchler, M.J., Rubini, M., Domann, F.E., Govil, M., Christensen, K., Bille, C. *et al.* (2008) Disruption of an AP-2alpha binding site in an IRF6 enhancer is associated with cleft lip. *Nat Genet*, **40**, 1341-1347.
- 16 Wang, X., Pasolli, H.A., Williams, T. and Fuchs, E. (2008) AP-2 factors act in concert with Notch to orchestrate terminal differentiation in skin epidermis. *J Cell Biol*, **183**, 37-48.
- 17 Li, W. and Cornell, R.A. (2007) Redundant activities of Tfap2a and Tfap2c are required for neural crest induction and development of other non-neural ectoderm derivatives in zebrafish embryos. *Dev Biol*, **304**, 338-354.
- 18 Popa, C., Dahler, A.L., Serewko-Auret, M.M., Wong, C.F., Smith, L., Barnes, L.M., Stratton, G.M. and Saunders, N.A. (2004) AP-2 transcription factor family member expression, activity, and regulation in human epidermal keratinocytes in vitro. *Differentiation*, **72**, 185-197.
- 19 Botti, E., Spallone, G., Moretti, F., Marinari, B., Pinetti, V., Galanti, S., De Meo, P.D., De Nicola, F., Ganci, F., Castrignano, T. *et al.* (2011) Developmental factor IRF6 exhibits tumor suppressor activity in squamous cell carcinomas. *Proc Natl Acad Sci U S A*, **108**, 13710-13715.
- 20 de la Garza, G., Schleiffarth, J.R., Dunnwald, M., Mankad, A., Weirather, J.L., Bonde, G., Butcher, S., Mansour, T.A., Kousa, Y.A., Fukazawa, C.F. *et al.* (2013) Interferon regulatory factor 6 promotes differentiation of the periderm by activating expression of grainyhead-like 3. *J Invest Dermatol*, **133**, 68-77.

- 21 Guttormsen, J., Koster, M.I., Stevens, J.R., Roop, D.R., Williams, T. and Winger, Q.A. (2008) Disruption of epidermal specific gene expression and delayed skin development in AP-2 gamma mutant mice. *Dev Biol*, **317**, 187-195.
- 22 Pyrgaki, C., Liu, A. and Niswander, L. (2011) Grainyhead-like 2 regulates neural tube closure and adhesion molecule expression during neural fold fusion. *Dev Biol*, **353**, 38-49.
- 23 Richardson, R.J., Dixon, J., Malhotra, S., Hardman, M.J., Knowles, L., Boot-Handford, R.P., Shore, P., Whitmarsh, A. and Dixon, M.J. (2006) Irf6 is a key determinant of the keratinocyte proliferation-differentiation switch. *Nat Genet*, **38**, 1329-1334.
- 24 Takeda, K., Takeuchi, O., Tsujimura, T., Itami, S., Adachi, O., Kawai, T., Sanjo, H., Yoshikawa, K., Terada, N. and Akira, S. (1999) Limb and skin abnormalities in mice lacking IKKalpha. *Science*, **284**, 313-316.
- 25 Holland, P., Willis, C., Kanaly, S., Glaccum, M., Warren, A., Charrier, K., Murison, J., Derry, J., Virca, G., Bird, T. *et al.* (2002) RIP4 is an ankyrin repeat-containing kinase essential for keratinocyte differentiation. *Curr Biol*, **12**, 1424-1428.
- 26 Lee, S., Kong, Y. and Weatherbee, S.D. (2013) Forward genetics identifies Kdf1/1810019J16Rik as an essential regulator of the proliferation-differentiation decision in epidermal progenitor cells. *Dev Biol*, **383**, 201-213.
- 27 Thomason, H.A., Zhou, H., Kouwenhoven, E.N., Dotto, G.P., Restivo, G., Nguyen, B.C., Little, H., Dixon, M.J., van Bokhoven, H. and Dixon, J. (2010) Cooperation between the transcription factors p63 and IRF6 is essential to prevent cleft palate in mice. *J Clin Invest*, **120**, 1561-1569.
- 28 Scibetta, A.G., Wong, P.P., Chan, K.V., Canosa, M. and Hurst, H.C. (2010) Dual association by TFAP2A during activation of the p21cip/CDKN1A promoter. *Cell Cycle*, **9**, 4525-4532.
- 29 Koinuma, D., Tsutsumi, S., Kamimura, N., Taniguchi, H., Miyazawa, K., Sunamura, M., Imamura, T., Miyazono, K. and Aburatani, H. (2009) Chromatin immunoprecipitation on microarray analysis of Smad2/3 binding sites reveals roles of ETS1 and TFAP2A in transforming growth factor beta signaling. *Mol Cell Biol*, **29**, 172-186.
- 30 Iwata, J., Suzuki, A., Pelikan, R.C., Ho, T.V., Sanchez-Lara, P.A., Urata, M., Dixon, M.J. and Chai, Y. (2013) Smad4-Irf6 genetic interaction and TGFbeta-mediated IRF6 signaling cascade are crucial for palatal fusion in mice. *Development*, **140**, 1220-1230.

- 31 Descargues, P., Sil, A.K., Sano, Y., Korchynskiy, O., Han, G., Owens, P., Wang, X.J. and Karin, M. (2008) IKKalpha is a critical coregulator of a Smad4-independent TGFbeta-Smad2/3 signaling pathway that controls keratinocyte differentiation. *Proc Natl Acad Sci U S A*, **105**, 2487-2492.
- 32 Marinari, B., Moretti, F., Botti, E., Giustizieri, M.L., Descargues, P., Giunta, A., Stolfi, C., Ballaro, C., Papoutsaki, M., Alema, S. *et al.* (2008) The tumor suppressor activity of IKKalpha in stratified epithelia is exerted in part via the TGF-beta antiproliferative pathway. *Proc Natl Acad Sci U S A*, **105**, 17091-17096.
- 33 Nair, M., Teng, A., Bilanchone, V., Agrawal, A., Li, B. and Dai, X. (2006) Ovol1 regulates the growth arrest of embryonic epidermal progenitor cells and represses c-myc transcription. *J Cell Biol*, **173**, 253-264.
- 34 Grandori, C., Cowley, S.M., James, L.P. and Eisenman, R.N. (2000) The Myc/Max/Mad network and the transcriptional control of cell behavior. *Annu Rev Cell Dev Biol*, **16**, 653-699.
- 35 Zervos, A.S., Gyuris, J. and Brent, R. (1993) Mxi1, a protein that specifically interacts with Max to bind Myc-Max recognition sites. *Cell*, **72**, 223-232.
- 36 Marinari, B., Ballaro, C., Koster, M.I., Giustizieri, M.L., Moretti, F., Crosti, F., Papoutsaki, M., Karin, M., Alema, S., Chimenti, S. *et al.* (2009) IKKalpha is a p63 transcriptional target involved in the pathogenesis of ectodermal dysplasias. *J Invest Dermatol*, **129**, 60-69.
- 37 Zhu, F., Xia, X., Liu, B., Shen, J., Hu, Y. and Person, M. (2007) IKKalpha shields 14-3-3sigma, a G(2)/M cell cycle checkpoint gene, from hypermethylation, preventing its silencing. *Mol Cell*, **27**, 214-227.
- 38 Restivo, G., Nguyen, B.C., Dziunycz, P., Ristorcelli, E., Ryan, R.J., Ozuysal, O.Y., Di Piazza, M., Radtke, F., Dixon, M.J., Hofbauer, G.F. *et al.* (2011) IRF6 is a mediator of Notch pro-differentiation and tumour suppressive function in keratinocytes. *EMBO J*.
- 39 Richardson, R.J., Dixon, J., Jiang, R. and Dixon, M.J. (2009) Integration of IRF6 and Jagged2 signalling is essential for controlling palatal adhesion and fusion competence. *Hum Mol Genet*, **18**, 2632-2642.
- 40 Bailey, C.M., Khalkhali-Ellis, Z., Kondo, S., Margaryan, N.V., Seftor, R.E., Wheaton, W.W., Amir, S., Pins, M.R., Schutte, B.C. and Hendrix, M.J. (2005) Mammary serine protease inhibitor (Maspin) binds directly to interferon regulatory factor 6: identification of a novel serpin partnership. *J Biol Chem*, **280**, 34210-34217.

- 41 Bailey, C.M., Abbott, D.E., Margaryan, N.V., Khalkhali-Ellis, Z. and Hendrix, M.J. (2008) Interferon regulatory factor 6 promotes cell cycle arrest and is regulated by the proteasome in a cell cycle-dependent manner. *Mol Cell Biol*, **28**, 2235-2243.
- 42 Sil, A.K., Maeda, S., Sano, Y., Roop, D.R. and Karin, M. (2004) IkappaB kinase-alpha acts in the epidermis to control skeletal and craniofacial morphogenesis. *Nature*, **428**, 660-664.
- 43 Ting, S.B., Wilanowski, T., Auden, A., Hall, M., Voss, A.K., Thomas, T., Parekh, V., Cunningham, J.M. and Jane, S.M. (2003) Inositol- and folate-resistant neural tube defects in mice lacking the epithelial-specific factor Grhl-3. *Nat Med*, **9**, 1513-1519.
- 44 Wu, C., Endo, M., Yang, B.H., Radecki, M.A., Davis, P.F., Zoltick, P.W., Spivak, R.M., Flake, A.W., Kirschner, R.E. and Nah, H.D. (2013) Intra-amniotic transient transduction of the periderm with a viral vector encoding TGFbeta3 prevents cleft palate in Tgfbeta3(-/-) mouse embryos. *Mol Ther*, **21**, 8-17.